ISSN 2413-5577

№ 1 Январь – Март 2025

Экологическая безопасность прибрежной и шельфовой зон моря

Ecological Safety of Coastal and Shelf Zones of Sea

No. 1 January – March 2025

ecological-safety.ru

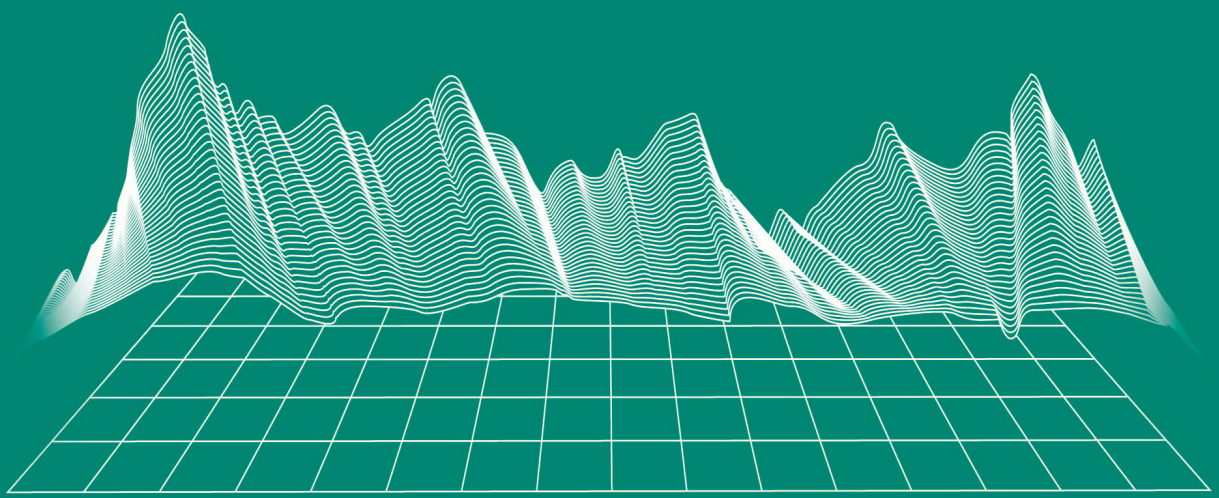

ISSN 2413-5577

No. 1, 2025
January – March

Publication frequency:
Quarterly

16+

ECOLOGICAL SAFETY OF COASTAL AND SHELF ZONES OF SEA

Scientific and theoretical peer reviewed journal

FOUNDER AND PUBLISHER:
Federal State Budget Scientific Institution
Federal Research Centre
"Marine Hydrophysical Institute of RAS"

The Journal publishes original research results, review articles (at the editorial board's request) and brief reports.

The Journal aims at publication of results of original scientific research concerning the state and interaction of geospheres (atmosphere, lithosphere, hydrosphere, and biosphere) within coastal and shelf areas of seas and oceans, methods and means of study thereof, ecological state of these areas under anthropogenic load as well as environmental protection issues.

The Journal's editorial board sees its mission as scientific, educational and regulatory work to preserve the ecological balance and restore the resource potential of coastal and shelf areas believing that despite the geographical limitations of the areas under study, the processes taking place within them have a significant impact on the waters of the seas and oceans and economic activity.

The Journal publishes original research materials, results of research performed by national and foreign scientific institutions in the coastal and shelf zones of seas and oceans, review articles (at the editorial board's request) and brief reports on the following major topics:
- Scientific basis for complex use of shelf natural resources
- Marine environment state and variability
- Coastal area state and variability; coast protection structures
- Monitoring and estimates of possible effects of anthropogenic activities
- Development and implementation of new marine environment control and monitoring technologies

The outcome of the research is information on the status, variability and possible effects of anthropogenic activities in the coastal and shelf marine areas, as well as the means to perform calculations and to provide information for making decisions on the implementation of activities in the coastal zone.

e-mail: ecology-safety@mhi-ras.ru

website: http://ecological-safety.ru

Founder, Publisher and Editorial Office address:
2, Kapitanskaya St.,
Sevastopol, 299011, Russia

Phone, fax: + 7 (8692) 54-57-16

EDITORIAL BOARD

РЕДАКЦИОННАЯ КОЛЛЕГИЯ

CONTENTS

№ 1. 2025 January – March, 2025

СОДЕРЖАНИЕ

№ 1. 2025 Январь – Март, 2025

Original paper

Assessment of SKIRON and ERA5 Atmospheric Forcing for the Reconstruction of the Black Sea Circulation Based on Hydrophysical Modeling Results

O. A. Dymova *, N. A. Miklashevskaya

Marine Hydrophysical Institute of RAS, Sevastopol, Russia

* *e-mail: olgdymova@mhi-ras.ru*

Abstract

A modeling of the Black Sea circulation for 2016 was carried out with different sets of atmospheric forcing data to determine the optimal atmospheric forcing for retrospective analysis of hydrophysical fields. An eddy-resolving z-model of Marine Hydrophysical Institute with a resolution of 1.6 km was used for the calculations. Differences in the circulation structure for the two experiments were revealed. It was shown that in the SKIRON experiment compared to ERA5, the cyclonic circulation of the Black Sea was weakened, the isopycnic surfaces were aligned, and the cold intermediate layer was not determined by the 8°C isotherm due to the underestimation of the solar radiation flux and weakening of the wind influence. A comparison of the model thermohaline characteristics calculated using ERA5 and SKIRON atmospheric forcings and measurement data of temperature and salinity obtained by ARGO profiling floats and onboard equipment in 87, 89, 91 cruises of R/V *Professor Vodyanitsky* was carried out. According to the validation results, it was obtained that in the upper 300-meter layer, for all measurement stations the mean RMSE of temperature and salinity in the ERA5 experiment were 28 and 17% lower, respectively, than the RMSE calculated from the SKIRON data.

Keywords: Black Sea, modeling, temperature, salinity, current velocity, *in situ* data, forcing, *ERA5*, *SKIRON*

Acknowledgment: The work was supported by the state assignment of MHI RAS on topic no. FNNN-2024-0001 (“Oceanological processes” code).

For citation: Dymova, O.A. and Miklashevskaya, N.A., 2025. Assessment of SKIRON and ERA5 Atmospheric Forcing for the Reconstruction of the Black Sea Circulation Based on Hydrophysical Modeling Results. *Ecological Safety of Coastal and Shelf Zones of Sea*, (1), pp. 6–25.

Оценка применимости атмосферных форсингов *SKIRON* и *ERA*5 для реконструкции циркуляции Черного моря на основе результатов моделирования гидрофизических полей

О. А. Дымова *, Н. А. Миклашевская

Морской гидрофизический институт РАН, Севастополь, Россия
** e-mail: olgdymova@rambler.ru*

Аннотация
Проведено моделирование циркуляции Черного моря в 2016 г. с разными наборами данных об атмосферном воздействии с целью определения оптимального атмосферного форсинга для проведения ретроспективного анализа гидрофизических полей. Для расчетов использована вихреразрешающая *z*-модель Морского гидрофизического института с разрешением 1.6 км. По результатам двух экспериментов выявлены различия в структуре циркуляции. Показано, что вследствие заниженного потока коротковолновой радиации и слабого ветрового воздействия по данным *SKIRON*, по сравнению с *ERA*5, циклоническая циркуляция Черного моря ослабевает, изопикнические поверхности выравниваются, а холодный промежуточный слой не определяется по изотерме 8 °С. Выполнено сопоставление модельных термохалинных характеристик, рассчитанных при использовании атмосферных форсингов *ERA*5 и *SKIRON*, с данными натурных наблюдений за температурой и соленостью, полученными буями-профилометрами *ARGO* и судовым оборудованием в 87, 89, 91-м рейсах НИС «Профессор Водяницкий». По результатам валидации получено, что в верхнем 300-метровом слое средние по всем станциям измерений среднеквадратические отклонения температуры и солености в эксперименте *ERA*5 меньше на 28 и 17 % соответственно, чем среднеквадратические отклонения, рассчитанные по данным эксперимента *SKIRON*.

Ключевые слова: Черное море, моделирование, температура, соленость, скорость течений, натурные наблюдения, форсинг, *ERA*5, *SKIRON*

Благодарности: работа выполнена в рамках госзадания ФГБУН ФИЦ МГИ по теме № FNNN-2024-0001.

Для цитирования: *Дымова О. А., Миклашевская Н. А.* Оценка применимости атмосферных форсингов *SKIRON* и *ERA*5 для реконструкции циркуляции Черного моря на основе результатов моделирования гидрофизических полей // Экологическая безопасность прибрежной и шельфовой зон моря. 2025. № 1. С. 6–25. EDN TPMTAZ.

Introduction

The Black Sea is a semi-enclosed basin connected to the World Ocean by a narrow shallow strait with a double-layer current. According to the type of vertical structure of currents in the Bosphorus Strait, the Black Sea belongs to the estuarine type of basins with outflow of more fresh water in the upper layer and inflow of more saline water in the lower one. Due to the fact that water exchange with the World Ocean is limited in such seas, their circulation pattern depends significantly on atmospheric conditions.

Based on comparative numerical analyses of the energy budget of semi-enclosed seas such as the Mediterranean, Red, Black and Baltic seas, it is shown in [1] that the basin circulation is significantly influenced by buoyancy fluxes

through the straits in addition to the wind work. The authors attribute qualitative aspects of the variability of currents in basins to differences between the relative contributions of the wind work and buoyancy work to the energy budget. Based on numerical modeling of the Caspian Sea water dynamics, it is shown in [2] that the level rise in the 1980–1990s was caused by changes in the volume of river runoff and atmospheric conditions over the basin. Correct reproduction of the water balance determined by atmospheric forcing helped to reproduce a sharp increase in the level (up to 2.5 m) in the Caspian Sea. In [3], the results of extreme surges modeling in the Sea of Azov are presented. It is shown that when using high-resolution WRF atmospheric data (10 km resolution), the accuracy of storm surge reproduction is higher than in the data calculated using ERA-Interim forcing (0.75° resolution). In [4], based on the results of numerical experiments, the effect of such atmospheric data as wind and thermohaline forcing on the Black Sea circulation is investigated and it is shown that the mean annual cyclonic vorticity of the wind field and the seasonal variability of the heat flux from the atmosphere support the large-scale cyclonic circulation in the basin. It is shown in [5] that changes in the intensity of the wind influence over the Black Sea lead to significant differences in the structure of current velocity field: if cyclonic vorticity of the wind field prevails over the sea, the velocity field is dominated by large-scale circulation; if the wind influence is weakened, an eddy circulation regime with predominance of mesoscale structures is formed.

In [1–5] above, the importance of atmospheric forcing in numerical analyses of the dynamics of enclosed and semi-enclosed seas is demonstrated. Therefore, the selection of external forcing data, especially wind stress, should be carefully controlled for retrospective analysis of the circulation of such seas. Despite the large number of high quality reanalyses of the Black Sea (see, e.g., [6, 7] and data set [1)]), in addition to thermohaline and hydrodynamic arrays, we also intend to calculate the circulation energy characteristics, which are not provided by the reanalyses known to us, in order to study the mechanisms of the observed trends in the variability of hydrophysical fields.

The aim of this paper is to validate the Black Sea circulation modeling results obtained by using different atmospheric datasets and to select the atmospheric forcing for the retrospective analysis of the Black Sea hydrophysical fields.

Numerical model

An eddy-resolving z-model of Marine Hydrophysical Institute (MHI model) was used to reconstruct the Black Sea circulation [8]. The model is based on full system of ocean thermohydrodynamics equations in the Boussinesq approximation, hydrostatics and incompressibility of seawater. The equation of state is represented

---

[1)] Lima, L., Masina, S., Ciliberti, S. A., Peneva, E. L., Cretí, S., Stefanizzi, L., Lecci, R., Palermo, F., Coppini, G. [et al.], 2020. *Black Sea Physical Reanalysis (CMEMS BS-Currents) (Version 1): Data set.* Copernicus Monitoring Environment Marine Service (CMEMS). https://doi.org/10.25423/CMCC/BLKSEA_MULTIYEAR_PHY_007_004

by a nonlinear dependence of density on temperature and salinity. The sea level is calculated from the equation obtained by fulfilling the linearized kinematic condition on the free surface, the vertical velocity is calculated from the continuity equation. In the context of solid lateral boundaries, the conditions of equality to zero of the normal velocity and the normal derivative of the tangential velocity are set for the components of the velocity vector; for temperature and salinity, the equality to zero of the normal derivatives is set. A no-slip condition and zero normal heat and salt fluxes are placed on the bottom. The model takes into account river runoff and water exchange through the straits, with Dirichlet conditions imposed on the liquid parts of the boundary. Wind stress, heat fluxes from the atmosphere, precipitation and evaporation are given as boundary conditions on the free surface. In addition, sea surface temperature is assimilated on the free surface when data are available. Vertical turbulent mixing is described using the Mellor–Yamada closure model [9], while horizontal viscosity and diffusion are described by the Laplace operator with constant coefficients. The sea level, temperature and salinity, horizontal components of the velocity vector are set at the initial moment of time. The model equations, boundary conditions and coefficients used are described in detail in [8].

The MHI model was implemented on grid C [10] with a resolution of 1.6 km in horizontal coordinates, which is sufficient to reproduce the mesoscale circulation features in both abyssal and coastal zones of the Black Sea [11], as it is smaller than the barotropic Rossby radius of deformation, which averages 15–17 km, and the baroclinic radius, which reaches 5 km in the coastal zone. According to [12], the term "mesoscale" will be used in this paper to denote eddy structures with sizes of 30–150 km. Vertically, 27 z-horizons were set with spacing from 2.5 m near the surface to 200 m in deep layers. Basin bathymetry was constructed from EMODnet [2)] data at a resolution of (1/8)′.

Numerical experiments and atmospheric forcing

Two numerical experiments were performed for 2016 with the same model settings but different atmospheric forcing. The initial fields for the experiments were the same and they were constructed from CMEMS reanalysis data for the Black Sea [1)]. Data from the Copernicus system [3)] were taken to set the sea surface temperature. Temperature, salinity and water discharge in rivers and straits correspond to monthly mean climatic values from atlas [13]. The first experiment (hereinafter referred to as the ERA5 experiment) used hourly data from the ERA5 reanalysis [4)] provided

---

[2)] European Commission. *European Marine Observation and Data Network (EMODnet)*. [online] Available at: https://www.emodnet-bathymetry.eu [Accessed: 3 March 2025].

[3)] CMEMS. *Black Sea - High Resolution and Ultra High Resolution L3S Sea Surface Temperature: Product ID.* SST_BS_SST_L3S_NRT_OBSERVATIONS_010_013E.U/CMEMS; Copernicus Marine Data Store. https://doi.org/10.48670/moi-00158

[4)] Hersbach, H., Bell, B., Berrisford, P., Biavati, G., Horányi, A., Muñoz Sabater, J., Nicolas, J., Peubey, C., Radu, R. [et al.], 2023. *ERA5 Hourly Data on Single Levels from 1959 to Present:* Data Set. Copernicus Climate Change Service (C3S) Climate Data Store (CDS). https://doi.org/10.24381/cds.adbb2d47

by the European Centre for Medium-Range Weather Forecasts for global climate, with a resolution of 0.25°. In the second experiment (hereinafter referred to as the SKIRON experiment), the atmospheric forcing included two-hourly data obtained by the SKIRON/Dust modeling system (Greece) with a spatial resolution of 0.1° [14].

Comparative analysis of SKIRON and ERA5 data showed a significant difference in wind forcing over the Black Sea region. The tangential wind stresses were calculated using an aerodynamic formula similar to [15] based on wind speed data at 10 m height. As can be seen from Fig. 1, for both forcings, strong winds over the Black Sea most often (about 10%) have a direction between northerly and northeasterly, which is consistent with climatic estimates [15]. This structure of wind fields favours the formation of cyclonic circulation of waters [5)] in the upper active layer [16]. However, the maximum values of wind stress differ almost by a factor of 1.4 and reach $5 \cdot 10^{-5}$ N/cm^2 according to ERA5 and $3.5 \cdot 10^{-5}$ N/cm^2 according to SKIRON, corresponding to wind speeds of about 23 and 18 m/s, respectively. Comparison with available observations shows that the wind speed from ERA5 data is closer to reality. In confirmation of the above, Fig. 2 presents the wind fields on 3 December 2016 plotted using ERA5 and SKIRON forcing data and obtained at the Remote Sensing Department of Marine Hydrophysical Institute from satellite data (available at: http://dvs.net.ru/mp/data/main_ru.shtml). It can be seen that the high wind speed areas in ERA5 (Fig. 2, *b*) are more representative.

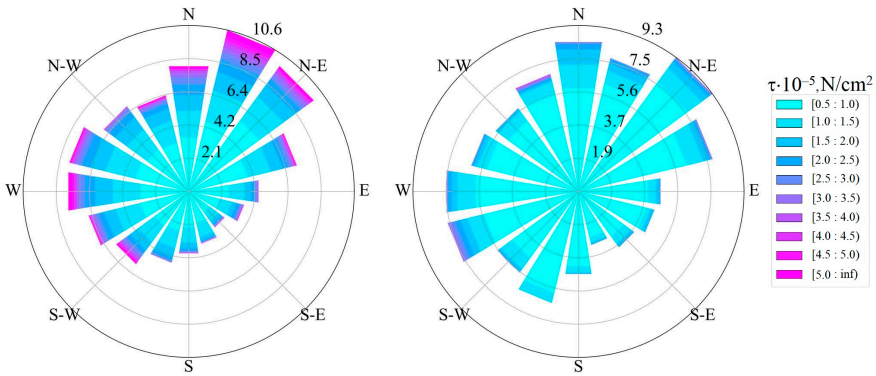

a ***b***

F i g. 1. Histograms of repeatability, %, of the wind directions and the wind stress values τ for the Black Sea in 2016: *a* – ERA5; *b* – SKIRON. The data are calculated from wind speed at a height of 10 m

[5)] Blatov, A.S., Bulgakov, N.P., Ivanov, V.A., Kosarev, A.N. and Tuljulkin, V.S., 1984. *Variability of the Black Sea Hydrophysical Fields*. Leningrad: Gidrometeoizdat, 240 p. (in Russian).

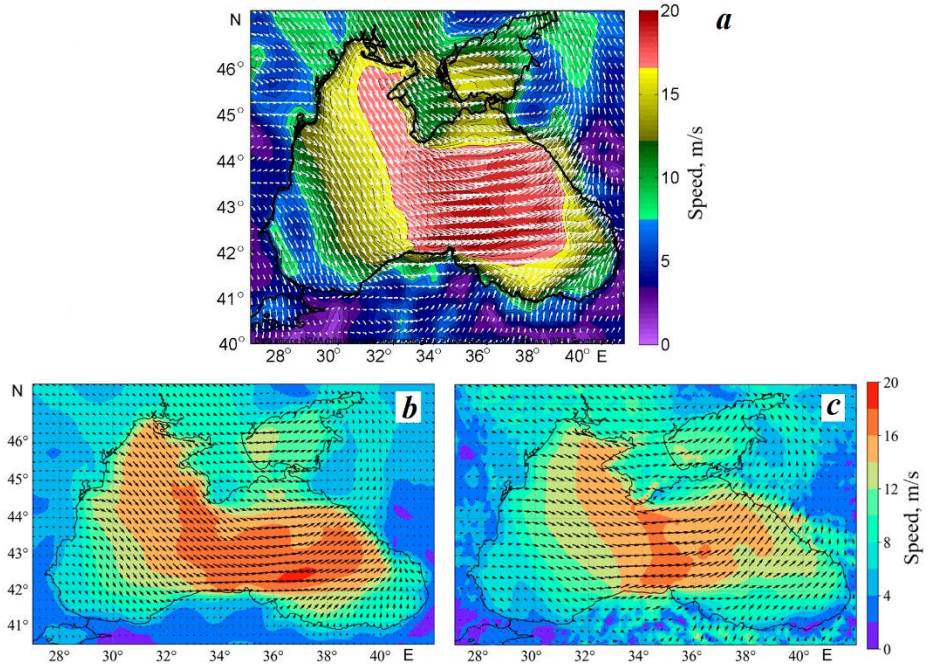

F i g. 2. Examples of presentation of the wind fields on 3 December 2016: *a* – from satellite data (http://dvs.net.ru/mp/data/vel/jpg/wind/wind_nomads_2016120306.jpg); *b* – from ERA5 data; *c* – from SKIRON data

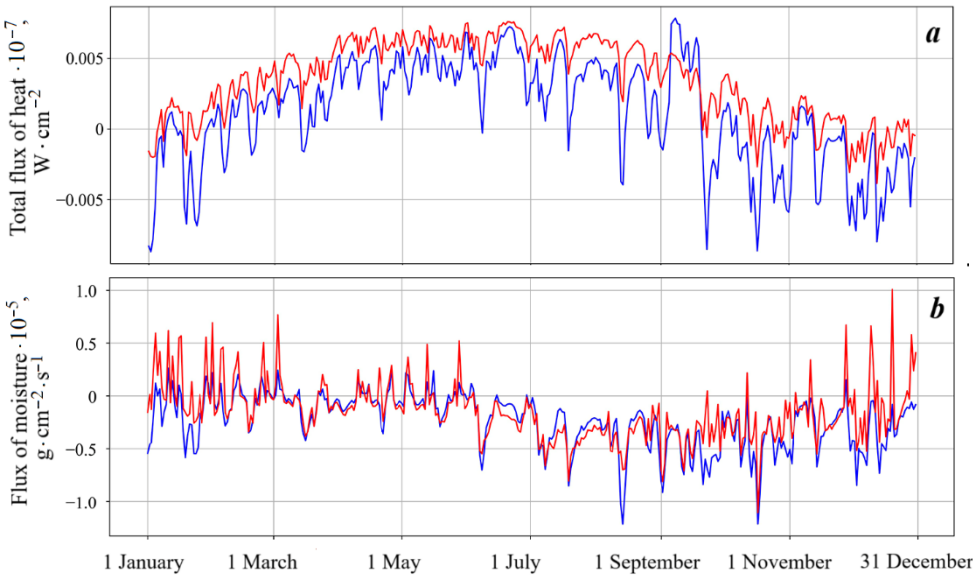

F i g. 3. Total fluxes of heat (*a*) and moisture (*b*) in 2016 according to ERA5 (red lines) and SKIRON (blue lines)

The temporal variability of other fluxes from the ERA5 and SKIRON forcing data is qualitatively similar. For area averages, the total heat flux (sensible and latent heat, thermal and solar radiation) during the year is 15–20% higher according to the ERA5 data (Fig. 3, *a*). For the moisture flux (precipitation minus evaporation), an increase in precipitation is observed in winter and autumn according to ERA5 (Fig. 3, *b*).

Results of modeling and validation

As a result of numerical experiments, daily temperature, salinity and current velocity fields as well as sea level data were obtained for the entire study period. To validate the results, we calculated the root mean square errors (RMSE) of the model temperature and salinity from the *in situ* data obtained by ARGO profiling floats [6)] and onboard equipment in 87, 89 and 91 cruises of R/V *Professor Vodyanitsky* [17] in 2016 provided by the Oceanographic Database of Marine Hydrophysical Institute [18] (Fig. 4, Table 1). The data array contained more than 200 thousand measurements obtained both in the coastal zone and in the deep sea. As can be seen from Fig. 4 and Table 1, the coasts of Crimea, Turkey and the central deep sea are well provided with observation data in the cold and warm seasons. For the North Caucasus coast, the data from two ARGO floats are available for autumn and winter 2016. No data are reported for the northwestern shelf and the area of the Batumi anticyclone.

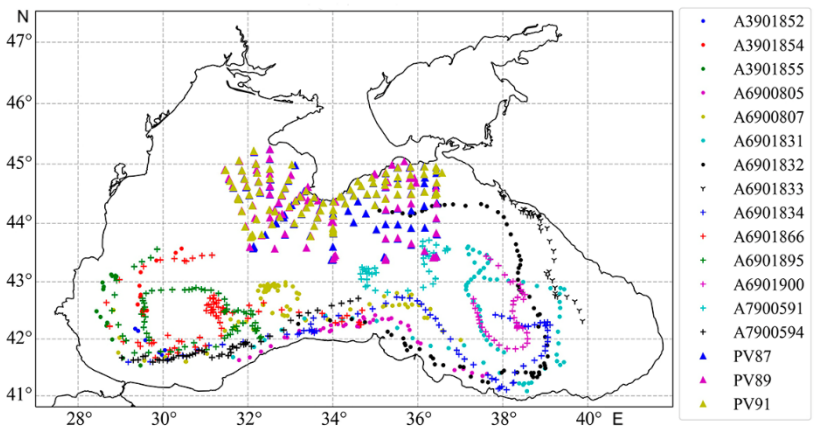

F i g . 4 . Map of location the temperature and salinity measurement stations conducted by ARGO floats and R/V *Professor Vodyanitsky* in 2016

[6)] IFREMER. *Coriolis Operational Oceanography*. [online] Available at: https://www.coriolis.eu.org/Data-Products/Data-selection [Accessed: 3 March 2025].

T a b l e 1. Information about temperature and salinity measurements in 2016

Identifier of float A / cruise PV	Date of stations	Number of stations	Number of measure-ments	Maximum pro-file depth, m
A3901852	6–28 December	6	624	1507
A3901854	2 November – 29 December	13	1507	1509
A3901855	22 October – 28 December	15	1461	1356
A6900805	2 January – 12 November	39	2354	1500
A6900807	2 January – 31 December	137	189737	991
A6901831	5 January – 30 December	74	7126	1513
A6901832	2 January – 27 December	73	6579	1520
A6901833	2 June – 29 December	42	3614	1517
A6901834	5 January – 30 December	74	6746	1505
A6901866	2 January – 28 December	74	96639	987
A6901895	2 January – 27 December	73	8321	723
A6901900	4 January – 22 July	41	10777	978
A7900591	11 January – 27 December	38	36836	1012
A7900594	3 January – 25 August	48	18307	1974
PV87	30 June – 18 July	124	108681	2180
PV89	30 September – 9 October	104	60741	2185
PV91	16 November – 3 December	107	48945	2068

For data obtained from each float, in each cruise and for each model, at the points closest to the measurement stations on the corresponding date, vertical averaging of profiles in six layers characterised by specific thermohaline conditions [5)] was carried out: upper layer (0–5 m), seasonal thermocline layer (5–30 m), cold intermediate layer (30–100 m), permanent halocline layer (100–300 m), two deep water layers (300–800 m and 800–1500 m). Then, along the tracks, the series of temperature and salinity deviations from the measured data were calculated and the RMSE were obtained. Analysis of the RMSE tables for all tracks (not presented in the paper) showed that the trend of the RMSE changes in the indicated layers was preserved for all data. The largest deviations from the observational data were obtained for the summer season temperature fields in the thermocline, and for the salinity fields in the halocline. Below a depth of 300 m, the RMSE values are small and close in two experiments, the difference between them does not exceed 0.025 °C and 0.036‰ for temperature and salinity, respectively. Table 2 further summarises the RMSE of temperature and salinity averaged over all tracks by the results of both experiments in the upper 300 m layer.

As can be seen from Table 2, in the whole layer, the values of temperature reproduction errors are smaller in the ERA5 experiment than in SKIRON. The highest RMSE of temperature in both experiments were found in the 5–30 m layer, with the RMSE values in the ERA5 experiment being 28% lower than in SKIRON. For salinity, the difference between the RMSE values in the 0–30 m layer is small, about 0.03‰, and in the halocline layer, the RMSE of salinity in the ERA5 experiment is about 17% less than in the SKIRON experiment.

Thus, the thermohaline characteristics in the layers of the permanent halocline and seasonal thermocline in the ERA5 experiment are closer to the measurement data than in the SKIRON experiment. The seasonal thermocline formation is primarily due to the warming of the upper water layer, hence, the increased heat flux in the ERA5 data (see Fig. 3, *a*) gives more realistic temperature fields. The error decrease in the halocline layer in the ERA5 experiment can be related both to the increase in the precipitation flux in autumn and winter (see Fig. 3, *b*) and to the change in the current field structure. The latter statement will be verified below by a comparative analysis of the current velocity and salinity fields in two experiments.

Table 2. RMSE of temperature and salinity by the results of the ERA5 and SKIRON experiments

Layer, m	Temperature RMSE, °C		Salinity RMSE, ‰	
	SKIRON	ERA5	SKIRON	ERA5
0–5	1.175	0.625	0.224	0.258
5–30	2.390	1.706	0.188	0.212
30–100	0.623	0.489	0.454	0.384
100–300	0.199	0.154	0.423	0.312

To analyse the differences between the experimental results, the spatial distributions of the fields of currents, temperature and salinity at different horizons during the year were compared. It was obtained that calculations with SKIRON data showed smoother fields of all considered thermohydrodynamic characteristics in the upper 20 m layer than in calculations with ERA5 forcing.

Let us consider in detail the peculiarities of the model temperature fields. From January to the end of April in the ERA5 experiment, the water temperature in the surface layer in the area of the northwestern shelf was 3–4 °C lower than in the second experiment. For the basin as a whole, this difference was 1–2 °C at the 5 m horizon, 0.5–1 °C at the 20 m horizon. From the third ten-day period of April, water began to warm up faster at both horizons in the first experiment than in the second one. According to the literature data [5)], as a result of the spring and summer warming, a thermocline layer is formed in the Black Sea, with a depth of the vertical gradient summer maximum of 15–20 m [19]. According to the validation (Table 2), the maximum RMSE of temperature were revealed in the 5–30 m layer by the results of both experiments.

Fig. 5 shows temperature distributions at the 20 m horizon on 15 June and 15 December calculated in two experiments. It can be seen that in June, the difference between temperature values from ERA5 and SKIRON data for the western part of the basin averaged 3–4 °C, for the eastern part – up to 3 °C (Fig. 5, *a*, *b*).

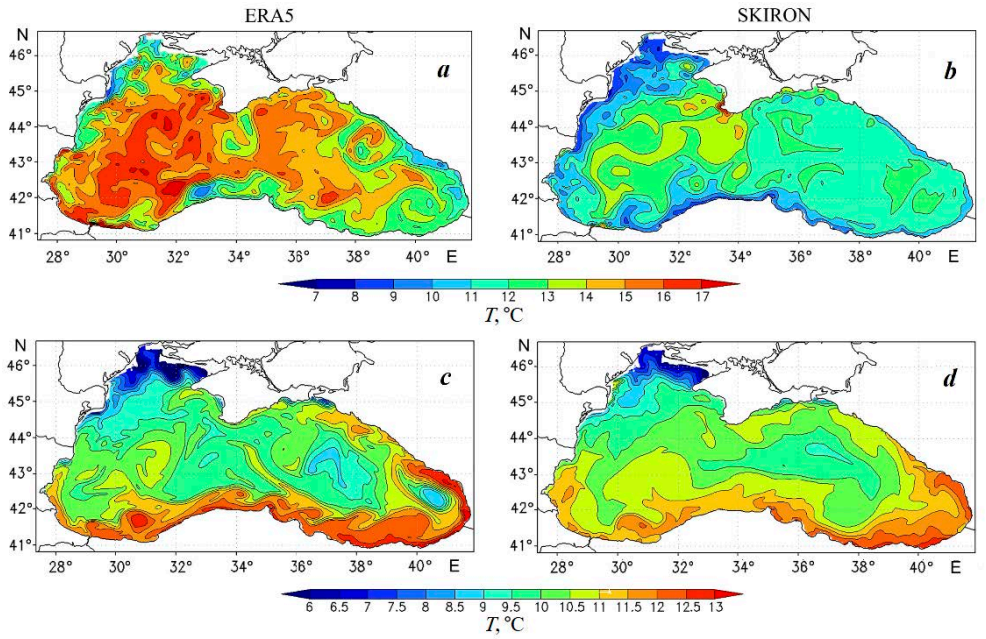

F i g . 5 . Temperature fields at the 20 m horizon on 15 June 2016 (*a*, *b*) and 15 December 2016 (*c*, *d*) obtained by using atmospheric forcings ERA5 (*a*, *c*) and SKIRON (*b*, *d*)

It should also be noted that for each experiment, the largest temperature difference of 3–5 °C between the western and eastern parts of the basin was observed in the zones of eddy activity.

In the ERA5 experiment, the eastern part warmed to almost the same temperature values (20–24 °C) as the western part by September. For the SKIRON experiment, the temperature difference at 20 m horizon between the western (22.5–24 °C) and eastern (12.5–15.5 °C) parts of the basin was about 10 °C by mid-September. Since late October, the temperature fields in two experiments differed insignificantly (0.5–1 °C) across all the horizon, except for the southeastern region of the sea, where, according to the ERA5 experiment, the temperature was 3–4 °C lower due to the effect of a cyclonic mesoscale eddy (Fig. 5, *c*).

For the summer period, the heat fluxes from the atmosphere were analysed and the reconstructed temperature was compared with the data obtained in 87th cruise of R/V *Professor Vodyanitsky* (30 June – 18 July 2016). It was found that the difference in the heating intensity of the upper water layer in two calculations (Fig. 5, *a*, *b*) was related to differences in the magnitude of the solar radiation flux. Thus, the monthly solar radiation flux at the sea surface for June 2016 was 249.51 and 187.43 W/m^2 according to ERA5 and SKIRON data, respectively. The spatial distribution of the flux (Fig. 6) is also consistent with the non-uniformity of the temperature distribution in the western and eastern parts of the sea: for both forcings, the solar radiation flux in the western part is higher than in the eastern one.

Estimates of deviations from the direct measurement data make it possible to determine which of two experiments gives results closer to the actual observed temperature. Fig. 7 shows the difference between the measured and calculated temperature at the 15 m horizon at the stations of 87th summer cruise of R/V *Professor Vodyanitsky* (see Fig. 4). It can be seen that the temperature deviations in the ERA5 experiment were lower than in the SKIRON experiment: the mean difference over all stations was almost twice as small in absolute value (Fig. 7) and the RMSE in the 5–30 m layer was 2.83 °C according to ERA5 data versus 3.65 °C according to SKIRON data.

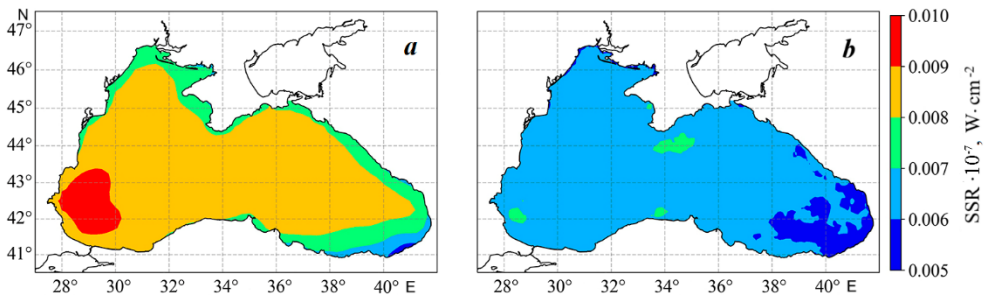

F i g . 6 . Monthly-mean solar radiation fields for June 2016 according to ERA5 (*a*) and SKIRON (*b*) data

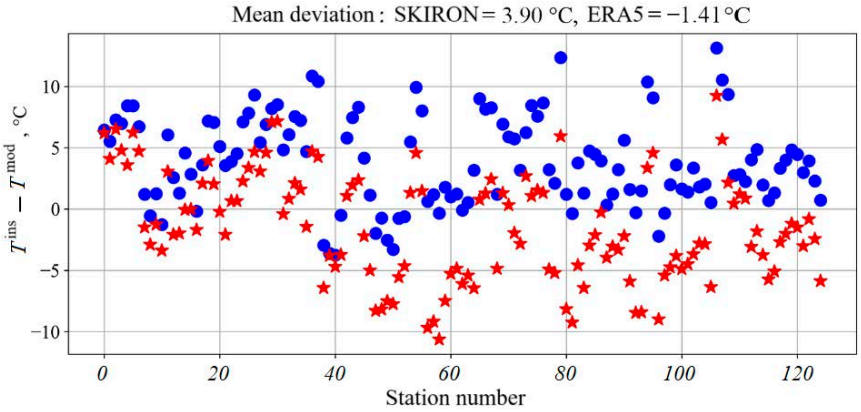

Fig. 7. Temperature deviation between the measurement data of 87th cruise of R/V *Professor Vodyanitsky* and the results of numerical experiments ERA5 (stars) and SKIRON (circles) at the 15 m horizon

It is known that the main contribution to the heat balance over the Black Sea comes from solar radiation (with a maximum in June) [19]. It should be expected that the differences in the magnitude of the total heat flux in the spring and summer season according to the ERA5 data observed in Fig. 3, *a*, will also be determined by this component of the balance. Fig. 6 confirms that the solar radiation from ERA5 is higher. Since the setup of the numerical experiments was identical, and only the atmospheric fluxes at the free surface differed, it can be argued that the underestimated solar radiation fluxes in the SKIRON forcing compared to ERA5 lead to significant temperature underestimation in the upper sea layer.

Analysis of the temperature distribution on a zonal section along 43.5°N showed that the temperature fields in the autumn and winter period were more homogeneous in the SKIRON experiment than in ERA5. In addition, calculations using SKIRON data showed that the water temperature in the upper mixed layer was about 0.5–1.0 °C higher in the first half of the year than using ERA5 data. Spring water warming in the SKIRON experiment started earlier than in the ERA5 experiment, but from the end of April the process intensified in the ERA5 experiment and the water started to warm faster than in the SKIRON experiment. Fig. 8, *a* shows that in the ERA5 experiment, the formation of a cold intermediate layer determined by the 8 °C isotherm is clearly observed, whereas in the SKIRON experiment, it is almost undetermined by the 8 °C isotherm (Fig. 8, *b*). Comparison of the model temperature with data from ARGO profiling float 6901831 (the trajectory of the float in the summer of 2016 was in the vicinity of 43°N – see Fig. 4) showed that the results of the ERA5 experiment were closer to the observational data, since the deviation of the model temperature from the observational data in the ERA5 experiment was 0.3–1 °C smaller than in SKIRON (Fig. 8, *c*). The vertical location of temperature isolines

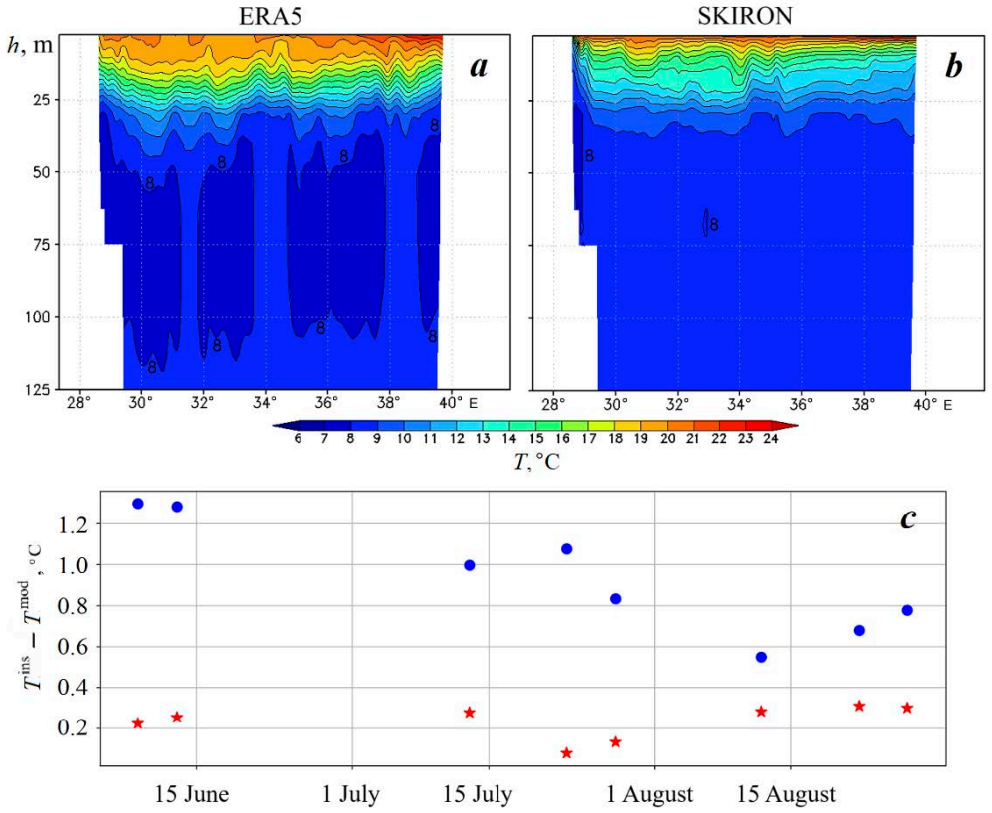

F i g . 8 . Zonal sections of temperature fields along 43.5° N for 15 June 2016 obtained by using atmospheric forcing ERA5 (*a*) and SKIRON (*b*). Temperature deviation between the measurement data of ARGO profiler float no. 6901831 and the modeling results of numerical experiments ERA5 (stars) and SKIRON (circles) (*c*) at the 75 m horizon

in the 50–110 m layer in Fig. 8 indicates the presence of frontal zones preventing horizontal mixing which can be stipulated by eddy dynamics in the central deep sea.

Salinity fields at horizons up to 20 m obtained from the results of two numerical experiments are quantitatively and qualitatively similar in the autumn and winter period (January–February and October–December), while differences appear from March to October. Thus, according to the results of calculations using ERA5 data, it was obtained that during this period at the 20 m horizon in the areas of the Danube, Dnieper and Dniester river mouths, quite extensive zones of waters with salinity below 16‰ were observed, whereas in the second experiment the salinity was higher than 16.75‰. In addition, during this period at the mentioned horizon,

more saline waters occupied a larger area according to the results of calculations using SKIRON data. Analysis of the sea surface moisture flux (precipitation minus evaporation) showed that during the spring and summer seasons, the forcing data were close (Fig. 3, *b*) and heat and mass fluxes in the mouths of rivers and in the straits were the same in both experiments. Consequently, change in stratification due to heating leads to rearrangement of velocity field and then salinity field as a result of advective transport. Therefore, we assume that differences in the spatial distribution of salinity field are related to the structure of current field.

Below the 30 m horizon, salinity fields differ more significantly throughout the entire calculation period. As can be seen from Table 2, the greatest difference between calculations is observed in the permanent halocline layer. Fig. 9 demonstrates salinity fields at the 100 m horizon in June and December 2016. It was obtained that in the SKIRON experiment, salinity in the continental slope zone was about 0.5‰ higher in summer (Fig. 9, *b*) and 1‰ higher in winter (Fig. 9, *d*) than in the ERA5 experiment. Salinity values are close in the zones of action of mesoscale eddies. By the end of the year, the salinity difference between the deep sea and the near-slope zone in the ERA5 experiment is larger (Fig. 9, *e*) than in the SKIRON experiment (Fig. 9, *f*), which indicates indirectly the intensification of the Rim Current and formation of the salinity field dome-shaped structure with higher values in the centre of the basin and lower ones in the periphery.

Comparison of model data and along-track measurements of salinity by ARGO floats at horizons in the constant halocline layer showed that the ERA5 data reproduced salinity more accurately. This is confirmed by the analysis of mean and root mean square deviations of salinity. Table 3 shows the RMSE of salinity from measurement data in the 100-300 m layer for some ARGO floats operating in deep water (Fig. 4). For most floats, the RMSE of salinity is smaller when using ERA5 forcing.

Fig. 10 demonstrates deviation between measured and calculated salinity values at 100 m horizon. It can be seen that in May–August, the RMSE of salinity in the ERA5 experiment is two to three times smaller than in the SKIRON experiment, and the annual mean deviation is about 20% smaller.

As shown by the analysis, the differences in the spatial distribution of salinity have little to do with the difference in the moisture flux from the atmosphere in two experiments and appear to be determined by a change in the velocity field structure. In the upper 20 m layer, current velocities and eddies from January to the end of April 2016 in the SKIRON experiment were less intense, especially in the area of the Anatolian Coast and Crimea. In January–April, the maximum velocities in the indicated areas according to the ERA5 experiment were 1.5 times greater than the values from the SKIRON data (at the 20 m horizon, 55–60 and 30–35 cm/s, respectively), with current directions remaining unchanged. In the second half of the year, the Rim Current is not formed as a single gyre in the SKIRON experiment, therefore a significant difference in the localisation of the currents is observed, especially in the area of formation of the Sevastopol anticyclone and also in the area of the Anatolian Coast. In July–October, maximum velocity values in the area of

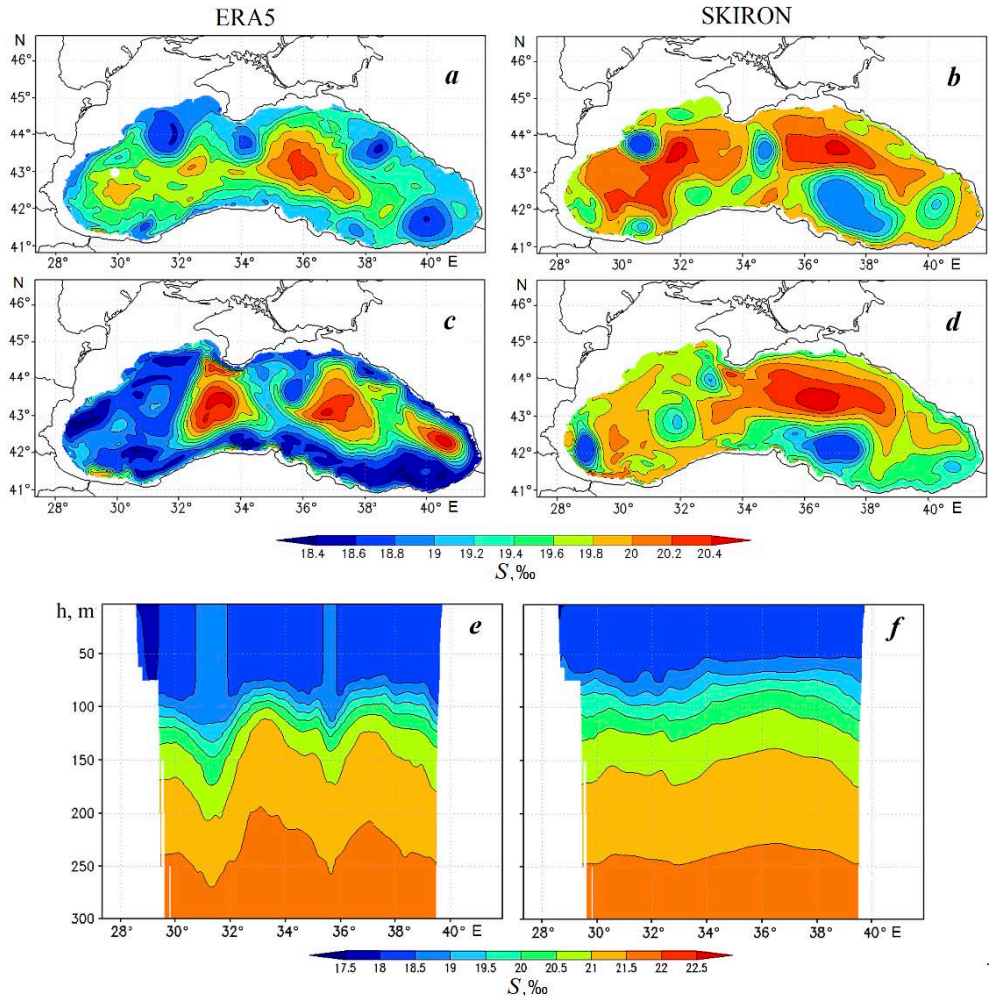

Fig. 9. Salinity fields on 15 June 2016 (*a, b*) and 15 December 2016 (*c*, *d*) at the 100 m horizon and zonal section of the salinity field along 43°N for 15 December 2016 (*e*, *f*), obtained by using atmospheric forcing ERA5 (*a*, *c*, *e*) and SKIRON (*b*, *d*, *f*)

Table 3. RMSE salinity, calculated in the ERA5 and SKIRON experiments, from ARGO data at a depth of 100–300 m

Forcing	Float identifier					
	6900805	6900807	6901832	6901834	7900591	7900594
ERA5	0.267	0.271	0.291	0.266	0.334	0.187
SKIRON	0.241	0.487	0.368	0.45	0.511	0.25

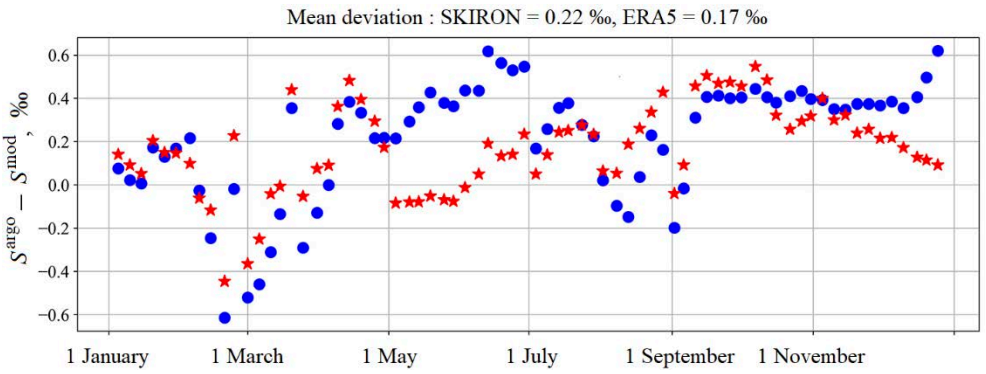

Fig. 10. The salinity deviation between the measurement data of ARGO profiler float 6901834 and the results of numerical experiments ERA5 and SKIRON at the 100 m horizon

the Sevastopol anticyclone became different by two to three times (55–60 cm/s for ERA5 and 20–25 cm/s for SKIRON at the 20 m horizon). And the current directed to the east near the coast of Turkey was not observed in the SKIRON experiment.

Fig. 11 shows time variability of mean current kinetic energy at the first z-level of the model grid in two experiments. Since the equations of motion include wind tangential stresses as boundary conditions at this level, the energy change of the currents here depends directly on the wind. According to Fig. 1, the wind over the Black Sea was more intense from ERA5 forcing data than from SKIRON data,

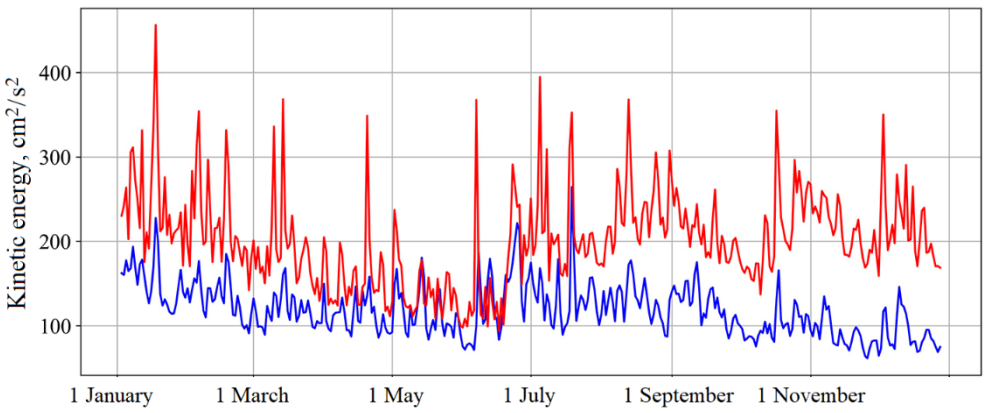

Fig. 11. Time variability of mean current kinetic energy in the upper model horizon according to data of ERA5 (red line) and SKIRON (blue line) experiments

which led to an increase in the velocity of surface currents. The curves in Fig. 11 confirm current velocity increase at the upper horizon in the ERA5 experiment and increasing difference between experiments in the second half of the year.

The change in the currents structure at the upper horizons was also reflected in the intensity of the Rim Current and mesoscale eddies in the deep layers. Fig. 12 shows model current velocity fields at the 100 m horizon in June and December 2016. It can be seen that the orbital velocities at the periphery of the mesoscale eddies reach 25–30 cm/s in two experiments in June (Fig. 12, *a*, *b*) and the Rim Current intensity (velocity in the core and current width) is higher according to the data of the ERA5 experiment. The ERA5 experiment shows clearly Sevastopol and Batumi anticyclones with velocities up to 36 and 28 cm/s, respectively, in the current field in December, when a chain of mesoscale anticyclones is also observed near the Anatolian Coast (Fig. 12, *c*). In the second experiment at a horizon of 100 m in winter, the number and intensity of mesoscale anticyclones at the periphery of the Rim Current are significantly lower, and the Rim Current velocity averages about 10 cm/s.

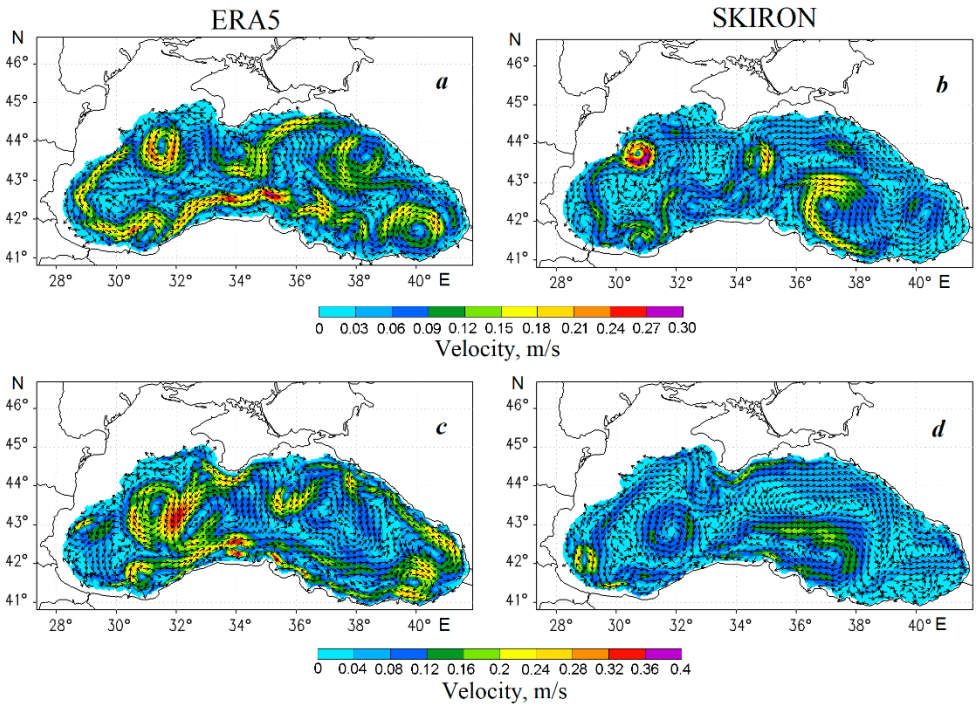

F i g . 1 2 . Current velocity fields obtained by using atmospheric forcing ERA5 (*a*, *c*) and SKIRON (*b*, *d*) at the 100 m horizon on 15 June 2016 (*a*, *b*) and 15 December 2016 (*c*, *d*)

Comparison of the current fields (Fig. 12) with the salinity fields (see Fig. 9) at the 100 m horizon confirms that the increase in the salinity gradient between the deep water and near-slope zones in the ERA5 experiment in winter is caused by more intense cyclonic circulation of waters and evolution of mesoscale anticyclones at the periphery of the Rim Current.

Conclusion

Two numerical experiments on the reconstruction of the Black Sea circulation for 2016 using the ERA5 and SKIRON atmospheric forcings were carried out. The results of temperature and salinity modeling were validated on the basis of contact measurements made by ARGO profiling floats and in the cruises of R/V *Professor Vodyanitsky*. The comparative analysis of hydrophysical fields obtained in two experiments was performed.

Validation of the model temperature and salinity fields showed that the thermohaline structure of the Black Sea waters was more accurately reconstructed using the ERA5 atmospheric forcing. For this experiment, the RMSE of temperature in the 5–30 m layer decreased by 28% and the RMSE of salinity in the 30–100 m layer decreased by about 17%.

Hydrophysical fields of the Black Sea for 2016, calculated using ERA5 data differ from those calculated from SKIRON data by the increase in the temperature of the upper 20 m layer in the spring and summer season, formation of the cold intermediate layer, increase in the horizontal salinity gradient between the periphery and the central part of the basin in the permanent halocline layer, intensification of the Rim Current and coastal mesoscale anticyclones (Sevastopol, Batumi anticyclones, Anatolian coastal eddies) in the upper 300 m layer.

When comparing the forcing data for 2016, it was obtained that ERA5 had higher wind intensity throughout the year and higher solar radiation intensity during the warm period of the year. According to the SKIRON experiment results, insufficient wind energy and underestimated heat flux lead to weakening of the Black Sea cyclonic circulation, alignment of isopycnic surfaces and temperature decrease in the 50–150 m layer. Thus, it is reasonable to use the ERA5 atmospheric reanalysis for retrospective analysis of the Black Sea hydrophysical fields.

REFERENCES

1. Cessi, P., Pinardi, N. and Lyubartsev, V., 2014. Energetics of Semienclosed Basins with Two-Layer Flows at the Strait. *Journal of Physical Oceanography*, 44(3), pp. 967–979. https://doi.org/10.1175/JPO-D-13-0129.1
2. Dyakonov, G.S. and Ibrayev, R.A., 2019. Long-Term Evolution of Caspian Sea Thermohaline Properties Reconstructed in an Eddy-Resolving Ocean General Circulation Model. *Ocean Science*, 15(3), pp. 527–541. https://doi.org/10.5194/os-15-527-2019
3. Fomin, V., Diansky, N., Korshenko, E. and Panasenkova, I., 2019. Assessment of Extreme Surge Simulation Accuracy in the Sea of Azov for Various Types of Atmospheric Forcing and Ocean Model Parameters. In: C. Grueau, R. Laurini and L. Ragia, eds., 2019. *Proceedings of the 5th International Conference on Geographical Information Systems Theory, Applications and Management. May 3–5, 2019, in Heraklion, Crete, Greece.* Vol. 1, pp. 340–344. https://doi.org/10.5220/0007836603400344

4. Oguz, T., Malanotte-Rizzoli, P. and Aubrey, D., 1995. Wind and Thermohaline Circulation of the Black Sea Driven by Yearly Mean Climatological Forcing. *Journal of Geophysical Research: Oceans*, 100(C4), pp. 6845–6863. https://doi.org/10.1029/95JC00022
5. Demyshev, S.G., Dymova, O.A. and Miklashevskaya, N.A., 2022. Spatio-Temporal Variability of Hydrophysical and Energy Characteristics of the Black Sea Circulation During Prevalence Movements of Different Scale. *Journal of Oceanological Research*, 50(3), pp. 27–50. https://doi.org/10.29006/1564-2291.JOR-2022.50(3).2
6. Korotaev, G.K., Knysh, V.V., Lishaev, P.N. and Sarkisyan, A.S., 2016. Reanalysis of Seasonal and Interannual Variability of Black Sea Fields for 1993–2012. *Izvestiya, Atmospheric and Oceanic Physics*, 52(4), pp. 418–430. https://doi.org/10.1134/S0001433816040071
7. Korotaev, G.K., Belokopytov, V.N., Dorofeev, V.L., Mizyuk, A.I. and Kholod, A.L., 2024. Acceleration of Climate Change in the Upper Layer of the Black Sea. *Doklady Earth Sciences*, 518(1), pp. 1550–1555. https://doi.org/10.1134/S1028334X24602797
8. Demyshev, S.G., 2012. A Numerical Model of Online Forecasting Black Sea Currents. *Izvestiya, Atmospheric and Oceanic Physics*, 48(1), pp. 120–132. https://doi.org/10.1134/S0001433812010021
9. Mellor, G.L. and Yamada, T., 1982. Development of a Turbulence Closure Model for Geophysical Fluid Problems. *Reviews of Geophysics*, 20(4), pp. 851–875. https://doi.org/10.1029/RG020i004p00851
10. Arakawa, A. and Lamb, V.R., 1981. A Potential Enstrophy and Energy Conserving Scheme for the Shallow Water Equation. *Monthly Weather Review*, 109(1), pp. 18–36. https://doi.org/10.1175/1520-0493(1981)109<0018:APEAEC>2.0.CO;2
11. Gruzinov, V.M., Diansky, N.A., Diakov, N.N. and Stepanov, D.V., 2018. Estimating the Coastal-Trapped Internal Wave Parameters in the Black Sea. In: I. M. Kabatchenko, ed., 2018. *SOI Proceedings*. Moscow: SOI. Iss. 219, pp. 66–87 (in Russian).
12. Chelton, D.B., Schlax, M.G. and Samelson, R.M., 2011. Global Observations of Nonlinear Mesoscale Eddies. *Progress in Oceanography*, 91(2), pp. 167–216. https://doi.org/10.1016/j.pocean.2011.01.002
13. Simonov, A.I. and Altman, E.N., eds., 1991. [*Hydrometeorology and Hydrochemistry of Seas of the USSR. Vol. 4. The Black Sea. Iss. 1. Hydrometeorological Conditions*]. Saint Petersburg: Gidrometeoizdat, 429 p. (in Russian).
14. Kallos, G., Nickovic, S., Papadopoulos, A., Jovic, D., Kakaliagou, O., Misirlis, N., Boukas, L., Mitikou, N., Sake laridis, G. [et al.], 1997. The Regional Weather Forecasting System SKIRON: An Overview. In: G. B. Kallos, V. Kotroni and K. Lagouvardos, eds., 1997. *Proceedings of the International Symposium on Regional Weather Prediction on Parallel Computer Environments. October 15–17, 1997. Athens, Greece*. University of Athens, pp. 109–122.
15. Shokurov, M.V. and Shokurova, I.G., 2017. Wind Stress Curl over the Black Sea under Different Wind Regimes. *Physical Oceanography*, (6), pp. 12–23. https://doi.org/10.22449/1573-160X-2017-6-12-23
16. Korotaev, G., Oguz, T., Nikiforov, A. and Koblinsky, C., 2003. Seasonal, Interannual, and Mesoscale Variability of the Black Sea Upper Layer Circulation Derived from Altimeter Data. *Journal of Geophysical Research: Oceans*, 108(C4), 3122. https://doi.org/10.1029/2002JC001508
17. Artamonov, Yu.V., Skripaleva, E.A., Alekseev, D.V., Fedirko, A.V., Shutov, S.A., Kolmak, R.V., Shapovalov, R.O. and Shcherbachenko, S.V., 2018. Hydrological Research in the Northern Part of the Black Sea in 2016 (87th, 89th and 91st Cruises of R/V *Professor Vodyanitsky*). *Physical Oceanography*, 25(3), pp. 229–234. https://doi.org/10.22449/1573-160X-2018-3-229-234

18. Bayankina, T.M., Godin, E.A., Zhuk, E.V., Ingerov, A.V., Isaeva, E.A. and Vetsalo, M.P., 2021. Information Resources of Marine Hydrophysical Institute, RAS: Current State and Development Prospects. In: T. Chaplina, ed., 2021. *Processes in GeoMedia – Volume II. Springer Geology*. Springer, Cham, pp. 187–197. https://doi.org/10.1007/978-3-030-53521-6_22
19. Ivanov, V.A. and Belokopytov, V.N., 2013. *Oceanography of the Black Sea*. Sevastopol: EKOSI-Gidrofizika, 210 p.

Submitted 15.06.2024; accepted after review 20.09.2024;
revised 17.12.2024; published 31.03.2025

About the authors:

Olga A. Dymova, Leading Research Associate, Marine Hydrophysical Institute of RAS (2 Kapitanskaya Str., Sevastopol, 299011, Russian Federation), PhD (Phys.-Math.), **ORCID ID: 0000-0003-4036-2447, ResearcherID: P-9669-2015**, *olgdymova@rambler.ru*

Nadezhda A. Miklashevskaya, Junior Research Associate, Marine Hydrophysical Institute of RAS (2 Kapitanskaya Str., Sevastopol, 299011, Russian Federation), **ORCID ID: 0000-0003-2619-343X, ResearcherID: P-2167-2017**, *nmikl@rambler.ru*

Contribution of the authors:

Olga A. Dymova – literature review on the study problem, concept exploration, outlining the study methodology, carrying out calculations, processing and description of the study results, results analysis and interpretation, data visualisation and their presentation in the text, critical analysis and revision of the text

Nadezhda A. Miklashevskaya – processing and description of the study results, qualitative and quantitative analysis of the results, data visualisation and their presentation in the text, preparation of the article text

All the authors have read and approved the final manuscript.

Original paper

Wind Field Retrieval in the Coastal Zone Using X-Band Radar Data at Large Incidence Angles

A. E. Korinenko *, V. V. Malinovsky

Marine Hydrophysical Institute of Russian Academy of Sciences, Sevastopol, Russia
* *e-mail: korinenko.alex@mhi-ras.ru*

Abstract

The paper aims to develop a geophysical model function that allows retrieval of the wind speed vector from a radar signal scattered from the sea surface. During *in situ* experiments on the stationary oceanographic platform in 2022–2024, a database was created which contained radar information, frequency spectra of sea surface elevations, wind speed and direction, and geometric properties of breaking wave crests in the active phase. An MRS-1011 360-degree marine radar (X-band, 3 cm wavelength) transmitting and receiving horizontally polarized signal at large incidence angles was used in the experiments. For these observation conditions, the main informative parameter that governs the radar cross section is the fraction of the sea surface covered by wind wave breaking crests (whitecap coverage). The role of this parameter is qualitatively confirmed by the fact that the radar power and whitecap coverage have similar wind speed dependencies. It was shown that the radar cross section was proportional to the whitecap coverage with 1.47 as the proportionality coefficient. The intensity of wave breaking also depends on the wave age, which leads to the dependency of the radar cross section on the wave development stage. The influence of the wave age on the radar signal level was confirmed experimentally. It was shown that the level of the wind dependency of the radar signal in the "up-wind" direction increased by a factor of 5 when the wave age increased from 0.1 to 1.2. Based on the *in situ* data and physical grounds of the sea surface radar backscatter formation, we suggest a geophysical model function allowing retrieval of wind speed fields in areas within a radius of about a kilometer. The error in wind speed vector magnitude and direction retrieved from radar data was 1.2 m/s and 30°, respectively, compared to the data obtained by the anemometer.

Keywords: navigation radar stations, radar images, normalized radar cross-section, sea surface, wind speed, in situ measurements, wave age, wave breaking

Acknowledgments: The study was carried out with financial support of the Russian Science Foundation grant no. 24-27-20105, https://rscf.ru/project/24-27-20105, and under the Agreement with the Department of Education and Science of Sevastopol no. 85 dated June 19, 2024. The authors thank K. A. Pampey for her assistance in *in situ* data processing

For citation: Korinenko, A.E. and Malinovsky, V.V., 2025. Wind Field Retrieval in the Coastal Zone Using X-Band Radar Data at Large Incidence Angles. *Ecological Safety of Coastal and Shelf Zones of Sea*, (1), pp. 26–41.

Восстановление полей ветра в прибрежной зоне по радиолокационным данным *X*-диапазона при больших углах наблюдения морской поверхности

А. Е. Кориненко *, В. В. Малиновский

Морской гидрофизический институт РАН, Севастополь, Россия
* *e-mail: korinenko.alex@mhi-ras.ru*

Аннотация
Цель статьи – разработать геофизическую модельную функцию, позволяющую по радиолокационному сигналу, отраженному от морской поверхности, восстанавливать модуль и направление скорости ветра. В ходе натурных экспериментов на стационарной океанографической платформе в 2022–2024 гг. была сформирована база данных, содержащая радиолокационную информацию, частотные спектры возвышений морской поверхности, скорость и направление ветра, геометрические размеры обрушений в активной фазе. В эксперименте использовалась радиолокационная станция *MRS*-1011 (*X*-диапазон, длина электромагнитной волны 3 см), работающая в круговом обзоре на горизонтальной поляризации передачи/приема сигнала при больших углах наблюдения. Для данных условий наблюдений основным информативным параметром, определяющим эффективную площадь рассеяния, является доля морской поверхности, покрытая обрушениями. Качественным подтверждением этого является совпадение ветровой зависимости радиолокационного сигнала с зависимостью от скорости ветра доли моря, занятой обрушениями. Показано, что зависимость эффективной площади рассеяния от суммарной площади обрушений на единице поверхности является линейной с коэффициентом 1.47. Интенсивность обрушений зависит также от возраста волн, что приводит к изменению эффективной площади рассеяния в зависимости от степени развития волнения. Экспериментально установлено влияние возраста волн на уровень сигнала радиолокатора. Показано, что уровень радиолокационного сигнала в направлении «на ветер» увеличивается в пять раз при изменении возраста волн от 0.1 до 1.2. На основании натурных данных и физических представлений о формировании отраженного от морской поверхности радиолокационного сигнала предложена геофизическая модельная функция, которая позволяет определять поля скорости ветра в акваториях радиусом около километра. Ошибка восстановленных по радиолокационным данным модуля и направления скорости ветра составила соответственно 1.2 м/с и 30° по сравнению с информацией, полученной анемометром.

Ключевые слова: радиолокационные станции, радиолокационные изображения, удельная эффективная площадь рассеяния, морская поверхность, скорость ветра, натурные измерения, возраст волн, обрушения ветровых волн

Благодарности: исследование выполнено за счет гранта Российского научного фонда № 24-27-20105, https://rscf.ru/project/24-27-20105, и соглашения с Департаментом образования и науки г. Севастополя № 85 от 19.06.2024 г.

Для цитирования: *Кориненко А. Е., Малиновский В. В.* Восстановление полей ветра в прибрежной зоне по радиолокационным данным *X*-диапазона при больших углах наблюдения морской поверхности // Экологическая безопасность прибрежной и шельфовой зон моря. 2025. № 1. С. 26–41. EDN JRCXNU.

Introduction

The most effective means of monitoring the aquatic environment under any meteorological conditions and at any time of day and night are radar systems. Currently, algorithms have been developed that use satellite radar information to determine wind speed and direction, surface wave characteristics, and to study eddies and frontal partitioning (see, for example, [1, 2] and the literature cited in these works). These data processing techniques are based on developed theoretical models of the formation of the radar signal reflected from the sea surface at incidence angles of 15–60° [3].

However, satellite data cannot be used for continuous monitoring of wind speed fields, currents and surface wave characteristics in ports, coastal waters and areas of heavy shipping. Navigation radar stations (RS) installed on offshore platforms, ships or onshore structures are used for real-time and continuous monitoring of the selected area. In order to analyse RS data, methods to recover velocity and direction of surface currents and determining characteristics of surface waves were developed and tested (see, for example, [4–6] and the literature cited in these works).

Wind speed reconstruction from radar images is mainly based on empirical models that establish the relationship between the radar signal intensity and wind speed vector magnitude U. In [7], it was proposed to use a third-order geophysical model function (GMF). At wind speeds of ~ 4 and 22 m/s, the errors in retrieved wind speeds were ~ 0.8 and ~ 0.1 m/s, respectively. To determine the wind speed direction, the radar signal intensity, depending on sea surface observation azimuth φ, is approximated by a harmonic function [8]. The value of the angle at which the maximum radar signal value is observed is taken as wind direction φ_U. To determine U, an empirical model function was proposed in [8], in which the radar signal integrated over all azimuth angles was used. Another way to retrieve wind speed vector from marine navigation radar images is to use neural networks [9].

Unfortunately, many papers describing algorithms for wind field retrieval from coastal or ship RS data do not provide information on the linearity of the characteristics of the radar receiving paths and its calibration dependencies. As a result, it is not possible to convert the signal intensity into normalized radar cross-section (NRCS) σ_0 and make comparisons with data from other sources and theoretical models. The empirical GMFs listed above are not based on physical ideas about the formation of the radio signal reflected from the sea surface at large sensing angles. Various methods of smoothing and filtering of the initial signal are applied, which makes it difficult to use the proposed techniques for other types of radars.

Onshore or shipboard radars operate generally in horizontal polarised transmission/reception mode at sea surface sensing angles of 75–89°. Under such observational conditions, the main contribution to the NRCS formation is made by wave breaking [1, 3, 10–12]. In current models, σ_0 depends on fraction of sea surface q with whitecap coverage. Accordingly, the NRCS changes with wind speed variation should be related to the wind dependency of q. At the same time, q depends on the wave age [13–15], which leads to a change in the level of σ_0 for the same wind but different wave ages.

Taking into account the physical state of the sea surface is particularly important for the retrieval of atmospheric parameters in the coastal waters, where the degree of wave development varies widely depending on the wind direction.

The paper aims to develop a semiempirical model of the wind dependency of the sea surface NRCS in the X-band at horizontal polarization of the signal transmission/reception at large incidence angles over a wide range of wave ages.

Experiment location and equipment

The *in situ* experiment was conducted in August – October 2022–2024 on a stationary oceanographic platform located in Blue Bay near the village of Katsiveli, the Southern Coast of Crimea (Fig. 1, *a*). With its coordinates 44°23′38″ N, 33°59′09″ E, the stationary oceanographic platform is constructed ~ 480 m from the nearest shore point. The depth at the measurement site is about 30 m.

An MRS-1011 (produced by Micran JSC, city of Tomsk) short-range vision radar with high range resolution (Δl = 0.79 m) transmitting and receiving horizontally polarized signal. The radar power is not more than 1 W, the width of the radiation pattern in the horizontal plane ($\Delta\varphi$) is 1°, in the vertical plane – 30°. In this radar, a continuous linearly modulated signal is generated at an operating frequency of 9430 MHz (wavelength λ_r = 3.2 cm) modulated by a periodic sawtooth function with a period of 7 ms. The bandwidth of the sensing signal is 200 MHz relative to the operating frequency. The received reflected signal is subjected to amplification and homodyne processing resulting in a beat signal, the spectrum of which represents the range and radar cross-section σ (RCS) of the target.

The radar was mounted on the oceanographic platform at a height of 15 m above sea level (Fig. 1, *b*, *c*) and was used during the experiment in the circular view mode with an antenna rotation angular velocity of 2.79 rad/s. Due to the radar specific location on the platform, the sea surface viewing sector ranged from 55° to 315° geographic azimuth.

As an example, the inset of Fig. 1, *a* shows a radar image of the sea surface, with clearly visible surface waves. The bright area in the upper left part is due to reflections of the radar signal from the shore. The dark area is the result of shading by the platform elements, in this sector the RS transmitter was not activated.

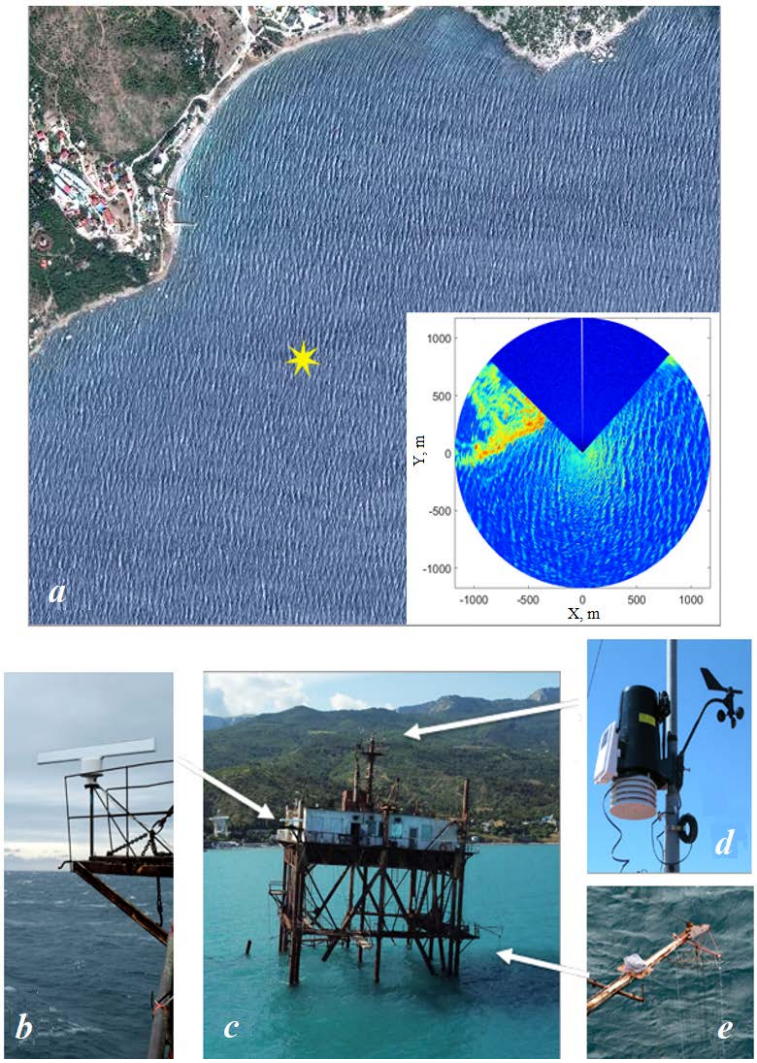

Fig. 1. Study area (*a*) and equipment used. The star indicates the location of the stationary oceanographic platform; the inset shows a radar image of the sea surface; *b* – MRS-1011 radar station; *c* – stationary oceanographic platform, the arrows indicate the location of the equipment shown in *b*, *d*, *e*; *d* – meteorological station; *e* – string wave recorder

Wind speed and direction, atmospheric pressure, air temperature and humidity were recorded using a Davis Vantage Pro2 6152 meteorological station located 23 m above sea level on the mast of the oceanographic platform (Fig. 1, *d*). Water temperature was measured at a depth of 3 m.

Wind speed at 10 m horizon for neutral stratification of the atmospheric boundary layer was calculated using meteorological and surface water temperature data with the COARE 3.0 methodology from [16].

Surface wave characteristics were recorded using a string wave recorder (Fig. 1, *e*). Frequency spectra of sea surface elevations $S(f)$ were obtained as a result of wave data processing. As a rule, during our measurements, in addition to wind waves, ripple waves were also observed. Approach [17] was used to divide the wave frequency spectrum into ripple waves and wind-generated waves. As a result, the values of spectral peak frequency f_p, wave peak frequency f_{pw} and wave age $\alpha = c_{pw}/U$, where c_{pw} is phase velocity of waves at the wave peak frequency, were determined.

The geometric characteristics of wave breaking were determined from video recordings of the sea surface made with a digital video camera. Additional information on the algorithm and calculation of various breaking parameters is given in [18, 19].

Fig. 2 demonstrates the histograms of values U, φ_U and α measured in the experiment. As can be seen from Fig. 2, *a*, wind speed ranged from 2 to 20 m/s, with the majority of observations being made in the U range of 5 to 15 m/s. During the experiments, winds were predominantly easterly (φ_U = 60–120°) and westerly (φ_U = 250°) (Fig. 2, *b*). The wave age distribution shown in Fig. 2, *c* shows that α varied from 0.1 to 3, with ~96 % of the wave age values ranging within 0.1–1.2.

Cases when the sea was dominated by ripples were excluded from further processing. Strong modulations of the radar signal caused by ripples can affect the mean values of σ_0 significantly, but are not studied in the paper.

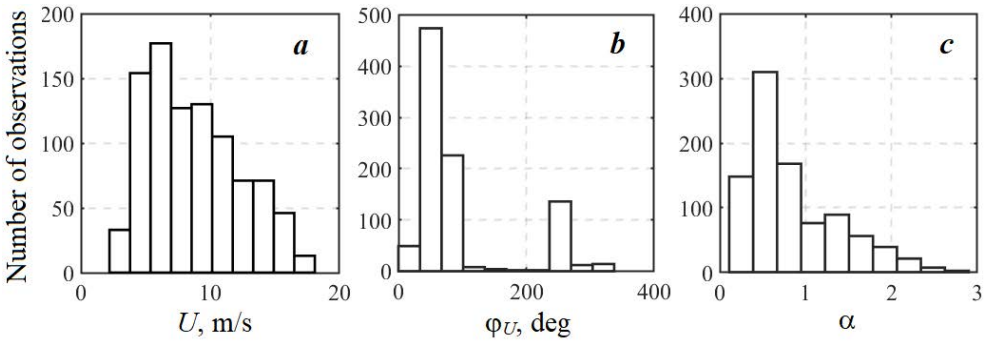

F i g . 2 . Histograms of wind and wave measurement conditions: *a* – wind speed; *b* – wind direction; *c* – wave age

Data preprocessing

A radar similar in its technical characteristics to the RS in [20], but with increased transmitter power, was used during the experiments.

To convert conventional units of the radar signal into absolute values of NRCS σ_0, the RS was calibrated. An inflatable polymer ball (wall thickness ~ 1 mm, diameter D_{Ball} = 67.5 cm) with added aluminum powder was used as a target. To give conductive properties, the ball was additionally coated with paint with the addition of aluminum powder. Given that $\lambda_r << D_{Ball}/2$, the ball RCS is $\sigma_{Ball} = 0.36$ m^2. In calm weather, the target was towed by an inflatable boat up to 1000 m from the platform.

Carrying out calibration works is necessary because the obtained values facilitate data interpretation, since the radar scattering models operate with absolute values of the signal. Note that the calibration constants are different for every device.

As was shown in [20], the receiver characteristics of the RS we use are nonlinear. Accordingly, we should expect that the received signal power from the ball P_R will not be described by the basic radar formula. Fig. 3 shows the dependency of P_R/σ_{Ball} value on the distance to the ball R. Measurement data can be described by the following power function

$$P_R / \sigma_{Ball} = C \cdot R^{-d}, \quad (1)$$

where coefficients $C = 1.1 \cdot 10^{12}$ and $d = 3.4$ are obtained by the least squares method.

The magnitude of the reflected signal scattered by the sea depends on the value of irradiated sea surface area S. To exclude this influence, the signal reflected from the sea surface is described as NRCS $\sigma_0 = \sigma / S$, where $S = 2\Delta l\, R \tan(\Delta\varphi/2)$.

Taking into account the calibration constants, the sea surface NRCS for all points of the radar image was defined as

$$\sigma_0 = C' P R^{2.4},$$

where $C' = 1/[2C\,\Delta l \tan(\Delta\varphi/2)]$; P is power of the received radar signal.

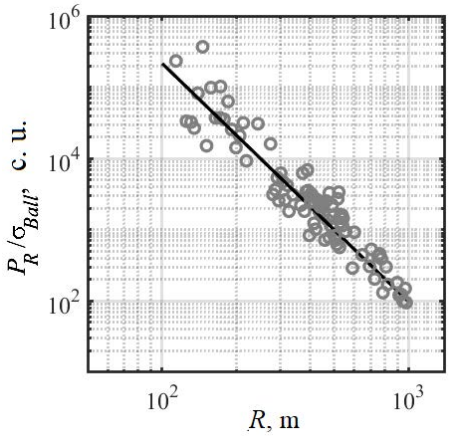

Fig. 3. Dependence of the received signal power normalized to the ball radar cross-section on the distance to the target. The straight line shows approximation by power function (1)

Model of non-Bragg scattering component

A model for the formation of the sea surface radar NRCS is considered in [3]. In general, σ_0 can be represented as the sum of Bragg σ_{0br} and non-Bragg σ_{0nb} scattering components

$$\sigma_0 = \sigma_{0br}(1 - q) + \sigma_{0nb}\, q.$$

According to [3], σ_{0nb} is formed under conditions of quasi-mirror reflections from very rough parts of the breaking zone, then the whitecap RCS is as follows

$$\sigma_{0nb}(\theta, \varphi) = \sigma_{0wb}(1 + M_{wb}\, \overline{\theta}_{wb}\, A_{wb}(\varphi)), \quad (2)$$

$$\sigma_{0nb}(\theta) = (\sec^4(\theta)/s_{wb}^2) \exp(-\tan^2(\theta)/s_{wb}^2) + s_{wb}/s_{wb}^2, \quad (3)$$

where θ is incidence angle from nadir; φ is observation azimuth of the radar station; M_{wb} is modulation transfer function; $\overline{\theta}_{wb}$ – is whitecap average inclination; $A_{wb}(\varphi)$ is coefficient determining the angular distribution of non-Bragg scattering and providing the difference between radar signals in "up-wind" and "down-wind" observations; ε_{wb}^2 is RMS slope of roughness of the breaking zone; ε_{wb} is constant equal to the ratio of the whitecap thickness to its length. At high incidence angles ($\theta > 75°$) [21], the main contribution to the horizontally polarized radar signal is made by σ_{0nb}, and the determining role in expression (3) is played by the second summand, hence, taking into account (2), σ_0 can be written as

$$\sigma_0 = (s_{wb}/s_{wb}^2)(1 + M_{wb}\, \overline{\theta}_{wb}\, A_{wb}(\varphi))\, q, \quad (4)$$

According to expression (4), σ_0 should not depend on the sea surface observation angle. For very large angles ($\theta > 88$–$89°$), the NRCS value can be influenced by the effects associated with shading of sea surface areas by long-wave crests. As follows from formula (4), the change in signal power will be determined by the fraction of the sea surface covered by wave breaking.

Traditionally, q is described by power function $q = B_0 U^n$ (see, e. g., [19, 22–24]). However, the large scatter in the data [13, 14] indicates that wind speed by itself does not explain all of the observed variability of q. In particular, according to [13–15], coefficient B_0 is wave age function $B_0 = f(\alpha)$. As function $f(\alpha)$ can be nonlinear, let us define it as power function $f(\alpha) = \alpha^b$. A general form expression for formula (5), which is an analogue of GMF, follows from the above:

$$\sigma_0(\varphi, \theta) = B(\varphi, \theta)\, \alpha^{b(\varphi, \theta)}\, U^{n(\varphi, \theta)}, \quad (5)$$

where $b(\varphi, \theta)$, $n(\varphi, \theta)$ and $B(\varphi, \theta)$ are constants.

Note that, since our data were obtained under conditions close to neutral stratification of the atmosphere, we will neglect the manifestation of stratification effects on wave breaking.

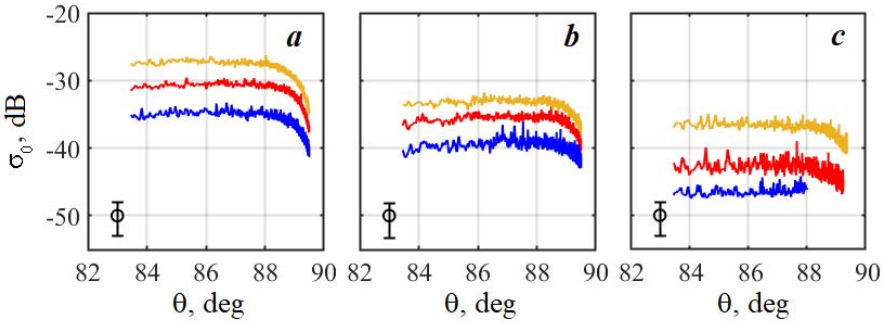

Fig. 4. Normalized radar cross-section (NRCS) of the sea surface s a function of the angle of observation for 'up-wind' (*a*), 'perpendicular to the wind' (*b*) and 'down-wind' (*c*) measurements. The blue line is data averaged over the range $U = 7.0 \pm 1.5$ m/s; the red line is 11.0 ± 1.5 m/s; the orange line is 15.0 ± 1.5 m/s. Confidence intervals are given in the bottom left part of the figure

Analysis of data obtained

Angular dependencies of radar signal

Fig. 4 shows the NRCS dependency on the incidence angle for "up-wind" σ_0^{up}, "perpendicular to the wind" σ_0^{cr} and "down-wind" σ_0^{dw} measurements. The RMS deviation averaged over realisations did not exceed 5 dB. As can be seen from Fig. 4, the sea surface NRCS for incidence angles $83.5 \le \theta \le 88°$ is almost unchanged, while at higher values of θ, the NRCS decreases due to the influence of shading by long-wave crests. In order to construct the GMF to recover the wind speed vector, we will consider the mean value of σ_0 over the range of angles (83.5–88°) and on the descending section of σ_0 for values of θ equal to 88 and 89°. For our observational conditions, this corresponds to a distance of 130–860 m.

Wind dependencies of radar signal

Fig. 5 shows an example of wind dependencies σ_0^{up}, σ_0^{cr}, σ_0^{dw} for the range of angles $83.5 \le \theta \le 88°$, with the colour of symbols corresponding to the wave age colour scale on the right side.

As follows from Fig. 5, power dependency of σ_0 on wind speed is observed. Note that for the same wind speed at the measurement level, the values of σ_0 increase with increasing α, i. e., in the process of wave development. This regularity is characteristic of all selected observation azimuths. With α changing from 0.1 to 1.2, the weakest growth of σ_0 by ~5 times is observed for σ_0^{up}, and the largest NRCS increase by about 30 times is characteristic for σ_0^{cr}. The obtained dependency of σ_0 on wind speed and wave age confirms the appropriateness of describing the sea surface NRCS in form (5).

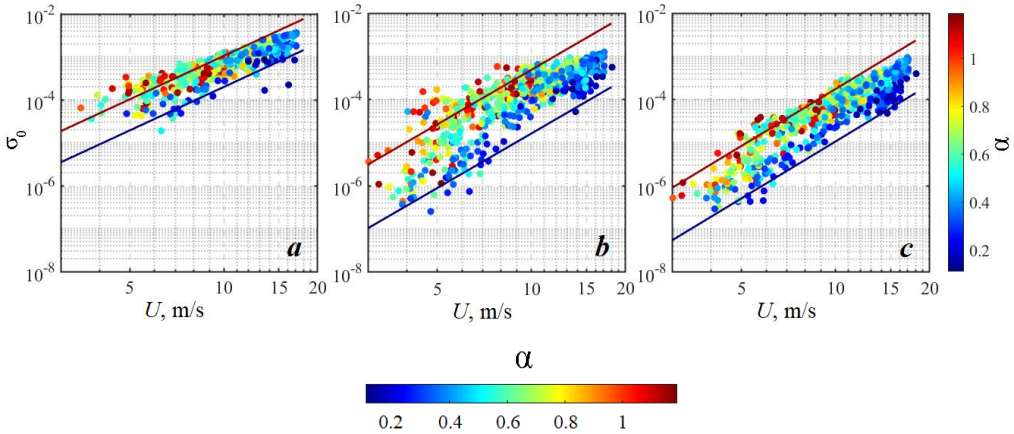

F i g . 5 . NRCS of the sea surface as a function of wind speed during 'up-wind' (*a*), 'perpendicular to the wind' (*b*) and 'down-wind' (*c*) sensing. The solid lines correspond to dependence (5) with coefficients given in the table for α = 0.1 (lower line) and α = 1.2 (upper line)

Coefficients of NRCS wind dependency

θ	φ = 0°			φ = 90°			φ = 180°		
	$10^7 B$	n	b	$10^8 B$	n	b	$10^8 B$	n	b
83.5–88	4.2	3.3	0.7	2.2	4.2	1.4	0.5	4.4	1.1
88.5	2.9	3.3	0.8	6.4	3.6	1.0	4.9	3.1	0.7
89	0.7	3.5	1.0	17.5	2.9	0.9	–	–	–

The values of coefficients B, b, n given in Table for different values of θ and azimuths in the interval $0.1 \le \alpha \le 1.2$ were determined by the least squares method from experimental arrays of simultaneous measurements of wind speed, wave age and $\sigma_0(\varphi, \theta)$. In the "up-wind" direction, the values of corresponding powers are almost the same for specified incidence angles θ. The decrease in B level at observation angles $\theta \ge 88.5°$ can be explained by shading conditions.

The obtained values of n fall within the range of wind coefficient estimates known from [14, 25, 26] for the fraction of the sea surface covered by breaking crests.

The NRCS model considered above at large incidence angles (4) indicates that σ_0 is determined by the value of q. Hence, wind dependency σ_0 should be determined by the dependency of q on U. Note that the first two terms in the right-hand side of expression (4) containing s_{wb}^2, M_{wb}, $\overline{\theta}_{wb}$,, can involve in $\sigma_0 = f(U)$, but we did not determine their values. Let us use the archive data of q and the values of σ_0 and q obtained simultaneously during measurements in the experiment.

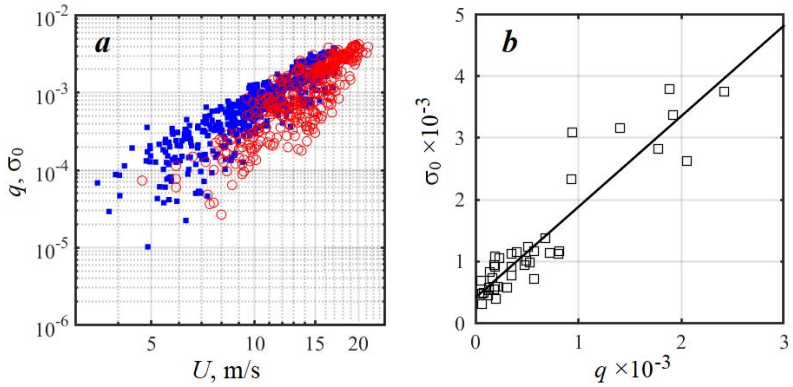

F i g . 6 . Fractions of the whitecap coverage and NRCS: *a* – wind dependencies q and σ_0; (■ – values of σ_0^{up} at $U = 2.2 \div 17.1$ m/s, ○ – values of q at $U = 4.7 \div 21.4$ m/s) *b* – dependency of NRCS on q derived from synchronous measurements

In Fig. 6, *a*, squares represent the values of σ_0^{up} at wind speeds from 2.2 to 17.1 m/s, circles represent the values of q obtained at $U = 4.7$–21.4 m/s. Both wind dependencies almost coincide, but a slight difference is observed at $U < 10$ m/s; in these cases, a stronger decrease in the value of q is observed with decreasing wind. This can be explained by the fact that during moderate and weak winds, small breaking crests that contribute significantly to the value of q are not identified during video processing [27, 28]. At the same time, such breaking is involved in the formation of the NRCS.

It is of interest to compare σ_0 and the fraction of the surface covered by the active phase of breaking. Indeed, according to model (4), simple relation $\sigma_0 \infty q$ should be observed. Fig. 6, *b* demonstrates the dependency of the NRCS on q obtained from our data as a result of synchronous measurements. As can be seen from Fig. 6, *b*, the dependency of the NRCS on q is satisfactorily described by the linear function shown by the solid line $\sigma_0 = 1.47q$. Such a linear dependency confirms model (4) of the NRCS formation at large incidence angles of the radar signal.

Azimuthal dependencies of radar signal

Previous studies [29–31] have shown that for maritime navigation stations operating on a horizontally polarised signal at $\theta > 75°$, the maximum value of the radar signal is observed in the "up-wind" direction. To describe the azimuthal dependency of the signal and to find the wind speed and direction, we approximate our data by a standard dependency in the form of a restricted Fourier series (see, e. g., [32])

$$\sigma(U, \varphi, \theta) = A_0 + A_1 \cos(\varphi - \varphi_w) + A_2 \cos[2(\varphi - \varphi_w)], \qquad (6)$$

where φ_w is direction of azimuthal dependency maximum; A_0, A_1, A_2 are coefficients, which generally depend on U, α, θ and, according to the work [1)], are written as

[1)] Ulaby, F.T., Moore, R.K. and Fung, A.K., 1986. *Microwave Remote Sensing: Active and Passive. Vol. 3*. Dedham, MA, USA: Artech House, 2126 p.

$$A_0 = (\sigma_0^{up} + \sigma_0^{cr} + \sigma_0^{dw})/4, \quad (7)$$

$$A_1 = (\sigma_0^{up} - \sigma_0^{dw})/2, \quad (8)$$

$$A_2 = (\sigma_0^{up} - 2\sigma_0^{cr} + \sigma_0^{dw})/4, \quad (9)$$

In our notations, direction $\varphi = \varphi_w$ corresponds to the "up-wind" measurements, $\varphi = \varphi_w + \pi$ – to the "down-wind" ones. In formulas (7)–(9), σ_0^{up}, σ_0^{cr}, σ_0^{dw} are described by expression (6), with the values of coefficients B, b, n given in Table. Fig. 7 shows the NRCS azimuthal dependencies for easterly and westerly wind directions. The line is for dependency (6) considering expressions (5) and (7)–(9). The unknowns in formula (6) are U_{RL} and φ_w, which were determined by the least squares method (with $U_{RL} = 10$ m/s, $\varphi_w = 80°$ for the line in Fig. 7, *a* and with $U_{RL} = 14$ m/s, $\varphi_w = 250°$ for the line in Fig. 7, *b*). The wave age in the radar measurements was calculated from the wind wave elevation spectra.

At moderate wind speeds (Fig. 7, *a*), azimuthal dependency $\sigma_0(\varphi)$ has one pronounced maximum when measuring "up-wind", with the minimum value observed "down-wind". When the wind speed increases (Fig. 7, *b*), the azimuthal dependency acquires a bimodal character, a second local maximum appears in the "up-wind" direction. The peculiarities of azimuthal dependencies at large sea surface observation angles are discussed in more detail in [20].

Speeds U_{RL} and φ_w were calculated for the whole data array by the least squares method according to formula (6) using *in situ* radar measurements. Fig. 8 shows the comparison of wind speed direction and vector magnitude retrieved from radar data with those retrieved from the anemometer.

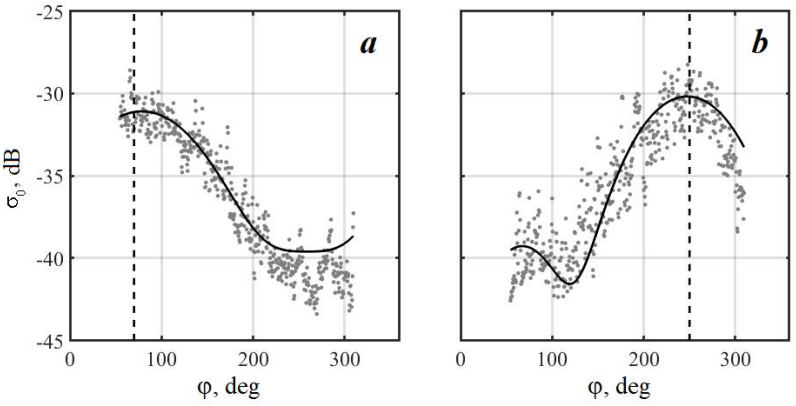

Fig. 7. The sea surface NRCS as an azimuth angle function at $U = 9$ m/s, $\varphi_U = 70°$, $\alpha = 0.8$ (*a*); $U = 15$ m/s, $\varphi_U = 250°$, $\alpha = 0.2$ (*b*). The dashed lines are for wind direction retrieved from the anemometer data

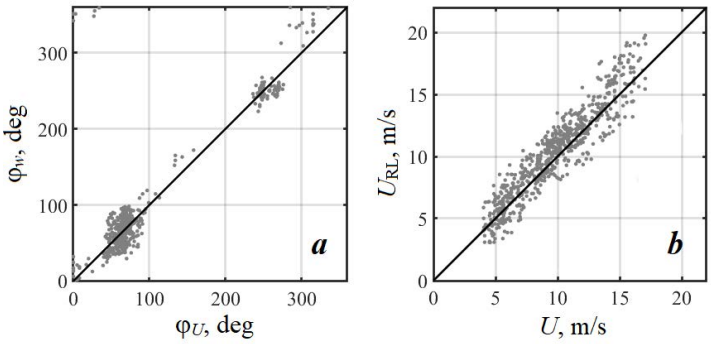

F i g . 8 . Wind speed direction (*a*) and vector magnitude (*b*) retrieved from the anemometer and radar data. The straight line corresponds to equal values of the two quantities

Fig. 8 shows a linear relationship between φ_w and φ_U as well as between U_{RL} and U, with standard deviations between these pairs of values being 30° and 1.2 m/s, respectively.

Conclusions

The semiempirical model of the wind dependency of the sea surface NRCS is proposed, which makes it possible to retrieve the driving wind speed for X-band radar sensing of the sea surface at large incidence angles. Radar, meteorological, waveform data and video recordings of the sea surface obtained during 2022-2024 at a stationary oceanographic platform in Blue Bay, the Southern Coast of Crimea, were used for the analysis. Measurements were carried out at wind speeds from 4 to 17 m/s. The observed wave age varied from 0.1 to 3, with 96% of the values of α being in the interval $0.1 \le \alpha \le 1.2$.

For radar sensing of the sea at large incidence angles, fraction of the sea surface q covered by breaking crests is the main informative parameter that governs NRCS σ_0. Dependency of the fraction of sea surface covered by breaking crests on wind speed and wave age α results in the corresponding dependencies of σ_0 on wind speed vector magnitude U and wave age.

The contribution of wave breaking to the sea surface NRCS was confirmed experimentally. The linear dependency of σ_0 on the fraction of the sea surface covered by breaking was obtained: $\sigma_0 = 1.47q$. Presented wind dependencies σ_0^{up} and q obtained *in situ*, are almost identical. This result confirms experimentally adopted model $\sigma_0(U) \propto q(U)$ and the essential role of wave breaking in the formation of the radar signal scattered by the sea surface at large incidence angles. It is shown that the degree of wave development affects the NRCS level, which increases five times with increasing wave age from 0.1 to 1.2 for the same “up-wind” direction.

The geophysical model function that takes into account wind speed and wave age α was constructed. Using the results obtained within the geophysical model function, wind speed and wind direction can be retrieved from the radar data. The wind speed vector magnitude and direction calculated from σ_0 coincided satisfactorily with the anemometer readings. The RMS errors of retrieved values U_{RL} and φ_w were 1.2 m/s and 30°, respectively.

References

1. Johannessen, J.A., Kudryavtsev, V., Akimov, D., Eldevik, T., Winther, N. and Chapron, B., 2005. On Radar Imaging of Current Features: 2. Mesoscale Eddy and Current Front Detection. *Journal of Geophysical Research*, 110(C7), C07017. https://doi.org/10.1029/2004JC002802ee
2. Kudryavtsev, V.N., Chapron, B., Myasoedov, A.G., Collard, F. and Johannessen, J.A., 2013. On Dual Co-Polarized SAR Measurements of the Ocean Surface. *IEEE Geoscience and Remote Sensing letters*, 10(4), pp. 761–765. https://doi.org/10.1109/LGRS.2012.2222341
3. Kudryavtsev, V., Hauser, D., Caudal, G. and Chapron, B., 2003. A Semiempirical Model of the Normalized Radar Cross-Section of the Sea Surface. 1. Background Model. *Journal of Geophysical Research: Oceans*, 108(C3), 8054. https://doi.org/10.1029/2001JC001003
4. Ivonin, D.V., Telegin, V.A. Bakhanov, V.V. Ermoshkin, A.V. and Azarov, A.I., 2011. Sample Application of a Low-Cost X-Band Monitoring System of Surface Currents at the Black Sea Shore. *Russian Journal of Earth Sciences*, 12(2), pp. 1–8. ES2003. https://doi.org/10.2205/2011ES000507
5. Ermoshkin, A.V. and Kapustin, I.A., 2019. Estimation of the Wind-Driven Wave Spectrum Using a High Spatial Resolution Coherent Radar. *Russian Journal of Earth Sciences*, 19(3), ES1005. https://doi.org/10.2205/2019ES000662
6. Ermoshkin, A.V., Kapustin, L.A., Molkov, A.A. and Bogatov, N.A., 2020. Determination of the Sea Surface Current by a Doppler X-Band Radar. *Fundamental and Applied Hydrophysics*, 13(3), pp. 93–103. https://doi.org/10.7868/S2073667320030089 (in Russian).
7. Vicen-Bueno, R., Horstmann, J., Terril, E., de Paolo, T. and Dannenberg, J., 2013. Real-Time Ocean Wind Vector Retrieval from Marine Radar Image Sequences Acquired at Grazing Angle. *Journal of Atmospheric and Oceanic Technology*, 30(1), pp. 127–139. https://doi.org/10.1175/JTECH-D-12-00027.1
8. Lund, B., Graber, H. C. and Romeiser, R., 2012. Wind Retrieval from Shipborne Nautical X-Band Radar Data. *IEEE Transactions on Geoscience and Remote Sensing*, 50(10), pp. 3800–3811. https://doi.org/10.1109/TGRS.2012.2186457
9. Dankert, H., Horstmann, J. and Rosenthal, W., 2003. Ocean Wind fields retrieved from radar-image sequences. *Journal of Geophysical Research*, 108(C11), 3352. https://doi.org/10.1029/2003JC002056
10. Malinovsky, V.V., 1992. Evaluation of the Relationship between Parameters of the Radar Signal Backscattered by the Sea Surface at Grazing Angles and the Wind Wave Breaking Characteristics. *Soviet Journal of Physical Oceanography*, 3(6), pp. 443–454. https://doi.org/10.1007/BF02197559
11. Hwang, P.A., Sletten, M.A. and Toporkov, J.V., 2008. Breaking Wave Contribution to Low Grazing Angle Radar Backscatter from the Ocean Surface. *Journal of Geophysical Research: Oceans*, 113(C9), C09017. https://doi.org/10.1029/2008JC004752
12. Ermoshkin, A.V., Bakhanov, V.V. and Bogatov, N.A., 2015. Development of an Empirical Model for Radar Backscattering Cross Section of the Ocean Surface at Grazing Angles. *Sovremennye Problemy Distantsionnogo Zondirovaniya Zemli iz Kosmosa*, 12(4), pp. 51–59 (in Russian).

13. Zhao, D. and Toba, Y., 2001. Dependence of Whitecap Coverage on Wind and Wind-Wave Properties. *Journal of Oceanography*, 57, pp. 603–615. https://doi.org/10.1023/A:1021215904955
14. Brumer, S.E., Zappa, C.J. Brooks, I.M., Tamura, H., Brown, S.M., Blomquist, B.W., Fairall, C.W. and Cifuentes-Lorenzen, A., 2017. Whitecap Coverage Dependence on Wind and Wave Statistics as Observed During SO GasEx and HiWinGS. *Journal of Physical Oceanography*, 47(9), pp. 2211–2235. https://doi.org/10.1175/JPO-D-17-0005.1
15. Dulov, V.A., Skiba, E.V. and Kubryakov, A.A., 2023. Landsat-8 Observations of Foam Coverage under Fetch-Limited Wave Development. *Remote Sensing*, 15(9), 2222. https://doi.org/10.3390/rs15092222
16. Fairall, C.W., Bradley, E.F., Hare, J.E., Grachev, A.A. and Edson, J.B., 2003. Bulk Parameterization of Air-Sea Fluxes: Updates and Verification for the COARE Algorithm / C. W. Fairall [et al.] // *Journal of Climate*. 16(4), pp. 571–591. https://doi.org/10.1175/1520-0442(2003)016<0571:BPOASF>2.0.CO;2
17. Hanson, J.L. and Phillips, O.M., 1999. Wind Sea Growth and Dissipation in the Open Ocean. *Journal of Physical Oceanography*, 29(8), pp. 1633–1648. https://doi.org/10.1175/1520-0485(1999)029<1633:WSGADI>2.0.CO;2
18. Mironov, A.S. and Dulov, V.A., 2008. Detection of Wave Breaking Using Sea Surface Video Records. *Measurement Science and Technology*, 19(1), 015405. https://doi.org/10.1088/0957-0233/19/1/015405
19. Korinenko, A.E., Malinovsky, V.V., Kudryavtsev, V.N. and Dulov, V.A., 2020. Statistical Characteristics of Wave Breakings and their Relation with the Wind Waves' Energy Dissipation Based on the Field Measurements. *Physical Oceanography*, 27(5), pp. 472–488. https://doi.org/10.22449/1573-160X-2020-5-472-488
20. Malinovsky, V.V., Korinenko, A.E. and Kudryavtsev, V.N., 2018. Empirical Model of Radar Scattering in the 3-cm Wavelength Range on the Sea at Wide Incidence Angles. *Radiophysics and Quantum Electronics*, 61(2), pp. 98–108. https://doi.org/10.1007/s11141-018-9874-7
21. Kudryavtsev, V., Akimov, D., Johannessen, J. and Chapron, B., 2005. On Radar Imaging of Current Features: 1. Model and Comparison with Observations. *Journal of Geophysical Research*, 110(C7), C07016. https://doi.org/10.1029/2004JC002505
22. Phillips, O.M., 1988. Radar Returns from the Sea Surface – Bragg Scattering and Breaking Waves. *Journal of Physic Oceanography*, 18(8), pp. 1065–1074. https://doi.org/10.1175/1520-0485(1988)018<1065:RRFTSS>2.0.CO;2
23. Monahan, E.C. and Woolf, D.K., 1989. Comments on "Variations of Whitecap Coverage with Wind Stress and Water Temperature". *Journal of Physical Oceanography*, 19(5), pp. 706–709. https://doi.org/10.1175/1520-0485(1989)019<0706:COOWCW>2.0.CO;2
24. Kleiss, J.M. and Melville, W.K., 2010. Observations of Wave Breaking Kinematics in Fetch-Limited Seas. *Journal of Physical Oceanography*, 40(12), pp. 2575–2604. https://doi.org/10.1175/2010JPO4383.1
25. Bortkovskii, R.S. and Novak, V.A., 1993. Statistical Dependencies of Sea State on Water Temperature and Wind-Wave Age. *Journal of Marine Systems*, 4(2–3), pp. 161–169. https://doi.org/10.1016/0924-7963(93)90006-8
26. Anguelova, M.D. and Webster, F., 2006. Whitecap Coverage from Satellite Measurements: A First Step Toward Modeling the Variability of Oceanic Whitecaps. *Journal of Geophysical Research: Oceans*, 111(C3), C03017. https://doi.org/10.1029/2005JC003158
27. Sutherland, P. and Melville, W.K., 2013. Field Measurements and Scaling of Ocean Surface Wave-Breaking Statistics. *Geophysical Research Letters*, 40(12), pp. 3074–3079. https://doi.org/10.1002/grl.50584

28. Korinenko, A.E., Malinovsky, V.V. and Kudryavtsev, V.N., 2018. Experimental Research of Statistical Characteristics of Wind Wave Breaking. *Physical Oceanography*, 25(6), pp. 489–500. https://doi.org/10.22449/1573-160X-2018-6-489-500
29. Trizna, D.B. and Carlson, D.J., 1996. Studies of Dual Polarized Low Grazing Angle Radar Sea Scatter in Nearshore Regions. *IEEE Transactions on Geoscience and Remote Sensing*, 34(3), pp. 747–757. https://doi.org/10.1109/36.499754
30. Hatten, H., Seemann, J., Horstmann, J. and Ziemer, F., 1998. Azimuthal Dependence of the Radar Cross Section and the Spectral Background Noise of a Nautical Radar at Grazing Incidence. In: T. I. Stein, ed., 1998. *Proceedings of IGARSS. Sensing and Managing the Environment. IEEE International Geoscience and Remote Sensing Symposium. Seattle, WA. USA. 6–10 July.* IEEE Publications. Vol. 5, pp. 2490–2492. https://doi.org/10.1109/IGARSS.1998.702255
31. Plant, W.J., Keller, W.C., Hayes, K. and Chatham, G., 2010. Normalized Radar Cross Section of the Sea for Backscatter: 1. Mean Levels. *Journal of Geophysical Research: Oceans*, 115(C9), C09032. https://doi.org/10.1029/2009JC006078
32. Wentz, F.J., Peteherych, S. and Thomas, L.A., 1984. A Model Function for Ocean Radar Cross Section at 14.6 GHz. *Journal of Geophysical Research: Oceans*, 89(C3), pp. 3689–3704. https://doi.org/10.1029/JC089iC03p03689

Submitted 11.07.2024; accepted after review 22.10.2024;
revised 17.12.2024; published 31.03.2025

About the authors:

Aleksandr E. Korinenko, Senior Research Associate, Marine Hydrophysical Institute of RAS (2 Kapitanskaya St., Sevastopol, 299011, Russian Federation), PhD (Phys.-Math.), **Scopus Author ID: 23492523000, ORCID ID: 0000-0001-7452-8703**, *korinenko.alex@mhi-ras.ru*

Vladimir V. Malinovsky, Senior Research Associate, Marine Hydrophysical Institute of RAS (2 Kapitanskaya St., Sevastopol, 299011, Russian Federation), PhD (Phys.-Math.), **ORCID ID: 0000-0002-5799-454X, ResearcherID: F-8709-2014, Scopus Author ID: 23012976200**, *vladimir.malinovsky@mhi-ras.ru*

Contribution of the authors:

Aleksandr E. Korinenko – development of techniques and carrying out the experimental studies, paper materials discussion, analysis and summary of the study results, preparation of the paper text

Vladimir V. Malinovsky – development of experimental study techniques, analysis and summary of the study results, preparation of the paper text

All the authors have read and approved the final manuscript.

ISSN 2413-5577, Ecological Safety of Coastal and Shelf Zones of Sea, 2025, No. 1, pp. 42–50.

Original article

The Danube River Water Discharge According to Satellite Optical Data of the Landsat Series

V. V. Suslin, S. A. Sholar, E. A. Podgibailov*, O. V. Martynov

Marine Hydrophysical Institute of RAS, Sevastopol, Russia
* *e-mail: e.podgibailov@yandex.ru*

Abstract
The paper aims to find the correlation relationship between the land–water area ratio for a fixed area of the Danube Delta and the total river discharge using Landsat series satellite products and SMHI Hypeweb hydrological model. The study period covered 1984–2010. We used a total of 132 satellite images in one band in the near-infrared spectral range with a spatial resolution of 30 m. Two study areas were selected: the delta area with channel and land (44.9–45.4°N, 29.55–29.60°E) and the control area of the mouth seashore (44.9–45.4°N and 29.80–29.85°E). For each of them a histogram was plotted which characterised the reflected light in relative units and their corresponding numbers of pixels. The signal from the first area was found to be in the range of 7000–26,000 r.u., whereas from the second one it was 7000–8000 r.u. This distinction allowed us to separate the delta areas occupied by river water from those of land. For this purpose, we calculated the ratio between the number of pixels corresponding to a value of 7000–8000 r.u. to all pixels in the area. Then we found the correlation between the river discharge from the SMHI Hypeweb hydrological model and the proportion of pixels corresponding to areas occupied by water. The regression $y = 7.78 \cdot 10^{-4} \cdot x^{0.09} - 5.98 \cdot 10^{-4}$ was obtained. The analysis of seasonal variability showed that in the studied delta area, the share of pixels related to water-occupied areas > 0.5 corresponds to the months from March to May, and the minimum values < 0.3 correspond to July–September. All this is consistent with the period of intensity of precipitation and snowmelt in the Danube River basin area. The data from this work may be useful to researchers assessing the impact of this river discharge on the hydrological regime and condition of the Black Sea.

Keywords: remote sensing, Danube River, river discharge, Landsat TM, SMHI Hypeweb, hydrological model, Black Sea

Acknowledgments: The work was carried out under state assignment of MHI RAS FNNN-2024-0012 “Analysis, diagnosis and operational forecast of the state of hydrophysical and hydrochemical fields of marine areas based on mathematical modeling using data from remote and contact measurement methods”.

For citation: Suslin, V.V., Sholar, S.A., Podgibailov, E.A. and Martynov, O.V., 2025. The Danube River Water Discharge According to Satellite Optical Data of the Landsat Series. *Ecological Safety of Coastal and Shelf Zones of Sea*, (1), pp. 42–50.

Расход воды реки Дуная по оптическим спутниковым данным серии *Landsat*

В. В. Суслин, С. А. Шоларь, Е. А. Подгибайлов *, О. В. Мартынов

Морской гидрофизический институт РАН, Севастополь, Россия
* *e-mail: e.podgibailov@yandex.ru*

Аннотация
Цель работы – найти корреляционную связь между соотношением площадей суши и воды для фиксированного района дельты Дуная и суммарным расходом реки, используя спутниковые продукты серии *Landsat* и гидрологическую модель *SMHI Hypeweb.* Период исследования охватывал 1984–2010 гг. Всего было использовано 132 спутниковых снимка в одном спектральном канале в ближнем инфракрасном диапазоне спектра с пространственным разрешением 30 м. Выбрали два района исследования: участок дельты с руслом и сушей (44.9–45.4° с. ш., 29.55–29.60° в. д.), а также контрольный участок устьевого взморья (44.9–45.4° с. ш., 29.80–29.85° в. д.). Для каждого из них строили гистограмму, характеризующую отраженный свет в условных единицах и соответствующие им количества пикселов. Получено, что сигнал, исходящий от первого района, находится в диапазоне 7000–26 000 у. е., а от второго – 7000–8000 у. е. Данное различие позволило отделить участки дельты, занятые речной водой, от суши. Для этого вычисляли отношение между числом пикселов, соответствующих значению 7000–8000 у. е., ко всем пикселам в данном районе. Затем находили корреляцию между расходом реки по гидрологической модели *SMHI Hypeweb* и долей пикселов, соответствующих занятым водой участкам. Получена регрессия $y = 7.78 \cdot 10^{-4} \cdot x^{0.09} - 5.98 \cdot 10^{-4}$. Анализ сезонной изменчивости показал, что в исследуемом участке дельты доле пикселов, соответствующих занятым водой участкам, превышающим 0.5, соответствуют месяцы с марта по май, а минимальные значения (менее 0.3) характерны для июля – сентября. Все это согласуется с периодом интенсивности выпадения осадков и таяния снегов в ареале бассейна р. Дуная. Данные этой работы могут быть полезны исследователям, оценивающим влияние стока указанной реки на гидрологические режим и состояние Черного моря.

Ключевые слова: дистанционные методы исследований, Дунай, расход рек, *Landsat TM*, гидрологическая модель, Черное море

Благодарности: работа выполнена в рамках государственного задания ФИЦ МГИ РАН FNNN-2024-0012 «Анализ, диагноз и оперативный прогноз состояния гидрофизических и гидрохимических полей морских акваторий на основе математического моделирования с использованием данных дистанционных и контактных методов измерений».

Для цитирования: Расход воды реки Дуная по оптическим спутниковым данным серии *Landsat* / В. В. Суслин [и др.] // Экологическая безопасность прибрежной и шельфовой зон моря. 2025. № 1. С. 42–50. EDN GJZXGP.

Introduction

The Black Sea occupies a unique geographical position due to the system of the Bosphorus, Dardanelles and Gibraltar Straits, making it the most isolated water body in the Atlantic Ocean basin. Under such conditions, the water mass coming from the estuaries has a particularly pronounced effect on the dynamics as well as the optical and biochemical characteristics of waters at the mouths of marine areas. For the Black Sea, the Danube River runoff is a decisive factor in physico-chemical processes both in the north-western shelf area and in the whole sea in general [1, 2]. The contribution of the Danube to long-term and seasonal changes in sea level is also significant [3]. Therefore, quantification of the volume of water flowing from the Danube into the Black Sea is highly demanded in different fields of scientific knowledge.

With the development of the Earth surface remote sensing from artificial satellites, new opportunities arise for monitoring the areas of the river mouth interface with a lake or sea [1), 2)].

The problem of studying river discharge from satellite data in the optical spectral range is not new. For example, this problem is addressed in [4–6]. In these works, a two-band approach [5] or an automatic classification system (ISODATA) [4] are used to separate the surface occupied by water and land. Application of the obtained results with synchronous measurements of river discharge at gauging stations made it possible to construct a regression relationship between these parameters, which can be used for monitoring the river discharge based on satellite measurements only.

Altimetric methods [7–9] and estimation with high-resolution data from the Sentinel-2 satellite [10–13] are also known. However, it should be noted that the above methods, despite their advantages, are difficult to use by domestic researchers, as access to satellite products is currently limited. The use of these methods requires consideration of many factors (vegetation cover, water chromaticity, atmosphere aerosol component, spectral indices based on several bands, etc.), which complicates the estimation of river discharge.

The paper aims to find the correlation relationship between the land–water area ratio and the total water discharge of the Danube River from observations of a fixed area of the river delta using medium resolution second level satellite data (i.e. after atmospheric correction) in the near-infrared spectral range, using one band. The article uses materials of the report on the XII All-Russian Conference with international participation “Current Problems in Optics of Natural Waters (ONW’2023)” [14].

---

1) Scott, J.W., Moore, L., Harris, W.M. and Reed, M.D., 2003. *Using the Landsat Enhanced Thematic Mapper Tasseled Cap Transformation to Extract Shoreline*. U.S. Geological Survey Open File Report OF 03-272. 14 p. https://doi.org/10.3133/ofr2003272

2) NASA. *The Thematic Mapper*. 2025. [online] Available at: https://landsat.gsfc.nasa.gov/thematic-mapper/ [Accessed: 11 February 2025].

Materials and methods

Reanalysis data obtained from the SMHI Hypeweb website [3)] were used as input data of the discharge at the Danube River mouth. The source provides information on daily water discharge (sector 9600704) from 1 January 1981 to 31 December 2010 (Fig. 1).

Landsat series satellite products (a joint project of the US Geological Survey and NASA) were obtained from the Landsat Missions website [4)]. For the study, cloud-free images of the second level, i. e. after atmospheric correction, were selected from the entire available image array in band 5, wavelength range 1.55–1.75 μm with a spatial resolution of 30 m. This satellite product characterises the reflection coefficient of natural sunlight (in r. u.) of the study area of the Earth surface, taking into account atmospheric influence and observation geometry. For the water surface, the reflection coefficient values themselves and its variability associated with the observation geometry are minimal, as when selecting scenes, we excluded data with sea surface glare. The choice of band was stipulated by its lower sensitivity to errors associated with aerosol in the atmosphere and high content of mineral suspension in river waters, which determined a better separation of land and water surface.

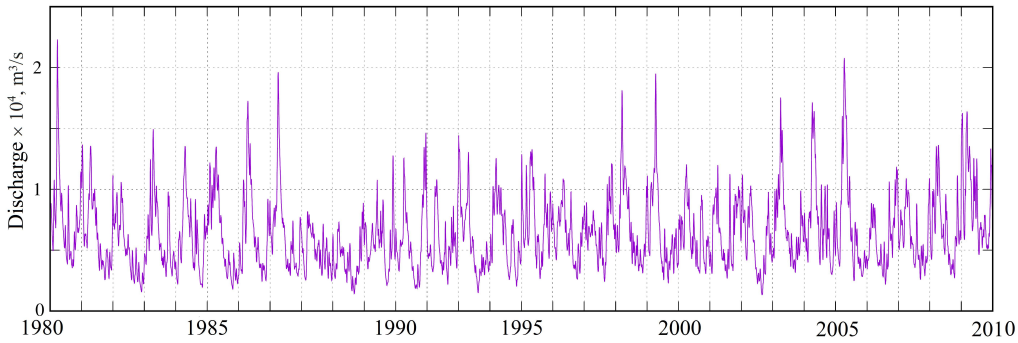

F i g . 1 . Water discharge at the Danube River mouth (sector 9600704) according to reanalysis data from the SMHI Hypeweb website

[3)] SMHI. *Europe Time Series*. 2025. [online] Available at: https://hypeweb.smhi.se/explore-water/historical-data/europe-time-series/ [Accessed: 11 February 2025].

[4)] U.S. Geological Survey. *Landsat Missions*. 2025. [online] Available at: https://www.usgs.gov/landsat-missions [Accessed: 11 February 2025].

A total of 132 images were selected for 1984–2010:

January	3	July	22
February	5	August	19
March	8	September	11
April	9	October	11
May	14	November	5
June	18	December	7

As would be anticipated, the largest number of suitable scenes is observed in the warm period of the year, a phenomenon primarily attributable to the frequency of cloud coverage throughout the year. The selected images are distributed uniformly over the years in the time interval under consideration, with an average of five months of the year being covered.

The study area (fixed delta area) coordinates are 44.9–45.4°N and 29.55–29.60°E (Fig. 2, *a*). In addition, a control area of the mouth seashore with coordinates 44.9–45.4°N and 29.80–29.85°E, located close to the study area, was selected (Fig. 2, *b*).

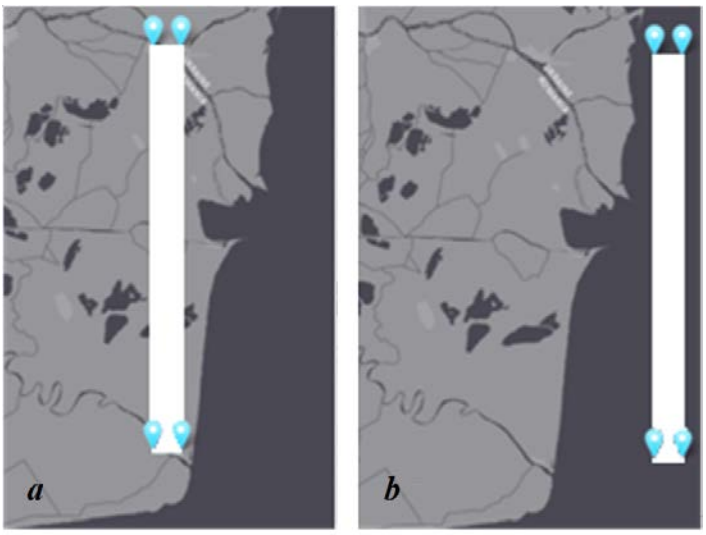

Fig. 2. Study areas: *a* – the fixed section of the delta; *b* – the control area of the mouth seashore (adopted from: https://earthexplorer.usgs.gov/)

For Band 5, histograms (Fig. 3) were plotted for the two selected areas (Fig. 2). The control area of the mouth seashore (Fig. 3, *b*) exhibits variability in signal amplitude from the water surface, ranging from 7000 to 8000 r. u. Conversely, the entire range of variability for the fixed delta area (Fig. 3, *a*) extends from 7000 to 26,000 r.u. Fig. 3 demonstrates the obvious fact that the signal from the water surface (Fig. 2, *b*) is significantly weaker than that from land (Fig. 2, *a*) for the near-infrared range.

Thus, the share of water-occupied surface at the fixed delta area in Fig. 2, *a* (*weight water*) was found as the ratio of the number of pixels in the histogram from the range of 7000–8000 r. u. to all pixels in the area. The relationship between the discharge of the Danube River and the *weight water* was determined by the corresponding date of the survey, i. e. the same day. Since the cross-section of the channel (effluents) varies with depth, there must be a relationship between the width of the channel (effluents) and the water discharge. At the same time, the width of the channel (effluents) is obviously related to the area covered by water observed on the satellite scene.

Results and discussion

Fig. 4 shows the result of the relationship between the proportion of pixels (*weight water*) occupied by water at a fixed delta site and the Danube River discharge for 1984–2010. The correlation coefficient is 0.78 and the total number of points is 132.

The choice of individual effluents in the Danube River delta as a fixed delta area has little effect on the nature of the obtained relationship (Fig. 4). A similar observation can be made regarding the increase in the fixed area within the delta.

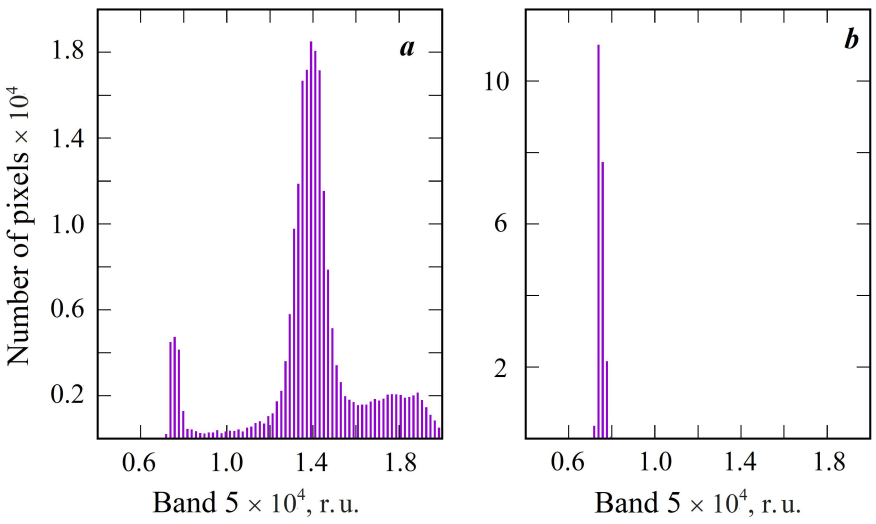

Fig. 3. An example of count in Band 5 (1.55–1.75 μm) signal histograms for the fixed delta area (*a*) and the control area of the mouth sea-shore (*b*) for 5 September 2009

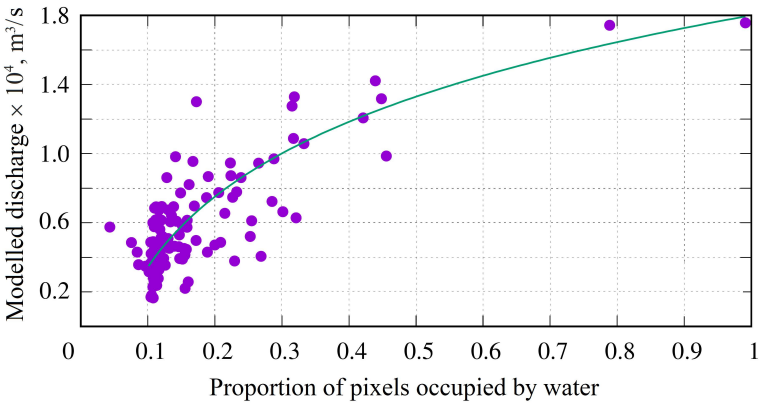

Fig. 4. Relationship between the proportion of pixels (*weight water*) occupied by water for the fixed delta area and the Danube River discharge for 1984–2010: the dots denote separate scenes and the line is the general regression relationship: $y = 7.78 \cdot 10^{-4} \cdot x^{0.09} - 5.98 \cdot 10^{-4}$

The nature of the obtained functional relationship can be qualitatively explained within the framework of a simple hypothesis, for which it is sufficient to consider two trivial cases of river channel cross-sections: rectangular and triangular. In the first case, the channel width is fixed; hence, a change in discharge will not affect the increase in channel width or surface area occupied by water, i.e. it is a period of low discharge. In the second case, the relationship will be a quadratic function of channel width, and all other variants with less steep channel cross-sections will approach the relationship obtained.

The seasonal variability analysis shows that *weight water* over 0.5 corresponds to the months from March to May, whereas the minimum values of *weight water* under 0.3 correspond to July–September. All this is consistent with the period of intensity of precipitation and snowmelt in the Danube River water intake area [5)].

Conclusions

To solve the problem of determining the Danube River discharge using Landsat series satellite products, a simple one-band method was proposed, which is characterised by its accessibility to a wide range of users. The possibility of dividing the river delta area into land- and water-occupied zones based on their signal in the near-infrared spectral range is shown. It was found that the water surface corresponded to the range of 7000–8000 r.u. and the land to 7000–26,000 r.u.

[5)] Ivanov, V.A. and Minkovskaya, R.Ya., 2008. [*Sea Estuaries of Rivers of Ukraine and Estuarine Processes*]. Sevastopol: ECOSI-Gidrofizika, 448 p. (in Russian).

By calculating the ratio of the number of pixels corresponding to water-occupied areas to all pixels of the selected delta area and relating this share to the river discharge from the hydrological model reanalysis data for the same date, we obtained regression relationship $y = 7.78 \cdot 10^{-4} \cdot x^{0.09} - 5.98 \cdot 10^{-4}$. The above relationship can be applied to calculate the inflow of the Danube river water into the Black Sea. It was found that water–land pixel ratio exceeding 0.5 was typical for spring months and less than 0.3 corresponded to summer – early autumn, which coincides with the period of precipitation intensity and snowmelt in the Danube River basin.

References

1. Tsyganova, M.V., Lemeshko, E.M. and Ryabtsev, Yu.N., 2023. Influence of Upwelling on River Plume Development in the Coastal Zone of the North-Western Black Sea Shelf Based on Numerical Modelling. *Ecological Safety of Coastal and Shelf Zones of Sea*, (1), pp. 20–30.
2. Kondratev, S.I., 2019. Three Typical Hydrological-Hydrochemical Situations near the Danube River Mouth Based on the Marine Hydrophysical Institute Research Expeditions in 1997–2013. *Physical Oceanography*, 26(4), pp. 326–340. https://doi.org/10.22449/1573-160X-2019-4-326-340
3. Goryachkin, Yu.N. and Ivanov, V.A., 2006. [*Black Sea Level: Past, Present and Future*]. Sevastopol: MHI NAS of Ukraine, 210 p. (in Russian).
4. Terekhov, A.G., Dolgikh, S.A., Pak, I.T. and Makarenko, N.G., 2015. [Satellite-Based Diagnostics of Water Discharge in Snow-Ice Fed Rivers Using the Kash River as an Example (PRC)]. In: IKI, 2015. [*Proceedings of the 13th All-Russian Open Conference "Current Problems of Remote Sensing of Earth from Space"*]. Moscow: IKI RAS, p. 140 (in Russian).
5. Mukhamedjanov, I.D., Konstantinova, A.M., Loupian, E.A. and Umirzakov, G.U., 2022. Evaluation of Satellite Monitoring Capabilities of Stream Runoff Based on the Amu Darya River State Analysis. *Sovremennye Problemy Distantsionnogo Zondirovaniya Zemli iz Kosmosa*, 19(1), pp. 87–103. https://doi.org/10.21046/2070-7401-2022-19-1-87-103 (in Russian).
6. Gleason, C.J. and Durand, M.T., 2020. Remote Sensing of River Discharge: A Review and a Framing for the Discipline. *Remote Sensing*, 12(7), 1107. https://doi.org/10.3390/rs12071107
7. Bjerklie, D.M., Birkett, C.M., Jones, J.W., Carabajal, C., Rover, J.A., Fulton, J.W. and Garambois, P.-A., 2018. Satellite Remote Sensing Estimation of River Discharge: Application to the Yukon River Alaska. *Journal of Hydrology*, 561, pp. 1000–1018. https://doi.org/10.1016/j.jhydrol.2018.04.005
8. Bjerklie, D.M., Dingman, S.L., Vorosmarty, C.J., Bolster, C.H. and Congalton, R.G., 2003. Evaluating the Potential for Measuring River Discharge from Space. *Journal of Hydrology*, 278(1–4), pp. 17–38. https://doi.org/10.1016/S0022-1694(03)00129-X
9. Sichangi, A.W., Wang, L., Yang, K., Chen, D., Wang, Z., Li, X., Zhou, J., Liu, W. and Kuria, D., 2016. Estimating Continental River Basin Discharges Using Multiple Remote Sensing Datasets. *Remote Sensing of Environment*, 179, pp. 36–53. https://doi.org/10.1016/j.rse.2016.03.019
10. Filippucci, P., Brocca, L., Bonafoni, S., Saltalippi, C., Wagner, W. and Tarpanelli, A., 2022. Sentinel-2 High-Resolution Data for River Discharge Monitoring. *Remote Sensing of Environment*, 281, 113255. https://doi.org/10.1016/j.rse.2022.113255

11. Mukhamediev, R.I., Terekhov, A., Sagatdinova, G., Amirgaliyev, Y., Gopejenko, V., Abayev, N., Kuchin, Y., Popova, Y. and Symagulov, A., 2023. Estimation of the Water Level in the Ili River from Sentinel-2 Optical Data Using Ensemble Machine Learning. *Remote Sensing*, 15(23), 5544. https://doi.org/10.3390/rs15235544
12. Mukhamedjanov, I.D., Konstantinova, A.M. and Loupian, E.A., 2020. The Use of Satellite Data for Monitoring Rivers in the Amu Darya Basin. *Regional Problems of Earth Remote Sensing*, 223, 03008. https://doi.org/10.1051/e3sconf/202022303008
13. Terekhov, A.G., Abayev, N.N., Sagatdinova, G.N., Mukhamediev, R.I. and Amirgaliyev, E.N., 2023. Satellite Estimation of River Water Level from Shoal Monitoring Data: The Case of the Transboundary Ili River (Central Asia). *Sovremennye Problemy Distantsionnogo Zondirovaniya Zemli iz Kosmosa*, 20(4), pp. 227–238. https://doi.org/10.21046/2070-7401-2023-20-4-227-238 (in Russian).
14. Suslin, V.V., Podgibailov, E.A., Martynov, O.V. and Sholar, S.A., 2023. Water Discharge of the Danube River According to Medium-Resolution Optical Satellite Data. In: IO RAS, 2023. *Proceedings of the XII All-Russian Conference with International Participation "Current Problems in Optics of Natural Waters". 25–27 October 2023, Saint Petersburg. Vol. 13*. Moscow: Shirshov Institute Publishing House, pp. 240–245 (in Russian).

Submitted 08.07.2024; accepted after review 30.09.2024;
revised 17.12.2024; published 31.03.2025

About the authors:

Vyacheslav V. Suslin, Head of Department of the Oceanic Processes Dynamics, Leading Research Associate, Marine Hydrophysical Institute of RAS (2 Kapitanskaya Str., 299011, Sevastopol, Russia), PhD (Phys.-Math.), **ORCID ID: 0000-0002-8627-7603, Scopus Author ID: 6603566261, ResearcherID: B-4994-2017**, *slava.suslin@mhi-ras.ru*

Stanislav A. Sholar, Research Associate, Marine Hydrophysical Institute of RAS (2 Kapitanskaya Str., 299011, Sevastopol, Russia), PhD (Tech.), **ORCID ID: 0000-0002-7242-3403, Scopus Author ID: 57189886286, ResearcherID: GSD-9744-2022**, *sa.sholar@mail.ru*

Evgeny A. Podgibailov, Leading Engineer, Marine Hydrophysical Institute of RAS (2 Kapitanskaya Str., 299011, Sevastopol, Russia), **ORCID ID: 0009-0002-2570-1367, Scopus Author ID: 58687010100, ResearcherID: KHZ-5622-2024,** *e.podgibailov@yandex.ru*

Oleg V. Martynov, Senior Research Associate, Marine Hydrophysical Institute of RAS (2 Kapitanskaya Str., 299011, Sevastopol, Russia), PhD (Tech.), **Scopus Author ID: 57201603369**, *oleg.martynov.49@mail.ru*

Contribution of the authors:

Vyacheslav V. Suslin – problem statement, concept development, results analysis, manuscript writing

Stanislav A. Sholar – graphical material construction, literature review on the study problem, discussion of results, formulation of conclusions

Evgeny A. Podgibailov – collection of study materials, primary processing and sorting of data, discussion of the results, article execution

Oleg V. Martynov – literature review on the study problem, discussion of the results, article execution

All the authors have read and approved the final manuscript.

ISSN 2413-5577, Ecological Safety of Coastal and Shelf Zones of Sea, 2025, No. 1, pp. 51–71.

Original paper

Transformation of the Western Branch of the Bakalskaya Spit (Northwestern Crimea) as a Result of the Storm on 26–27 November 2023

V. V. Krylenko [1] *, Yu. N. Goryachkin [2], M. V. Krylenko [1], B. V. Divinsky [1]

[1] *Shirshov Institute of Oceanology of RAS, Moscow, Russia*

[2] *Marine Hydrophysical Institute of RAS, Sevastopol, Russia*

* *e-mail: krylenko.slava@gmail.com*

Abstract

Accumulative marine coastal forms of the Black Sea are exposed to a number of natural threats, including sea level rise and increased wave action. Monitoring of accumulative forms dynamics in order to timely identify adverse trends in their development is a necessary component for coastal zone management and the development of coastal protection measures. The aim of the work is to determine the qualitative and quantitative characteristics of the transformation of the western branch of the largest accumulative form in the northwestern coast of Crimea – the Bakalskaya Spit – as a result of the storm on 26–27 November 2023. We used cartographic, literary and archival sources as well as remote sensing data, materials of long-term monitoring observations and results of mathematical modeling. In terms of wave parameters and overall power, the 26–27 November 2023 storm was extremely strong but not unique, and in terms of power and other wave parameters it is comparable to the 11 November 2007 storm. It was found that during the extreme storm, the accumulative body shifted to the east. The magnitude of the displacement varies significantly along the length of the spit and exceeds the magnitude of the main shore retreat. The position of zones with different magnitudes of the coastal bar displacement or formation of washouts does not coincide with that in previous storms. Differences in the character and scale of the accumulation body transformation are determined by local in terms of time and space conditions, primarily by the relief of the underwater slope and beach at the time of storm formation. Monitoring of the accumulative body dynamics following the storm recorded self-restoring processes confirming that the lithodynamic system had not been not brought out of the dynamic equilibrium.

Keywords: Black Sea, Crimean Peninsula, Bakalskaya Spit, extreme storm, relief, coastline

Acknowledgments: The work was carried out under state assignment of IO RAS no. FMWE-2024-0027 and that of MHI RAS no. FNNN-2024-0016.

For citation: Krylenko, V.V., Goryachkin, Yu.N., Krylenko, M.V. and Divinsky, B.V., 2025. Transformation of the Western Branch of the Bakalskaya Spit (Northwestern Crimea) as a Result of the Storm on 26–27 November 2023. *Ecological Safety of Coastal and Shelf Zones of Sea*, (1), pp. 51–71.

Трансформация западной ветви Бакальской косы (Северо-Западный Крым) в результате шторма 26–27 ноября 2023 года

В. В. Крыленко [1] *, Ю. Н. Горячкин [2], М. В. Крыленко [1], Б. В. Дивинский [1]

[1] *Институт океанологии им. П. П. Ширшова РАН, Москва, Россия*

[2] *Морской гидрофизический институт РАН, Севастополь, Россия*

* *e-mail: krylenko.slava@gmail.com*

Аннотация

Аккумулятивные морские береговые формы Черного моря подвержены ряду природных угроз, в числе которых подъем уровня моря и усиление волнового воздействия. Мониторинг динамики аккумулятивных форм для своевременного выявления неблагоприятных тенденций их развития является необходимой составляющей для управления береговой зоной и разработки мер по защите берегов. Цель работы – определение качественных и количественных характеристик трансформации западной ветви крупнейшей аккумулятивной формы северо-западного побережья Крыма – Бакальской косы – в результате шторма 26–27 ноября 2023 г. Использованы картографические, литературные и архивные источники, данные дистанционного зондирования, материалы многолетних мониторинговых наблюдений, результаты математического моделирования. По волновым параметрам и общей мощности шторм 26–27 ноября 2023 г. является чрезвычайно сильным, но не уникальным, а по мощности и другим параметрам волнения сравним со штормом 11 ноября 2007 г. Установлено, что в ходе шторма произошло смещение аккумулятивного тела на восток. Величина смещения существенно различается на протяженности косы и превышает величину отступания коренного берега. Положение зон с разными величинами смещения берегового вала или образованием промоин не совпадает с положением таких зон в прошлые штормы. Различия в характере и масштабе трансформации аккумулятивного тела определяются локальными во времени и пространстве условиями, прежде всего рельефом подводного склона и пляжа на момент формирования шторма. Мониторинг динамики аккумулятивного тела после шторма зафиксировал процессы самовосстановления, подтверждающие, что литодинамическая система не была выведена из состояния динамического равновесия.

Ключевые слова: Черное море, полуостров Крым, Бакальская коса, экстремальный шторм, рельеф, береговая линия

Благодарности: работа выполнена в рамках государственных заданий ИО РАН FMWE-2024-0027 и ФИЦ МГИ РАН FNNN-2024-0016.

Для цитирования: Трансформация западной ветви Бакальской косы (Северо-Западный Крым) в результате шторма 26–27 ноября 2023 года / В. В. Крыленко [и др.] // Экологическая безопасность прибрежной и шельфовой зон моря. 2025. № 1. С. 51–71. EDN NJYEOA.

Introduction

The Bakalskaya Spit is located in the Karkinitsky Gulf of the Black Sea on the northwestern coast of the Crimean Peninsula. The principal difference between the Bakalskaya Spit and other large accumulative forms of the Black Sea is its location in the depth of the Karkinitsky Gulf, where the action of a number of natural factors is weakened and of some others is intensified. It is a unique natural object determining the hydrodynamic regime of the Karkinitsky Gulf and, at the same time, exposed to hazardous natural phenomena. Transformation of the accumulative body, on the one hand, is a consequence of certain natural impacts (e. g. storms or surges) and, on the other hand, is caused by changes in lithodynamic, hydrodynamic or hydrochemical processes in the bay water area. It is important that the lithodynamic system of the Bakalskaya Spit is little changed anthropogenically, which allows studying the natural transformation of large marine coastal accumulative forms under conditions of sea level rise and increased storm activity [1, 2].

Specialists of Marine Hydrophysical Institute and Southern Branch of Shirshov Institute of Oceanology have been monitoring the Bakalskaya Spit. The scientific material obtained during the expeditions as well as by remote sensing and mathematical modeling methods is reflected in works [3–7]. In the Black Sea, an increasing tendency to frequency and intensity of storm waves was noted [8–11]. Storms, especially extreme ones, lead to the transformation of coastal accumulative forms [12, 13] and in some cases to their degradation [14]. Meanwhile, the impact of extreme storms on accumulative forms is most often considered theoretically [15–17].

In November 2023, the Black Sea was exposed to a series of strong Mediterranean cyclones. Winds of up to 40 m/s were observed over much of the water area [18].

On 26–27 November 2023, a storm surge was formed, the parameters of which reached or exceeded the level of previously observed storms in the region. This allows classifying this storm as an extreme natural phenomenon [19]. As the scientific observations on the transformation of marine coastal accumulative forms of the Black Sea during extreme storms are limited, it seems relevant to consider the impact of the storm on the Bakalskaya Spit. In [20], the impact of this storm on another accumulative form, the Lake Bogaily barrier beach, was considered. It was shown that as a result of the storm, the structure of relief and vegetation cover within the barrier beach that had existed for several decades was completely transformed. The Bogaily barrier beach has undergone a much greater transformation than in the preceding period of 40 years.

It should be noted that the Bakalskaya Spit and the adjacent water area have the status of a landscape and recreational park of regional significance. Nevertheless, sketch projects for the development of a large recreational zone have already been developed by order of local authorities. Unfortunately, these projects ignore

completely natural processes taking place on the coast, including dangerous ones. It is expected that the comparison of new data with the results of previous studies will make it possible to assess the changes that occurred during a single storm in comparison with the previous long-term dynamics.

The work aims to determine the qualitative and quantitative characteristics of the transformation of the Bakalskaya Spit western branch as a result of the extreme storm on 26–27 November 2023.

Materials and methods of study

Satellite images of different years from open sources (Google Earth, Yandex, Bing, etc.) were used to analyse the coastal relief dynamics. Data from the European Space Agency Sentinel-2 spacecraft imagery were used to provide a rapid assessment of the changes caused by the storm on 26–27 November 2023 [1)]. To achieve accurate spatial reference, geometric correction of satellite data was carried out [20]. The sea and lake (lagoon) edge line, coastal bar and cliff's edge were digitised from the images. As a spatial reference of the obtained results, we used a system of virtual reference profiles (RP) drawn through points located at a distance of 200 m from each other. As a result of this work, information on the dynamics of the water's edge and other morphological elements in different time periods was obtained.

The detailed study of the relief and its dynamics required the creation of digital elevation models (DEM). Aerial photographs from unmanned aerial vehicles (UAV) were used [21, 22]. Using the photogrammetric processing technology implemented in Agisoft Metashape software, orthophotos with 0.1 m resolution and DEMs with grid spacing of 0.15 × 0.15 m were constructed.

In addition to remote sensing materials, data from granulometric analysis of beach and bottom sediment samples, morphometric characteristics, archival materials and geobotanical descriptions obtained during expeditions were used.

Calculations of climatic characteristics of wind waves in the Black Sea were carried out using modern spectral wave model MIKE 21 SW [2)]. Full description of the model as well as issues of its verification and adjustment are outlined in [23]. Based on the results of calculations, the array of spatial fields of surface wave parameters with a discreteness of 1 h was formed for the entire sea area for the period from January 1979 to December 2023.

[1)] European Space Agency. *Sentinel-2*. 2023. [online] Available at: https://sentinel.esa.int/web/sentinel/technical-guides/sentinel-2-msi/level-1c/product-formatting [Accessed: 12 December 2023].

[2)] DHI, 2007. *MIKE 21/3 Coupled Model FM: Step-by-Step Training Guide: Coastal Application*. Hørsholm, Denmark: DHI, 190 p.

General characteristics of the Bakalskaya Spit

Morphologically, the Bakalskaya Spit (Fig. 1) is a free double accumulative form up to 8 km long [24]. Both branches are rooted adjacent to active cliffs developed in the Pliocene and Quaternary clay strata. At the junction point of the western branch, the main shore changes its direction sharply from northeastern to eastern. The spit western branch extends almost straight from the point where it is adjacent to the main shore. During the first 4 km, the western branch forms a narrow (60–100 m) barrier beach separating the lagoon (Lake Bakalskoe) from the sea.

The underwater slope in the vicinity of the Bakalskaya Spit is asymmetric, reflecting the development of the spit. The underwater slope to the west of the spit is a shallow water plain descending westwards, with a sharp drop in depth to 7 m on the eastern side close to the shore, followed by a flat gulf bottom. The coastal bar and sediments up to a depth of 2–6 m consist of shell sand with a large admixture of oolites, gravel and pebbles. A layer of grey lake silt emerges on the seabed at depths of up to 2 m against the Lake Bakalskoe barrier beach front.

The geographical position determines the specificity of the hydrodynamic regime of the water area adjacent to the Bakalskaya Spit. The periods with the predominant influence of either waves or currents alternate in the development of

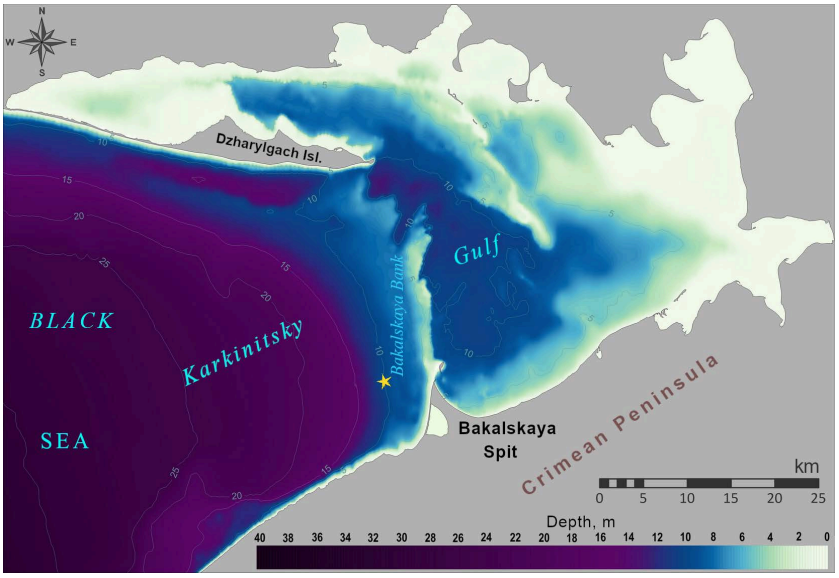

Fig. 1. Schematic map of the Karkinitsky Gulf in the Black Sea (data on underwater topography are given using SonarChart™ materials) (available at https://webapp.navionics.com). The star denotes the point for which the main wave parameters were calculated

the accumulative form. The recurrence and velocities of currents from the open sea to the Karkinitsky Gulf and back are comparable, while the wave regimes for the western and eastern sides of the spit are different [25–28]. Northerly and westerly winds are prevailing but the acceleration length is not the same for them. Westerly winds generate a large long open sea wave, while northerly winds generate a low short wave. In terms of power and duration of action, westerly and southwesterly winds exceed considerably easterly and northeasterly winds: average power values to the west of the spit are about 1 kW/m and to the east – 0.5 kW/m [25]. Episodically, storm waves can develop, which are several times more powerful than average storms. For the spit western branch, the most severe storms were observed in 1981 and 1992, north-northwesterly; in 2007, west-northwesterly; in 1981, 2000, 2017, west-southwesterly; and in 1981, 2008, south-southwesterly. The 2007 storm was the most powerful – 60 kW/m. Such extreme events determine the lithodynamic appearance of the spit in many respects. The characteristic trend components of climatic variability of wind waves in the area of the Bakalskaya Spit since 1979 are as follows:

– decrease in the recurrence of west-southwesterly storms;

– significant decrease in the average wave height during north-northwesterly and south-southwesterly storms;

– increase in wave height during west-northwesterly and north-northeasterly storms.

The wave regime determines the cardinal difference in the relief structure and dynamics of the western and eastern branches of the spit. In the multi-year regime, the dominant role of the eastward-directed wave can be observed. The accumulative body of the Bakalskaya Spit (including the underwater part – the Bakalskaya Bank) shifted eastward during its development, which is reflected in the transverse profile of the spit (Fig. 1): the western slope is gentle, while the eastern slope is steep [29]. For the above-water part of the spit, this process is manifested by washout of its western branch and accumulation on the eastern shore. The sediment budget depends on the products of coastal abrasion and shell directly from the underwater slope. Although the main volume of sediments enters the lithodynamic system from the west, the western branch shifts eastwards (the shore retreats) in the form of a coastal bar 1.2–1.6 m high and 20–50 m wide. In waves with a significant longshore component, the movement of sediment here occurs in a distal direction; in cross-shore waves, the previous sediments are washed out, transporting material to the inner part of the spit. The eastern branch advances into the sea area (accumulation is observed) as new generations of coastal bars 0.5–1.2 m high and 5–10 m wide are formed.

Thus, the current development of the Bakalskaya Spit is determined by changes in the number, direction and intensity of storms, fluctuations in the volume of sediment input and anthropogenic sediment extraction [1, 7, 24].

Structure of the western branch

The relief of the above-water part of the western branch of the Bakalskaya Spit is based on a full profile sand-shell beach (Fig. 2). Within the western branch, the following main zones can be distinguished, traced in one form or another along almost the entire length of the spit:

1. Active beach zone. It is characterised by the most variable relief, exposed to the action of waves throughout most of its development. The width is rarely more than 10 m (Figs. 2, 3) and the slope towards the sea is characteristic. Within the beach, a storm bank (less often several) is usually formed, and sometimes culp formation is observed. When the longshore currents intensify and are accompanied by material export, a beach scarp is formed (Fig. 3, *c*). Dense matting of algal remnants is occasionally formed at the root part of the spit along the edge (Fig. 3, *a*). As the shore retreats near the water's edge, sediments of the inner part of the spit are exposed, i.e. bars (shell, sand, pebbles, often lithified) or inter-bar depressions (silt with a mixture of shell, with a framework of vegetation remnants). The latter are more resistant to washout and contribute to the formation of capes (Fig. 3, *c*). The greatest variability of the plan position of the coastline, formation and destruction of storm banks and terraces are observed near the distal part of the coastline (Fig. 3, *e*), where fluctuations in the volume of sediments moving in different directions are most significant.

2. Ridge zone. The most elevated part of the coastal bar (from 0.6 m at the Lake Bakalskoe barrier beach to 1.4 m at the root and northern parts), it is located 10–15 m from the sea's edge (Fig. 2). The main features of the relief of this zone are formed during the strongest storms, when wave overtopping of the ridge of the coastal bar is observed along its entire length and is accompanied by the transfer of material to the rear side. During moderate storms, the wave splash crosses the ridge only through depressions in it, where seawater flowing into the inner part of the spit is concentrated and runoff troughs are formed. Between storms, runoff troughs are transformed into erosion cuts under the action of precipitation. Within the ridge zone, a more or less developed vegetation cover is present, which is destroyed during strong storms. Aeolian forms with associated vegetation have formed in places on the most elevated parts of the western branch central part.

3. Rear zone (lagoon for the Lake Bakalskoe barrier beach). Transition zone where migration of Lake Bakalskoe material transported by waves from the sea slope or surface runoff from the ridge zone is completed. The relief is represented by the surface sloping away from the sea, dissected by runoff troughs. The transition to the surface of the inner part of the spit has a pronounced bend, the transition to the bottom of the lagoon is smoother and is distinguished only by the composition of sediments. Areas of splash flow discharge are characterised by tongue-shaped protrusions (Fig. 3, *f*), frequency and configuration of which differ significantly along the length of the spit. The zone is usually characterised by developed vegetation cover.

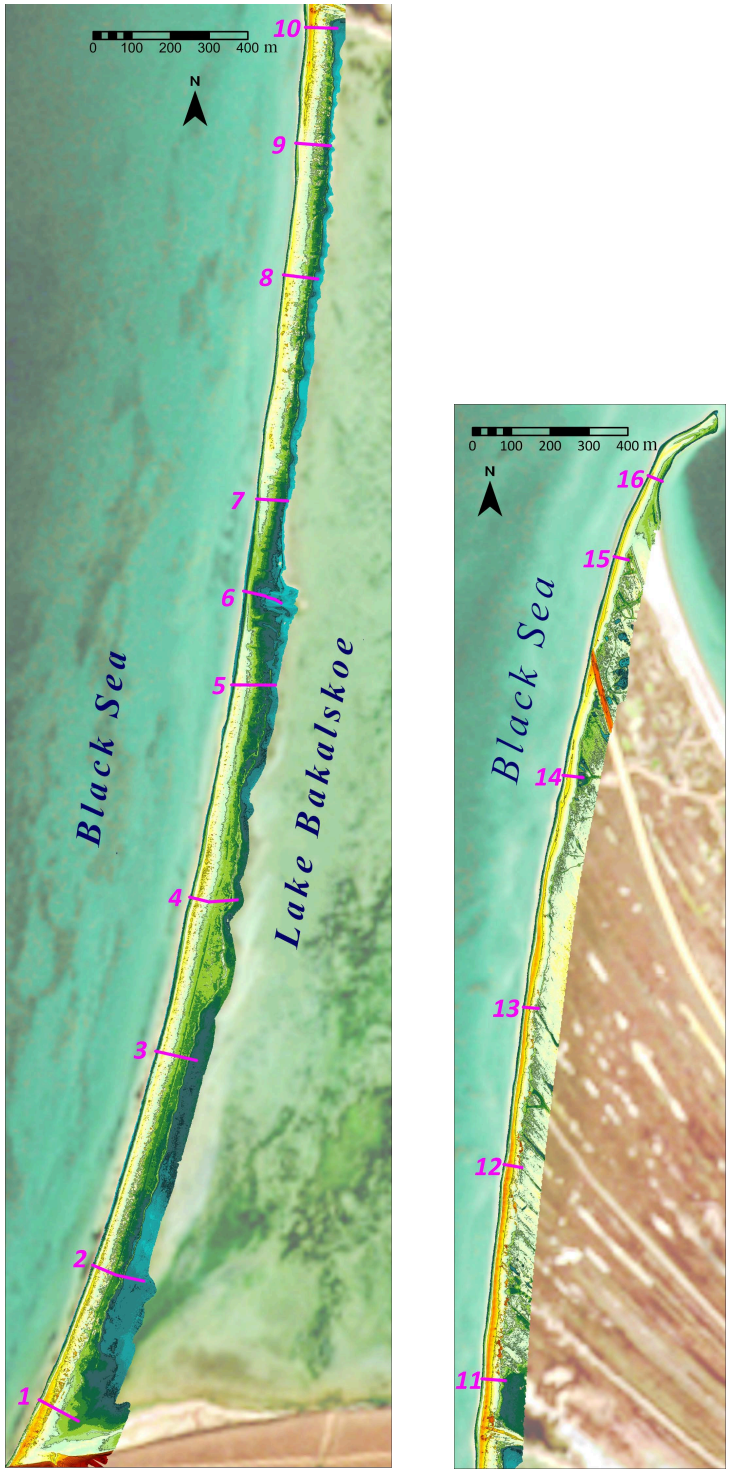

F i g . 2 . The relief of the Bakalskaya Spit western branch (a), transverse profiles (b): left – barrier beach of Bakalskoe Lake, right – main part of the spit. The numerals indicate the numbers of the profiles

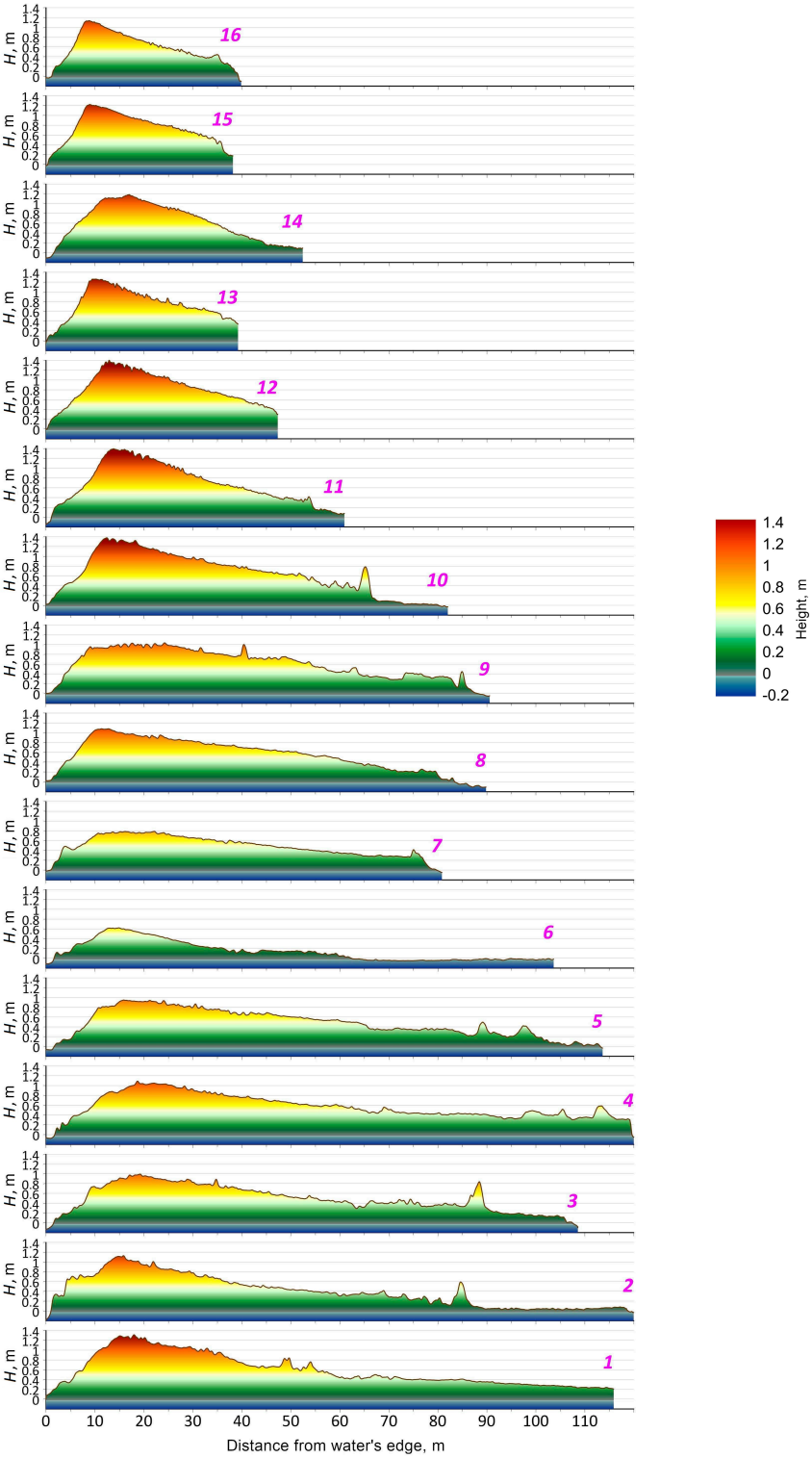

Continued Fig. 2.

Fig. 3. The western branch of the Bakalskaya Spit: *a* – the root part; *b* – the barrier beach of Bakalskoe Lake; *c* – a cape formed at the sea water's edge as a result of the exposure of vegetation remnants of the inner part of the spit; *d* – the beach in the central part of the spit; *e* – the distal part of the spit; *f* – the overflow cone on the shore of Bakalskoe Lake

4. Shore of Lake Bakalskoe along the barrier beach. This zone is developed under the influence of the sea. The overtopping of waves over the barrier beach ridge is accompanied by the transport of material from the sea slope and the washout of the runoff troughs, resulting in the formation of numerous alluvial fans on the lakeshore (Fig. 3, *f*), which create a kind of culp configuration. The development of the shores of Lake Bakalskoe is significantly influenced by lake level fluctuations caused by seasonal changes in the amount of precipitation or seawater input during strong storms. Complete drying of the lake was not observed. The lakeshore, with the exception of active fans, is covered with near-water halophytic herbaceous vegetation, which in dry years develops part of the drying area. During the seasonal development of algae accompanied by a drop in the lake water level, a solid cover 15–30 cm thick is formed of dead vegetation remnants in shallow waters and the drying area. This cover further reduces wave action on the lakeshores. During periods of high standing water, a bank of vegetation

and debris is formed along the lake shoreline under the action of waves. Along the barrier beach, during heavy storms at sea, this bank is usually destroyed by the splash currents and a new one begins to form. No active longshore redistribution of material can be observed along most of the lake shoreline, which can be explained by the low intensity of the corresponding wave direction or the absence of sediments.

Characteristics of the storm on 26–27 November 2023

To analyse the nature of storm impact on the shore, the main wave parameters (significant wave heights, peak periods of the spectrum, average propagation directions) were calculated. The calculation point was located 5200 m from the shore at an isobath of 10 m (Fig. 1). In addition, the wave power was calculated, which is a representative characteristic since it depends on two integral wave parameters, namely wave height and wave energy period. Simplifying a little, we can say that the energy period is the period of a monochromatic wave with a power equivalent to the power of given irregular waves. Wave power is expressed in kilowatts per metre of wave front.

Fig. 4 shows maximum wave heights and power of particular storms west of the Bakalskaya Spit over the last 45 years. Storms were analysed that developed waves with significant heights exceeding the 2.5 m level. If this threshold was not met in a particular year, the characteristics of just the largest storm were chosen for that year. As can be seen in Fig. 4, over the last 45 years, the 26–27 November 2023 storm is comparable in energy and wave height to the 11 November 2007 storm.

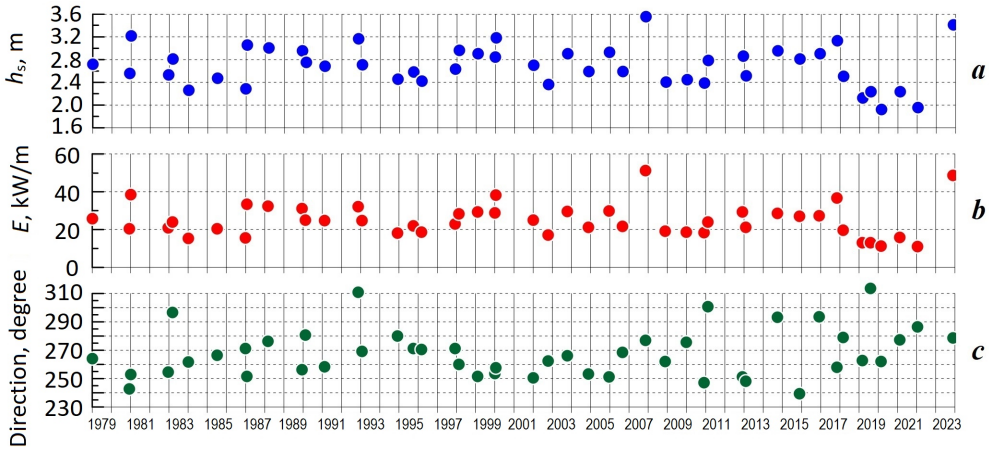

F i g . 4 . Parameters of the largest storms west of the Bakalskaya Spit: *a* – maximum significant wave heights; *b* – maximum wave power; *c* – general directions of storms

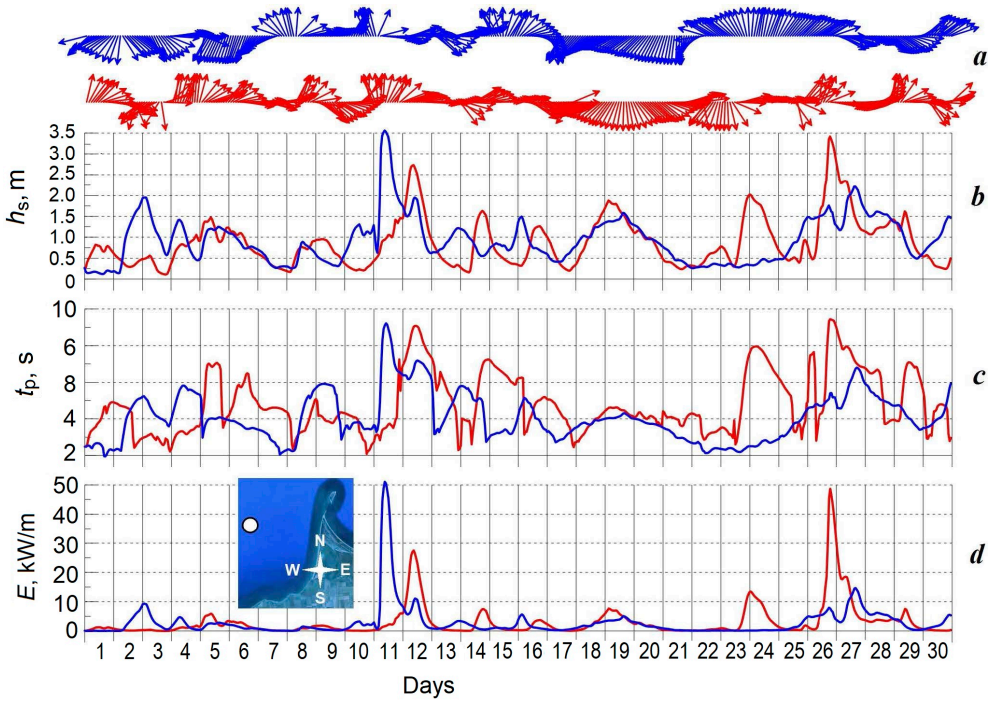

Fig. 5. The main parameters of wind waves for the water area west of the Bakalskaya Spit in November 2007 (blue) and 2023 (red): *a* – propagation directions; *b* – significant wave heights; *c* – peak and mean wave periods; *d* – wave power

Fig. 5 presents a series of significant wave heights, periods, power and wave directions for the water area west of the Bakalskaya Spit in November 2023. In addition, the figure provides graphs of the same parameters for November 2007 to compare. It can be seen that both in November 2007 and November 2023 the western branch of the Bakalskaya Spit was under the influence of significant waves, including a storm with a power of over 25 kW/m on 12 November 2023. At the time of the greatest development of the storm on 26 November 2023 at an isobath of 10 m, the wave parameters were as follows: significant wave height – 3.4 m, period – 7 s, length – 75 m. The wave surge height during the storm was 0.15–0.55 m. It should be noted that the November 2007 storm is slightly higher in power than the similar storm of 2023. Most likely, these two cases characterise the degree of possible maximum wind wave development for the water area under consideration.

Transformation of the western branch during the storm on 26–27 November 2023

As shown in [18, 30], the storm of 26–27 November 2023 is extreme for the Western Crimea on the scale of several decades in terms of wave parameters and overall power. A somewhat different picture is observed in the area of the Bakalskaya Spit located in the Karkinitsky Gulf. According to the scale and nature of changes in the shore configuration and coastal bar relief of the western branch of the Bakalskaya Spit, it can be concluded that the storm in question was extremely strong but not unique. This storm is comparable to the storm of 11 November 2007 in terms of power and other wave parameters (Fig. 5).

During the 2007 and 2023 storms, wave action with overtopping of the beach ridge was observed along the entire length of the coastal bar on the spit western branch. The bar surface was levelled and existing vegetation was either destroyed or buried under a layer of sand. The coastal bar width increased considerably, with clearly visible tongues of sand streams, which were pushing on the inner part of the spit (Fig. 6). Numerous washouts were formed in the Lake Bakalskoe barrier beach, with pronounced traces of sediment movement from the seashore to the lakeshore (Fig. 6).

Figs. 7 and 8, *a* demonstrate the western branch sea's edge retreat values from 03.09.2023 (pre-storm) to 02.09.2024 (post-storm and restoration of bar integrity). It can be seen that the amount of retreat varies considerably along the entire spit. In the section of the main shore south of the spit, the retreat is either absent (RP *1*) or does not exceed 5 m (RP *2* – RP *3*). At the root part of the spit, the edge retreat is relatively small (10–12 m), and at the RP *8* – RP *11* section it does not exceed 5 m. In the northern part of the Lake Bakalskoe barrier beach (RP *12* – RP *22*), the retreat values increase significantly, averaging 28 m and reaching 45 m at RP *16*. In the section where the western branch is a bar extending over the inner part of the spit (RP *23* – RP *33*), the retreat is slightly less, averaging 16.2 m. Within the distal end (RP *34* – RP *36*), the western shore retreated approximately 60 m.

Fig. 6. Transformation of the western branch of the Bakalskaya Spit during the storm: *left* – a washout in the barrier beach of Bakalskoe Lake; *right* – movement of sand from the seashore to the inner part of the spit

Figs. 7 and 8, *b* show the western branch sea's edge displacement values from 03.09.2023 (pre-storm) to 02.09.2024 (post-storm and restoration of bar integrity). It can be seen that the amount of displacement varies considerably along the entire spit. The edge retreat is small (10 m on average) at the root part of the spit (RP *3* – RP *13*), while it is either absent or does not exceed 5 m on profiles *10* and *13*. In the northern part of the Lake Bakalskoe barrier beach (RP *12* – RP *22*), the displacement values increase significantly, averaging 49.5 m

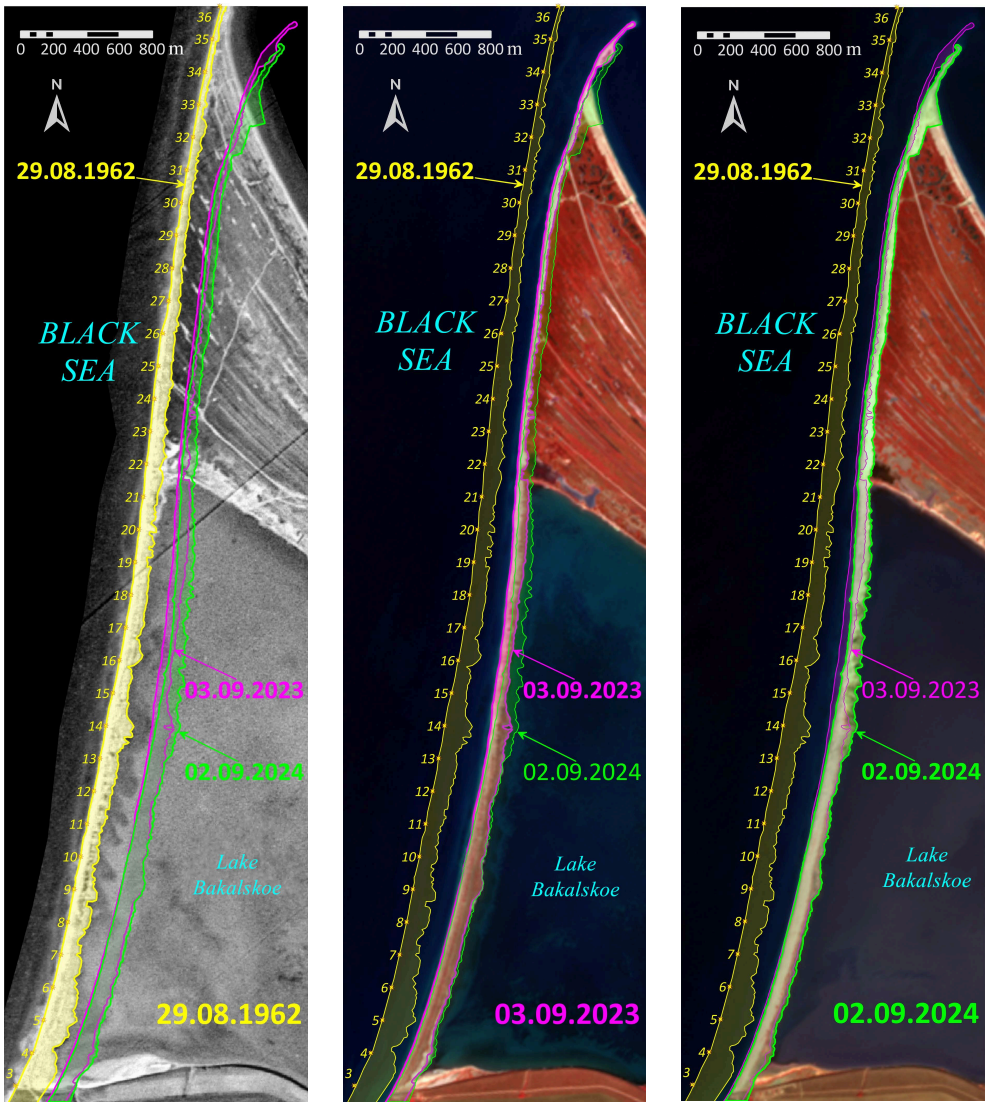

Fig. 7. The transformation scheme of the western branch of the Bakalskaya Spit since 1962 and during the storm on 26–27 November 2023

and reaching 80 m at RP *15*. In the section where the western branch is a bar extending over the inner part of the spit, the displacement remains high between RP *23* and RP *29* (43 m on average) and decreases sharply to 16–18 m between RP *30* and RP *31*. It is possible that the decline at this section is due to the presence of a high crushed shell limestone roadbed extending at an acute angle to the edge. To the north of the road, the bar displacement increases sharply, reaching 80 m at RP *33*. A strong (up to 60 m) displacement to the east of the distal end was noted (RP *34* – RP *36*). During the storm, the distal length was reduced by 380 m and subsequently restored by 220 m.

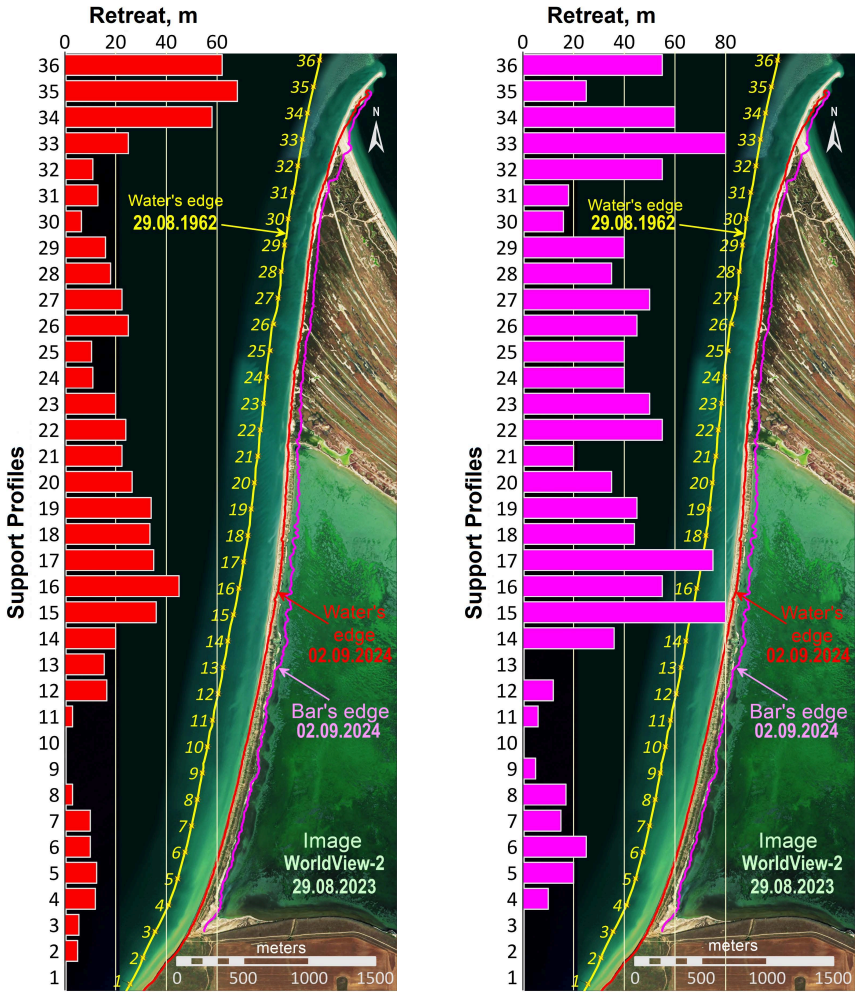

F i g . 8 . Retreat of the sea water's edge (*left*) and the rear part of the beach bar (*right*) of the western branch of the Bakalskaya Spit during the storm on November 26–27, 2023. The numbers indicate the numbers of the support profiles, the distance between the profiles is 200 m

It should be noted that for the entire length of the western branch no evidence of longshore sediment movement during storms is observed, all changes being caused by cross-shore water movements. This is probably due to the long wave lengths. The front of the waves approaching from the open sea, when in contact with the seabed, turned parallel to the shoreline at a considerable distance from the shore and approached it almost at normal.

Transformation of the western branch after the storm of 26–27 November 2023

During the storm, the Lake Bakalskoe barrier beach underwent the greatest changes. In its northern part, two groups of continuous washouts with lengths of 550 and 150 m along the barrier beach were formed (image from 30.11.2023 in Fig. 9). During the storm, the flow of both water and sediments was directed towards the lake. Excess water in the lake led to flooding of the low-lying areas of the inner part of the spit. After the end of the storm and the lowering of sea level, the water began to backflow through the washouts, accompanied by the transport of sand to the seashore. After the levels normalised, the cross-water movement stopped and conditions were created for the barrier beach integrity to be restored. During the month following the storm, the northern group of washouts disappeared completely (image from 01.01.2024 in Fig. 9), while the largest scour holes remained in the southern group, and they were significantly shallower. After another month, only one washout was observed within the barrier beach (image from 31.01.2024 in Fig. 9), which also disappeared during the following two months (image from 09.03.2024 in Fig. 9).

The restoration of the barrier beach was accompanied by changes in the position of both sea and lagoon's edges. Furthermore, most of the changes in the configuration of the lagoon shoreline were associated with fluctuations in lake level. On the seashore, the changes in configuration were associated with the redistribution of sediment both longitudinally and transversely. In contrast to the Lake Bogaily barrier beach [20], where the seaward movement of the sea's edge was observed during the post-storm period, on the western branch of the Bakalskaya Spit, the shore retreat continued after the end of the storm. The washouts were closed by sediments from adjacent shoreline areas. As a result, the highest values of shore retreat following the storm were observed in the northern part of the Lake Bakalskoe barrier beach, where washouts had been formed during the storm.

It should be noted that the areas of washout formation and shore retreat during storms are not stationary. Fig. 9 (images from 08.06.2003 and 15.06.2004) shows that after a series of October 2003 storms with a power of 25 and 34.2 kW/m, washout formation and shore retreat occurred in the southern part of the Lake Bakalskoe barrier beach. Such irregularity is most likely caused by fluctuations in the volume and location of sediment stores on the underwater slope adjacent to the Bakalskaya Spit from the west. The presence of sediment stores is indicated by underwater bars along the spit western branch (see Fig. 2). The irregular nature of storm passage and the mosaic distribution of sediment accumulations cause significant variations in the volume of material entering the near-edge zone. Analysis of space images shows that "plumes" of sediments are periodically formed along the spit western branch, gradually shifting along the shore from the foot

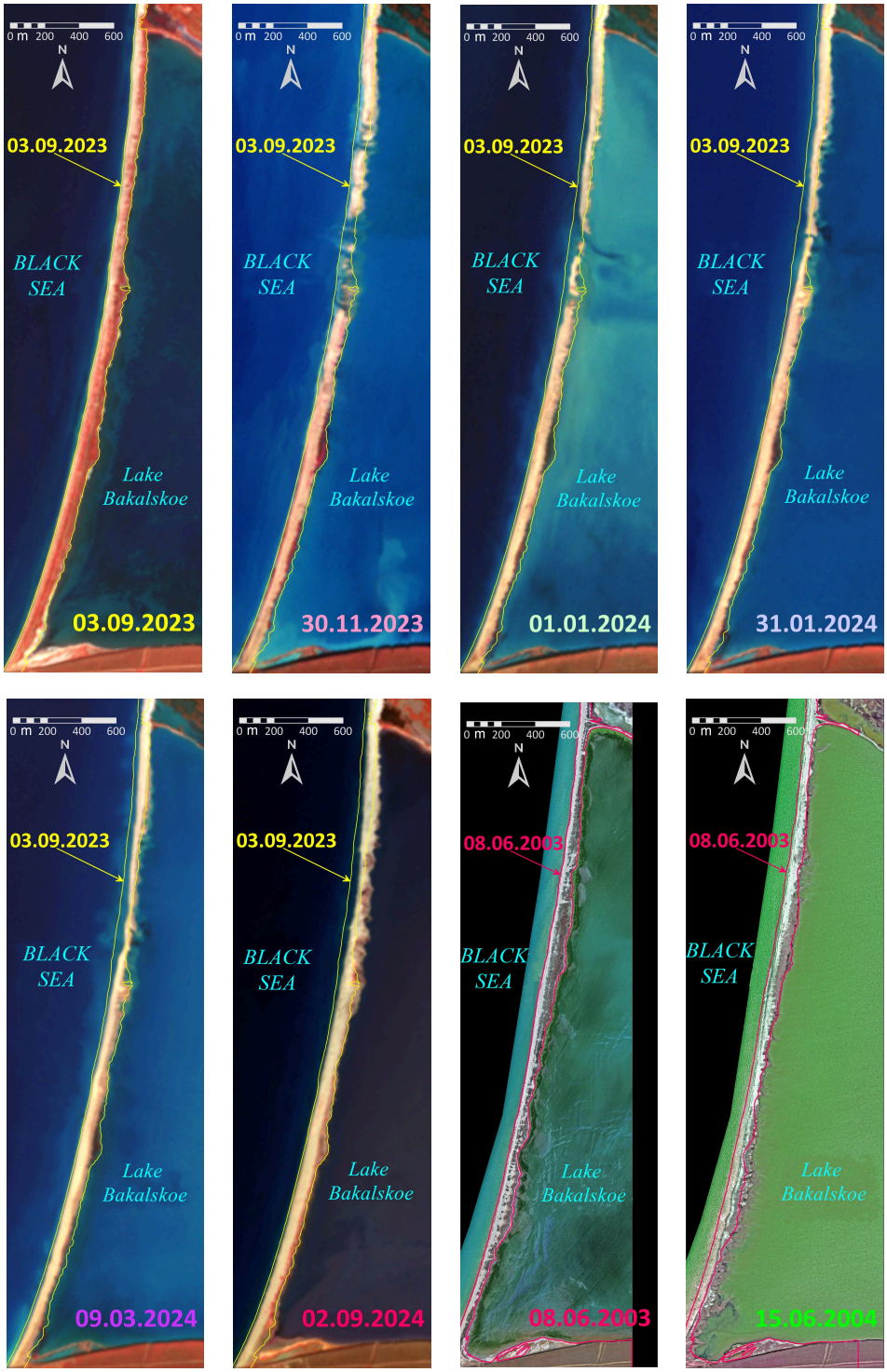

Fig. 9. Transformation of the barrier beach of Lake Bakalskoe after the storm on 26–27 November 2023. For comparison, illustrations of the transformation of the barrier beach in 2003–2004 are given

of the spit to the distal, which causes significant changes in the relief of the underwater slope, configuration of the shoreline, beach width and profile. It is this feature that contributes to changing the position of washouts formed during storms.

Another consequence of the storm was the destruction of vegetation within the entire coastal bar. By autumn 2024, the vegetation within the coastal bar had not yet been restored, which is clearly visible when comparing the images from 03.09.2023 and 02.09.2024 (Fig. 9).

Conclusion

In terms of wave parameters and overall power, the 26–27 November 2023 storm is extreme for Western Crimea on the scale of several decades. However, in the area of the Bakalskaya Spit located in the Karkinitsky Gulf, the storm in question is extremely strong but not unique, and it is comparable to the storm of 11 November 2007 in terms of power and other wave parameters. A similar conclusion can be drawn from the scale and nature of changes in the shore configuration and coastal bar relief of the western branch of the Bakalskaya Spit. Most likely, these two storms determine the limits of possible maximum wind wave development for the water area under consideration, and the differences in the nature and scale of the accumulation body transformation are determined by local conditions in time and space, primarily the relief of the underwater slope and beach at the time of storm formation.

The relief of the above-water part of the western branch of the Bakalskaya Spit is based on a full profile beach, within which the main zones are distinguished, which can be traced almost along the entire length of the spit. During the 26–27 November 2023 storm, wave action with overtopping of the beach ridge was observed along the entire length of the coastal bar of the spit western branch. All zones underwent significant transformation. The coastal bar width increased significantly due to its displacement to the inner part of the spit by a distance that exceeded the retreat of the sea's edge. The bar surface was leveled and vegetation was either destroyed or buried under a layer of sand. Numerous washouts were formed on the Lake Bakalskoe barrier beach, which transported sediments from the seashore to the lakeshore.

In general, the effects of the 26–27 November 2023 storm on the western branch of the Bakalskaya Spit are large-scale but not critical. As can be seen from the dynamics of the barrier beach following the storm, self-restoring processes can be traced, confirming that the lithodynamic system was not brought out of the dynamic equilibrium.

REFERENCES

1. Goryachkin, Yu.N. and Kosyan, R.D., 2018. The Bakalskaya Spit is a Unique Natural Object of the Crimean Peninsula (Review). *Ecological Safety of Coastal and Shelf Zones of Sea*, (4), pp. 5–14. https://doi.org/10.22449/2413-5577-2018-4-5-14 (in Russian).
2. Zenkovich, V.P., 1955. [The Bakalskaya Spit]. In: IO RAS, 1955. *Sbornik Rabot Instituta Okeanologii AN SSSR*, (4), pp. 86–101 (in Russian).

3. Ivanov, V.A., Goryachkin, Yu.N., Udovik, V.F., Kharitonova, L.V. and Shutov, S.A., 2012. Current State and Evolution of the Bakal Spit. *Ecological Safety of Coastal and Shelf Zones of Sea*, 26(1), pp. 8–15 (in Russian).
4. Krylenko, M.V. and Krylenko, V.V., 2018. Study of the Granulometric Composition of Beach and Bottom Sediments of the Bakalskaya Spit. *Ecological Safety of Coastal and Shelf Zones of Sea*, (4), pp. 40–49. https://doi.org/10.22449/2413-5577-2018-4-40-49 (in Russian).
5. Goryachkin, Yu.N. and Kharitonova, L.V., 2018. Dynamics of the Shoreline in the Area of the Bakalskaya Spit. *Ecological Safety of Coastal and Shelf Zones of Sea*, (4), pp. 22–30. https://doi.org/10.22449/2413-5577-2018-4-22-30 (in Russian).
6. Rudnev, V.I., 2018. Peculiarities of the Bottom Relief of the Bakalskaya Spit Foreshore. *Ecological Safety of Coastal and Shelf Zones of Sea*, (4), pp. 15–21. https://doi.org/10.22449/2413-5577-2018-4-15-21 (in Russian).
7. Kosyan, A.R., 2018. Role of Coastal Shells in the Formation of Carbonate Sediments of the Bakalskaya Spit. *Ecological Safety of Coastal and Shelf Zones of Sea*, (4), pp. 81–91. https://doi.org/10.22449/2413-5577-2018-4-81-91 (in Russian).
8. Belokopytov, V.N., Fomin, V.V. and Ingerov, A.V., 2017. On Multidisciplinary Investigations of Dangerous Natural Phenomena in the Azov–Black Sea Basin. *Physical Oceanography*, (3), pp. 28–44. https://doi.org/10.22449/1573-160X-2017-3-28-44
9. Divinsky, B.V., Kubryakov, A.A. and Kosyan, R.D., 2020. Interannual Variability of the Wind-Wave Regime Parameters in the Black Sea. *Physical Oceanography*, 27(4), pp. 337–351. https://doi.org/10.22449/1573-160X-2020-4-337-351
10. Kharitonova, L.V. and Fomin, V.V., 2012. Statistical Characteristics of Wind Waves in the Coastal Area of the Western Crimea according to Retrospective Estimation During 1979–2010. *Ecological Safety of Coastal and Shelf Zones of Sea*, 26(1), pp. 24–33 (in Russian).
11. Gippius, F.N. and Arkhipkin, V.S., 2017. Interannual Variability of Storm Waves in the Black Sea According to Numerical Modeling Results. *Vestnik Moskovskogo Universiteta. Seria 5, Geografia*, (1), pp. 38–47 (in Russian).
12. Goryachkin, Yu.N., Ivanov, V.A. and Kharitonova, L.V., 2013. Is a New Island in the Black Sea? *Reports of the National Academy of Sciences of Ukraine*, (8), pp. 100–104 (in Russian).
13. Rudnev, V.I., Divinskiy, B.V. and Kosyan, R.D., 2020. Changes in Topography of the Coastal Zone of the Bakalskaya Spit from 2018 to 2019. *Ecological Safety of Coastal and Shelf Zones of Sea*, (1), pp. 22–35. https://doi.org/10.22449/2413-5577-2020-1-22-35 (in Russian).
14. Kosyan, R.D. and Krylenko, V.V., 2014. *The Current State of Marine Accumulative Shores of Krasnodar Region and their Use*. Moscow: Nauchnyy Mir, 256 p. (in Russian).
15. Leont'yev, I.O., 2021. Estimating the Vulnerability of a Sandy Coast to Storm-Induced Erosion. *Oceanology*, 61(2), pp. 254–261. https://doi.org/10.1134/S0001437021020119
16. Leont'yev, I.O., Ryabchuk, D.V. and Sergeev, A.Y., 2015. Modeling of Storm-Induced Deformations of a Sandy Coast (Based on the Example of the Eastern Gulf of Finland). *Oceanology*, 55(1), pp. 131–141. https://doi.org/10.1134/S000143701406006X
17. Bugajny, N., Furmańczyk, K., Dudzińska-Nowak, J. and Paplińska-Swerpel, B., 2013. Modelling Morphological Changes of Beach and Dune Induced by Storm on the Southern Baltic Coast Using XBeach (Case Study: Dziwnow Spit). *Journal of Coastal Research*, 65(sp1), pp. 672–677. https://doi.org/10.2112/SI65-114.1

18. Dulov, V.A., Yurovskaya, M.V., Fomin, V.V., Shokurov, M.V., Yurovsky, Yu.Yu., Barabanov, V.S. and Garmashov, A.V., 2024. Extreme Black Sea Storm in November, 2023. *Physical Oceanography*, 31(2), pp. 295–316.

19. Bogdanovich, A.Yu., Lipka, O.N., Krylenko, M.V., Andreeva, A.P. and Dobrolyubova, K.O., 2021. Climate Threats in the North-West Caucasus Black Sea Coast: Modern Trends. *Fundamental and Applied Climatology*, 7(4), pp. 44–70. https://doi.org/10.21513/2410-8758-2021-4-44-70 (in Russian).

20. Krylenko, V.V., Goryachkin, Yu.N., Krylenko, M.V. and Divinsky, B.V., 2024. Transformation of Lake Bogaily Barrier Beach (Western Crimea) under the Influence of Extreme Storms. *Ecological Safety of Coastal and Shelf Zones of Sea*, (3), pp. 59–78.

21. Krylenko, V.V. and Rudnev, V.I., 2018. Technique of Photographic Aerial Survey of the Bakalskaya Spit. *Ecological Safety of Coastal and Shelf Zones of Sea*, (4), pp. 59–64. https://doi.org/10.22449/2413-5577-2018-4-59-64 (in Russian).

22. Krylenko, M. and Krylenko, V., 2020. Features of Performing High-Precision Survey of the Abrasion Coast Relief by UAV. *Bulletin of Science and Practice*, 6(2), pp. 10–19. https://doi.org/10.33619/2414-2948/51/01 (in Russian).

23. Divinsky, B. and Kosyan, R., 2017. Spatiotemporal Variability of the Black Sea Wave Climate in the Last 37 Years. *Continental Shelf Research*, 136, pp. 1–19. https://dx.doi.org/10.1016/j.csr.2017.01.008

24. Goryachkin, Yu.N. and Dolotov, V.V., 2019. *Sea Coasts of Crimea*. Sevastopol: Colorit, 256 p. (in Russian).

25. Divinsky, B.V., 2018. Hydrodynamic Water Conditions in the Bakalskaya Spit Area. *Ecological Safety of Coastal and Shelf Zones of Sea*, (4), pp. 31–39. https://doi.org/10.22449/2413-5577-2018-4-31-39 (in Russian).

26. Goryachkin, Yu.N. and Repetin, L.N., 2009. [Storm Wind and Wave Regime near the Black Sea Coast of Crimea]. *Ekologicheskaya Bezopasnost' Pribrezhnoy i Shel'fovoy Zon i Kompleksnoe Ispol'zovanie Resursov Shel'fa* [Ecological Safety of Coastal and Shelf Zones and Comprehensive Use of Shelf Resources], 19, pp. 56–69 (in Russian).

27. Fomin, V.V., Alekseev, D.V. and Kharitonova, L.V., 2013. [Modeling of the Bakalskaya Spit Morphodynamics]. *Ekologicheskaya Bezopasnost' Pribrezhnoy i Shel'fovoy Zon i Kompleksnoe Ispol'zovanie Resursov Shel'fa* [Ecological Safety of Coastal and Shelf Zones and Comprehensive Use of Shelf Resources], 27, pp. 374–380 (in Russian).

28. Fomin, V.V. and Lazorenko, D.I., 2020. Hydrodynamic Process Peculiarities in the Bakalskaya Spit Area as per Computational Modeling Data. *Ecological Safety of Coastal and Shelf Zones of Sea*, (3), pp. 31–47. https://doi.org/10.22449/2413-5577-2020-3-31-47 (in Russian).

29. Krylenko, V.V., Krylenko, M.V. and Aleinikov, A.A., 2019. Research of the Bakalskaya Bank Underwater Relief by Sentinel-2 Satellite Images. *Ecological Safety of Coastal and Shelf Zones of Sea*, (2), pp. 30–39. https://doi.org/10.22449/2413-5577-2019-2-30-39 (in Russian).

30. Divinsky, B.V. and Saprykina, Ya.V., 2024. Extreme Wind Waves on the Northeastern Shelf of the Black Sea. *Doklady Earth Sciences*, 517, pp. 1224–1233. https://doi.org/10.1134/S1028334X24601676

Submitted 18.08.2024; accepted after review 02.10.2024;
revised 17.12.2024; published 31.03.2025

About the authors

Viacheslav V. Krylenko, Senior Research Associate, Shirshov Institute of Oceanology of RAS (36 Nakhimov Avenue, Moscow, 117997, Russian Federation), PhD (Geogr.), **ORCID ID: 0000-0001-8898-8479, ResearcherID: N-1754-2017**, *krylenko.slava@gmail.com*

Yuri N. Goryachkin, Chief Research Associate, Marine Hydrophysical Institute of RAS (2 Kapitanskaya St., Sevastopol, 299011, Russian Federation), DSc (Geogr.), **ORCID ID: 0000-0002-2807-201X, ResearcherID: I-3062-2015,** *yngor@mhi-ras.ru*

Marina V. Krylenko, Leading Research Associate, Shirshov Institute of Oceanology of RAS (36 Nakhimov Avenue, Moscow, 117997, Russian Federation), PhD (Geogr.), **ORCID ID: 0000-0003-4407-0548, ResearcherID: R-2210-2016**, *krylenko@mail.ru*

Boris V. Divinsky, Senior Research Associate, Shirshov Institute of Oceanology of RAS (36 Nakhimov Avenue, Moscow, 117997, Russian Federation), PhD (Geogr.), **ORCID ID: 0000-0002-2452-1922, ResearcherID: C-7262-2014**, *divin@ocean.ru*

Contribution of the authors:

Viacheslav V. Krylenko – task setting, processing, analysis and description of research results, preparation of the text and graphic materials

Yuri N. Goryachkin – task setting, processing and analysis of literary sources, field studies, preparation of the article text

Marina V. Krylenko – processing and analysis of the results of field research, preparation of the text of the article and the list of references

Boris V. Divinsky – mathematical modeling of hydrodynamic processes

All the authors have read and approved the final manuscript.

Original paper

Testing of a Piled (Permeable) Breakwater Made of Composite Materials for Coastal Protection. Part 2. Evaluation of Impact on the Shore State

B. V. Chubarenko [1], D. I. Dikii [1] *, D. A. Domnin [1], R. B. Zakirov [1], A. N. Babakov [1], V. T. Paka [1], A. A. Kondrashov [1], A. O. Korzh [1], E. M. Burnashov [2], K. V. Karmanov [3], O. V. Bass [4], V. I. Efremov [5], O. I. Ryabkova [4]

[1] *Shirshov Institute of Oceanology of Russian Academy of Sciences, Moscow, Russia*
[2] *GBU KO Baltberegozashchita, Svetlogorsk, Russia*
[3] *Kaliningrad State Technical University, Kaliningrad, Russia*
[4] *Immanuel Kant Baltic Federal University, Kaliningrad, Russia*
[5] *LLC Trading House Basalt Pipes, Moscow, Russia*
* *e-mail: dimandikiy@mail.ru*

Abstract
The paper analyzes the effectiveness of a pile breakwater structure *Grebenka* for coastal protection purposes. From 03.10.2020 to 30.04.2023, full-scale testing of the structure was conducted on the northern shore of the Kaliningrad Oblast near the city of Zelenogradsk between the eroded and accumulative shore segments. Four breakwater modules were installed in a single line in the groin pocket at a depth of about 2 m offshore of the groin end but did not completely overlap the pocket. One module was installed in the immediate vicinity of the shoreline. The experiment covered several seasons of severe storms, which allowed us to compare the shoreline dynamics at the breakwater installation site and in the neighbouring areas. We carried out regular measurements of the beach width, aerial survey, repeated depth measurement at the installation site and assessed the underwater slope dynamics. We also determined the thickness of the sand cover layer at the structure installation site and placed tilting flow velocity sensors on the breakwater. It was found that the beach width at the breakwater installation site and in adjacent areas was changing synchronously. The absence of an obvious accumulative effect behind the installed breakwater was, first, due to the displacement of the breakwater modules and their partial immersion in the sand and, second, due to the limited line length of the offshore modules in proportion to their distance from the shoreline. A temporary positive effect was achieved only for a solitary module as periodic beach progradation to the root of an old groin adjacent thereto from the east. The results of the full-scale test will be used to further improve the breakwater design.

Keywords: breakwater, shore protection, Baltic Sea, field experiment, beach dynamics, underwater slope dynamics, coastal erosion

Acknowledgments: The experiment in terms of creating and installing the breakwater (as well as conducting part of visual surveys and measurement works in 2022, preparation of flow measuring instruments) was funded entirely by the developer, LLC Trading House Basalt Pipes, Moscow. Expeditionary work to determine long-term changes in the width of the beach, aerial visual surveys 2022-2023, measurement works 2023, underwater survey and determination of the thickness of loose sediment 2022, measurement of currents were carried out with the support of topic no. FMWE-2021-0012, while the analysis of the experiment results and preparation of this article were performed with the support of topic no. FMWE-2024-0025 of the state assignment of the P.P.Shirshov Institute of Oceanology of the Russian Academy of Sciences. The authors thank the engineering staff of IO RAS and personally A.P. Podufalov, M.I. Nemtsov and Yu.N. Perov for their highly professional contribution to the expedition work.

For citation: Chubarenko, B.V., Dikii, D.I., Domnin, D.A., Zakirov, R.B., Babakov, A.N., Paka, V.T., Kondrashov, A.A., Korzh, A.O., Burnashov, E.M., Karmanov, K.V., Bass, O.V., Efremov, V.I. and Ryabkova, O.I., 2025. Testing of a Piled (Permeable) Breakwater Made of Composite Materials for Coastal Protection. Part 2. Evaluation of Impact on the Shore State. *Ecological Safety of Coastal and Shelf Zones of Sea*, (1), pp. 72–95.

Испытание свайного (проницаемого) волнолома из композитных материалов для берегоукрепления. Часть 2. Оценка влияния на состояние берега

Б. В. Чубаренко [1], Д. И. Дикий [1] *, Д. А. Домнин [1], Р. Б. Закиров [1], А. Н. Бабаков [1], В. Т. Пака [1], А. А. Кондрашов [1], А. О. Корж [1], Е. М. Бурнашов [2], К. В. Карманов [3], О. В. Басс [4], В. И. Ефремов [5] О. И. Рябкова [4]

[1] *Институт океанологии им. П. П. Ширшова РАН, Москва, Россия*

[2] *ГБУ КО «Балтберегозащита», Светлогорск, Россия*

[3] *Калининградский государственный технический университет, Калининград, Россия*

[4] *Балтийский федеральный университет имени Иммануила Канта, Калининград, Россия*

[5] *ООО «Торговый дом «Базальтовые трубы», Москва, Россия*

* *e-mail: dimandikiy@mail.ru*

Аннотация

Проанализирована эффективность применения свайного сооружения вида волнолом «Гребенка» для целей берегозащиты. С 03.10.2020 по 30.04.2023 были проведены натурные испытания данной конструкции на границе абразионного и аккумулятивного сегментов северного побережья Калининградской области вблизи г. Зеленоградска. Четыре модуля волнолома были установлены в одну линию в бунном кармане на глубине около 2 м мористее конца бун, но не перекрывали этот карман полностью. Один прибрежный модуль был установлен в непосредственной близости от линии уреза. Эксперимент охватил несколько сезонов сильной штормовой активности, что позволило сравнить динамику береговой линии в месте установки волнолома и на соседних участках. Проводились регулярные измерения ширины пляжа, аэрофотосъемка, повторное измерение глубин в месте установки, оценка динамики подводного вала, определение толщины слоя песчаного чехла в месте установки конструкции, размещение инклинометрических датчиков скорости течения на волноломе. Выявлено, что

ширина пляжа в месте установки волнолома и на смежных участках изменялась синхронно. Отсутствие очевидного аккумулятивного эффекта позади волнолома связано, во-первых, со смещением модулей и их частичным погружением в песок, а во-вторых, с недостаточной длиной линии мористых модулей по отношению к их удалению от уреза. Временный положительный эффект был достигнут только позади отдельно стоящего модуля и выражался в периодическом выдвижении пляжа к корню примыкающей к нему с востока старой буны. Результаты проведенного натурного испытания будут применены для дальнейшего совершенствования конструкции волнолома.

Ключевые слова: волнолом, берегоукрепление, Балтийское море, натурный эксперимент, динамика пляжа, подводный склон, абразия берега

Благодарности: создание и установка волнолома, а также проведение части визуальных обследований и промерных работ 2022 г., подготовка средств измерения течений выполнены за счет разработчика волнолома «Гребенка» – ООО «Торговый дом «Базальтовые трубы», г. Москва. Работы были поддержаны двумя темами государственного задания Института океанологии им. П. П. Ширшова РАН: работы по определению долговременных изменений ширины пляжа, аэровизуальные обследования 2022–2023 гг., промерные работы 2023 г., подводная съемка и определение толщины рыхлого осадка 2022 г. и измерение течений проводились при поддержке темы № FMWE-2021-0012, а анализ результатов эксперимента и подготовка статьи – при поддержке темы № FMWE-2024-0025. Авторы благодарят инженерный состав института и персонально А. П. Подуфалова, М. И. Немцова, Ю. Н. Перова за высокопрофессиональный вклад в проведение экспедиционных работ.

Для цитирования: Испытание свайного (проницаемого) волнолома из композитных материалов для берегоукрепления. Часть 2. Оценка влияния на состояние берега / Б. В. Чубаренко [и др.] // Экологическая безопасность прибрежной и шельфовой зон моря. 2025. № 1. С. 72–95. EDN TPHYNA.

Introduction

The widespread retreat of the marginal seas coastline [1] is also characteristic of the Baltic Sea. There is a pronounced trend towards increased coastal erosion in the southern Baltic [2–4], which is related to geological characteristics [5]. Negative dynamics is observed primarily for sandy shores, which are affected by storms of north-western, western, south-western directions [6, 7]. The storm impact along with the increased sea level [8, 9] is one of the main external factors contributing to the coastal erosion and retreat. Sea level rise as one of the vivid manifestations of regional climate change [10] is a characteristic phenomenon for the open coast of the South-Eastern Baltic, where the rate of sea level rise in the 20th century was 1.3–1.5 cm / 10 years [11].

During 2007–2017 [7], the coastal retreat in the Kaliningrad Oblast was estimated to be 0.2 m/year for the Baltic Spit, 0.4 m/year for the Curonian Spit, 0.5 m/year for the western coast of the Sambia Peninsula and 0.2 m/year for the northern coast.

In the Kaliningrad Oblast, various measures have been taken to counteract coastal erosion [12], such as installation of breakwaters and groins, reinforcement of cliff slopes with gabions or geosynthetic covers [13]. There is experience of coastal protection by inwash of sand obtained as a result of slope terracing

near the village of Filino [14, 15]. This inwash provided shoreline maintenance for several years. Experimental dumping of bottom material near Baltiysk obtained during maintenance dredging of navigation canal [16] did not lead to the expected result as the near-bottom currents in this area [17] do not allow the material to deposit at the water's edge [18].

The most impressive is the example of a long-term discharge of material obtained by hydraulic washing of rock during amber extraction by the Kaliningrad Amber Combine. This discharge resulted in a complete change in the natural dynamics of the western coast of the Sambia Peninsula, namely, in the prevalence of accumulation over the naturally occurring erosion and the progradation of the water's edge by hundreds of metres [19]. The cessation of discharges allowed finding out that annual nourishment of at least 20% of the previously discharged volume is required to support the material washed up on the open coast [20].

Coastal breakwaters [1)] have never been used before on the Kaliningrad coast. There is experience in the application of such structures on the neighbouring coast of Poland [21], but it is not always positive [22], as the success depends largely on local conditions.

The aim of the work is to confirm or reject the hypothesis that it is possible to protect the coast from erosion using a relatively inexpensive permeable breakwater *Grebenka* (the comb) [23] and to identify its positive and negative aspects. Within the coastal protection concept for the coast of the Kaliningrad Oblast [24], it was recommended to apply underwater breakwaters, taking into account the existing conditions, so *in situ* testing of possible solutions was extremely useful. The creation of a permeable version of the structure was driven by the desire to obtain a lighter and cheaper construction compared to a monolith breakwater.

The experiment was conducted on the coast of the south-eastern Baltic Sea (Fig. 1, *a*, *b*), in the coastal zone of the Kaliningrad Oblast near the town of Zelenogradsk, on the border of a stable and erosion coast (site *BC* in Fig. 1, *c*). The tested breakwater of permeable construction *Grebenka* [23, 25] consisted of four 12-metre modules (seaward modules *1–4*, Fig. 1, *d*), installed at a depth of 2.5 m at a distance of 75–80 m from the water's edge, the distance between modules being 1.5–2 m. The modules were installed within the easternmost inter-groin pocket of a group of old semi-destroyed groins of the early 20th century, located to the west of Zelenogradsk. Module *5* was installed at a depth of 1.5 m at a distance of 35 m from the water's edge near the middle of the visible part of the easternmost part of the destroyed old groins.

[1)] A coastal breakwater is a structure located in the water area along the shore to protect the shoreline from destruction by wave action and to accumulate and retain sediment from movement (Russian state standard GOST P 54523-2011).

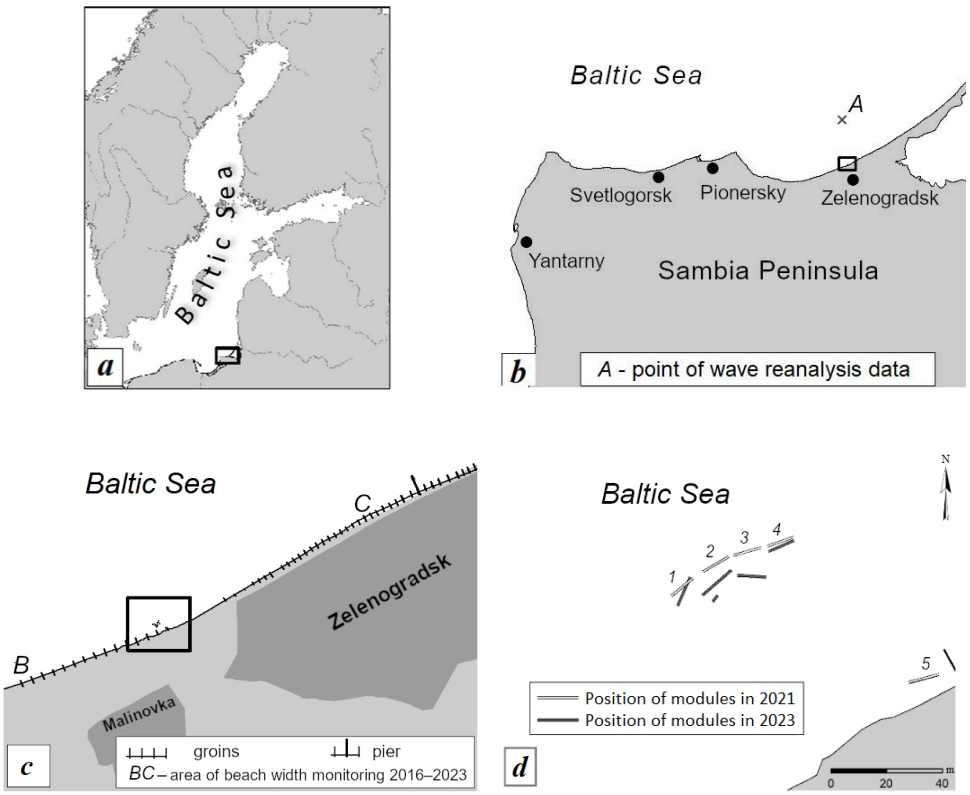

Fig. 1. Testing site: *a* – the Baltic Sea; *b* – enlarged image of the area contoured in fragment *a*: the northern shore of the Sambia Peninsula, Kaliningrad Oblast; *c* – enlarged image of the area contoured in fragment *b*: a section of the shore adjacent to the Zelenogradsk city beach from the west; the rectangle highlights the breakwater installation site, *BC* – observation area for long-term dynamics of the beach width; *d* – location of the modules in 2021 (after installation) and in 2023 (during final inspection)

Details of the breakwater installation and changes in its design during the experiment are given in the paper [23]. This work uses the materials of the XXX All-Russian Conference 'The Coastal Zone of the Seas of Russia in the XXI Century' [2)].

[2)] Ogorodov, S.A., ed., 2024. [*Coastal Zone of Seas of Russia in the XXI Century: Proceedings of the XXX All-Russian Conference. Moscow, 3–7 June 2024*]. Moscow: Geograficheskiy Fakultet MGU, pp. 150–151 (in Russian).

Experimental area and meteorological conditions

In the study area, the deposit flow, on average directed from west to east, is quite saturated. At depths between 18 and 28 m, there is an extensive relic sand lens [3)] with an area of about 7 km^2.

Within the group of old groins of the early 20th century (2 km long), installed in 1925–1927, which traps and retains sand, the shore is quite stable with a beach of an average width of 30–40 m and foredune up to 6–8 m high (Fig. 2, *a*). The adjacent from the east shady section of the shore (Fig. 2, *b*) is more dynamic and characterised by a clearly pronounced erosion tendency.

a ***b*** ***c*** ***d***

F i g . 2 . State of the beach: *a* – stable beach at the western tip of the old groins site (the early 20th cent.) (27.04.2012); *b* – lee erosion at the eastern tip of the old groins site (27.04.2012); *c* – seasonal beach restoration identified by a strip of washed sand, including in the shady zone of the groins (27.04.2012) (photo by A. N. Babakov); *d* – the state before the period of autumn-winter storms in 2020, 19.10.2020. The arrows indicate the future position of the breakwater modules

[3)] Orlenok, V.V., 1992. [*Study of Stratigraphy and Lithology of Bottom Sediments of the Sambia Peninsula Based on Drilling and Seismic Profiling Data*]. Report of KGU. Kaliningrad, 64 p.(in Russian).

The rate of cliff retreat [4] in the western part of Zelenogradsk in 1963–1974 reached 0.6 m/year, whereas in terms of volume it was 7.2 m^3/(running meter·year).

Only after the construction of a new group of groins in early 2017, the beach in the previously erosion-prone urban section recovered quickly. However, in the 700 m interval between the groups of old and modern groins, the beach is actively eroded by storm events (Fig. 2, *d*).

The dumping of dredged material from the construction of the International Marine Terminal in Pionersky, Kaliningrad Oblast (Fig. 1, *b*), was one of the sources of sediment in the area under consideration. The marine dump is located 5 km east of Pionersky within the same lithodynamic cell where the breakwaters were located. Prevailing westerly winds contribute to the alongshore transport of material [26]. A total of 834,000 m^3 of dredged material was delivered to the marine dump from 2018 to 2023: 291,000 m^3 in 2018–2019 and 347,000, 185,000 and 11,000 m^3 annually from 2021 to 2023, respectively.

The underwater slope of the study area typically has an underwater bar 50–150 m from the water's edge with a depth above the top of the bar being approximately 1.3–1.7 m. The bottom topography is uniform along the shore, but there are localised features in the form of depressions and shallow areas that actively migrate depending on the conditions of the last storm.

According to various estimates, the depth of closure for this area ranges from 7.5 m [27] to 8.4 m [28]. The wave breaker zone begins at a distance of more than 200 m from the water's edge [29].

Seasonal dynamics at this site are traditional. Autumn and winter storms wash sand away and transport it along and across the beach. Material arriving on the underwater slope from the west and east during the spring–summer period is rewashed onto the beach by more moderate waves, restoring the beach width (Fig. 2, *c*). Erosion and accumulation alternate continuously over a period of several years, and the installation of the breakwaters appears to have occurred during a phase of active erosion.

During the experiment (spring 2021 – spring 2023), several storms were recorded on the northern coast of the Sambia Peninsula. The longest and most destructive of them occurred during the autumn–winter period: 19–20 November 2021, 13–21 January 2022, 27–31 January 2022, 17–21 February 2022, 4–8 April 2022, 18–21 February 2023. The average wind speed on these dates exceeded 15 m/s and the direction was predominantly westerly. The consequences of their impact on the shores are shown in the work [30].

According to the reanalysis data, for a point with a depth of 17.5 m seaward of the breakwater location (point *A* in Fig. 1), the highest waves during the study period were recorded on 30 January 2022, their height being about 6 m and the direction of wave motion being from the northwest. The number of days during which a significant wave height reached 2 m was 105. The majority of these days were recorded in October–March (85%). The largest contributions were January 2022

[4] Ryabkova, O.I., 1987. [*Coastal Dynamics of the Sambia Peninsula and Curonian Spit in Relation to Coastal Protection Problems. Extended Abstract of Doctoral Dissertation*]. Moscow, 17 p. (in Russian).

Parameters of main registered storm events during the experiment

Storm date	H_{max}, m	H_{max}_3h, m	H_{mean}_3h, m	Wave direction	Wave period, s
13–22 January 2022	5.52	5.31	2.80	Northern, north-western	5.42
26–31 January 2022	6.09	6.01	2.64	Northern, north-western	5.01
17–25 February 2022	3.73	3.60	1.80	Northern	3.60
30 January – 02 February 2023	3.06	3.02	1.93	South-western	4.22
17–21 February 2023	5.84	5.78	2.33	South-western	4.60

Note. H_{max} – maximum significant wave height: H_{max}_3h – maximum significant wave height for moving average 3 hours; H_{mean}_3h – average significant wave height for moving average 3 hours (re-analysis data).

with 17 days, February 2022 with 12 days, February 2023 with 11 days, and November and December 2021 with 10 days each. The total number of hours in which waves with a significant height exceeding 2 m were observed during the study period was 1139. Thus, the period of the experiment was rich in prolonged and rather severe storm events (Table).

Methods and scope of conducted studies

The position of the breakwater, beach and water's edge on the satellite images was referenced to the coordinates of fixed reference points; the location of the breakwater modules and tracing of the water's edge were carried out using GPS (error up to 2 m).

Aerial visual observation using a DJI Mini2 unmanned aerial vehicle (UAV) recorded the position of the shoreline and the boundaries of the underwater bar (in autumn–summer 2022 and winter–spring 2023). UAV were flying at an altitude of 120 m, with a longshore coverage of over 900 m, limited to the width of the beach (inland), and 100 m (seaward) in the transverse direction to the water's edge.

The underwater longshore bar was identified visually by its typical yellow colour without automated techniques. The top of the bar was defined as the area of the most intense yellow colour in the image.

Periodic beach width measurements (11 measurements between 15 March 2022 and 12 April 2023) near the breakwater were made on three profiles (line *5* in Fig. 3). The central profile was located between the breakwater modules, the left (west) profile was located on the traverse of the penultimate old groin, and the right (east) profile was in the central part of the lee erosion zone at a distance from the central profile approximately equal to the width of the inter-groin pocket. The data obtained by optical levelling were used to construct beach height profiles. Beach width measurements were taken after the winter 2022 measurement period: on 15 March – 21 April 2022 with a frequency of approximately one week, as well as on 1 July 2022, 22 November 2022, 1 December 2022, 12 April 2023. Changes in the beach width over a long-term period were assessed from the data of the beach width measurements in 2016–2023 using a set of profiles in the section from the western edge of the early 20th century groin group (previously mentioned old groins) to the western end of the promenade in Zelenogradsk (section *BC* in Fig. 1, *c*, lines *8* in Fig. 3).

The thickness of the loose sand layer at the cross-section passing through the breakwater modules (line *7* in Fig. 3) was determined by the hydraulic washing method: an electric water pump was used to create a constant water pressure, which was fed into a probing metal tube with a diameter of 20 mm. Under the water pressure, the soil was washed out and the probe was deepened. The measurements were carried out on 23 April 2023 and the results were normalised to the mean annual sea level according to the tide gauge in the port of Pionersky.

The bottom relief in the coastal zone changes from year to year due to various natural factors. At the breakwater location, depths were surveyed (with 40 m survey line spacing) on 7 September 2022 and 23 April 2023 (Fig. 3). A single-beam echosounder with navigation reference using a Garmin GPSMAP 421s chartplotter was used for the survey. The measurement results were referenced to mean annual sea level and interpolated to a grid with 10 × 10 m spacing. A differential digital relief model was then obtained by surface subtraction, from which bottom deformation zones were identified and the amount of sand loss and gain between the survey dates of 7 September 2022 and 23 April 2023 was calculated.

In order to quantify the effect of wave energy attenuation during its passage through the breakwater, two inclinometer-type current velocity meters were used [31]. One meter was attached to the seaward and the other to the rear part of module *3* (Fig. 3, *b*). As brackets for the inclinometers suspension, we used stapled together flexible glass-fiber reinforced bars with a diameter of 10 mm, the upper ends of which were fixed horizontally in the upper part of the module. Lead weights were tied to the free ends of the brackets. The weights dragged the brackets to the bottom and sank the inclinometers. The flexibility of the glass reinforcement prevented the weights from subsiding into the sand. The inclinometers were

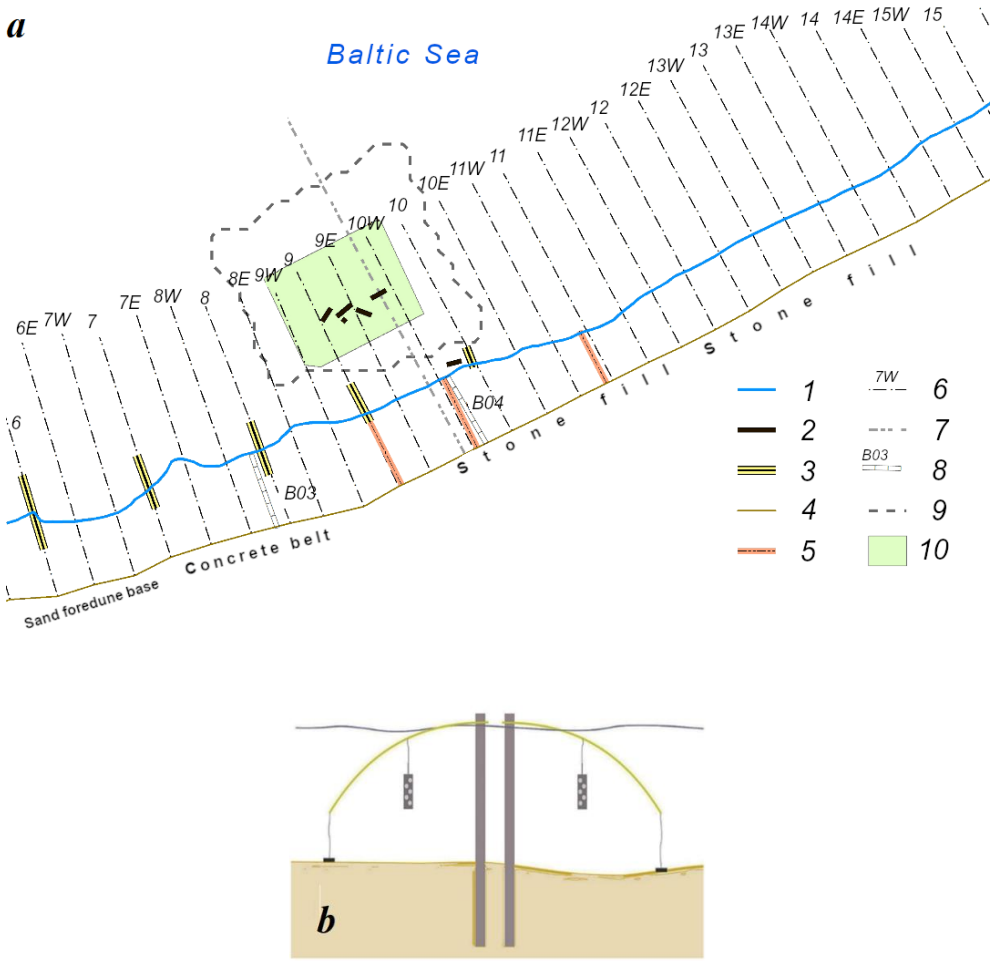

F i g . 3 . Work layout: *a* – basic reference lines and layout of the *Grebenka* breakwater modules, cross sections and work areas: *1* – the water's edge on 24.09.2022; *2* – *Grebenka* breakwater modules; *3* – old wooden groins; *4* – basic reference line; *5* – profiles for determining the beach width (GBU KO *Baltberegozashchita*); *6* – profiles for estimating the width of the underwater bar and its distance from the water's edge; *7* – profile for determining the loose sediment thickness; *8* – profiles for measuring the seasonal dynamics of the beach width (data from previous years were used); *9* – the boundary of the measuring range; *10* – the polygon for calculating the deformation of the underwater slope; *b* – inclinometer installation diagram

attached to 30 cm rope leashes so that they were positioned 1 m from the module and 1 m from the surface. The inclinometers recorded (at a frequency of 5 Hz) the absolute value of wave-induced current velocity and longshore transport from 12:00 on 23 April 2023 to 12:00 on 28 April 2023.

Results and discussion

Observations of beach condition and dynamics were carried out in 2016–2023 along with the eastern wing of the Zelenograd concavity, from the village of Priboy to the western edge of the Zelenogradsk promenade (section *BC* in Fig. 1, *c*, lines *8* in Fig. 3). The boundaries of the section are 2 km west and 2 km east of the breakwater installation site. Periodic surveys revealed marked variations in beach width depending on wind-wave and surge activity, as well as the amount of sediment input from the marine dump of the Pionersky port.

Photo survey of the water's edge position showed its periodic progradation after spring-summer moderate waves (Fig. 4, *a*, *e*), and beach erosion and narrowing after autumn-winter storms (Fig. 4, *b–d*, *f*). But the resulting stable beach attachment to the coastal module did not occur. The beach width varied here within the same range as before the breakwater installation.

A trend towards winter erosion of the beach (22 December 2016, 17 December 2021, 2 February 2022, 22 February 2023) and its re-expansion under weak wave action (5 May 2022, 25 August 2022, 19 December 2022, 12 May 2023) was observed along the entire section from the village of Priboy to Zelenogradsk (Fig. 5). Active beach erosion after the extreme storms of February 2022, during which wind speeds above 20 m/s were recorded on five occasions and the sea level exceeded the long-term average by 0.5–1 m, is indicative. The beach in the western section was half washed out to 20 m, while to the east of the old groins it was washed away completely to the base of the bouldery berm (see the graph for 02.02.2022 in Fig. 5).

The beach width within the early 20th century old groins (0–2 km) varies seasonally from 20–30 m in winter to 30–55 m in summer with a maximum of up to 45–55 m at the eastern end of the section (Fig. 5). Historical data [5)] (October 1976 – 43 m, July 1977 – 28 m, August 1978 – 43 m, September 1979 – 19 m, October 1981 – 25 m, August 1982 – 28 m) indicate the same.

The western two-kilometer section is fairly stable under any waves and features a wider beach than the typically eroded eastern section (2–3.7 km) even after the installation of new groins on the eastern section in 2017.

A noticeable beach protrusion at the eastern end of the early 20th century groin group, near the breakwaters, was observed throughout the measurement period (2016–2023), before and after their installation. The local beach dynamics was similar to that of adjacent sections, indicating that the breakwaters did not influence on the beach morphodynamics.

The orientation of the wind-wave vector also plays an important role in the dynamics of the studied beach. Westerly and northerly winds contribute to surge

[5)] Personal archive of O. I. Ryabkova.

F i g . 4 . The beach dynamics after the installation of the breakwaters in 2021–2023: *a* – summer accumulation, 06.09.2021; *b* – beach narrowing after extreme storms, 02.02.2022; *c* – the state of the beach after the storm period, 05.05.2022; *d* – beach nourishment in the finishing phase of the winter storm, 19.12.2022; *e* – the beach restored by moderate spring waves, 12.05.2023; *f* – beach narrowing due to a noticeable increase in the sea level, 11.08.2023. Photo by A.N. Babakov

and beach erosion, while easterly and southerly winds restore the beach. Thus, in April–June 2023, moderate easterly winds dominated, which led to the sea level drop by 10–15 cm below the long-term average water level and the formation of a very wide beach (see the chart for 12 May 2023 in Fig. 5). However, a reversal of moderate wind to the southwestern quarter (July–August) resulted in a 45 cm rise in level and a marked narrowing of the beach (11 August 2023). It should be added that the beach was even narrower during a moderate south-westerly storm (8 August 2023), but three days after the end of the storm, an 8–12-meter wide sandy strip had already been washed up across the entire section.

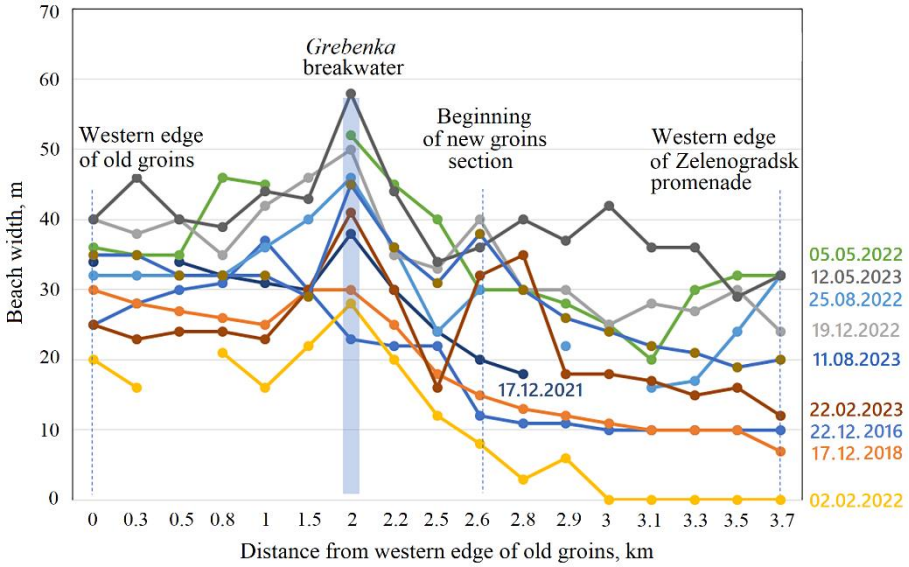

Fig. 5. Seasonal dynamics of the beach width (for 2016–2023) in the area from the western edge of the wooden groins (early 20th cent.), including the area of new groins, up to the western edge of the promenade in Zelenogradsk. The location of the breakwaters is shown with a blue bar

Monitoring by the State Budgetary Institution Baltberegozashchita in 2020–2023 near the breakwater also recorded the presence of a stable wide beach both before and after the breakwater installation. The fact that after the installation of the breakwater modules by 23.06.2021, the beach became slightly narrower than before the installation, confirms the absence of accumulative effect in the shade of the breakwater (Fig. 6). Apparently, the beach narrowing is related to the above-mentioned sea level and wave activity fluctuations, whereas the longitudinal variations of the water's edge are related to the spatial heterogeneity of the wave field and morphology of the underwater slope.

Detailed measurements of the beach width at three cross-sections opposite the breakwater from March 2022 to August 2023 confirmed the close dependence of beach dynamics on wind and wave action. Weak, unstable winds (March to June 2022) following a series of February storms contributed to significant beach widening, but wind transition to the south-westerly quarter and its intensification to 12–15 m/s was accompanied by beach narrowing. Subsequent alternation of easterly winds (December 2022, March–May 2023) with southwesterly winds (January–February 2023, July–August 2023) caused corresponding beach widening and narrowing (Fig. 7).

An analysis of aerial photographs showed that during the experiment period the underwater bar was no more than 100 m away from the water's edge. The width of the bar (according to the data taken at the cross-sections: polygons *4*, *5*, *6* in Fig. 8) varied significantly from 10 to 70 m and the width of the beach varied

Fig. 6. Interannual dynamics of the water's edge near the breakwater before and after its installation (2014 – GoogleEarth source, 2018 – satellite image ResursP, 2021 – GPS tracing)

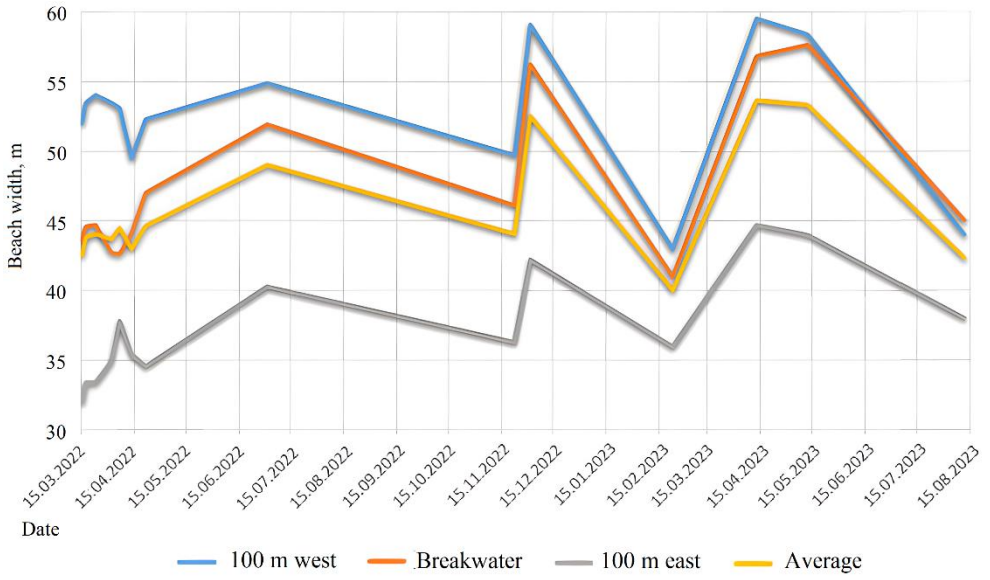

Fig. 7. Intra-annual beach dynamics on a 200 m long section opposite the breakwater according to measurements of GBU KO *Baltbergozashchita* at three cross sections (lines *5* in Fig. 3), 15.03.2022–11.08.2023

from 10 to 15 m. No correlation between the longshore distributions of width values was observed (correlation coefficients from –0.15 to 0.34 on different dates). Alongshore variations in the distance from shore of the coastal and seaward boundaries of the underwater bar on some days correlated with a coefficient of 0.64–0.70.

An analysis of the underwater bar dynamics showed significant variability in its configuration, width and location of its seaward and coastal boundaries (Fig. 8). It is clearly seen that the structure of the underwater bar does not correlate with the presence of groins and the shoreline irregularity. The presence of the *Grebenka* breakwater does not affect the structure of the underwater bar and the water's edge position. Of note, in the area without groins, the shoreline is more flattened. A festooned shoreline structure was recorded several times in the section with groins, when the festoons edges overlapped the position of the groins.

In the study area, the underwater coastal slope between 0 and 5 m depth is characterised by an average inclination of about 0.016 (or 1:64). At the time of the 07.09.2022 survey, the top of the longshore underwater bar (Fig. 9) was adjacent to the breakwater line. However, this was a coincidental event in the dynamics of the underwater bar, as, e. g., during measurements on 23.04.2023, its top was 30 m seaward than the breakwater line and the depth in the area of the seaward breakwater modules increased by 0.5 m (Fig. 9).

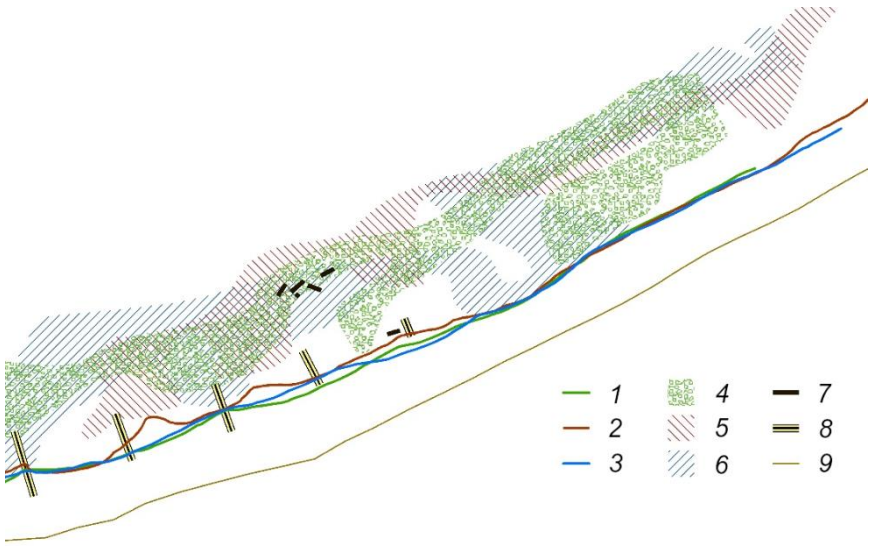

Fig. 8. The visible position of the water's edge on 10.08.2022 (*1*), 24.09.2022 (*2*), 01.11.2022 (*3*) and the underwater longshore bar on 10.08.2022 (*4*), 24.09.2022 (*5*), 01.11.2022 (*6*). The figure shows positions of the breakwater modules (*7*), old wooden groins (*8*) and the reference line of the artificial foredune edge (*9*)

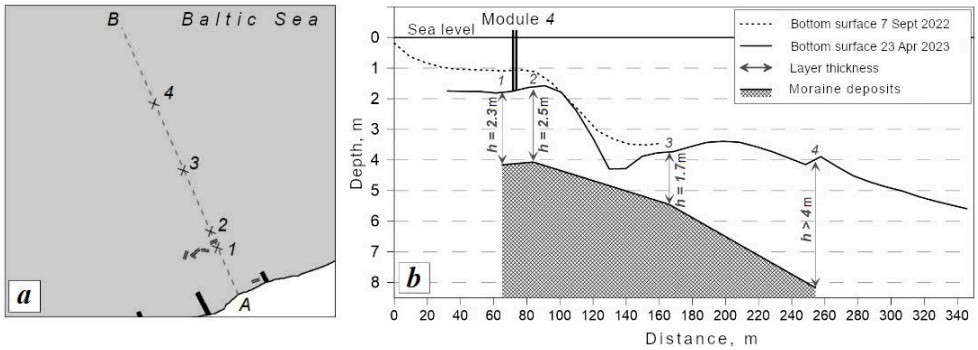

Fig. 9. The profile of the coastal slope and the loose sediment thickness: *a* – the layout of the profile line and points of measurement of the loose sediment thickness; *b* – profiles of depths and the loose sediment thickness

The measurements on 7 September 2022 and 23 April 2023 illustrate the variability in the depth profile around the seaward modules associated with the migration of the underwater bar due to storm events in January 2023 (see Table).

At the maximum overlap area of the 7 September 2022 and 23 April 2023 measurement areas of 19,000 m^2 (Fig. 10), 5,000 m^3 of sand was lost between 7 September 2022 and 23 April 2023, with an average depth increase of 26 cm. In the area of the *Grebenka* breakwater modules (contoured by the black rectangular in Fig. 10, with an area of 6,700 m^2 covering the top of the underwater bar and its rear part behind the breakwaters), 2.7 thousand m^3 of sand was lost and the depth increased by 41 cm on average. The calculated deformation values ranged [–2.4...–0.9] m.

The measurements illustrate the changes in depth structure around the breakwater modules associated with the impact of the winter 2023 storm: a general deepening across the section and a lowering of depths behind the breakwaters. Given that depths around the breakwater modules were over 2 m in spring 2021 and approximately 1 m in September 2022 (measured on 7 September 2022), it is reasonable to conclude that storm characteristics vary significantly.

In order to assess the possible dynamics of the underwater shoreline slope around the breakwater over a longer period, we used the results of measurements for a similar area near the Zelenogradsk pier. The pier is located within the same lithodynamic shore segment 2 km east of the breakwater. Along the eastern edge of the pier (140 m long), which runs perpendicular seawards, depth was measured from early 2016 with a hand lead three to four times per year in 8.5 m increments, which corresponded to half the distance between the pier piles. The typical depth at the end of the pier was 3.5–4.5 m. On rare occasions of the underwater bar top's displacement towards the pier end at low sea level, the depth there was 2.0–2.2 m (20 April 2017 and 12 May 2023).

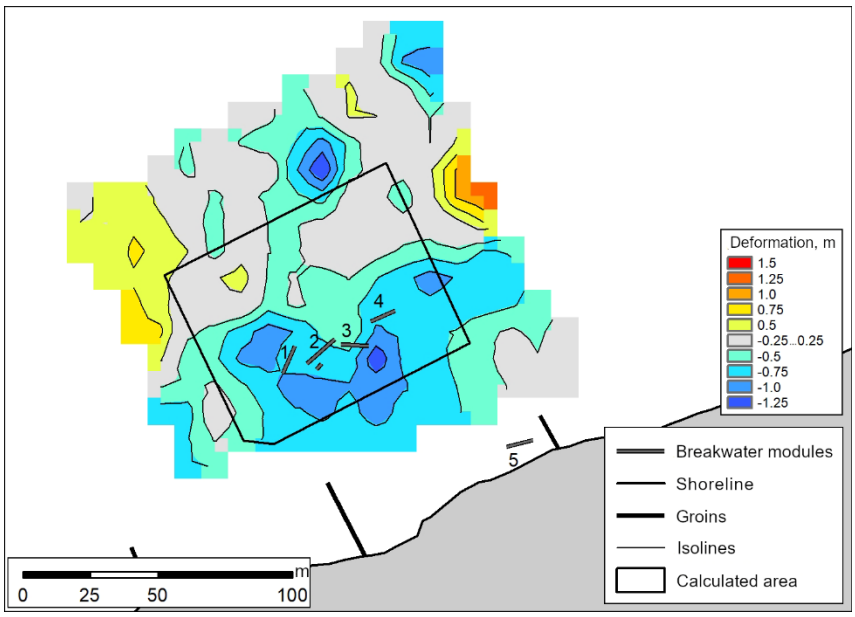

Fig. 10. Diagram of the bottom relief deformation for 07.09.2022–23.04.2023 (positive values – accumulation, negative values – erosion), the calculated area for estimation of volumetric deformations of the coastal slope is delineated in black

The section near the pier of Zelenogradsk may serve as an analogue to the section with modules only in terms of deformations associated with underwater bar migration, but not in terms of absolute depths and inclination of the underwater shore slope. This is because the thickness of the sandy sediments layer (loose sediments) in the area of the old groins (where the breakwater modules are located) is generally significantly greater than in the area of the pier in Zelenogradsk. For this reason, in March 2022, when the Baltic Sea level was extremely low, exposures of the underwater bar closest to the edge were observed along the entire section of the early 20th century groins and elsewhere along the shore, but not near the Zelenogradsk pier.

The data of measurements along the pier in 2016–2023 illustrate various situations: both when the top of the underwater bar was close to the water's edge (a quieter period of the year, at a depth of 2.2–3.7 m), and when it was significantly seaward (a storm period, at a depth of 4–5 m). By analogy to the breakwater section, it can be said that deformation of the underwater shore slope due to the migration of the coastal bar near the breakwater modules could be 2–2.7 m. This is comparable to the height of the structures themselves and may cause their subsidence to sand almost up to their full height.

We used the results of measurements (23 April 2023) carried out by the hydraulic washing method to construct a plot of thickness variations of the loose sediment (sand) layer along the profile perpendicular to the shore and passing through module 4 of the breakwater (Fig. 9). The loose sediment layer thickness was 2 m thick at a distance of 70 m from the water's edge at the rear of the breakwater (Fig. 9, *b*), from 3 m at the underwater bar top, from 0.5 m at the seaward base of the underwater bar, and 4 m at the seaward end of the profile. The inclination of the underlying surface was approximately 0.017 (or 1:59). Based on the geometric characteristics of the breakwater, its modules did not reach the level of the moraine bedrock when subsided in loose sediment (sand). Their subsidence was 0.5–1.5 m.

For technical reasons, the currents were measured from 12:00 on 23.04.2023 to 12:00 on 28.04.2023, and only a short-term episode of wind strengthening and wave increase was recorded. According to the surface wave reanalysis data in point *A* (Fig. 1), a westerly wind persisted during the inclinometric measurements and forming waves (the significant wave height averaged 0.6 m and the period averaged 2.3 s) propagating southeasterly (Fig. 11).

The most active waves were observed on 26–28 April 2023 under rather weak westerly wind with an average speed up to 5 m/s and gusts up to 13 m/s. The waves formed in the westerly wind, refracting on the relief, although turning towards the shore, ran over the breakwater module virtually with zero angle of attack, very close to the line of its strike. That is why the obtained record is not so indicative to judge the damping of waves on the breakwater module. The instantaneous (pulsation) values of wave velocities (Fig. 11) obtained from the two sides of the breakwater module did not differ significantly, and the current velocities from the seaward side of the breakwater slightly exceeded those from the shore side.

For the averaged characteristics, the opposite situation is observed: the average velocities from the frontal side of the breakwater are slightly less than the velocities behind the breakwater, which may be a consequence of the calculation of integral velocities using vector averaging laws. Wave motions from the seaward side

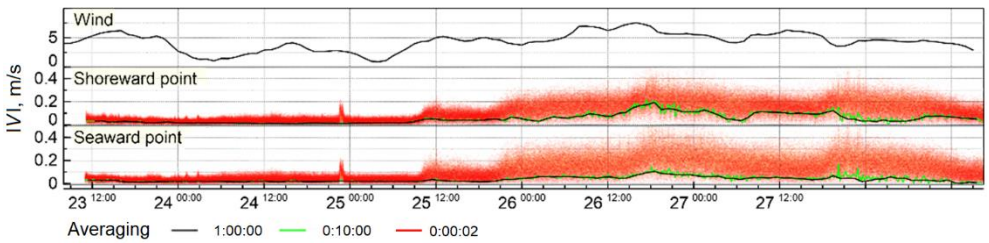

Fig. 11. Results of registration of the absolute flow velocity with inclinometers from 12:00 on 23.04.2023 to 12:00 on 28.04.2023. Red colour is instantaneous values of current velocities, green colour is 10-minute averaging, black colour is one-hour averaging

a ***b***

Fig. 12. Exposure of the top of the underwater alongshore bar in March 2022 shortly before its attachment to the water's edge at an extremely low sea level: *a* – the shore segment where the breakwater was installed (red arrows); *b* – the shore segment 400 m west of the breakwater installation site

of the breakwater are naturally asymmetric due to wave deformation on the relief, so their average value is not equal to zero. However, the waves from the shore side of the breakwater are significantly more asymmetric due to its influence, and as a result, the averaged (integral) current velocities may turn out to be larger than the velocities of the incoming wave.

The episode of extreme sea level lowering in March 2022 should be discussed separately (Fig. 12). Within a few weeks, the shoals near the water's edge along the entire coast became exposed in places where the underwater bar was in a state prior to its seasonal attachment to the beach in May 2022 (see the characteristic increase in beach width on 05.05.2022 in Fig. 5).

Notably, this exposure was most substantial in the inter-groin segment where the breakwater was installed (Fig. 12, *a*), although there were similar exposures nearby 200 m to the east and in other inter-groin segments to the west (Fig. 12, *b*). This probably indicates the influence of the breakwater when it retained its original configuration. It is not possible to state this reliably as in-depth monitoring was not undertaken at that time.

Conclusions

The studies showed that the beach width on the eastern flank of the Zelenograd concavity, including that at the location of the experimental breakwater installation, experiences natural seasonal and synoptic variations depending on sea level and wave action. We recorded a significant variability in the configuration of the underwater alongshore bar, the location of its seaward and coastal boundaries, and its width. The structure of the underwater bar correlated with neither the presence of groins, nor the shoreline irregularity, nor the presence of the breakwater. The migration

of the alongshore bar provided significant depth variations (up to 1 m) at the breakwater location. Deformation during the 2022–2023 autumn–winter storms varied between [–2.4...0.9] m. Storm movements in the sandy base (the recorded values of loose cover thickness were from 0.5 to 2 m) contributed to subsidence of the structures by 0.5–1.5 m.

The beach width at the location of the *Grebenka* breakwater and at adjacent sections changed synchronously, which indicates a unified response to external impacts of the entire lithodynamic segment of the shore within which the breakwaters were installed.

It was expected that after the breakwater installation, the experiment would show progradation of the water's edge relative to the neighbouring areas and, under favourable conditions, formation of a tombolo behind the breakwater. However, no positive effect of the installed modules on beach dynamics was noted on either a seasonal or inter-annual time scale. The exception was the extreme low sea level event in March 2022, when the exposure of the tops of the underwater bar was more clearly observed (compared to similar neighbouring sections) in the intergroin segment where the breakwater was installed.

The absence of an obvious resulting accumulative effect from the seaward group of breakwater modules is due to their displacement and partial subsidence in sand under the action of the wave, which disrupted the linearity of the entire structure, as well as to the decreased area of their resistance to the wave front. After the 2021–2022 winter storm period, each module was already acting as a separate structure. It was not possible to register the response of the shore before this period, since careful observations were made after the structure had been breached. Another factor that did not allow achieving a positive effect from the structure installation was the limited length of the structure relative to its distance from the water's edge.

During certain moderate waves, the beach progradated and attached itself to the coastal module creating a temporary tombolo. However, a similar progradation of the water's edge was also noted at adjacent sections. The fact that the water's edge adjoined the base of the last, easternmost groin, and this position was kept in 2023, may indicate a possible temporal (no attachment in spring 2024) positive effect for the water's edge in the shade of the coastal module.

The question of whether the permeable breakwater *Grebenka* can protect the shore from erosion was only answered in part in the course of the work due to the flaws in the design of the breakwater, which determined a very weak effect of the structure on the shore dynamics. An important result of the work is the testing of the life-size structure directly in natural conditions. The experience gained has shown the usefulness of such tests and the need for their comprehensive planning with the involvement of a wide range of specialists to assist the design engineers in taking full account of all the peculiarities of hydro-lithodynamics, geomorphological and geological features.

References

1. Mentaschi, L., Vousdoukas, M.I., Pekel, J.-F., Voukouvalas, E. and Feyen, L., 2018. Global Long-Term Observations of Coastal Erosion and Accretion. *Scientific Reports*, 8, 12876. https://doi.org/10.1038/s41598-018-30904-w
2. Kaehler, C., Cantré, S., Schweiger, C. and Saathoff, F., 2022. Dune Erosion at the German Baltic Coast–Investigation and Analysis of a Large-Scale Field Experiment Compared to Life Dunes. *Journal of Marine Science and Engineering*, 10, 1605. https://doi.org/10.3390/jmse10111605
3. Łabuz, T.A., 2014. Erosion and its Rate on an Accumulative Polish Dune Coast: the Effects of the January 2012 Storm Surge. *Oceanologia*, 56(2), pp. 307–326. https://doi.org/10.5697/oc.56-2.307
4. Šakurova, I., Kondrat, V., Baltranaitė, E., Vasiliauskienė, E. and Kelpšaitė-Rimkienė, L., 2023. Assessment of Coastal Morphology on the South-Eastern Baltic Sea Coast: The Case of Lithuania. *Water*, 15(1), 79. https://doi.org/10.3390/w15010079
5. Harff, J., Furmanczyk, K. and von Storch, H., eds., 2017. *Coastline Changes of the Baltic Sea from South to East. Past and Future Projection*. Cham: Springer. Vol. 19, 388 p. https://doi.org/10.1007/978-3-319-49894-2
6. Bagdanavičiūtė, I., Kelpšaitė, L. and Daunys, D., 2012. Assessment of Shoreline Changes Along the Lithuanian Baltic Sea Coast During the Period 1947–2010. *Baltica*, 25(2), pp. 171–184. https://doi.org/10.5200/baltica.2012.25.17
7. Karmanov, K., Burnashov, E. and Chubarenko, B., 2018. Contemporary Dynamics of the Sea Shore of Kaliningrad Oblast. *Archives of Hydro-Engineering and Environmental Mechanics*, 65(2), pp. 143–159. https://doi.org/10.1515/heem-2018-0010
8. Sokolov, A.N., Chubarenko, B.V. and Karmanov, K.V., 2016. Hydrodynamic Conditions in the Coastal Zone of the Vistula Spit and the Sambian Peninsula: The Case of the Storm in January 2012. *KSTU News*, 43, pp. 67–77 (in Russian).
9. Bobykina, V.P., Stont, Zh.I. and Kileso, A.V., 2021. Deformations of the Marine Coastline of the Curonian Spit (South-Eastern Baltic Sea) During Autumn-Winter Season of 2018–2019. *IKBFU's Vestnik. Series: Natural and Medical Sciences*, (2), pp. 73–83 (in Russian).
10. Stont, Z.I., Navrotskaya, S.E. and Chubarenko, B.V., 2020. Long-Term Tendencies in Variations of Hydro-Meteorological Characteristics in Kaliningrad Oblast. *Journal of Oceanological Research*, 48(1), pp. 45–61. https://doi.org/10.29006/1564-2291.JOR-2020.48(1).3 (in Russian).
11. Navrotskaya, S.E. and Chubarenko, B.V., 2017. On the Increase of the Annual and Seasonal Values of Water Level in the Mouth of the Pregolya River (the Baltic Sea) in 1996–2015. *Proceedings of the Russian Geographical Society*, 149(2), pp. 16–30 (in Russian).
12. Bass, O.V., 2015. [Modern Concept of Coastal Protection and Hydraulic Engineering on Sea Shores of the Kaliningrad Region]. *IKBFU's Vestnik*, (1), pp. 138–144 (in Russian).
13. Chubarenko, B., Domnin, D., Simon, F.-G., Scholz, P., Leitsin, V., Tovpinets, A., Karmanov, K. and Esiukova, E., 2023. Change over Time in the Mechanical Properties of Geosynthetics Used in Coastal Protection in the South-Eastern Baltic. *Journal of Marine Science and Engineering*, 11(1), 113. https://doi.org/10.3390/jmse11010113
14. Boldyrev, V.L. and Ryabkova, O.I., 2001. [Coastal Processes Dynamics on the Kaliningrad Coast of the Baltic Sea]. *Proceedings of the Russian Geographical Society*, 133(5), p. 41 (in Russian).
15. Ryabkova, O.I. and Levchenkov, A.V., 2016. Contribution of German, Soviet and Russian Researchers to the Study of the Sambia Peninsula Coast. *IKBFU's Vestnik. Series: Natural and Medical Sciences*, (3), pp. 44–70 (in Russian).

16. Chechko, V., Sokolov, A., Chubarenko, B., Dikii, D. and Topchaya, V., 2015. Dynamics of Sediments Disposed in the Marine Coastal Zone near the Vistula Lagoon Inlet, South-Eastern Part of the Baltic Sea. *Baltica*, 28, pp. 189–199. https://doi.org/10.5200/baltica.2015.28.16
17. Babakov, A.N. and Chubarenko, B.V., 2019. The Structure of the Net Alongshore Sediment Transport in the Eastern Gulf of Gdansk. *Water Resources*, 46(4), pp. 515–529. https://doi.org/10.1134/S0097807819040031
18. Sokolov, A. and Chubarenko, B., 2018. Numerical Simulation of Dynamics of Sediments Disposed in the Marine Coastal Zone of South-Eastern Baltic. *Baltica*, 31(1), pp. 13–23. https://doi.org/10.5200/baltica.2018.31.02
19. Bass, O.V. and Zhindarev, L.A., 2007. Technogenesis in the Sand Coastal Zone of Inland Seas (Paper 1. The Mineral Industry Impact on Morpholitodynamics of South-Eastern Baltic Coastal Zone). *Geomorfologiya*, (4), pp. 17–24 (in Russian).
20. Burnashov, E., Chubarenko, B. and Stont, J., 2010. Natural Evolution of Western Shore of a Sambian Peninsula on Completion of Dumping from an Amber Mining Plant. *Archives of Hydro-Engineering and Environmental Mechanics*, 57(2), pp. 105–117.
21. Marcinkowski, T. and Szmytkiewicz, M., 2013. Performance of Submerged Breakwaters as Improvement of Beach Fill Effectiveness in Gdynia, Poland. *Journal of Coastal Research*, 65(sp1), pp. 326–331. https://doi.org/10.2112/SI65-056.1
22. Kubowicz-Grajewska, A., 2015. Morpholithodynamical Changes of the Beach and the Nearshore Zone Under the Impact of Submerged Breakwaters – a Case Study (Orłowo Cliff, the Southern Baltic). *Oceanologia*, 57(2), pp. 144–158. https://doi.org/10.1016/J.OCEANO.2015.01.002
23. Dikii, D.I., Efremov, V.I., Chubarenko, B.V., Domnin, D.A., Zakirov, R.B., Burnashov, E.M., Karmanov, K.V. and Bass, O.V., 2024. Testing of a Piled (Permeable) Breakwater Made of Composite Material for Coastal Protection. Part 1: Installation Conditions and Stability Assessment. *Ecological Safety of Coastal and Shelf Zones of Sea*, (3), pp. 79–92.
24. Burnashov, E.M., Chubarenko, B.V., Cherkasov, S.S. and Karmanov, K.V., 2022. Shore Protection System for Coastal Region: Experience of the Kaliningrad Oblast. In: B. V. Chubarenko, ed., 2022. *Proceedings of All-Russian Conference with International Participation "XXIX Coastal Conference: Field-Based and Theoretical Research in Shore Use Practice"*. Kaliningrad, April 18–24, 2022. Kaliningrad: Izd-vo BFU im. I. Kanta, pp. 17–19 (in Russian).
25. Bass, O.V., Vasutkin, E.S. and Efremov, B.I., 2021. Approach to Reducing Shore Erosion Based on Application of Composite Pile Breakwater "Comb". *Construction Economic and Environmental Management*, (3), pp. 124–133. https://doi.org/10.37279/25194453-2021-3-124-133 (in Russian).
26. Sokolov, A.N. and Chubarenko, B.V., 2017. Efficiency Analysis of the Sea Disposal of Dredging Material from the Coastal Protection Point of View. *KSTU News*, 45, pp. 102–111 (in Russian).
27. Ostrowski, R. and Stella, M., 2016. Sediment Transport Beyond the Surf Zone Under Waves and Currents of the Non-Tidal Sea: Lubiatowo (Poland) Case Study. *Archives of Hydro-Engineering and Environmental Mechanics*, 63(1), pp. 63–77. https://doi.org/10.1515/heem-2016-0005
28. Leont'yev, I.O., 2012. Predicting Shoreline Evolution on a Centennial Scale Using the Example of the Vistula (Baltic) Spit. *Oceanology*, 52(5), pp. 700–709. https://doi.org/10.1134/S0001437012050104

29. Chubarenko, B.V., Sokolov, A.N. and Dikii, D.I., 2023. Variability of the Coastal Currents, Waves and Wind Surge Along the Shore of the South-Eastern Baltic (Kaliningrad Oblast, Russian Federation). *Regional Studies in Marine Science*, 57, 102762. https://doi.org/10.1016/j.rsma.2022.102762

30. Stont, Z.I., Bobykina, V.P. and Ulyanova, M.O., 2023. "Diving" Cyclones and Consequences of Their Impact on the Coast of the South-Eastern Baltic Sea. *Russian Journal of Earth Sciences*, 23(2). https://doi.org/10.2205/2023ES000827

31. Paka, V.T., Nabatov, V.N., Kondrashov, A.A., Korzh, A.O., Podufalov, A.P., Obleukhov, S.D., Golenko, M.N. and Shchuka, S.A., 2019. On the Improvement of the Tilting Bottom Current Meter. *Journal of Oceanological Research*, 47(2), pp. 220–229. https://doi.org/10.29006/1564-2291.JOR-2019.47(2).13 (in Russian).

Submitted 25.07.2024; accepted after review 02.11.2024;
revised 17.12.2024; published 31.03.2025

About the authors:

Boris V. Chubarenko, Leading Research Associate, Head of the Laboratory of Coastal Systems, Shirshov Institute of Oceanology of Russian Academy of Sciences (36 Nakhimovskiy Ave., Moscow, 117997, Russian Federation), PhD (Phys.-Math.), **ORCID ID: 0000-0001-7988-1717, Scopus Author ID: 6507102508**, *chuboris@mail.ru*

Dmitry I. Dikii, Junior Research Associate, Shirshov Institute of Oceanology of Russian Academy of Sciences (36 Nakhimovskiy Ave., Moscow, 117997, Russian Federation), PhD (Tech.), **ORCID ID: 0000-0002-8819-8423, Scopus Author ID: 56998707400**, *dimandikiy@mail.ru*

Dmitry A. Domnin, Senior Research Associate, Shirshov Institute of Oceanology of Russian Academy of Sciences (36 Nakhimovskiy Ave., Moscow, 117997, Russian Federation), PhD (Geogr.), **ORCID ID: 0000-0001-8627-2055, Scopus Author ID: 9250345600**, *dimanisha@gmail.com*

Ruslan B. Zakirov, Research Associate, Shirshov Institute of Oceanology of Russian Academy of Sciences (36 Nakhimovskiy Ave., Moscow, 117997, Russian Federation), PhD (Geogr.), **Scopus Author ID: 57222497041**, *zakirov.ruslan.kaliningrad@yandex.ru*

Aleksandr N. Babakov, Senior Research Associate, Shirshov Institute of Oceanology of Russian Academy of Sciences (36 Nakhimovskiy Ave., Moscow, 117997, Russian Federation), PhD (Geogr.), **ORCID ID: 0000-0002-8824-8929, Scopus Author ID: 41261066200,** *babakov_temp@mail.ru*

Vadim T. Paka, Chief Research Associate, Shirshov Institute of Oceanology of Russian Academy of Sciences (36 Nakhimovskiy Ave., Moscow, 117997, Russian Federation), DSc (Phys.-Math.), **ORCID ID: 0000-0003-0316-1961, Scopus ID: 7003547709,** *vpaka@mail.ru*

Aleksey A. Kondrashov, Junior Research Associate, Shirshov Institute of Oceanology of Russian Academy of Sciences (36 Nakhimovskiy Ave., Moscow, 117997, Russian Federation), **ORCID ID: 0000-0002-3684-2184, Scopus ID: 36657225800,** *kondrashoff1984@yandex.ru*

Andrey O. Korzh, Leading Engineer, Shirshov Institute of Oceanology of Russian Academy of Sciences (36 Nakhimovskiy Ave., Moscow, 117997, Russian Federation), **ORCID ID: 0000-0001-6409-8228, Scopus ID: 15080985900,** *andrey.korzh@atlantic.ocean.ru*

Evgeny M. Burnashov, Deputy Director for Monitoring and Security of Hydraulic Facilities, GBU KO *Baltberegozashhita* (1 Khutorskaya Str., Kaliningrad Oblast, Svetlogorsk, 238560, Russian Federation), PhD (Geogr.), **Scopus Author ID: 41261235800**, *burnashov_neo@mail.ru*

Konstantin V. Karmanov, Graduate Student, Kaliningrad State Technical University (1 Sovetsky Drive, Kaliningrad, 236000, Russian Federation), **Scopus Author ID: 55377991800**, *konstantin.karmanoff@yandex.ru*

Oleg V. Bass, Associate Professor, Institute of High Technology, Immanuel Kant Baltic Federal University (14 Aleksandra Nevskogo Str., Kaliningrad, 236041, Russian Federation), PhD (Geogr.), **Scopus Author ID: 57219593321**, *o.bass@mail.ru*

Vladimir I. Efremov, Executive Director, LLC Trading House Basalt Pipes (29, Bldg 4, Petrovsko-Razumovsky Drive, Moscow, 127287, Russian Federation), *zbt@bk.ru*

Olga I. Ryabkova, Associate Professor, Immanuel Kant Baltic Federal University (14 Aleksandra Nevskogo Str., Kaliningrad, 236041, Russian Federation), PhD (Geogr.), **ORCID ID: 0000-0002-4562-4162**, *ryabko5195@mail.ru*

Contribution of the authors:

Boris V. Chubarenko – work supervision, analysis of all results and drawing general conclusions, planning and final editing of the paper text

Dmitry I. Dikii – analysis of storm activity reanalysis data, collection of material for the review, preparation of the first paper version, grouping of material and finalization of the paper text

Dmitry A. Domnin – aerial survey, analysis of the results and preparation of illustrations on the underwater bar dynamics

Ruslan B. Zakirov – measurement works, participation in loose sediment thickness determination, analysis of measurement results, preparation of relevant illustrations on measurements and loose sediment thicknesses

Aleksandr N. Babakov – collection and analysis of data on long-term beach dynamics and underwater slope dynamics in the Zelenogradsk area, detailed analysis of data on the relationship between beach dynamics and meteorological conditions

Vadim T. Paka – supervision of measurements of currents and loose sediment thickness, analysis of the results and drawing appropriate conclusions

Aleksey A. Kondrashov – carrying out currents measurements, including preparation of the tool set, analysis of measurement results

Andrey O. Korzh – carrying out works and mathematical analysis of the results of currents measurements, preparation of appropriate illustrations

Evgeny M. Burnashov – analysis of the results and contribution to overall conclusions

Konstantin V. Karmanov – leveling and aerial surveys, observations of beach widths, analysis of the data obtained

Oleg V. Bass – participation in structure installation, taking measurements in 2022, photographing the structure condition, participation in drawing conclusions on the structure

Vladimir I. Efremov – development of the breakwater design, supervision of and participation in installation, photographing the structure condition, partial funding of the works, drawing conclusions and recommendations regarding the structure

Olga I. Ryabkova – analysis of data on the source of sediment from dredging operations in the Pionersky port

All the authors have read and approved the final manuscript.

Original paper

Intensity of Coastal Upwellings of the Southern Coast of Crimea and their Impact on the Oxygen Regime of the Water Area

E. E. Sovga [1] *, T. V. Khmara [1], I. V. Mezentseva [2]

[1] *Marine Hydrophysical Institute of RAS, Sevastopol, Russia*

[2] *Sevastopol Branch of the Federal State Budgetary Institution N.N. Zubov State Oceanographic Institute, Sevastopol, Russia*

* *e-mail: science-mhi@mail.ru*

Abstract

The paper analyses long-term data of the MHI Oceanological Data Bank for spring-summer seasons (May–September) of 1986–2000 and 2007–2023 and assesses the conditions of upwelling occurrence, their duration, influence on the change of temperature and oxygen regimes and content of nutrients in the water area of Goluboy and Yalta Bays. Fourteen upwellings were detected during the mentioned periods. The volume of analysed data was 3288 values of depth, temperature, sigma-t, oxygen content and nutrients. Upwellings recorded in the first period (1986–2000) were observed only in the Yalta Bay water area. They are characterised by large temperature variations, significant changes in sigma-t and for May upwellings by very high values of oxygen content. An analysis of the current MHI database from 2007 to 2023 allowed us to identify upwellings in the waters of Goluboy Bay, including the area of the stationary oceanographic platform, in July 2007, May 2010, 2012 and 2013, June and September 2013 and June 2021. We compared the temperature, coastal sigma-t and oxygen content for May and June 2012, 2013 and June 2021 and concluded that the intensity of upwellings had significantly decreased, the reasons for which are still unclear and may require further research. The paper considers differences in the content of biogenic nitrogen and phosphorus in the coastal water areas of the Southern Coast of Crimea during upwellings. These differences were manifested in the increase in the content of mineral forms of phosphorus and insignificant change in the content of mineral complexes of nitrogen. The analysis of the used database for these periods showed the insufficiency of target measurements and the need to adjust the monitoring system, especially in the spring–summer period, when the probability of upwelling is maximum.

Keywords: coastal upwelling, Southern Coast of Crimea, temperature regime, oxygen regime, nutrients

Acknowledgements: The work was performed under state assignment of MHI RAS on topic FNNN-2024-0016 “Studies of spatial and temporal variability of oceanological processes in the coastal, near-shore and shelf zones of the Black Sea influenced by natural and anthropogenic factors on the basis of in situ measurements and numerical modelling”.

For citation: Sovga, E.E., Khmara, T.V. and Mezentseva, I.V., 2025. Intensity of Coastal Upwellings of the Southern Coast of Crimea and their Impact on the Oxygen Regime of the Water Area. *Ecological Safety of Coastal and Shelf Zones of Sea*, (1), pp. 96–111.

Интенсивность прибрежных апвеллингов Южного берега Крыма и их влияние на кислородный режим акватории

Е. Е. Совга [1] *, **Т. В. Хмара** [1], **И. В. Мезенцева** [2]

[1] *Морской гидрофизический институт РАН, Севастополь, Россия*

[2] *Севастопольское отделение Государственного океанографического института им. Н. Н. Зубова, Севастополь, Россия*

* *e-mail: science-mhi@mail.ru*

Аннотация

Проанализированы многолетние данные Банка океанологических данных МГИ за весенне-летние сезоны (май – сентябрь) 1986–2000 и 2007–2023 гг., оценены условия возникновения апвеллингов, их продолжительность, влияние на изменение температурного и кислородного режимов и содержание биогенных элементов в акватории Голубого и Ялтинского заливов. В указанные периоды обнаружено 14 апвеллингов. Объем проанализированных данных составил 3288 значений глубины, температуры, плотности, содержания кислорода и биогенных элементов. Апвеллинги, зафиксированные в первый период (1986–2000 гг.), отмечены только в акватории Ялтинского залива, для них характерны большие перепады температуры, существенные изменения плотности воды, а для майских апвеллингов – очень высокие значения содержания кислорода. Анализ современной базы данных МГИ с 2007 по 2023 г. позволил выявить апвеллинги в акватории Голубого залива, включая район расположения стационарной океанографической платформы, в июле 2007 г., мае 2010, 2012 и 2013 гг., июне и сентябре 2013 г. и июне 2021 г. В результате сравнения температуры, плотности прибрежных вод и содержания в них кислорода за май, июнь 2012, 2013 гг. и июнь 2021 г. сделан вывод о существенном снижении интенсивности апвеллингов, причины которого пока неясны и могут стать предметом дальнейших исследований. Рассматриваются различия в содержании биогенных азота и фосфора в прибрежных акваториях Южного берега Крыма в периоды прохождения апвеллингов. Эти различия проявились в увеличении содержания минеральных форм фосфора и незначительном изменении содержания минеральных комплексов азота. Анализ используемой базы данных за указанные периоды показал недостаточность целевых измерений и необходимость корректировки системы мониторинга, особенно в весенне-летний период, когда максимальна вероятность возникновения апвеллингов.

Ключевые слова: прибрежный апвеллинг, Южный берег Крыма, температурный режим, кислородный режим, биогенные элементы

Благодарности: работа выполнена в рамках государственного задания ФГБУН ФИЦ МГИ по теме FNNN-2024-0016 «Исследование пространственно-временной изменчивости океанологических процессов в береговой, прибрежной и шельфовой зонах Черного моря под воздействием природных и антропогенных факторов на основе контактных измерений и математического моделирования».

Для цитирования: *Совга Е. Е., Хмара Т. В., Мезенцева И. В.* Интенсивность прибрежных апвеллингов Южного берега Крыма и их влияние на кислородный режим акватории // Экологическая безопасность прибрежной и шельфовой зон моря. 2025. № 1. С. 96–111. EDN VKPHBI.

Introduction

The coastal zone of the Southern Coast of Crimea (SCC) is characterized by significant dynamic activity, as evidenced by numerous cases of upwelling on the sea surface. Upwelling occurs when, due to the Coriolis force and viscosity, the longshore wind direction deflects surface water away from the shore and deep water moves up instead. Generally accepted criterion for determining temperature upwelling corresponds to cases with a sharp (more than 5 °C) decrease in surface water temperature [1, 2]. The structure and dynamics of coastal upwelling near the SCC were described in [3], where the authors consider two types of coastal upwelling near the SCC – Ekman wind-driven and reverse storm surge ones. Characteristics of their occurrence conditions for 1980–1985 were given and it was shown that the most intensive and long-lasting Ekman upwellings were formed near the urban-type settlement of Katsiveli (Goluboy Bay). The paper also considers the influence of upwellings on the uplift of the cold intermediate layer core closer to the surface up to 30 m horizon.

In [4], the authors consider that circulation of the coastal anticyclonic eddy is one of the internal causes creating conditions for the development of upwelling near the coast of Crimea even with the absence of wind stress longshore component or when it is weak. According to the authors of [4], the main hydrodynamic processes contributing to the occurrence of upwelling in the SCC water area are as follows:

– intense western and south-western flows of the Rim Current along the southern shores of Crimea;

– interaction of the Rim Current northern periphery with the shelf relief heterogeneities (capes, bays) of the Crimean Peninsula;

– longshore eastern and north-eastern flows of the northern peripheries of anticyclonic dynamic formations, realising the Ekman effect at longshore wind intensification;

– reverse storm surge winds from the western and northern sectors, normal to the shore.

The interaction of these factors determines complex structure and dynamics of coastal waters and influences the process of upwelling formation.

The results of determining the regularities of coastal upwelling development in the Black Sea using satellite data are presented in [5]. The Black Sea water area was zoned according to the frequency of coastal upwellings. It was shown that upwellings were more frequently observed in the north-western part of the sea and much less frequently in the area of Yalta, Feodosiya, Novorossiysk and especially near the coast of Turkey. These areas are characterised by the absence of upwellings in certain years. Their occurrence frequency is 1–8 days per month.

Identification of areas with the highest frequency of coastal upwellings during the warm period for the Black Sea was carried out in [2]. A number of satellite

images of the entire Black Sea area obtained from AVHRR sensors of NOAA satellites in 1997–2011 were analysed. The observation time interval was extended to 2015 for the SCC. Significant interannual variability of the total duration of upwellings was noted over the period under consideration. For the SCC, estimates of the interaction of the upwelling with the surrounding multiscale dynamic structures, such as the area of active anticyclonic eddies formation, under the influence of the Rim Current southwest of the SCC were presented. As a result, the width of the developed upwelling can reach 30 km near the SCC. According to the authors of [2], upwellings are a kind of windows in which the thermocline and subthermocline waters interact with the atmosphere during the warm period of the year.

An analysis of intra- and inter-annual variability of the frequency, speed and duration of westerly winds contributing to the occurrence of upwellings near the SCC is presented in [6]. Six-hourly data on wind speed components at 10 m height obtained from atmospheric reanalysis ERA5 for 1979–2021 and temperature monitoring data at the Black Sea hydrophysical subsatellite polygon of Marine Hydrophysical Institute (MHI) were used.

Upwelling is detected as temperature decreases due to the rise of colder deep waters, most often from April to October, when the surface temperature is higher than the subsurface water temperature [7]. This is most contrasting in the summer months, with the highest vertical temperature gradient in the thermocline. Such upwelling is determined by the sea surface temperature obtained from contact measurements [1], including thermistor chains installed in shelf zones [8–10], as well as from satellite data [2, 11, 12].

Using modern methods of mathematical modeling (multi-scale coupled ocean–atmosphere modeling platform NOW (NEMO-OASIS-WRF) with a resolution of 2 km), one of the cases of wind-driven coastal upwelling in the Black Sea near the SCC on 24–25 September 2013 was studied in [13], where the authors applied this model successfully in order to reproduce a sharp decrease in sea surface temperature by 10 °C within two days. The increased spatial resolution of the simulation made it possible to identify upwelling features associated with the relief and shape of the coastline.

The above studies did not assess the impact of upwelling on the water area oxygen regime, nor did they analyse the associated change in the content of hydrochemical parameters, in particular, such ecosystem components as elements of the main biogenic cycle, with their content affecting the productivity of marine coastal zone ecosystems significantly [11, 14]. Rise of deep waters saturated with nutrients provides growth of phytoplankton biomass and other components of the biosphere [15].

In [16], it was shown that the area of Goluboy Bay was a convenient polygon for synchronous remote and subsatellite studies of natural oceanological processes and impact of coastal anthropogenic sources of pollution on the state of the marine coastal environment. An undoubted advantage of this polygon is the location of

a stationary oceanographic platform (SOP) in its south-western part at a distance of 430 m from the coast near Katsiveli with a sea depth of 27 m at the sampling point, which makes it possible to monitor promptly the development of upwelling in the SCC area based on changes in surface water temperature. In [11], the upwelling that occurred in May 2010 was studied using not only contact methods but also satellite data. In [16], the authors discuss the results of expedition research conducted on the SOP by the MHI Marine Biogeochemistry Department in 2009–2014 and analyse the impact of upwelling mainly on the content of individual components of the carbonate system, dissolved oxygen and elements of the main biogenic cycle. It was shown that not affecting the content of inorganic forms of nitrogen, the powerful upwelling observed in May 2014 in the SOP area led to an increase in phosphate concentration by 3–4 times compared to background values.

In the present study, the conditions of upwelling occurrence in the water area of Goluboy (including the SOP near Katsiveli) and Yalta Bays, their duration and influence on the changes in temperature and oxygen regimes and the content of nutrients were studied. We analysed data for May–September of these periods as the season of the most frequently occurring upwellings, easily registered due to the large temperature difference between surface and deep water layers.

Given the importance of upwelling for assessing the ecological state of coastal waters, further study of this phenomenon, especially its seasonal dynamics with detailed information on oxygen and nutrient content, is particularly relevant.

The aim of the paper is to assess the intensity and duration of coastal upwellings formed in spring and summer in the water areas of Goluboy and Yalta Bays by analysing changes in sigma-t, their temperature and oxygen regimes and the content of nutrients.

Materials and methods of study

The paper analysed long-term data of the MHI Oceanological Data Bank (ODB) for 1986–2000 and 2007–2023 in order to assess the conditions of upwelling occurrence in the water area of Goluboy (including the SOP near Katsiveli) and Yalta Bays. We assessed the intensity and duration of upwelling, as well as its influence on changes in temperature and oxygen regimes, sigma-t and content of nutrients (inorganic and total phosphorus and inorganic nitrogen) for May–August. The data analysed for the selected upwellings for the 1986–2000 period (July 1986, May 1987 and 1989, July 1997) comprised 2108 values of all water parameters including oxygen and nutrients. The distribution of values by year was found to be uneven, namely, 580 – in 1986, 575 – in 1987, 666 – in 1989 and 287 – in 1997.

In 2007–2023, upwellings were recorded in July 2007, May 2010, 2012 and 2013, June and September 2013, June 2021. The analysed data comprised 1180 values of the above parameters. The distribution of values by year was found to be uneven, namely, 384 values of all analysed parameters in 2007, 224 – in 2010,

137 – in 2012, 323 – in 2013 and 112 – in 2021. Only one upwelling was identified in the provided database on 7 September 2013 with a maximum temperature difference of up to 14 °C. In the analysed MHI ODB, upwellings were not recorded for 2014 (data for July and August only), 2015 (September), 2016 (May and July), 2017 (June and September), 2018 (July), 2019 (July), 2020 (September). In the 2022 and 2023 spring–summer period (data for May–September), no upwellings were recorded in the water area of Yalta and Goluboy Bays, which was confirmed by the conclusion of the authors of [5] that the SCC coastal waters belong to the part of the Black Sea where upwellings are not registered every year.

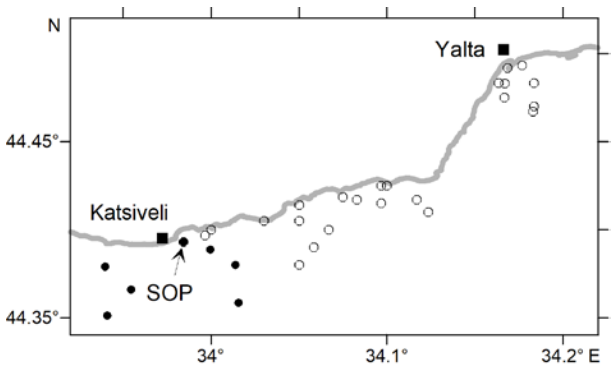

Fig. 1. Study area. The circles are stations performed in 1986–2000 and the dots are those performed in 2007–2023

Fig. 1 shows the location scheme of sampling stations.

It should be noted that three of the analysed upwellings were observed in Yalta Bay (1986–1989) and 11 ones in Goluboy Bay (1997, 2007–2021).

Results and discussion

In the SCC coastal zone (summer 1986–2000), the characteristics of coastal waters during the period of upwellings in the water area of Goluboy (including the SOP near Katsiveli) and Yalta Bays were considered. The duration of upwellings during this period varied from 6 to 28 h with a temperature decrease by 8–9 °C.

The 6 h upwelling observed on 14 July 1986 was accompanied by a decrease in temperature in the surface water layer by 8.33 °C and an increase in oxygen content to 7.76 mL/L, while before the upwelling, this value in the surface water layer was 5.39 mL/L. During the upwelling period, a vertical increase in sigma-t from 13.3 kg/m^3 near the surface to 14.1 kg/m^3 at a depth of 20 m was observed as well as an increase in oxygen content from 7.76 to 8.12 mL/L, an increase with depth in phosphates and total phosphorus content about three times, with unchanged inorganic forms of nitrogen (nitrites and nitrates).

The upwelling duration in the Yalta Bay water area on 25 May 1987 was more than a day (beginning – 25 May at 7:56 a.m., termination – 26 May at 11:00 a.m.), with a temperature difference of 8 °C (15.60–7.60 °C). The upwelling was accompanied by an increase in surface water oxygen content to 8.65 mL/L (7.04 mL/L before upwelling). Sigma-t also increased from 12.30 to 14.30 kg/m^3. An increase in phosphorus and nitrite nitrogen content was recorded on the second day of upwelling at a depth of 5 m. It should be noted that upwelling in May was also

characterised by a decrease in ammonium content as compared to the previous period.

The upwelling duration in the Yalta Bay water area on 11 May 1989 was 6 h with a temperature difference of more than 9 °C. Sigma-t also increased from 13.24 to 14.10 kg/m^3 during the upwelling and decreased up to 11.78 kg/m^3 looking past it. Of note is the higher oxygen content (8.70–9.01 mL/L) in the bay waters during the upwelling period, which persisted (8.63 mL/L) even after the upwelling termination on 15 May 1989. During the upwelling period, an increased content of total phosphorus was noted at the surface horizon, while the content of nitrates, phosphates and nitrites did not change at depth.

In the Goluboy Bay water area, the upwelling was recorded on 22 July 1997. Its duration was 7 h, with a temperature decrease of more than 9 °C. Sigma-t before its beginning was 10.47 kg/m^3 and during the upwelling period – 13.02–14.19 kg/m^3. Dissolved oxygen concentration in the surface layer was 5.86 mL/L on 18 July 1997 and 7.27–6.11 mL/L during the upwelling period. The content of biogenic compounds (phosphates, total phosphorus and nitrites) did not change vertically, with nitrates content only increased in the surface water layer.

Thus, in the first period under study, upwellings, regardless of their duration and temperature difference, were always accompanied by an increase in oxygen content and sigma-t. No such unambiguous conclusion can be made with regard to nutrients. An increase in the content of only total phosphorus and phosphates was recorded during three upwellings in July 1986, May 1987 and 1989 in the Yalta Bay water area and on 20 July 2007 in the Goluboy Bay water area, where the phosphates content increased almost three times and that of total phosphorus – one and a half times. The content of inorganic nitrogen did not change with depth during the upwelling period. A similar situation is described in [15], when under the influence of a powerful upwelling lasting one day in May 2014 in the SOP area, the content of inorganic nitrogen did not change, while the phosphates concentration increased 3–4 times compared to the background values. The reason can include differences in the cycles of these nutrients: for nitrogen, it is the water–atmosphere system and for phosphorus, it is the water–bottom system. Unlike inorganic nitrogen, phosphorus has no gaseous forms in water and its ability to accumulate near the bottom and return to the water column as a result of oxygen decrease under reducing conditions is well known. These differences are particularly evident in other water areas. Such conditions were recorded in Sevastopol Bay and described in [17]. Since upwelling is the rise of deep water, an increase in phosphorus is understandable.

In 2007–2023, the upwelling was revealed in the Goluboy Bay water area in July 2007, May 2010, 2012 and 2013, June and September 2013, June 2021. On the SOP, samples were collected at surface, 0.5 and 5.0 m horizons.

The upwelling duration on 20 July 2007 was one day, with a temperature decrease of about 10°C, sigma-t increase from 9.96 kg/m^3 (before the upwelling) to 13.86 kg/m^3 (during the upwelling) and dissolved oxygen concentration increase

from 5.5 to 7.96 mL/L at 1 m depth. The upwelling was accompanied by an increase in phosphates concentration almost three times (from 1.6 to 4.3 μg/L) and in total phosphorus – one and a half times (from 4.3 to 7.4 μg/L), with almost no effect on the content of nitrites and nitrates.

The 24 h upwelling recorded in May 2010 was accompanied by a decrease in temperature by 7.5 °C, an increase in sigma-t by about two units and a slight (up to 7.14 mL/L) increase in dissolved oxygen content.

In May 2012, several upwellings were observed: on 24 and 25 May with duration from 6 to 48 h with temperature decrease by 9.4–10.4 °C, and on 30–31 May with duration of a day with temperature decrease by more than 9 °C. All three upwellings of May 2012 were accompanied by an increase of oxygen content in the surface water layer up to 7.36 mL/L, with its content before the upwelling at 5.86 mL/L. During all three upwellings, sigma-t increased from 11.91 to 14.07 kg/m^3 (Table). The content of nutrients during the upwelling period in May 2012 was not measured.

Parameters of coastal upwellings in Yalta and Goluboy Bays found in 1986–2021

Upwelling date	Upwelling duration, h	Range of		
		sigma-t, kg/m^3	temperature, °C	oxygen content, mL/L
14.07.1986	6	11.40–13.40	13.20–21.03	5.39–7.72
25.05.1987	28	12.30–14.30	7.60–15.60	7.04–8.65
11.05.1989	6	11.80–14.10	8.30–17.30	8.63–9.01
22.07.1997	7	10.50–13.23	11.70–22.20	5.89–7.27
20.07.2007	24	10.01–13.96	14.90–25.00	5.50–7.96
27.05.2010	24	11.83–13.47	11.46–18.95	6.68–7.14
24.05.2012	6	11.91–14.03	8.15–18.61	5.86–7.36
25.05.2012	48	12.50–14.03	8.60–17.80	6.74–7.22
30.05.2012	24	12.50–14.07	8.62–18.00	6.74–7.25
25.05.2013	30	12.10–13.89	10.00–18.58	6.54–6.90
28.05.2013	5	12.01–13.78	10.20–18.76	6.25–6.83
01.06.2013	2	11.50–13.46	12.00–20.00	5.95–7.15
07.09.2013	24	11.30–13.79	10.12–21.50	5.60–7.11
02.06.2021	13	12.62–13.60	11.19–17.54	6.30–6.72

Note: The ranges of sigma-t, temperature and oxygen content are given for the surface horizon.

The overview table of all coastal upwellings detected in the MHI ODB for two periods 1986–2000 and 2007–2023 makes it possible to compare their influence on the change of water mass parameters such as sigma-t, temperature and dissolved oxygen saturation of the SCC coastal water areas on the example of Yalta and Goluboy Bays. Table does not present data on changes in the concentration of nutrients during the upwelling period because in the MHI ODB, these elements were determined only during the upwelling period in May 1987 and 1989, in July 1986, 1997 and 2007 and in September 2013. Nutrients were not determined during other upwelling periods.

The data in Table show that regardless of the upwelling duration, the change in oxygen content depends mainly on the change in sigma-t and temperature difference during the upwelling period. During the identified upwellings, temperature decreases ranged from 8 to 10.5 °C in May and July, 6.5 to 8 °C in June, with a maximum of 11.4 °C in September 2013. The increase in sigma-t resulted from the upwelling was maximum (by 2.0–2.73 kg/m^3) in July 1997 and 2007 and minimum (by 1.33 kg/m^3) in 2021. The maximum increase in dissolved oxygen content was observed in July 1986 (2.33 mL/L) and 2007 (2.46 mL/L). In May 1987 and 2012, it was 1.20–1.61 mL/L and the remaining upwellings were characterised by an increase in aeration by no more than 0.58 mL/L.

Figs. 2–5 show changes in coastal water parameters (temperature, sigma-t, oxygen content) under the influence of coastal upwellings in the Goluboy Bay water area around the SOP location in the modern period (2012–2021).

When comparing the information presented in Figs. 2, *a* and 2, *c*, a clear dependence of oxygen content on water temperature can be seen: at the upwelling, lower temperatures are accompanied by higher oxygen content. Sigma-t (Fig. 2, *b*) increases slightly at the upwelling but in contrast to temperature and oxygen content, separate decreased sigma-t lenses are observed at the surface and 5 m horizon up to a value of 12.60 kg/m^3. Later, at the upwelling over the whole area until 31 May, the sigma-t field is almost homogeneous with a value of 13.40 kg/m^3. Fig. 2, *b* also demonstrates that decreased sigma-t lenses location corresponds to the area of low oxygen concentrations.

The upwelling of 30 h duration recorded on 25 and 26 May 2013 differed from the upwelling in May 2012 by a decrease in temperature by about 8 °C and a lower difference in sigma-t from 12.10 to 13.80 kg/m^3, which was also reflected in a slight (6.54–6.86 mL/L) change in the surface water layer oxygen content (Fig. 3).

The upwelling recorded on 28 May 2013 was characterised by a duration of 5 h, temperature decrease by 8.5 °C and comparable changes in sigma-t and dissolved oxygen content (see Table). A very short (2 h) upwelling took place on 1 June 2013 (Fig. 3), with a temperature decrease of about 8 °C. It was accompanied by a decrease in oxygen content from 7.15 mL/L during the upwelling period to 5.95 mL/L

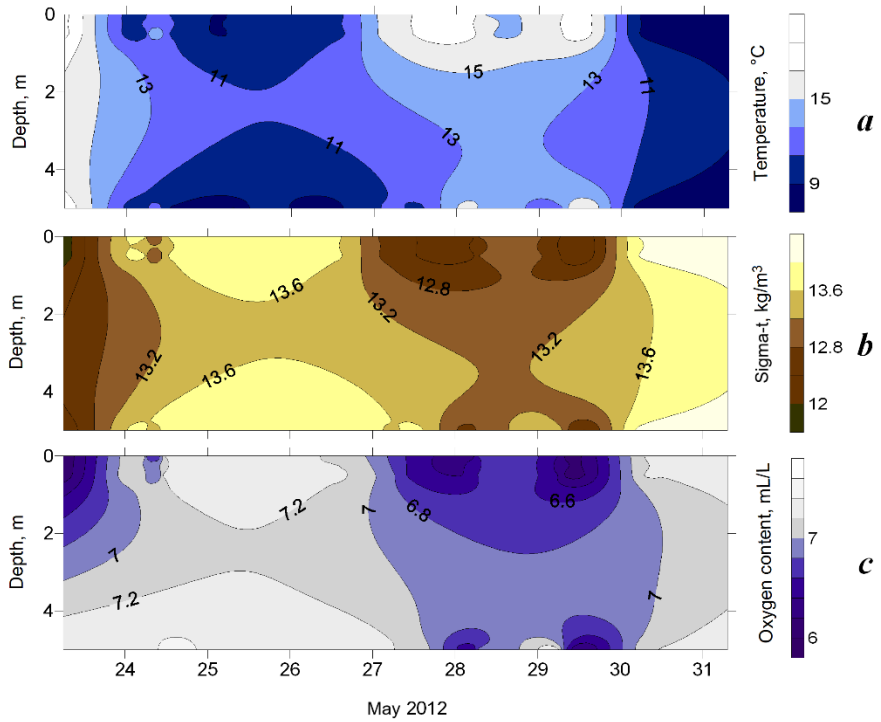

Fig. 2. Parameters of coastal waters: temperature (*a*), sigma-t (*b*) and oxygen content (*c*) during upwellings from 24 to 30 May 2012 in the Goluboy Bay water area (stationary oceanographic platform – SOP)

after its termination. Sigma-t at the surface horizon increased to 13.46 kg/m^3 during the upwelling period and decreased to 11.50 kg/m^3 after its termination.

When comparing the data presented in Figs. 2 and 3, it can be noted that in May 2013 the observed upwellings were characterised by a smaller temperature difference, sigma-t and oxygen content changes than in May 2012.

On 7 September 2013, the upwelling of 24 h duration was recorded in the Goluboy Bay water area, with a temperature difference of more than 10 °C (from 21.5 to 10.12 °C), sigma-t increase from 11.34 to 13.79 kg/m^3 and subsequent decrease after the upwelling to 5.6 mL/L with an increase in dissolved oxygen content to 7.11 mL/L (Fig. 4). In addition, the phosphates content doubled as at the upwelling in July 2007. This is also noted in the findings of [15], where the upwelling of May 2014 was described.

Higher upwelling intensity of on 7 September 2013 compared to May and June of the same year can be related to the effect of such a climatic factor as wind. In [6], in which the duration of winds favourable for the upwelling occurrence was

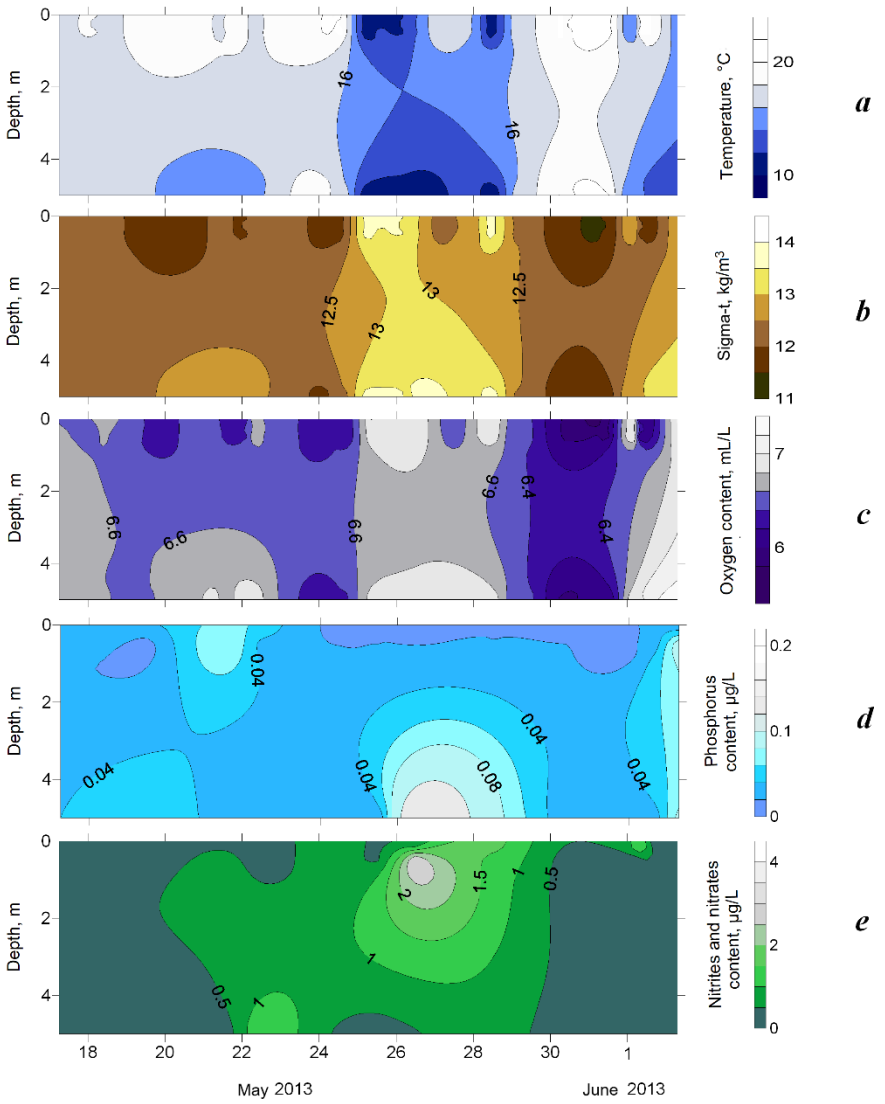

Fig. 3. Parameters of coastal waters: temperature (*a*), sigma-t (*b*), oxygen content (*c*), biogenic phosphorus (*d*) and sum of nitrites and nitrates (*e*) during upwellings from 26 to 30 May 2013 and 1 June 2013 in the Goluboy Bay water area (SOP)

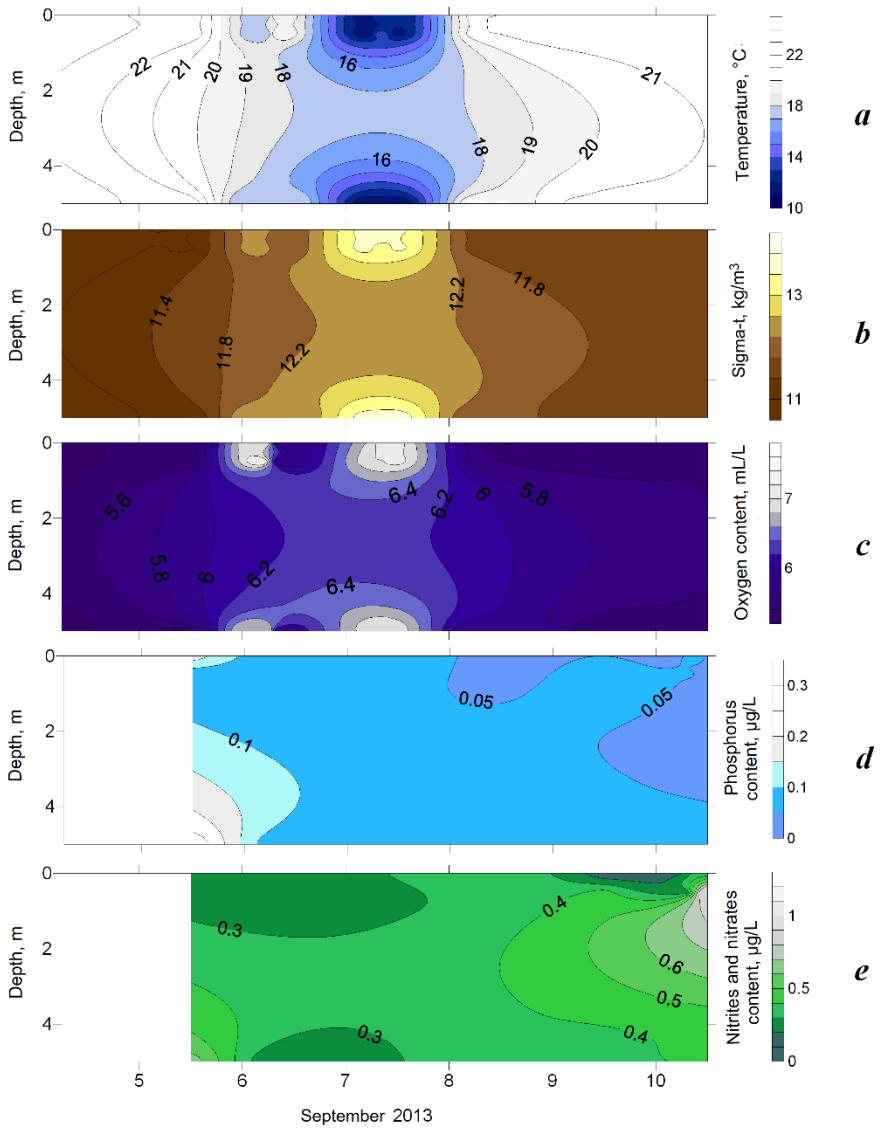

Fig. 4. Parameters of coastal waters: temperature (*a*), sigma-t (*b*), oxygen content (*c*), biogenic phosphorus (*d*) and sum of nitrites and nitrates (*e*) during an upwelling on 7 September 2013 in the Goluboy Bay water area (SOP)

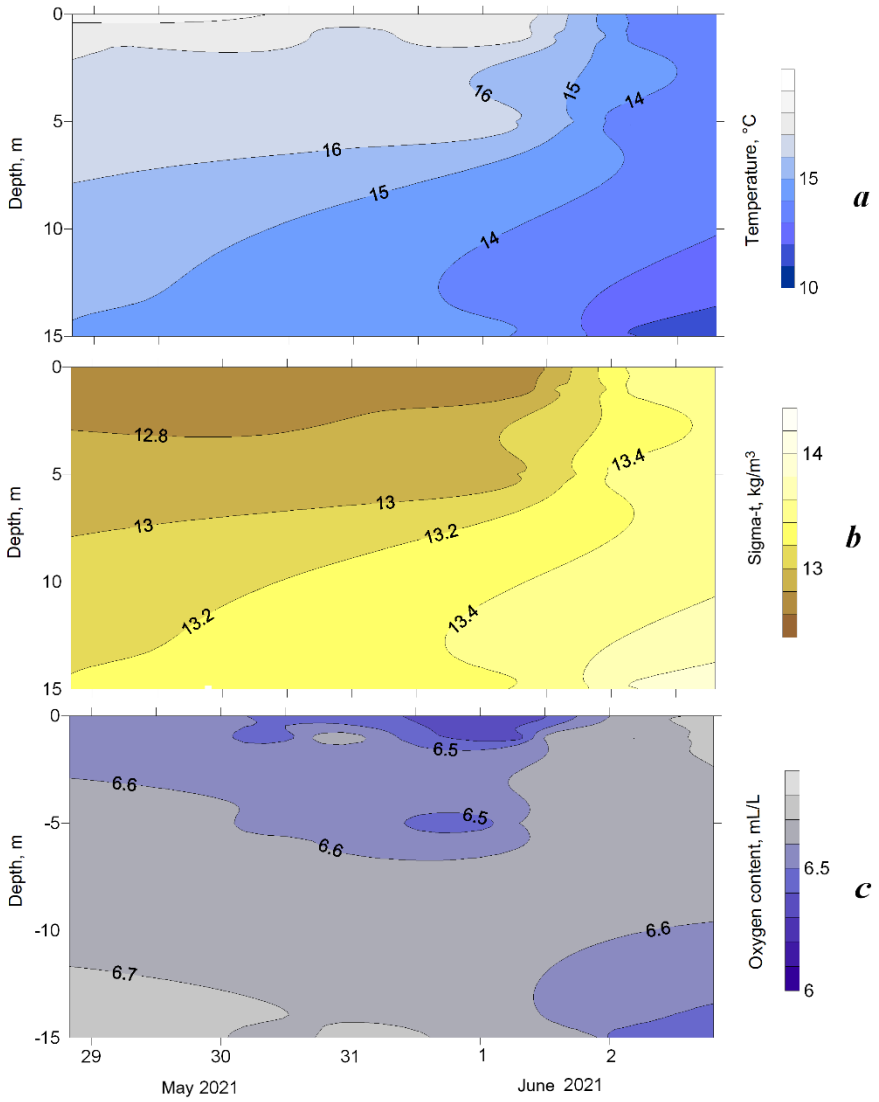

Fig. 5. Parameters of coastal waters: temperature (*a*), sigma-t (*b*) and oxygen content (*c*) during an upwelling on 2 June 2021

studied, it was shown that the longest duration (from 6 h to several days) of westerly winds had been recorded from 29 August to 8 September 2013.

The duration of the upwelling on 2 June 2021 was about 13 h (Fig. 5).

Fig. 5 shows that the upwelling of June 2021 can be characterised by minimal values of temperature difference (by about 6.5 °C), minimal change in sigma-t (by 1.33 kg/m^3) and the slightest change in oxygen content (by 0.16–0.42 mL/L).

Analysis of the information presented in Figs. 2–5 makes it possible to conclude that during the upwelling on 2 June 2021, the temperature decrease was the lowest one since 2012. This is probably why the distribution of oxygen content across all horizons (6.56–6.72 mL/L) was fairly uniform and sigma-t variation was negligible (from 12.62 to 13.52 kg/m^3).

According to the MHI ODB data, analysis of seasonal dynamics of upwelling occurrence in the SCC coastal water areas showed that eight upwellings were recorded in May, three – in July, two – in June and only one – in September.

The reasons for our finding of a slight decrease in upwelling intensity in the spring–summer period from 2012 to 2021 remain unclear, as more intense upwelling was observed in September 2013. In consideration of the intricacy of the processes that occur in the SCC coastal water areas, which are subject to factors of diverse natures, it is evident that further observations and the enhancement of the monitoring system are imperative to address the raised queries.

Conclusion

Based on the analysis of the MHI ODB *in situ* data for two periods 1986–2000 and 2007–2023, assessments of the influence of coastal upwellings on changes in temperature and oxygen regimes and content of nutrients in the Goluboy Bay water area, including the SOP in Katsiveli, and in the Yalta Bay water area were obtained. The maximum frequency of upwelling occurrence in the spring–summer season was confirmed.

It is shown that as a factor of change in water aeration, the upwelling contributes to the increase in dissolved oxygen content at any duration of its effect as a result of the accompanying temperature difference and change in sigma-t.

The upwellings recorded during the first period were noted in the Yalta Bay (three upwellings) and Goluboy Bay (one upwelling) water areas. They were characterised by large temperature differences, significant changes in sigma-t, and for the May upwellings – by very high oxygen content both before and after the upwelling. The reasons for such variability of parameters of the identified upwellings have still been unclear.

The analysis of the data for the second period (2007–2023) showed that the formed upwellings were detected in the Goluboy Bay waters, including the SOP area. Comparative analysis of information on the upwelling intensity for May and June 2012, 2013 and June 2021 made it possible to identify a significant decrease in the upwelling intensity based on changes in coastal water parameters (temperature, sigma-t and oxygen content), the reasons for which remain unclear and can be further studied.

It was concluded that the rise of deep water resulted from the upwelling contributed to the increase in the content of mineral forms of phosphorus and affected insignificantly the concentration of mineral complexes of nitrogen. The assumption that the difference in changes in the content of these biogenic complexes under the effect of the coastal upwelling is associated with differences in the systems of their circulation and requires further research.

The analysis of the used database for these periods showed the insufficiency of target measurements and the need to adjust the monitoring system, especially in the spring–summer period, when the probability of upwelling is maximum.

References

1. Lovenkova, E.A. and Polonskii, A.B., 2005. Climatic Characteristics of Upwelling near the Crimean Coast and their Variability. *Russian Meteorology and Hydrology*, (5), pp. 31–37.
2. Stanichnaya, R.R. and Stanichny, S.V., 2021. Black Sea Upwellings. *Sovremennye Problemy Distantsionnogo Zondirovaniya Zemli iz Kosmosa*, 18(4), pp. 195–207. https://doi.org/10.21046/2070-7401-2021-18-4-195-207 (in Russian).
3. Ivanov, V.A. and Mikhailova, E.N., 2008. [*Upwelling in the Black Sea*]. Sevastopol: ECOSI-Gidrofizika, 91 p. (in Russian).
4. Repetin, L.N., Romanov, A.S. and Churilova, T.Ya., 2010. Upwelling in the Area of Anticyclone Vorticity on the South Crimea Shelf. *Ecological Safety of Coastal and Shelf Zones and Comprehensive Use of Shelf Resources*, 22, pp. 205–227 (in Russian).
5. Borovskaya, R.V., Panov, B.N., Spyrydonova, E.O., Leksikova, L.A. and Kyrylova, M.V., 2005. Black Sea Near-Coastal Upwelling and Interannual Variability of its Intensity. *Ecological Safety of Coastal and Shelf Zones and Comprehensive Use of Shelf Resources*, 12, pp. 42–48 (in Russian).
6. Shokurova, I.G., Plastun, T.V., Kasianenko, T.E., Stanichnaya, R.R., Krasheninnikova, S.B. and Simonova, Yu.V., 2023. Winds Favorable for Upwellings near the Southern Coast of Crimea. *Physical Oceanography*, 30(4), pp. 398–409.
7. Ivanov, V.A. and Belokopytov, V.N., 2013. *Oceanography of the Black Sea*. Sevastopol: EKOSI-Gidrofizika, 210 p.
8. Tolstosheev, A.P., Motyzhev, S.V. and Lunev, E.G., 2020. Results of Long-Term Monitoring of the Shelf Water Vertical Thermal Struture at the Black Sea Hydrophysical Polygon of RAS. *Physical Oceanography*, 27(1), pp. 69–80. https://doi.org/10.22449/1573-160X-2020-1-69-80
9. Silvestrova, K.P., Zatsepin, A.G. and Myslenkov, S.A., 2017. Coastal Upwelling in the Gelendzhik Area of the Black Sea: Effect of Wind and Dynamics. *Oceanology*, 57(4), pp. 469–477. https://doi.org/10.1134/S0001437017040178
10. Ocherednik, V.V., Zatsepin, A.G., Kuklev, S.B., Baranov, V.I. and Mashura, V.V., 2020. Examples of Approaches to Studying the Temperature Variability of Black Sea Shelf Waters with a Cluster of Temperature Sensor Chains. *Oceanology*, 60(2), pp. 149–160. https://doi.org/10.1134/S000143702001018X
11. Sur, H.İ., Özsoy, E. and Ünlüata, Ü., 1994. Boundary Current Instabilities, Upwelling, Shelf Mixing and Eutrophication Processes in the Black Sea. *Progress in Oceanography*, 33(4), pp. 249–302. https://doi.org/10.1016/0079-6611(94)90020-5
12. Borovskaja, R.V., Lomakin, P.D., Panov, B.N. and Spiridonova, E.O., 2008. Structure and Interannual Variability of Characteristics of Inshore Black Sea Upwelling on Basis of Satellite Monitoring Data. *Issledovanie Zemli iz Kosmosa*, (2), pp. 26–36 (in Russian).
13. Efimov, V.V., Iarovaya, D.A. and Barabanov, V.S., 2023. Numerical Modelling of Upwelling near the South Coast of Crimea on 24–25 September 2013. *Ecological Safety of Coastal and Shelf Zones of Sea*, (1), pp. 6–19.

14. Pérez, F.F., Padín, X.A., Pazos, Y., Gilcoto, M., Cabanas, M., Pardo, P.C., Doval, M.D. and Farina-Busto, L., 2010. Plankton Response to Weakening of the Iberian Coastal Upwelling. *Global Change Biology*, 16(4), pp. 1258–1267. https://doi.org/10.1111/j.1365-2486.2009.02125.x

15. Chavez, F.P. and Messié, M., 2009. A Comparison of Eastern Boundary Upwelling Ecosystems. *Progress in Oceanography*, 83(1–4), pp. 80–96. https://doi.org/10.1016/j.pocean.2009.07.032

16. Kondratev, S.I., Varenik, A.V., Vnukov, Yu.L., Gurov, K.I., Kozlovskaya, O.N., Kotelianets, E.A., Medvedev, E.V., Orekhova, N.A., Svishchev, S.V., Khoruzhiy, D.S. and Konovalov, S.K., 2016. Blue Bay as a Sub-Satellite Ground for Evaluating Hydrochemical Characteristics in the Shelf Areas of the Crimea. *Physical Oceanography*, (1), pp. 48–59. https://doi.org/10.22449/1573-160X-2016-1-48-59

17. Sovga, E.E., Mezentseva, I.V. and Khmara, T.V., 2022. Simulation of Seasonal Hydrodynamic Regime in the Sevastopol Bay and of Assessment of the Self-Purification Capacity of its Ecosystem. *Fundamental and Applied Hydrophysics*, 15(2), pp. 110–123. https://doi.org/10.48612/fpg/92ge-ahz6-n2pt (in Russian).

Submitted 18.06.2024; accepted after review 03.09.2024;
revised 17.12.2024; published 31.03.2025

About the authors:

Elena E. Sovga, Leading Research Associate, Marine Hydrophysical Institute of RAS (2 Kapitanskaya St., Sevastopol, 299011, Russian Federation), DrSci (Geogr.), **ORCID ID: 0000-0002-0670-4573, ResearcherID: A-9774-2018**, *science-mhi@mail.ru*

Tatiyana V. Khmara, Research Associate, Marine Hydrophysical Institute of RAS (2 Kapitanskaya St., Sevastopol, 299011, Russian Federation), **Scopus Author ID: 6506060413, ResearcherID: C-2358-2016**, *xmara@mhi-ras.ru*

Irina V. Mezentseva, Senior Research Associate, Sevastopol Branch of the N. N. Zubov State Oceanographic Institute (61 Sovetskaya St., Sevastopol, 299011, Russian Federation), PhD (Geogr.), **ORCID ID: 0000-0001-9771-0380**, *mez-irina@mail.ru*

Contribution of the authors:

Elena E. Sovga – study task statement, database analysis, discussion of the results, article writing and editing

Tatiyana V. Khmara – preparation of graphic material, discussion of the results, article editing

Irina V. Mezentseva – provision and analysis of database on Yalta Bay, discussion of the results

All the authors have read and approved the final manuscript.

ISSN 2413-5577, Ecological Safety of Coastal and Shelf Zones of Sea, 2025, No. 1, pp. 112–123.

Original paper

Organic Matter in Waters of the Russian Sector of the Caspian Sea

L. V. Degtyareva [1] *, O. I. Bakun [2], M. A. Ocheretniy [1]

[1] *Caspian Marine Scientific Research Center, Astrakhan, Russia*

[2] *LLC LUKOIL-Nizhnevolzsknev, Astrakhan, Russia*

**e-mail: kaspmniz@mail.ru*

Abstract

The paper aims to analyse the results of long-term studies of dissolved and suspended organic matter content in the waters of the Northern Caspian and Middle Caspian in the Russian sector of the Caspian Sea. The paper analyses the main sources of input of organic matter, its seasonal and inter-annual variability, features of its spatial distribution and causes (allochthonous organic matter flow, production and destruction, water temperature, sea level changes, etc.) determining the spatial and temporal dynamics of organic matter content. The paper is written on the results of production environmental monitoring conducted at the licensed areas of LLC LUKOIL-*Nizhnevolzhskneft* in 2017–2021. The organic matter amount was estimated by organic carbon. The dissolved organic carbon concentration was found to vary from 0.10 to 9.30 mg/dm^3 in the surface water layer and from 0.10 to 9.60 mg/dm^3 in the bottom layer. The maximum enrichment of waters with dissolved organic matter was noted in the northern part of the water area. The concentration of suspended organic carbon in the surface water layer varied within 0.10–23.40 mg/dm^3, whereas in the bottom water layer it ranged within 0.05–19.40 mg/dm^3. The spatial distribution of suspended organic matter was characterized by seasonal shifts of the area with maximum concentrations northwards. The main factors affecting the organic matter content in water were water temperature, suspended matter concentration in water and hydrogen ion concentration. The level of dissolved and suspended organic matter has not changed in the last 20 years of studies. The dependence of dissolved and suspended organic matter concentrations on environment pH indicates the natural origin of the organic matter in the waters of the monitored sea area.

Keywords: Caspian Sea, productivity, organic matter, dissolved organic matter, suspended organic matter, allochthonous organic matter, autochthonous organic matter

For citation: Degtyareva, L.V., Bakun, O.I. and Ocheretniy, M.A., 2025. Organic Matter in the Waters of the Russian Sector of the Caspian Sea. *Ecological Safety of Coastal and Shelf Zones of Sea*, (1), pp. 112–123.

Органическое вещество в водах российского сектора Каспийского моря

Л. В. Дегтярева [1] *, О. И. Бакун [2], М. А. Очеретный [1]

[1] *Федеральное государственное бюджетное учреждение «Каспийский морской научно-исследовательский центр», Астрахань, Россия*

[2] *Общество с ограниченной ответственностью «ЛУКОЙЛ-Нижневолжскнефть», Астрахань, Россия*

**e-mail: kaspmniz@mail.ru*

Аннотация

Цель работы заключается в анализе результатов многолетних исследований содержания растворенного и взвешенного органического вещества в водах акватории Северного и Среднего Каспия в российском секторе Каспийского моря. Проанализированы основные источники поступления органического вещества, его сезонные и межгодовые изменения, особенности его пространственного распределения и причины (сток аллохтонного органического вещества, продукционно-деструкционные процессы, температура воды, изменения уровня моря и проч.), определяющие пространственную и временную динамику содержания органического вещества. Работа написана по результатам производственного экологического мониторинга, проведенного на лицензионных участках ООО «ЛУКОЙЛ-Нижневолжскнефть» в 2017–2021 гг. Количество органического вещества оценивали по органическому углероду. Установлено, что концентрация растворенного органического углерода изменялась от 0.10 до 9.30 мг/дм^3 в поверхностном слое воды и от 0.10 до 9.60 мг/дм^3 в придонном. Областью максимального обогащения вод органическим веществом в растворенной форме была северная часть акватории. Концентрация взвешенного органического углерода в поверхностном слое воды изменялась в интервале 0.10–23.40 мг/дм^3, в придонном – в интервале 0.05–19.40 мг/дм^3. Пространственное распределение органического вещества во взвешенной форме характеризовалось сезонным смещением области максимальных концентраций к северу. Основными факторами, влияющими на содержание органического вещества в воде, являются температура воды, а также концентрация взвешенного вещества в воде и водородный показатель. Уровень содержания растворенного и взвешенного органического вещества за последние 20 лет исследований не изменился. Зависимость концентрации растворенного и взвешенного органического вещества от pH среды подтверждает естественную природу органического вещества в водах исследуемой акватории.

Ключевые слова: Каспийское море, продуктивность, органическое вещество, растворенное органическое вещество, взвешенное органическое вещество, аллохтонное органическое вещество, автохтонное органическое вещество

Для цитирования: *Дегтярева Л. В., Бакун О. И., Очеретный М. А*. Органическое вещество в водах российского сектора Каспийского моря // Экологическая безопасность прибрежной и шельфовой зон моря. 2025. № 1. С. 112–123. EDN FNEADY.

Introduction

Potential biological productivity of a marine ecosystem is estimated by organic matter (OM) reserves in the water body. Being a product of vital activity of plants and animals, OM determines physical and chemical properties of water and bottom sediments and serves as a source of nutrients [1)].

[1)] Maystrenko, Yu.G., 1965. [*Organic Matter of Water and Bottom Sediment of Ukrainian Rivers and Water Bodies (the Dnieper and Danube Basins)*]. Kiev: Naukova Dumka, 239 p. (in Russian).

Representative indicators of dissolved organic matter (DOM) and suspended organic matter (SOM) are dissolved organic carbon (DOC) and suspended organic carbon (SOC) concentrations, respectively [1].

In the Caspian Sea, the incoming part of the OM balance is formed by allochthonous and autochthonous organic material, with autochthonous OM playing the leading role [2)]. Phytoplankton is the main producer of autochthonous OM [2)-4)]. Allochthonous OM comes mainly with river runoff [2, 3]. Main items of the consumption part of the balance are the OM bottom sedimentation and consumption during mineralisation [2)].

OM is present in the Caspian waters in dissolved and suspended forms [4]. Carbohydrates and lipids are main biochemical components of DOM [5], while lipids and proteins are those of SOM [3]. OM of allochthonous origin is characterised by a high content of the insoluble fraction [2), 3)].

According to literature, in the Russian sector of the Caspian Sea, the maximum DOM and SOM content is registered in the north-western part of the Northern Caspian, in the estuaries of the Terek and Sulak Rivers, as well as in the hydrologic front zone. The OM concentration decreases seaward [5)] [2, 5].

The OM concentration decreases with depth as a result of aerobic destruction [6]. Biochemical processes intensify in the bottom layer due to periodic turbulence of bottom sediments [6)]. In shallow water areas, OM is distributed uniformly throughout the water column due to intensive mixing [5)].

OM is characterised by seasonal changes: in spring, during phytoplankton blooming, the OM content in the photic water layer increases, and in autumn, it decreases due to the development of destruction and sedimentation [7, 8]. Suspended matter (SM) is the predominant form through which OM transitions from water to sediments [7)].

The rate of destruction of organic compounds depends on water temperature, environment pH and aeration conditions [3)]. Increase in water temperature adds to the intensity of mineralisation of organic compounds [9]. Increase in the environment pH indicates more active OM formation under conditions of production intensification, causing a decrease in the partial pressure of carbon dioxide in water, and OM destruction accompanied by an increase in the partial pressure of carbon dioxide

---

2) Datsko, V.G., 1957. [Content of Organic Matter in the Caspian Sea Waters and its Approximate Balance]. *Gidrokhimicheskie Materialy*, XXVII, pp. 10–20 (in Russian).

3) Romankevich, E.A., 1977. [*Geochemistry of Organic Matter in the Ocean*]. Moscow: Nauka, 256 p. (in Russian).

4) Bordovskiy, O.K. and Ivanenkov, V.N., eds., 1979. [*Ocean Chemistry. Vol. 1. Chemistry of Ocean Waters*]. Moscow: Nauka, 521 p. (in Russian).

5) Pakhomova, A.S. and Zatuchnaya, B.M., 1966. [*Hydrochemistry of the Caspian Sea*]. Leningrad: Gidrometeoizdat, 342 p. (in Russian).

6) Fedosov, M.V., 1957. [Chemical Basis of Southern Seas Fodder and their Water Regime]. *Informatsionny Sbornik VNIRO*, (1), pp. 14–19 (in Russian).

7) Romankevich, E.A., Artemiev, V.E., Belyaeva, A.N. and Lyutsarev, S.V., 1982. [Biogeochemistry of Dissolved and Suspended Organic Matter in the Ocean]. In: A.V. Sidorenko and A. A. Geodekian, eds., 1982. [*Organic Geochemistry of Waters and Exploration Geochemistry: Proceedings of the 8th International Organic Chemistry Congress*]. Moscow: Nauka, pp. 7–17 (in Russian).

leads to a decrease in pH. Oxygen, as the main oxidant in the bottom water layer, is used for mineralisation of organic compounds. The decrease in oxygen concentration in water depends on the amount of oxidised OM [4)].

An important role in OM mineralisation belongs to bacteria capable of decomposing dead OM (including oil products) and transforming its destruction products into forms suitable for assimilation by aquatic vegetation [8)] [10].

Study of the peculiarities of OM content and distribution in water bodies subject to organic pollution is especially relevant.

In the Russian sector of the Caspian Sea, deterioration of the quality of the marine environment has been observed in the modern period, which is primarily caused by the inflow of pollutants, including organic compounds (petroleum hydrocarbons, phenols, organochlorine pesticides, synthetic surfactants) from the Volga, Terek, and Sulak rivers [9)] [11–15]. In addition, eutrophication has been intensively occurring in the Northern Caspian and Middle Caspian, leading to an increase in the DOM and SOM amount [4, 16].

Sea level fluctuations result in quantitative changes in OM. Recent studies of OM distribution in the Caspian Sea waters in 2010–2015 showed that during that period of sea level decline, the DOC concentration had been almost unchanged [10]. However, the Caspian Sea level has decreased by more than 70 cm since 2016, and its further decline is predicted [17].

Under these conditions (continuing pollution, eutrophication, sea level decrease), it is necessary to estimate the OM content in the Caspian Sea waters in the modern period.

The work aims to determine the main sources of organic matter in the water area of the Russian sector of the Caspian Sea and the factors determining the spatial and temporal dynamics of the content of organic matter, its suspended and dissolved forms.

Materials and methods

The paper is written on the results of production environmental monitoring conducted at the licensed areas of LLC *LUKOIL-Nizhnevolzhskneft* in 2017–2021. Monitoring was carried out twice a year (spring–summer and autumn periods). Samples were taken consecutively at 58 stations (Fig. 1) in the surface and bottom layers.

First day analyses (water temperature, pH) were carried out by standard methods. Water samples (347 items) were processed in accredited laboratories. Nationally recognised test methods, certified measurement procedures, calibrated and verified measuring instruments were used in the chemical analyses. The amount of organic matter was estimated by organic carbon in accordance

---

[8)] Bordovsky, O.K., 1964. [*Accumulation and Transformation of Organic Matter in Marine Sediments (Study on the Origin of Oil)*]. Moscow: Nedra, 128 p. (in Russian).

[9)] Gurpanbur, Sh.B., 2010. [Ecological Problems of the Caspian Sea]. *Molodoy Ucheny*, I(5), pp. 128–131 (in Russian).

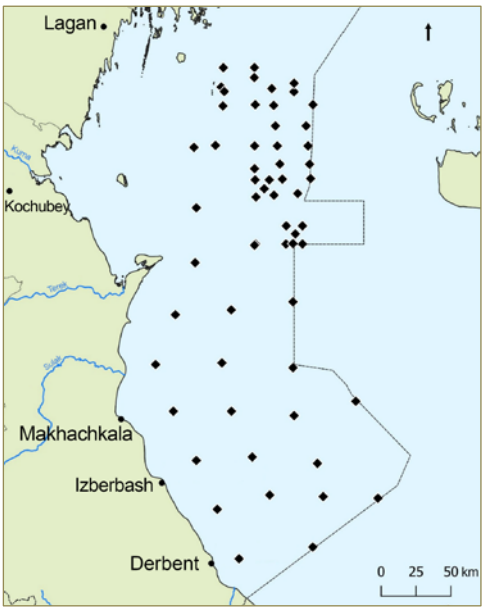

Fig. 1. Sampling scheme

with GOST 31958-2012. Statistical analysis was carried out according to paper [10].

Results and discussion

The hydrochemical regime was characterised by an increase in water temperature from spring to summer with preservation of sufficiently high temperature values in autumn (Table 1). Seasonal increase in hydrogen index values indicates production activation in summer and autumn period. The decrease in the amount of suspended sediment in summer and autumn is explained by the seasonal decrease in the volume of solid runoff with the Volga waters.

The DOC concentration varied from 0.10 to 9.30 mg/dm^3 in the surface layer and from 0.10 to 9.60 mg/dm^3 in the bottom layer (Table 2). On average, during the entire study period, the DOC content was higher near the surface due to the OM primary production in the photic layer and OM decomposition in the water column. However, due to the shallowness of the study area, vertical differences were minimal. The correlation between the values of DOC concentration in the surface and bottom layers was revealed. In spring, under high flood conditions and, consequently, high hydrodynamic

Table 1. Average values of hydrochemical indicators

Season	Water temperature, °C		Water pH		Suspended matter, mg/dm^3	
	Surface	Bottom	Surface	Bottom	Surface	Bottom
Spring	15.5	11.1	8.36	8.37	6.44	5.76
Summer	25.6	19.6	8.40	8.38	6.21	4.91
Autumn	19.5	17.0	8.46	8.43	2.88	2.51

[10] Smagunova, A.N. and Karpukova, O.M., 2012. [*Methods of Mathematical Statistics in Analytic Chemistry*]. Rostov-on-Don, Feniks, 346 p. (in Russian).

Table 2. Concentration of organic carbon in the water of the Northern Caspian, mg/dm^3

Season	Layer	Dissolved organic carbon		Suspended organic carbon	
		Range	Average	Range	Average
Spring	Surface	0.10–9.30	3.12	0.20–23.40	3.06
	Bottom	0.10–9.60	2.81	0.10–19.40	2.49
Summer	Surface	1.50–4.11	2.35	0.10–13.30	1.64
	Bottom	1.18–3.50	2.19	0.10–9.20	1.36
Autumn	Surface	0.75–6.00	2.43	0.10–6.86	1.17
	Bottom	0.45–5.00	2.21	0.05–4.80	0.96

activity, the correlation coefficient (r) was lower ($r = 0.48$; $n = 134$; $\alpha = 0.05$) than in summer ($r = 0.74$; $n = 72$; $\alpha = 0.05$) and autumn ($r = 0.79$; $n = 142$; $\alpha = 0.05$).

Despite the increase in the hydrogen ion concentration (pH) indicating the activation of OM primary production (Table 1), a decrease in the DOC content was observed from spring to autumn, both in the surface and bottom layers, which is explained by the increased insolation inhibiting photosynthesis in the summer and autumn period [11].

During the study period, the area of maximum DOC concentration was the northern part of the water area (Fig. 2).

The SOC concentration varied in the range of 0.10–23.40 mg/dm^3 in the surface water layer and in the range of 0.05–19.40 mg/dm^3 in the bottom water layer (Table 2). The SOC vertical distribution and seasonal dynamics repeated changes in the SM concentration (Table 1). The maximum SOC values recorded in the spring period are explained by the input of allochthonous organic matter with the Volga River runoff during the high flood period. However, from spring to autumn, the correlation between SOC content in the surface and bottom water layers became weaker. Thus, correlation coefficient was 0.66 ($n = 134$; $\alpha = 0.05$) in spring; 0.61 ($n = 72$; $\alpha = 0.05$) in summer; 0.48 ($n = 142$; $\alpha = 0.05$) in autumn. The decrease in the correlation ratio between these parameters is due to the fact that in spring SOC was a part of allochthonous (hard-to-mineralise) OM supplied with the Volga waters during high floods, and almost did not decompose in the water column, while in autumn it was a part of autochthonous (easily acidifiable) OM mineralised in the whole water column.

[11] Boulion, V.V., 1983. [*Primary Prodution of Plankton of Inland Water Bodies*]. Leningrad: Nauka, 150 p. (in Russian).

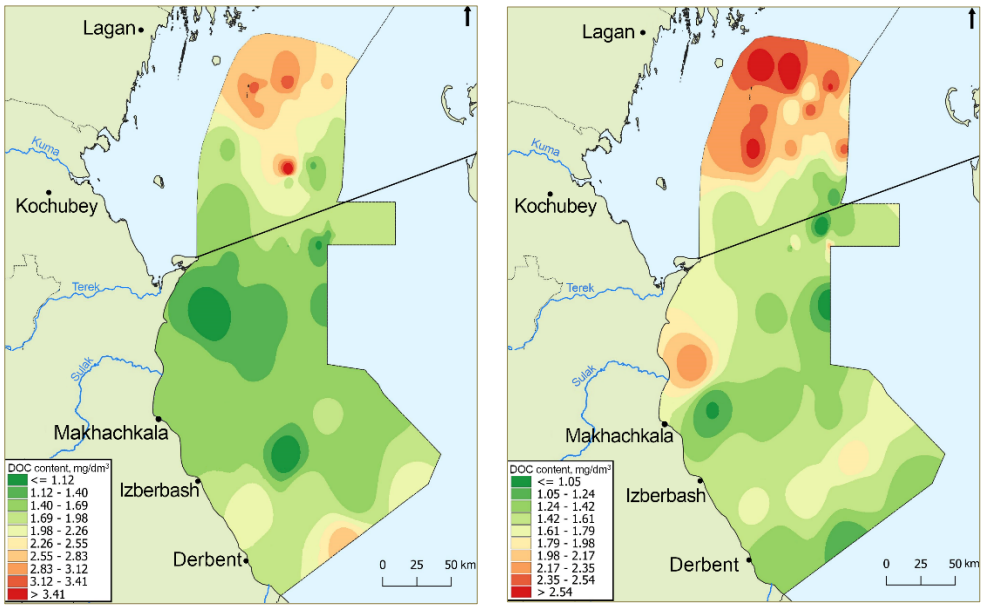

a ***b***

F i g . 2 . Spatial distribution of dissolved organic carbon (mg/dm^3) in the surface water layer in spring 2020 (*a*) and autumn 2021 (*b*). The line denotes the border between the Northern and Middle Caspian

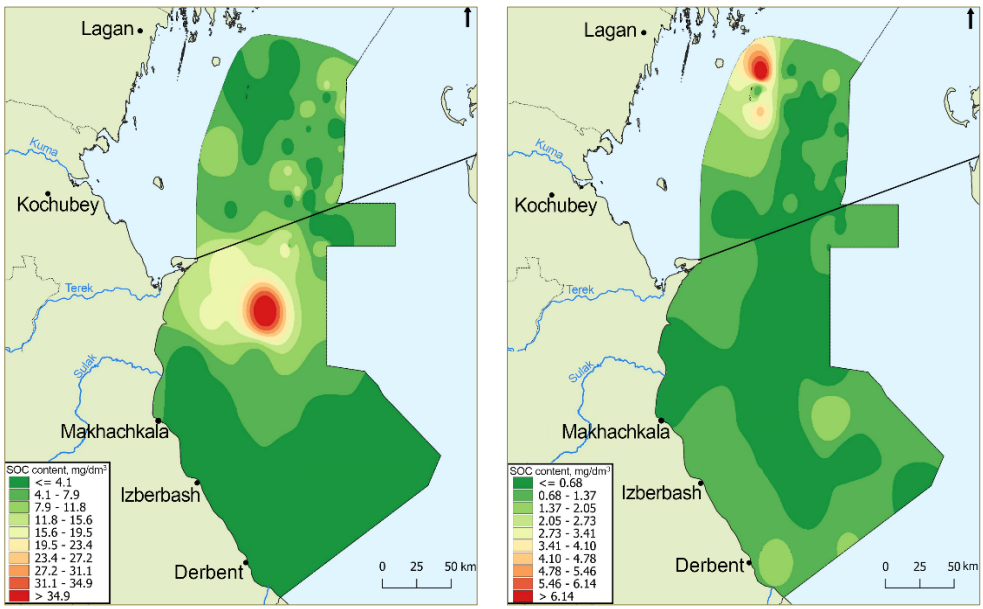

a ***b***

F i g . 3 . Spatial distribution of suspended organic carbon (mg/dm^3) in the surface water layer in spring 2020 (*a*) and autumn 2021 (*b*). For the line notation see Fig. 2

The SOC spatial distribution corresponded to the DOC distribution in autumn (Fig. 3). In the spring period, the area of the highest values was located on the traverse of the Agrakhan Peninsula, which can be caused by the Volga water export to this area against the background of increased water flow.

No statistically significant correlation between the content of DOC and SOC was found throughout the study period. The level of content as well as the characteristic features of the spatial distribution of DOC and SOC have not changed over the last 20 years of studies [18].

In the spring period, the DOC concentration was inversely related to water temperature. Correlation coefficient was –0.46 (Fig. 4) for the surface layer and –0.35 for the bottom one ($n = 137$; $\alpha = 0.05$). The SOC content was in direct correlation with the SM amount: $r = 0.77$ (surface) (Fig. 5) and $r = 0.71$ (bottom) with $n = 137$; $\alpha = 0.05$. This indicates that SOC occurs as part of allochthonous, hard-to-mineralise OM in the spring period.

Correlation dependence of DOC and SOC concentration on water pH was revealed in summer. The SOC dependence of pH ($r = 0.67$ and 0.62 for the surface (Fig. 6) and bottom layer, respectively) was stronger than the DOC dependence of pH ($r = 0.48$ and 0.57 for the surface and bottom layer, respectively). For all the above mentioned dependencies, $n = 74$; $\alpha = 0.05$.

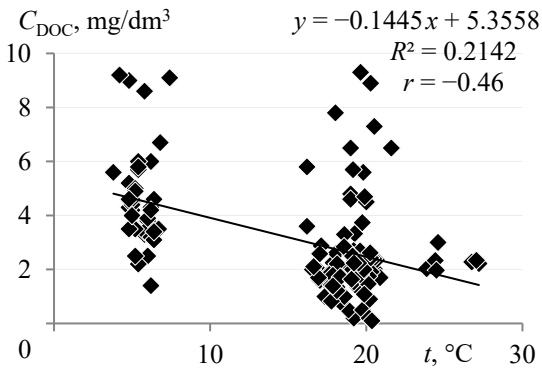

Fig. 4. Dependence of dissolved organic carbon C (mg/dm³) on water temperature (°C) in the surface water layer during spring

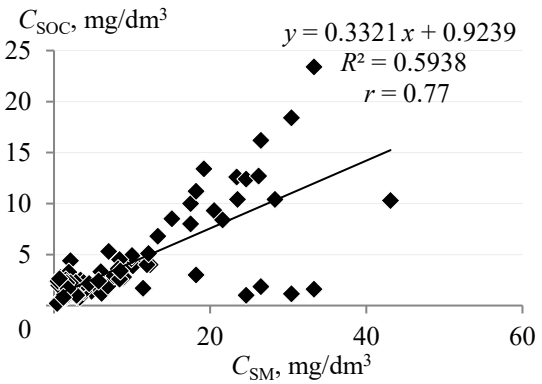

Fig. 5. Dependence of suspended organic carbon concentration (mg/dm³) on suspended matter concentration (mg/dm³) in the surface water layer during spring

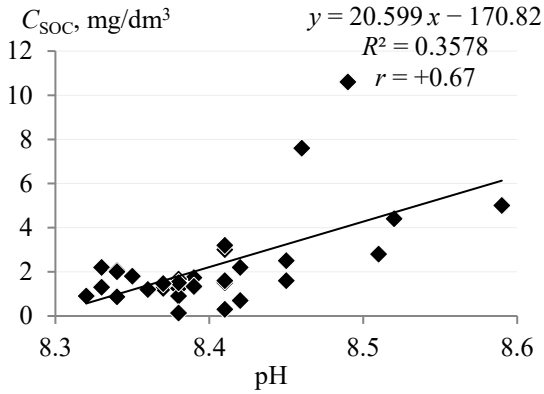

Fig. 6. Dependence of suspended organic carbon concentration (mg/dm^3) on pH in the surface water layer during summer

No statistically significant correlations were found in the data array for the autumn period.

The seasonal dynamics of SM, DOC and SOC differed at different stages of the marginal filter.

According to literature, the maximum amount of SM is registered in the "mud area" (water area with salinity not exceeding 4‰) [19]. However, our studies revealed that this pattern was observed only in summer and autumn (Table 3). In spring, during high floods, the main part of SM is carried further seaward. The increase in the SM and SOC content was observed in summer, in the DOC content – in spring.

In the "elementorganic area" (water area with salinity of 4–7‰), transition of organic substances into bottom sediments takes place as a result of flocculation and sorption activation [19]. Decrease in DOC concentration in water in the "elementorganic plug" in comparison with the "mud area" is observed only in spring. In summer and autumn, SOC decreases in the "elementorganic plug" (in autumn only in the surface layer).

In the "biological part" of the marginal filter (with salinity over 7‰), the OM bioassimilation takes place due to intensification of living organisms activity. The DOC and SOC concentration decreases compared to the OM content in the "elementorganic area". The DOC concentration decreased insignificantly, the SOC concentration decreased 3.3 times in the surface water layer and 4 times in the bottom water layer in summer. The SOC sharp decrease near the surface is a consequence of destruction, which is more intensive in the surface water layer under conditions of high oxygen saturation of water. Sharp decrease in the SOC amount in the bottom horizon is probably caused by the development of such filter-feeding molluscs as *Cerastoderma glaucum* (Bruguière, 1789) inhabiting at salinities of at least 5‰; *Monodacna colorata* (Eichwald, 1829), optimum salinity for which is 6–10‰; *Didacna protracta* (Eichwald, 1829) preferring salinities above 8‰, etc., in the biological part of the marginal filter [20, 21].

Table 3. Average concentration of suspended and organic substances in the water of the Northern Caspian, mg/dm^3

Season	Suspended matter		Dissolved organic carbon		Suspended organic carbon	
	Surface	Bottom	Surface	Bottom	Surface	Bottom
Salinity < 4‰						
Spring	1.55	1.60	7.75	5.75	1.25	1.05
Summer	11.15	3.55	2.38	2.32	7.80	6.68
Autumn	7.33	1.42	2.11	2.00	2.42	0.10
Salinity 4–7‰						
Spring	6.40	5.52	3.53	2.93	3.36	2.51
Summer	9.22	9.12	2.82	2.56	4.12	4.07
Autumn	3.83	4.06	3.08	2.54	1.59	1.23
Salinity > 7‰						
Spring	6.53	5.86	2.99	2.75	3.06	2.51
Summer	5.82	4.62	2.32	2.16	1.25	1.01
Autumn	2.71	2.36	2.37	2.17	1.10	0.94

Conclusion

The DOC and SOC concentration in the surface water layer of the Russian sector of the Caspian Sea is higher than in the bottom one due to the primary production of OM in the photic layer and decomposition of OM in the water column. Seasonal dynamics is characterised by a decrease in DOC and SOC from spring to autumn, which is explained by natural hydrochemical reasons (increased insolation inhibiting photosynthesis in the summer and autumn period, beginning of the destruction development in autumn and decrease in allochthonous OM input with the Volga River runoff).

The main factors affecting the OM content in water are water temperature (negative trend) and the amount of suspended sediment and water pH (positive trend).

The level of DOM and SOM has not changed in the last 20 years of studies. The dependence of DOM and SOM concentrations on environment pH assumes the natural origin of the organic matter in the waters of the monitored sea area.

REFERENCES

1. Agatova, A.I., Lapina, N.M., Torgunova, N.I. and Kodryan, K.V., 2021. Organic Matter and its Transformation Rates in Different Barents Sea Ecosystems. In: A. P. Lisitsin, ed., 2021. *The Barents Sea System*. Moscow: Izdatelstvo GEOS, pp. 212–235. https://doi.org/10.29006/978-5-6045110-0-8 (in Russian).
2. Gershanovich, D.E., Zinkovsky, A.B., Mordasova, N.V. and Sanina, L.V., 1990. [Suspended Matter, Phytoplankton, Chlorophyll in the Caspian Sea]. In: A. N. Kosarev, ed., 1990. [*The Caspian Sea: The Structure and Dynamics of Waters*]. Moscow: Nauka, pp. 49–61 (in Russian).
3. Khachaturova, T.A., 1981. Suspended Matter of the Caspian Sea and its Biochemical Composition. *Oceanology*, 21(1), pp. 70–76.
4. Salmanov, M.A., 1999. [*Ecology and Biological Productivity of the Caspian Sea*]. Baku: PITS Ismail, 398 p. (in Russian).
5. Agatova, A.I., Kirpichev, K.B., Lapina, N.M., Luk'yanova, O.N., Sapozhnikov, V.V. and Torgunova, N.I., 2005. Organic Matter in the Caspian Sea. *Oceanology*, 45(6), pp. 795–804.
6. Ohle, W., 1962. Der Stoffhaushalt der Seen als Grundlage einer Allgemeinen Stoffwechseldynamik der Gewässer. *Kieler Meeresforschungen*, 18(3), S. 107–120. URL: https://oceanrep.geomar.de/id/eprint/55674 [Zugriffsdatum: 22.01.2025].
7. Agatova, A.I., Lapina, N.M. and Torgunova, N.I., 2008. Organic Matter of the North Atlantic. *Oceanology*. 48(2). pp. 182–195. https://doi.org/10.1134/S0001437008020045
8. Lisitsyn, A.P., 1994. A Marginal Filter of the Oceans. *Oceanology*. 34(5), pp. 735–747 (in Russian).
9. Lobkovskii, L.I., Levchenko, D.G., Leonov, A.V. and Ambrosimov, A.K., 2005. [Geoecological Portrait of the Caspian Sea Ecosystem]. In: C. C. Lappo, ed., 2005. *Geoecological Monitoring of Marine Water Arias Containing Gas and Oil*. Moscow: Nauka, 326 p. (in Russian).
10. Agatova, A.I., Torgunova, N.I., Serebryanikova, E.A. and Dukhova, L.K., 2019. Space and Time Variations of Organic Matter in Caspian Sea Water. *Water Resources*, 46(1), pp. 76–86. https://doi.org/10.1134/S0097807819010020
11. Abdusamadov, A.S., Abdurakhmanov, G.M., Dohtukaeva, A.M. and Dudurhanova, L.A., 2011. Contamination of the Shallow Coastal Zone and Desalinated Shelf West of the Caspian Sea and its Impact on Biota and Reproduction of Fish. *The South of Russia: Ecology, Development*. (2), pp. 37–62 (in Russian).
12. Karygina, N.V., 2019. [On the Content, Distribution and Genesis of Hydrocarbons in the Waters of the Northern Caspian Sea]. In: D. V. Kashin, ed., 2019. [*Problems of Preservation of the Caspian Ecosystem During Oil And Gas Fields Development: Proceedings of the 7th Scientific and Practical Conference with International Participation. Astrakhan, 18 October 2019*]. Astrakhan, KaspNIRKH, pp. 83–88 (in Russian).
13. Karygina, N.V., Popova, E.S., Lvova, O.A., Galley, E.V. and Yatsun, E.V., 2020. On Oil and Pesticide Pollution of the Lower Volga and the Northern Part of the Caspian Sea. In: IngSU, 2020. [*Ecology and Nature Management: Proceedings of International Scientific and Practical Conference. Magas, 21–23 October 2020*]. Nazran: OOO KEP, pp. 250–257 (in Russian).
14. Ostrovskaya, E.V. and Umrikha, A.V., 2019. Oil Pollution of the North-Western Part of the Caspian Sea: Current State and Main Sources. In: V. M. Gruzinov, ed., 2019. *Proceedings of N.N. Zubov State Oceanographic Institute*. Moscow, pp. 209–220 (in Russian).

15. Shipulin, S.V., 2021. [State of Aquatic Bioresources in the Volga-Caspian Basin and Measures for their Conservation under Oil Production Development]. In: D. V. Kashin, ed., 2019. [*Problems of Preservation of the Caspian Ecosystem During Oil And Gas Fields Development: Proceedings of the 7th Scientific and Practical Conference with International Participation. Astrakhan, 22 October 2021*]. Astrakhan, KaspNIRKH, pp. 306–309 (in Russian).
16. Skopitsev, B.A. and Larionov, Yu.V., 1979. [Organic Matter in Suspensions of Some Lakes with Different Trophic Status]. *Vodnye Resursy*, (5), pp. 159–170 (in Russian).
17. Ostrovskaya, O.V., Gavrilova, E.V. and Varnachkin, S.A., 2022. [Changes in the Hydrological and Hydrochemical Regime of the North Caspian Sea Under Changing Climate Conditions]. In: O. V. Ostrovskaya and L.V. Degtyareva, eds., 2022. [*Proceedings of the International Scientific Conference "Climate Change in the Caspian Sea Area". 27–28 October 2021*]. Astrakhan: Izdatel Sorokin R.V., pp. 75–77 (in Russian).
18. Agatova, A.I., Lapina, N.M., Torgunova, N.I. and Kirpichev, K.B., 2001. Biochemical Study of Brackish-Water Marine Ecosystems. *Water Resources*. 28(4). pp. 428–437. https://doi.org/10.1023/A:1010401907179
19. Nemirovskaya, I.A. and Brekhovskikh, V.F., 2008. Origin of hydrocarbons in the particulate matter and bottom sediments of the northern shelf of the Caspian Sea. *Oceanology*, 48(1), pp. 43–53. https://doi.org/10.1134/S0001437008010062
20. Zhirkov, I.A., 2010. [*Biogeography and Bioecology of Benthos*]. Moscow: T-vo Nauchnykh Izdaniy KMK, 453 p. (in Russian).
21. Yablonskaya, E.A., 1975. [Long-Term Changes in the Biomass of Various Trophic Benthic Groups of the Northern Caspian]. *Trudy VNIRO*, CVIII, pp. 50–64 (in Russian).

Submitted 25.07.2024; accepted after review 13.09.2024;
revised 17.12.2024; published 31.03.2025

About the authors:

Larisa V. Degtyareva, Leading Research Associate, Caspian Marine Scientific Research Center (14 Shiryaeva St., Astrakhan, 414045, Russian Federation), PhD (Biol.), **ORCID ID: 0000-0003-1337-2797,** *kaspmniz@mail.ru*

Olga I. Bakun, Leading Engineer for Environmental Protection, LLC *LUKOIL-Nizhnevolzhskneft* (1, Bldg. 2 Admiralteyskaya St., Astrakhan, 414000, Russian Federation), PhD (Biol.), **ORCID ID: 0000-0002-8149-9389**, *ozornikova@mail.ru*

Maxim A. Ocheretniy, Research Associate, Caspian Marine Scientific Research Center (14 Shiryaeva St., Astrakhan, 414045, Russian Federation), **ORCID ID: 0009-0008-0667-9292**, *kaspmniz@mail.ru*

Contribution of the authors:

Larisa V. Degtyareva – initiation of the study, setting goals and objectives of the study, carrying out calculations, analysis of calculation results, formulation of conclusions

Olga I. Bakun – review of literature on the study issue, manuscript editing

Maxim A. Ocheretniy – creation of maps and tables, writing the abstract

All the authors have read and approved the final manuscript.

Original paper

Assimilation Capacity of Azov Sea Bottom Sediments with Respect to Copper and Zinc

M. V. Bufetova

Sergo Ordzhonikidze Russian State University for Geological Prospecting, Moscow, Russia

e-mail: mbufetova@mail.ru

Abstract

The work aims to assess the assimilation capacity of bottom sediments of the Sea of Azov with respect to copper and zinc by the level of their elimination into the geological depot as a result of sedimentation. The paper analyses metal concentrations in water and bottom sediments in 1991–2023. In 1998–2023, the average values of copper in sea water exceeded maximum permissible concentration (5 μg/L) and ranged 5.2–12 μg/L. The average concentration of copper in the bottom sediments of the Sea of Azov in 1991–1999 was 29.8 μg/g, in 2000–2010 it was 35.5 μg/g and in 2011–2023 it was 9.3 μg/g. The copper flux from the water to the bottom sediments of the open part of the sea ranged 14–381 t/year, whereas in Taganrog Bay it was 16–153 t/year. Sediment turnover periods of copper in the open sea and in Taganrog Bay averaged 0.5 and 1.6 years, respectively. The assimilation capacity of bottom sediments for copper in the open sea was 135.6 t/year and for Taganrog Bay it was 75.7 t/year. The zinc concentration in water exceeded its maximum permissible concentration (50 μg/L) in different years (up to 79 μg/L in Kuban-Akhtarsky and Kuban-Temryuksky districts). In the bottom sediments, the zinc concentration during the entire observation period was in the range of 17.1–98 μg/g in the open sea and 19.0–111 μg/g in the bay. The flux of sedimentation self-purification of water from zinc in the open sea was in the range of 175–902 t/year and in Taganrog Bay it was 76–407 t/year. The zinc turnover period in the open part of the sea varied within 0.7–39.8 years and in the bay, it was 0.1–4.8 years. The assimilation capacity of the bottom sediments with respect to zinc was 313.6 t/year for the open part of the sea and 169.1 t/year for Taganrog Bay. Determination of assimilation capacity of bottom sediments allows normalizing planned inputs of copper and zinc into the water area of the Sea of Azov.

Keywords: Sea of Azov, copper, zinc, pollution, heavy metal flux, accumulation coefficient, self-purification, copper flux, zinc flux, assimilation capacity

Acknowledgments: The author is grateful to *Azovmorinformtsentr*, a branch of *Tsentrregionvodkhoz*, for long-term cooperation and provided data.

For citation: Bufetova, M.V., 2025. Assimilation Capacity of Azov Sea Bottom Sediments with Respect to Copper and Zinc. *Ecological Safety of Coastal and Shelf Zones of Sea*, (1), pp. 124–136.

Ассимиляционная способность донных отложений Азовского моря в отношении меди и цинка

М. В. Буфетова

Российский государственный геологоразведочный университет имени Серго Орджоникидзе (МГРИ), Москва, Россия
e-mail: mbufetova@mail.ru

Аннотация
Цель работы – оценить ассимиляционную способность донных отложений Азовского моря в отношении меди и цинка по уровню их элиминации в геологическое депо в результате седиментационных процессов. Анализировались концентрации металлов в воде и донных отложениях в 1991–2023 гг. В 1998–2023 гг. средние значения меди в воде моря превышали ПДК (5 мкг/л) и находились в диапазоне 5.2–12 мкг/л. Концентрация меди в донных отложениях Азовского моря в 1991–1999 гг. составляла в среднем 29.8 мкг/г, в 2000–2010 гг. – 35.5 мкг/г, в 2011–2023 гг. – 9.3 мкг/г. Поток меди из воды в донные осадки открытой части моря варьировал в пределах 14–381 т/год, в Таганрогском заливе – 16–153 т/год. Периоды седиментационного оборота меди в открытом море и в Таганрогском заливе в среднем составляли 0.5 и 1.6 лет соответственно. Ассимиляционная способность донных отложений в отношении меди составила в открытой части моря 135.6 т/год, в Таганрогском заливе – 75.7 т/год. Концентрация цинка в воде превышала ПДК (50 мкг/л) в разные годы (в Кубано-Ахтарском и Кубано-Темрюкском районах – до 79 мкг/л). В донных осадках концентрация цинка весь период наблюдений находилась в диапазоне 17.1–98 мкг/г в открытом море и 19.0–111 мкг/г в заливе. Поток седиментационного самоочищения вод от цинка в открытой части моря находился в интервале 175–902 т/год, в Таганрогском заливе – 76–407 т/год. Период оборота цинка в открытой части моря варьировал в пределах 0.7–39.8 года, в заливе – 0.1–4.8 года. Ассимиляционная способность донных отложений в отношении цинка составила 313.6 т/год в открытой части моря и 169.1 т/год в Таганрогском заливе. Определение ассимиляционной способности донных осадков позволяет нормировать плановые поступления меди и цинка в акваторию Азовского моря.

Ключевые слова: Азовское море, медь, цинк, загрязнение, потоки тяжелых металлов, коэффициент накопления, самоочищение, поток меди, поток цинка, ассимиляционная способность

Благодарности: автор благодарна филиалу «Азовморинформцентр» ФГБВУ «Центррегионводхоз» за многолетнее сотрудничество и предоставленные данные.

Для цитирования: *Буфетова М. В.* Ассимиляционная способность донных отложений Азовского моря в отношении меди и цинка // Экологическая безопасность прибрежной и шельфовой зон моря. 2025. № 1. С. 124–136. EDN YPQPAB.

Introduction

Assessment of the water area self-purification ability by calculating the assimilation capacity (AC) of bottom sediments with respect to a particular pollutant can serve as a scientific and technical basis for finding ways to normalize the ecological state of marine ecosystems. Self-purification of the aquatic environment is a complex set of dilution, migration and redistribution of pollutants [1].

It was shown in [1)] that from the point of view of self-purification, the AC could be understood as a transformable and irreversibly eliminated flux of pollution from the marine environment as a result of abiotic and biotic processes [1)].

According to V. N. Yegorov, on the one hand, the marine environment AC means the amount of pollutant that can be diluted in the water areas so that the concentration of pollutant in critical biotic components of ecosystems does not exceed maximum permissible values. On the other hand, the AC is a differential criterion, i. e. the marginal flux of pollution eliminated to aquatic or geological depots [2, p. 238]. This approach to the AC assessment was implemented in [3], where on the basis of estimates of ultimate elimination fluxes of radionuclides, mercury and chlororganic compounds from the aquatic environment into bottom sediments (geological depots) of Sevastopol Bay, the AC values of bottom sediments were obtained with respect to these pollutants. The authors obtained the AC values of bottom sediments with respect to the mentioned pollutants. In particular, the authors obtained that the AC of bottom sediments in relation to mercury is 32.7 t/year [3]. The methodology for calculating the maximum permissible flux was also used in [4] to assess the AC of bottom sediments in the Azov Sea concerning lead. A similar method of assessment of the AC of bottom sediments with respect to copper and zinc is applied in this work.

The Sea of Azov is a relatively small shallow water body, which experiences high anthropogenic load. Among the most significant pollutants entering the water area of the Sea of Azov are heavy metals including such essential trace elements as copper and zinc, which are necessary for the metabolism of hydrobionts in low concentrations but become toxic to them in higher concentrations.

The work aims to assess the assimilation capacity of bottom sediments of the open part of the Sea of Azov and Taganrog Bay with respect to copper and zinc by their elimination into the geological depot as a result of sedimentation.

In this process, the following objectives were addressed:

1. To study the dynamics of water and bottom sediments pollution of the sea proper and Taganrog Bay by copper and zinc for 1991–2023.

2. To study the dependence of copper and zinc concentration in bottom sediments on their concentration in water, taking into account the accumulation coefficient.

3. To assess annual fluxes of copper and zinc deposition from water to bottom sediments during the studied period.

4. To determine the sediment turnover period of copper and zinc in the aquatic environment.

This study continues the series of works commenced by paper [4].

[1)] Polikarpov, G.G. and Egorov, V.N., 1986. [*Marine Dynamic Radiochemoecology*]. Moscow: Energoatomizdat, 176 p. (in Russian).

Materials and methods

The data on copper and zinc concentration in water and bottom sediments in 2010–2023, provided by *Azovmorinformtsentr* branch of *Tsentrregionvodkhoz* within the cooperation with the Department of Ecology and Environment Management of Sergo Ordzhonikidze Russian State University for Geological Prospecting (MGRI) were used in this paper. To determine interannual trends, we also used the literature data on copper and zinc content in the water of the Sea of Azov in 1991–2009 [5, 6].

The maximum permissible concentration (MPC_w) of copper in marine waters of fishery objects is 5 μg/ L, while that of zinc – 50 μg/L. Zinc and copper are classified as hazard class 3 (moderately hazardous) and have a toxicological limiting indicator of harmfulness [2)].

Since no quality standards for bottom sediments have been established in the Russian Federation, assessment of the degree of contamination of the sediments under study can be carried out according to [3)] where maximum permissible concentration (MPC) of metals in bottom sediments is specified. Thus, MPC of copper is 73 μg/g dry wt. and that of zinc is 620 μg/g dry wt.

Water samples were taken for the analysis by PE-1220 sampling system according to standard GOST 31861-2012 and RD 52.24.309-2016 from the surface horizon (0–5 m) at 32 points (Fig. 1). Dissolved forms of metals were determined. Bottom sediments were sampled for the analysis at the same stations as water samples using a bottom sampler DCH-0.034 according to standard GOST 17.1.5.01-80 in the surface layer of soils (0–5 cm). Sampling and chemical analysis of water samples and bottom sediments was carried out according to standard methods.

To estimate fluxes F (t/year) of annual deposition of copper and zinc in bottom sediments, expression [2] was used

$$F = C_{bs}\, S\, v_{sed}, \tag{1}$$

where C_{bs} is metal concentration in the surface layer of bottom sediments, μg/g; S is area of the water area under consideration, km^2; v_{sed} is sedimentation rate, $g \cdot m^{-2} \cdot year^{-1}$.

Sediment turnover period of heavy metal in the aquatic environment T (years) equal to the ratio of its volume in water to the deposition flux into bottom sediments reflects the time scale of sedimentation self-purification in waters [2]:

$$T = (C_w S\, h_m) / F, \quad \text{or} \quad T = (C_в V) / F, \tag{2}$$

where C_w is metal concentration in water, μg/L; V is volume of the analysed water area, km^3; h_m is average depth of the analysed water area, m.

[2)] Ministry of Agriculture of Russia, 2016. *On the Approval of Water Quality Standards for Water Bodies of Commercial Fishing Importance, Including Standards for Maximum Permissible Concentrations of Harmful Substances in the Waters of Water Bodies of Commercial Fishing Importance:* Order of the Ministry of Agriculture of Russia dated December 13, 2016, No. 552. Moscow: Ministry of Agriculture of Russia (in Russian).

[3)] Warmer, H. and van Dokkum, R., 2002. *Water Pollution Control in the Netherlands. Policy and Practice 2001:* RIZA Report 2002.009. Neue Niederlandische Liste. Altlasten Spektrum 3/95. Lelystad, 77 p. Available at: https://edepot.wur.nl/674312 [Accessed: 2 March 2025].

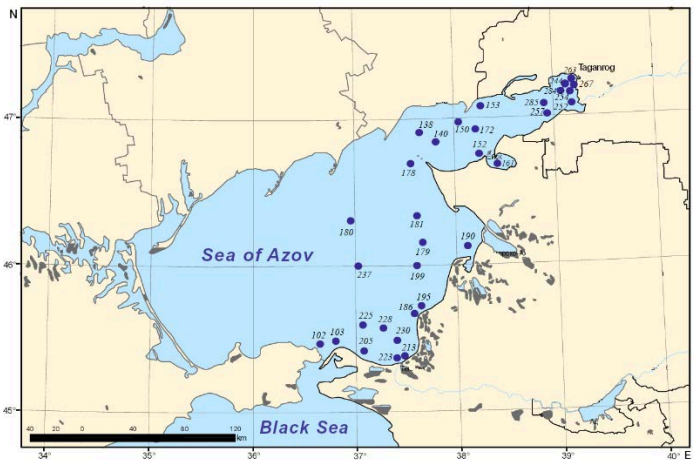

Fig. 1. Map of water and bottom sediments sampling in 2010–2023 (numbering of stations by *Azovmorinformcenter* branch of *Tsentrregionvodkhoz*)

Coefficients (C_a) of accumulation of heavy metals by bottom sediments were calculated according to formula [2]:

$$C_a = 1000\ (C_{bs}/C_w).$$

Relationship between coefficient of accumulation of metals in bottom sediments (C_a) and their concentration in water (C_w) is described by equation of straight line on the graphs with a logarithmic scale on the ordinate axes ($C_a - C_w$). This indicates that the processes of sorption interaction of bottom sediments with dissolved heavy metals in water are described by power function, which coincides with Freundlich adsorption equation:

$$C_a = C_{bo}/C_w = a\,C_w^{-n}, \quad (3)$$

where a is coefficient which corresponds to adsorption and depends on the nature of adsorbent and adsorbate, it is determined graphically; n is power exponent.

AC of bottom sediments of water areas is determined from relationship [2, p. 283]

$$Q = S\,v_{sed}\,C_{bs}, \quad (4)$$

where S is area of the water area under consideration, km^2; v_{sed} is sedimentation rate, g·m^{-2}·year^{-1}. Taking into account formula (3) and equation (4), expression $C_{bs} = C_w\,C_a$ is transformed into a ratio that can be used for normalization according to ecotoxicological criteria (with C_w = MPC):

$$Q = S\,v_{sed}\,C_w\,a\,C_w^{-n}, \quad (5)$$

where S is area of the water area under consideration, km^2; v_{sed} is sedimentation rate, g·m^{-2}·year^{-1}; C_w is metal concentration in water, μg/L; a is coefficient which corresponds to adsorption and depends on the nature of adsorbent and adsorbate, it is determined graphically (highlighted in bold in the equation of the power function in Figs. 2, *e* and 3, *e*); n is power exponent.

Parameters of the studied areas

Area	Total area, km^2 [7]	Volume, km^3 [7]	Average depth, m [7]	Average rate of sedimentation [1)], $g \cdot m^{-2} \cdot year^{-1}$
Taganrog Bay	5600	25	4.9	700
Open sea	33,400	231	7	300

The AC of bottom sediments in the open sea and in Taganrog Bay (Table) was calculated for the period of 1991–2023 for copper, for the period of 1993–2023 for zinc.

Results and discussion

Copper. The most powerful source of anthropogenic input of copper into the environment – up to 75% of the total – is non-ferrous metal production [8]. This trace element is intensively transported with atmospheric fluxes. Up to 13% of the total concentration of copper in surface waters of the seas is the share of dry deposition with wind dust and atmospheric precipitation [5]. River runoff of the Don and Kuban rivers is also a significant source of copper intake. Thus, according to the results of studies [9], in the lower reaches of the Don River copper concentration exceeded MPC_w for fresh waters of fishery objects everywhere, and in [10] it ranged from 1–14 μg/L (average value 3.5 μg/L). Partially copper comes with the products of coastal abrasion, which causes its high content in the Taganrog Bay coastal zone [11]. In addition, copper can enter the ecosystem of the Sea of Azov with diffuse wash-off of mineral fertilizers and chemical plant protection products from agricultural lands located on the catchments of the Don and Kuban rivers [12], as well as with wastewater from industrial, household and municipal services enterprises [5, 9–11]. Thus, according to generalized data, the discharge of copper as part of wastewater into the Sea of Azov within the boundaries of the Rostov Region, according to data from the federal statistical report according to form 2-TP (*Vodkhoz*) for 2023, is 64.7 kg (data from the Water Resources Department of the Rostov Region, Don Basin Water Administration, Rostov-on-Don).

Copper concentrations in the water of the Sea of Azov exceeded MPC_w in different years. In 1991–1995, its concentration in the water of the open part of the sea and Taganrog Bay decreased (Fig. 2, *a*), and then an increasing trend of

copper contamination of water in both areas was observed. In 2010–2017, the annual average concentration of copper in the open sea exceeded MPC_w and ranged from 5.2 to 8.1 μg/L. According to the results of the 2020–2023 surveys, the annual average values of copper in the open sea and in Taganrog Bay exceeded MPC_w and were 9.5 and 6.2 μg/L, respectively.

The physical and chemical composition of bottom sediments provides information on the accumulation and distribution of heavy metals over a longer period of time than water analysis, which characterizes its quality only at a given moment [13]. The sorption of ions and compounds of heavy metals by suspended matter and bottom sediments plays a special role among in-water processes, which, in the opinion of many researchers, are determinant, making the greatest contribution to the self-purifying capacity of a water body. The intensity of sorption depends on the pH and Eh values of the medium, the presence of clay particles, ligands, humic acids, ferromanganese oxides and a number of copper-binding cations [14].

The spatial distribution of copper in bottom sediments of the Sea of Azov was characterized by mosaic and variability. Thus, copper concentration was in the range of 21.0–37.0 μg/g dry wt. (average 29.8 μg/g dry wt.) in 1991–1999, 33.0–42.0 μg/g dry wt. (average 35.5 μg/g dry wt.) in 2000–2005 and further decreased with an increase in some years (Fig. 2, *b*). According to the data, no values exceeding the MPC value were observed during the specified periods. In 2011–2023, offshore concentrations ranged from 1.4 to 30 μg/g dry wt. (average 9.3 μg/g dry wt.) and those in Taganrog Bay were from 4.1 to 40 μg/g dry wt. (average 15.2 μg/g dry wt.). The highest concentrations of copper in bottom sediments were recorded in the areas of clay silt development, namely, in the central, north-western and western parts of Taganrog Bay, Yasen Bay, southern and central parts of the sea as well as on the Kuban River seashore.

Calculations based on formula (1) showed that the sedimentation flux of copper deposition into bottom sediments ranged in different years from 14 to 381 t/year (average 217 t/year) in the open sea and from 16 to 153 t/year (average 95 t/year) in Taganrog Bay (Fig. 2, *c*). Periods of sediment turnover of copper in the sea proper and in Taganrog Bay calculated by formula (2) at different concentrations of copper in water amounted to 0.5 and 1.6 years on average, respectively (Fig. 2, *d*). The dependence of the coefficient of copper accumulation by bottom sediments on its content in the aquatic environment shows moderate relationship and is described by equation of straight line in logarithmic scales along the ordinate axes (Fig. 2, *e*). When these data were approximated by the power function equation, the following was obtained for the open part of the sea: $C_a = 33{,}831\ C_w^{-1.569}$, for Taganrog Bay: $C_a = 30{,}976\ C_w^{-1.293}$. It is shown that the parameters of these equations are indicators of the AC of bottom sediments with respect to copper. They can be used for the purposes of ecological standardization taking into account sanitary and hygienic norms. If we assume $C_w = MPC_w$, then C_a of copper for the open part of the sea is 2708 and that for Taganrog Bay is 3866. To assess the AC of bottom sediments of the open part of the Sea of Azov, substituting corresponding values into expression (5) and taking into account the dimensionality, we obtain Q = 135.6 t/year and for Taganrog Bay Q = 75.7 t/year.

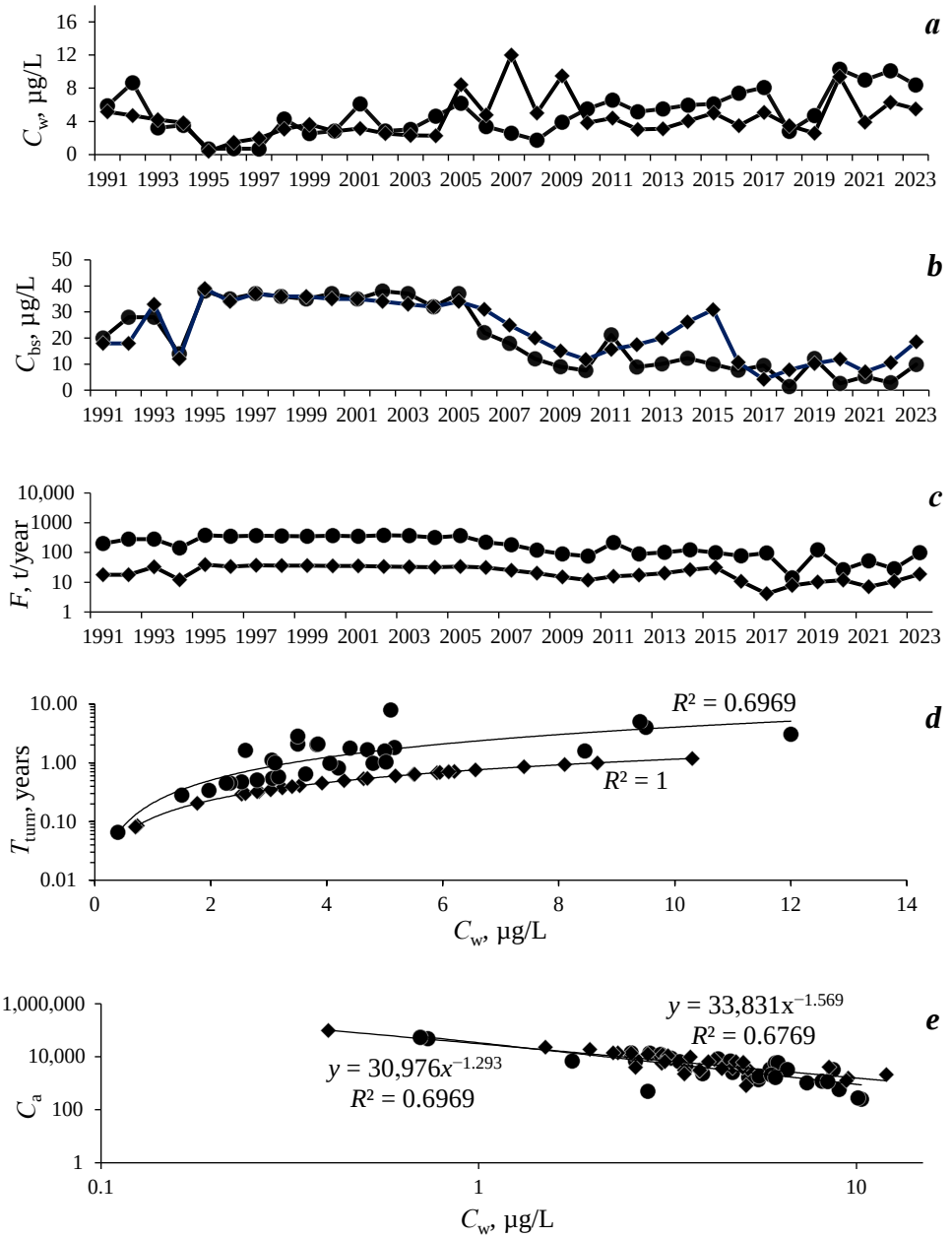

Fig. 2. Characteristics of copper distribution in open sea (•) and Taganrog Bay (♦): concentration in water, µg/L (*a*); concentration in the surface layer of bottom sediments, µg/g dry mass (*b*); flux of copper deposition into bottom sediments, t/year (*c*); period of sediment turnover of copper in water, years (*d*); dependence of the change in the coefficient of copper accumulation in bottom sediments on its concentration in water (*e*)

It should be noted that in addition to sedimentation, sediment is agitated at the water-bottom interface. At high values of dynamic velocity near the bottom, this sediment is agitated and then reenters the water. This is especially important for the Sea of Azov because of its shallow water and the tendency of the upper layer of bottom sediments to resuspend. Taking into account the results of [15, 16] and our own data, it was assumed in our study that the settling rate of particles after agitation was 7.5 mm/s (aleurite) and 0.04 mm/s (silt). Thus, the period of gravitational return of suspended sediments from the surface layers of the sea to the bottom sediments at a depth of up to 15 m will not exceed 28–30 h, i. e. it will be estimated on a daily time scale. In our case, annual average time scale of the study was considered. Therefore, the effect of turbulence was taken into account integrally when assessing the rate of sedimentation processes.

Zinc. Zinc enters natural waters as a result of the breakdown and dissolution of rocks and minerals (ZnS – sphalerite, ZnO – zincite, $ZnSO_4 \times 7H_2O$ – goslarite, $ZnCO_3$ – smithsonite, etc.) as well as with wastewater from mining and processing plants and electroplating shops, production units of parchment paper, mineral paints, viscose fibre [17]. For example, zinc discharge into the Sea of Azov as part of wastewater from enterprises of the Rostov Region was 570 kg in 2023 (according to form 2-TP (*Vodkhoz*)). Zinc is one of the vital elements for the biota. Hormonal metabolism, immune reactions, stabilization of ribosomes and cell membranes of hydrobionts are impossible without zinc participation [4)]. Zinc content in unpolluted water bodies is usually 0.5–15 μg/L. Zinc occupies an intermediate position between mercury and copper, on the one hand, and lead and cadmium, on the other hand, in terms of toxic effects on the biota, affecting significantly the behavioural and reproductive functions of fishes [1)].

In the Sea of Azov, the 1993–2006 period is characterized by low annual average zinc concentrations in the range of 2.2–12.2 μg/L in the open sea and 2.2–22.3 μg/L in Taganrog Bay (Fig. 3). In 2007–2014, a gradual increase in the annual average concentration was observed up to 38 μg/L in the open sea and 27 μg/L in Taganrog Bay. In 2020–2023, zinc content was 21.5 μg/L in the open sea and 6.9 μg/L in Taganrog Bay (Fig. 3, *a*). Zinc concentration in several water samples exceeded MPC_w in different years, mainly in Kuban-Akhtarsky and Kuban-Temryuksky districts (up to 79 μg/L), which is explained by the influence of the towns of Primorsko-Akhtarsk and Temryuk, metal removal with the Kuban River water, polluted discharges from rice paddies and runoff from adjacent fields as well as removal of contaminants with storm water of residential areas [18]. In the water sample taken in the Taganrog Bay central part on 16.10.2014, zinc concentration of 750 μg/L was recorded. Such an abnormally high value can be related to severe flooding on 24.09.2014 in Taganrog Bay and the Don estuary when the water level rose by 251 cm. The Don River waters are a significant source of zinc input into Taganrog Bay. In [10], the data on the content of dissolved forms

---

[4)] Moore, J.W. and Ramamoorthy, S., 1984. *Heavy Metals in Natural Waters*. Springer, 268 p. https://doi.org/10.1007/978-1-4612-5210-8

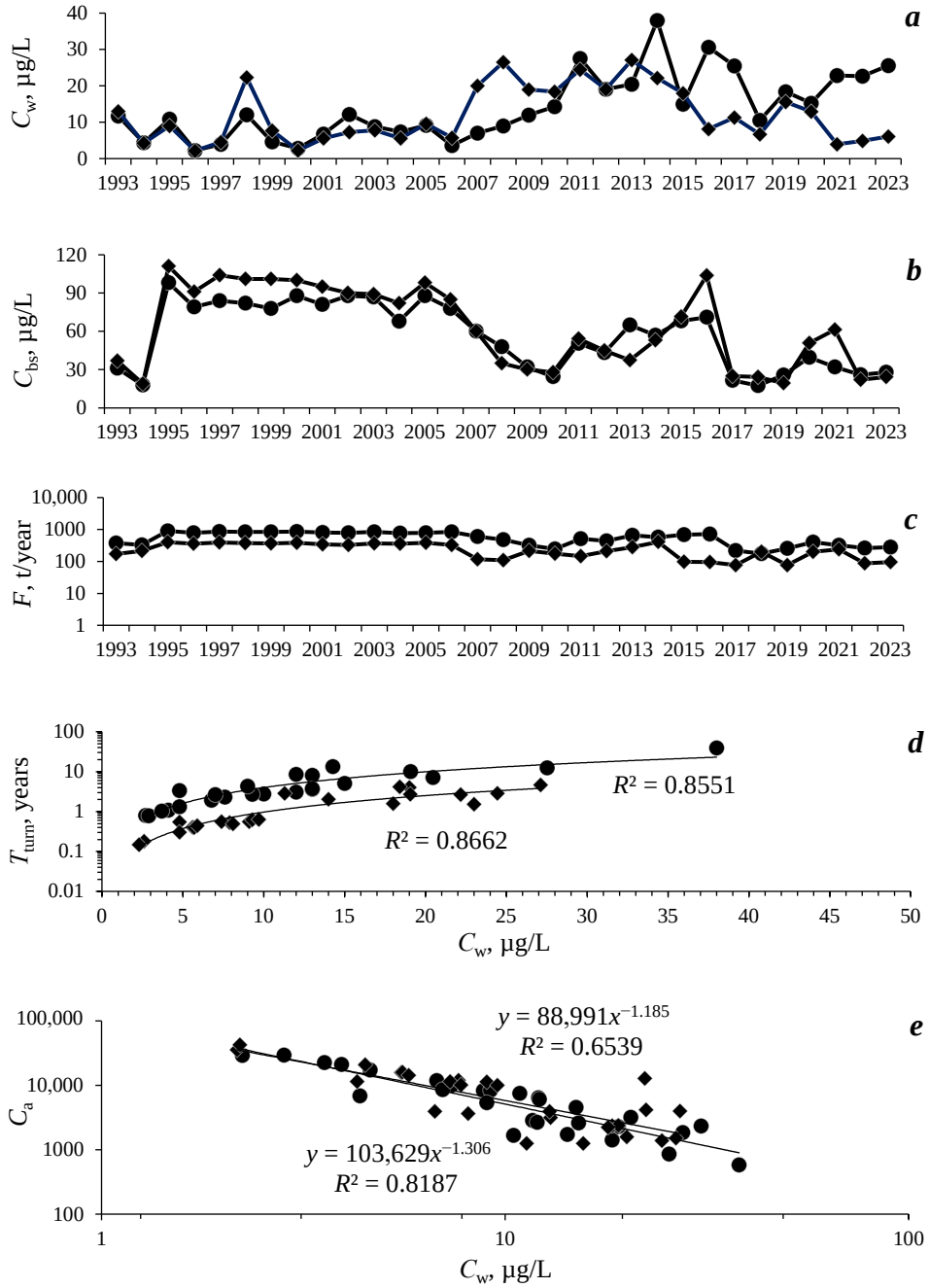

Fig. 3. Characteristics of zinc distribution in the open sea (•) and Taganrog Bay (♦): concentration in water, µg/L (*a*); concentration in the surface layer of bottom sediments, µg/g dry mass (*b*); flow of zinc deposition into bottom sediments, t/year (*c*); period of sediment turnover of zinc in water, years (*d*); dependence of the change in the coefficient of zinc accumulation by bottom sediments on its concentration in water (*e*)

of zinc in the lower reaches of the Don River are given. Thus, zinc concentration ranged from 1 to 10 μg/L (average value 5.6 μg/L) [18].

In bottom sediments, zinc concentrations did not reach MPC for the entire observation period and ranged from 17.1 to 98.0 μg/g in the sea proper and from 19.0 to 111.0 μg/g in the bay (Fig. 3, *b*). Higher zinc values correspond to the zone of clay silt distribution.

The results of assessment of zinc deposition fluxes in bottom sediments using formula (1) indicate (Fig. 3, *c*) that the flux of sedimentation self-purification of waters from this trace element was 175–902 t/year (with an average of 601 t/year) in the open sea and 76–407 t/year (average 256 t/year) in Taganrog Bay. Fig. 3, *d* shows that the sediment turnover period of zinc was 0.7–39.8 years in the open sea and 0.1–4.8 years in Taganrog Bay (Fig. 3, *d*). Fig. 3, *d* demonstrates that the dependence of changes in coefficients of the accumulation of zinc by bottom sediments at different concentrations of zinc in water is described with a sufficient degree of adequacy by equation of straight line in logarithmic scale along the ordinate axes (Fig. 3, *e*). For the open part of the sea, it was $C_a = 103{,}629\ C_w^{-1.306}$ and for Taganrog Bay, is was $C_a = 88{,}991\ C_w^{-1.185}$. If we assume $C_w = MPC_w$, then C_a is 626 for the open part of the sea and 863.1 for Taganrog Bay.

The AC of bottom sediments with respect to zinc calculated by relation (5) was 313.6 t/year for the open part of the sea and 169.1 t/year for Taganrog Bay.

The obtained calculated AC values of bottom sediments can be used for normalization of copper and zinc discharges into the ecosystem of the Sea of Azov.

Conclusions

According to the data for the 30-year period of studies, it was established that annual average concentrations of copper in dissolved form in water in different years exceeded MPC_w for water bodies of fishery importance by 1.5–2 times both in the open sea and in Taganrog Bay. In some samples, copper concentration values reached 4–5 MPC_w, mainly in the Kuban-Akhtarsky district and in the eastern part of Taganrog Bay. In the open sea, annual average copper concentrations for the last five years were slightly higher than in the bay. Annual average zinc concentrations in the water of the Sea of Azov did not exceed MPC_w for the entire study period. Higher values in the open sea were recorded in the Kuban-Akhtarsky and Kuban-Temryuksky districts, in Taganrog Bay – in the area of the Mius Liman and in the zone of influence of the town of Yeysk.

The content of copper and zinc in the bottom sediments of the Sea of Azov did not reach MPC, with the highest values of these metals recorded in the areas of clay silt distribution.

Data on sedimentation rates and concentrations of copper and zinc in bottom sediments made it possible to assess the fluxes of sedimentation self-purification of water from these metals. Deposition fluxes lead to a decrease in the content of pollutants in water, i.e. the effect of the flux is aimed at compensating for the causes of the flux. Thus, the flux of metals deposited in bottom sediments demonstrates the manifestation of the Le Chatelier–Braun principle under natural conditions.

Copper deposition flux averaged 217 t/year in the open sea and 95 t/year in Taganrog Bay. Zinc flux from water to bottom sediments averaged 601 t/year in the open sea and 256 t/year in Taganrog Bay.

Sediment turnover periods reflect the time scale of sedimentation self-purification of waters. This parameter for copper averaged 0.5 years in the open sea and 1.6 years in Taganrog Bay. The zinc turnover period averaged 7.7 years in the open sea and 1.8 years in Taganrog Bay.

The study of the trend of changes in the coefficient of copper and zinc accumulation by bottom sediments showed that the increased intensity of sedimentation self-purification of waters at low concentrations of copper and zinc in water was provided by high (with $C_a > n \cdot 10^4$ units) concentrating ability of bottom sediments. With increasing degree of water pollution by copper and zinc, the value of Kn decreased; accordingly, the contribution of sedimentation processes to water self-purification also decreased.

The AC values of bottom sediments expressed through flux dimensions can be accepted as quantitative criteria for normalization of the maximum permissible amount of pollutants entering the water area, at which their concentration in water will not exceed MPC_w. Thus, for the normal functioning of the ecosystem, no more than 135.6 t/year of copper and 313.6 t/year of zinc should enter the open part of the Sea of Azov, while in Taganrog Bay, the input limits are 75.7 t/year for copper and 169.1 t/year for zinc.

REFERENCES

1. Goldberg, G.A. and Zats, V.I., 1991. *Modelling of Selfpurification Processes of the Shelf Zone Sea Water*. Sevastopol: IBSS, 59 p. (in Russian).
2. Egorov, V.N., 2019. *Theory of Radiousotope and Chemical Homeostasis of Marine Ecosystems*. Sevastopol: IBSS, 356 p. (in Russian).
3. Egorov, V.N., Gulin, S.B., Malakhova, L.V., Mirzoeva, N.Y., Popovichev, V.N., Tereshchenko, N.N., Lazorenko, G.E., Plotitsina, O.V., Malakhova, T.V., Proskurnin, V.Y., Sidorov, I.G., Stetsyuk, A.P. and Gulina, L.V., 2018. Rating Water Quality in Sevastopol Bay by the Fluxes of Pollutant Deposition in Bottom Sediments. *Water Resources*, 45(2), pp. 222–230. https://doi.org/10.1134/S0097807818020069
4. Bufetova, M.V. and Egorov, V.N., 2023. Lead Contamination of Water and Sediments of Taganrog Bay and the Open Part of the Sea of Azov in 1991–2020. *Ecological Safety of Coastal and Shelf Zones of Sea*, (2), pp. 105–119. https://doi.org/10.29039/2413-5577-2023-2-105-119
5. Klenkin, A.A., Korpakova, I.G., Pavlenko, L.F. and Temerdashev, Z.A., 2007. [*Ecosystem of the Sea of Azov: Anthropogenic Pollution*]. Krasnodar: OOO "Prosveshcheniye-Yug", 324 p. (in Russian).
6. Korablina, I.V., Sevostyanova, M.V., Barabashin, T.O., Gevorgyan, J.V., Katalevsky, N.I. and Evseeva, A.I., 2018. Heavy Metals in the Ecosystem of the Azov Sea. *Problems of Fisheries*, 19(4), pp. 509–521. https://doi.org/10.36038/0234-2774-2018-19-4-509-521
7. Goptarev, N.P., Simonov, A.I., Zatuchnaya, B.M. and Gershanovich, D.E., eds., 1991. [*Hydrometeorology and Hydrochemistry of Seas of the USSR. Vol. 5. The Sea of Azov*]. St. Petersburg: Gidrometeoizdat, 236 p. (in Russian).
8. Putilina, V.S., Galitskaya, I.V. and Yuganova, T.I., 2013. *Sorption When Groundwater Contaminating by Heavy Metals and Radioactive Elements. Copper*. Novosibirsk: GPNTB SO RAN. Iss. 100, 95 p. (in Russian).

9. Matishov, G.G., Stepan'yan, O.V., Har'kovskii, V.M., Startsev, A.V., Bulysheva, N.I., Semin, V.V., Soier, V.G., Kreneva, K.V., Glushchenko, G.Y. and Svistunova, L.D., 2016. Characteristic of Lower Don Aquatic Ecosystem in Late Autumn. *Water Resources*, 43(6), pp. 873–884. https://doi.org/10.1134/S009780781606004X
10. Garkusha, D.N., Fedorov, Yu.A. and Predeina, L.M., 2022. Spatiotemporal Dynamics of Copper and Zinc Concentrations in the Lower Don Water. *Russian Meteorology and Hydrology*, 47(3), pp. 232–240. https://doi.org/10.3103/S1068373922030098
11. Khrustalev, Yu.P., 1999. *The Fundamental Problems of the Sedimentogenesis Geochemistry in the Azov Sea*. Apatity: Publishing house of the KSC RAS, 247 p. (in Russian).
12. Bufetova, M.V., 2020. Analysis of Changes in the Coefficient of Bottom Accumulation of Heavy Metals from their Concentration in the Water of the Sea of Azov. *Scientific Notes of V.I. Vernadsky Crimean Federal University. Geography. Geology*, 6(2), pp. 193–206 (in Russian).
13. Davydova, O.A., Korovina, E.V., Vaganova, E.S., Guseva, I.T., Krasun, B.A., Isaeva, M.A., Martseva, T.Y., Mulyukova, V.V., Klimov, E.S. and Buzaeva, M.V., 2016. Physical-Chemistry Aspects of Migratory Processes of Heavy Metals in Natural Aqueous Systems. *Bulletin of South Ural State University. Series Chemistry*, 8(2), pp. 40–50. https://doi.org/10.14529/chem160205 (in Russian).
14. Saeva, O.P., Yurkevich, N.V., Kabannik, V.G. and Kolmogorov, Y.P., 2013. Determining the Effectiveness of Natural Reactive Barriers for Acid Drainage Neutralization Using Sr-Xrf Method. *Bulletin of the Russian Academy of Sciences: Physics*, 77(2), pp. 214–216. https://doi.org/10.3103/S1062873813020305
15. Martyanov, S.D., Ryabchenko, V.A. and Rybalko, A.E., 2011. Modelling of Sediment Resuspension in the Neva Bay. *Proceedings of the Russian State Hydrometeorological University*, 20, pp. 13–26 (in Russian).
16. Gerasyuk, V.S. and Berdnikov, S.V., 2021. Experimental Estimation of the Deposition Rate of Water Suspended Particulate Matter in the Mouth of the Don River and in Taganrog Bay. *Oceanology*, 61(5), pp. 687–696. https://doi.org/10.1134/S0001437021040056
17. Putilina, V.S., Galitskaya, I.V. and Yuganova, T.I., 2013. *Sorption When Groundwater Contaminating by Heavy Metals and Radioactive Elements. Zinc*. Novosibirsk: GPNTB SO RAN. Iss. 102, 99 p. (in Russian).
18. Bufetova, M.V., 2024. Dynamics of multi-year variability of copper and zinc content in the Azov Sea water (1991–2023). In: IBSS, 2024. *Study of Aquatic and Terrestrial Ecosystems: History and Modernity: Book of Abstracts of the 3rd International Scientific and Practical Conference, 2–7 September, 2024, Sevastopol, Russian Federation*. Sevastopol: IBSS, pp. 198–199 (in Russian).

Submitted 15.05.2024; accepted after review 10.09.2024;
revised 17.12.2024; published 31.03.2025

About the author:

Marina V. Bufetova, Associate Professor of the Department of Ecology and Nature Management, Faculty of Ecology, Sergo Ordzhonikidze Russian State University for Geological Prospecting (23 Miklukho-Maklaya St., Moscow, 117997, Russian Federation), Associate Professor, PhD (Geogr.), **ORCID ID: 0000-0002-6247-1698**, *mbufetova@mail.ru*

The author has read and approved the final manuscript.

Original paper

The Dynamics of the Mollusks *Mytilaster lineatus* Settlement in the Black Sea Waters with Different Degrees of Petroleum Pollution

Yu. S. Tkachenko *, E. A. Tikhonova, T. V. Viter

A. O. Kovalevsky Institute of Biology of the Southern Seas of RAS, Sevastopol, Russia
* *e-mail: yulechkatkachenko.90@mail.ru*

Abstract
The paper estimates the dynamics of the settlement of mytilasters in the coastal water area with different degrees of petroleum pollution using the example of Sevastopol Bay (high level of anthropogenic load) and Laspi Bay (conditionally clean water area). To assess the marine environment quality at the sites of mytilaster fouling in the mentioned bays, data on the petroleum hydrocarbons content in the water was analysed (2012, 2015, 2018). The study material was samples of *Mytilaster lineatus* mollusks and bottom sediments taken in Sevastopol Bay from 2012 to 2018 at depths from 7 to 17 m during three sanitary and biological surveys. The abundance of mytilasters on various natural and artificial substrates of Sevastopol Bay in 2012, 2015 and 2018 under conditions of chronic oil pollution was analysed. It was revealed that the abundance of mytilasters on solid substrates was primarily influenced not by pollution of the marine environment but by water temperature and surf-wave phenomena. The values of the functional abundance index show that under chronic petroleum pollution, mytilasters, inhabiting artificial substrates of Sevastopol Bay, make a more significant contribution to transformation of matter and energy. At the same time, the energy significance of the studied mollusks in the soils of Sevastopol Bay is considerably lower than that in the conditionally clean water area (Laspi Bay). An analysis of average abundance and biomass of mollusks for 2012, 2015 and 2018 showed that the number of mytilasters in the marine soils of Sevastopol Bay increased. It was established that the quality of life of the community was influenced by the physical and chemical parameters of bottom sediments, which either accelerate or slow down the oxidation processes, thereby changing the oxygen level in the bottom sediments. According to the correlation analysis results, there is a direct relationship between the abundance, biomass of mollusks and concentrations of chloroform-extractable substances, petroleum hydrocarbons and redox potential. It was revealed that in the soils of Laspi Bay, the quantitative indicators of mytilasters were four times higher than in Sevastopol Bay.

Keywords: coastal waters, Mytilaster, artificial substrates, natural substrates, petroleum hydrocarbons, Black Sea

Acknowledgments: This work was carried out under IBSS state research assignment “Study of biogeochemical patterns of radioecological and chemoecological processes in the ecosystems of water bodies of the Sea of Azov-Black Sea Basin in comparison with other areas

of the World Ocean and individual aquatic ecosystems of their drainage basins to ensure sustainable development in the southern seas of Russia" (No. 124030100127-7).

For citation: Tkachenko, Yu.S., Tikhonova, E.A. and Viter, T.V., 2025. The Dynamics of the Mollusks *Mytilaster lineatus* Settlement in the Black Sea waters with Different Degrees of Petroleum Pollution. *Ecological Safety of Coastal and Shelf Zones of Sea*, (1), pp. 137–154.

Динамика поселения моллюсков *Mytilaster lineatus* в черноморской акватории с различной степенью нефтяного загрязнения

Ю. С. Ткаченко *, Е. А. Тихонова, Т. В. Витер

Институт биологии южных морей имени А. О. Ковалевского РАН, Севастополь, Россия

* *e-mail: yulechkatkachenko.90@mail.ru*

Аннотация

Оценена динамика поселения митилястеров в прибрежной акватории с различной степенью нефтяного загрязнения на примере бухт Севастопольской (высокий уровень антропогенной нагрузки) и Ласпи (условно чистая акватория). Для оценки качества морской среды в местах отбора обрастаний митилястеров в бухтах Севастопольской и Ласпи проанализировали данные о содержании нефтяных углеводородов в воде (2012, 2015 и 2018 гг.). Материалом для исследования послужили пробы моллюсков *Mytilaster lineatus* и донных осадков, отобранные в Севастопольской бухте с 2012 по 2018 г. с глубин от 7 до 17 м в рамках трех санитарно-биологических съемок. Проанализировано обилие митилястеров на различных естественных и искусственных субстратах б. Севастопольской в 2012, 2015 и 2018 гг. в условиях хронического нефтяного загрязнения. Выявлено, что на обилие митилястеров на твердых субстратах в первую очередь влияет не загрязнение морской среды, а температура воды и прибойно-волновые явления. Значения индекса функционального обилия показывают, что в условиях хронического нефтяного загрязнения митилястеры, обитающие на искусственных субстратах б. Севастопольской, вносят более значимый вклад в преобразование вещества и энергии. При этом энергетическая значимость исследуемых моллюсков в грунтах б. Севастопольской значительно ниже, чем в условно чистой акватории (б. Ласпи). Анализ средних значений численности и биомассы моллюсков в 2012, 2015 и 2018 гг. показал, что обилие митилястеров в морских грунтах б. Севастопольской увеличилось. Установлено, что на качество жизни сообщества оказывают влияние физико-химические показатели донных осадков, которые либо ускоряют, либо замедляют процессы окисления, изменяя тем самым содержание кислорода в донных отложениях. По результатам корреляционного анализа наблюдается прямая взаимосвязь между численностью, биомассой моллюсков и концентрациями хлороформ-экстрагируемых веществ, нефтяных углеводородов и окислительно-восстановительным потенциалом. Выявлено, что в грунтах б. Ласпи количественные показатели митилястеров в четыре раза выше, чем в б. Севастопольской.

Ключевые слова: прибрежная акватория, митилястеры, искусственные субстраты, естественные субстраты, нефтяные углеводороды, Черное море

Благодарности: работа выполнена в рамках государственного задания ФИЦ ИнБЮМ по теме «Изучение биогеохимических закономерностей радиоэкологических и хемоэкологических процессов в экосистемах водоемов Азово-Черноморского бассейна в сравнении с другими акваториями Мирового океана и отдельными водными экосистемами их водосборных бассейнов для обеспечения устойчивого развития на южных морях России» (№ гос. регистрации 124030100127-7).

Для цитирования: *Ткаченко Ю. С., Тихонова Е. А., Витер Т. В.* Динамика поселения моллюсков *Mytilaster lineatus* в черноморской акватории с различной степенью нефтяного загрязнения // Экологическая безопасность прибрежной и шельфовой зон моря. 2025. № 1. С. 137–154. EDN YFOTIP.

Introduction

Mytilaster (*Mytilaster lineatus* (Gmelin, 1791)) is a mass and widespread Black Sea species of coastal communities, forming settlements on various natural and artificial substrates. These mollusks contribute significantly to the filtration activity of mytilid settlements [1, 2], acting as a powerful natural biofilter [3]. Mytilasters are known to filter water 18 h/day [1)], removing bacterial suspension from it [4]. They are able to reduce the level of organic pollution of the water area significantly, including the concentration of petroleum products [5].

The mollusks under study are distributed quite widely and can be found on the Atlantic coast of southern Europe as well as in all seas of the Mediterranean basin [3]. They have been introduced to the Caspian Sea, where they are widely distributed [2)]. Mytilasters dominate in most areas of the Sea of Azov [6], forming settlements in muds under conditions of hypoxia and elevated temperatures as well as at increased content of petroleum products in bottom sediments [7].

Mytilasters are found in the Black Sea from the water edge to depths of 50–70 m. However, they form permanent breeding settlements only at shallow depths (3–8 m), mainly in the coastal zone. There, mytilasters are found on rocks among cystosira thickets (natural substrate) and on hydraulic structures (artificial substrate) [8, 9]. Mollusks also form mud communities, but less abundant than on hard substrates [3]. An increase in the abundance and biomass of Mytilaster species is observed in sheltered parts of bays where the surf action is weakened [10].

In recent years, the mytilid fouling of the Crimean coast has undergone a significant transformation [11, 12]. Mussels become smaller and less abundant, and mytilasters inhabit free spaces on both natural and artificial substrates [9]. The dominance of the studied mollusk species was previously observed on hydraulic structures of various coastal waters of Sevastopol [13]. In 2008–2009, the bivalve

---

[1)] Mironov, G.N., 1948. [Filtration and Nutrition of Black Sea Mussels]. *Trudy Sevastopolskoy Biologicheskoy Stantsii*, 6, pp. 338–352 (in Russian).

[2)] Scarlato, O.A. and Starobogatov, Ya.I., 1972. Class Bivalvia. In: V. A. Vodyanitskiy, ed., 1972. [*Field Guide for the Black Sea and the Sea of Azov Fauna*]. Kiev: Naukova Dumka. Vol. 3, pp. 178–249 (in Russian).

Mytilaster lineatus was also clearly dominant among other macrozoobenthos species in terms of abundance, biomass, and occurrence in all seasons and at all depths on the rocky soil of Karantinnaya Bay (Sevastopol) [14].

From 2009 to 2014, mytilasters were recorded on natural hard substrates in the waters of such reserves of the Crimean Peninsula as Cape Martyan Reserve, Karadag, Opuk, Kazantip Nature Reserves as well as in the water area of the Tarkhankut National Nature Park [15]. At the same time, this mollusk found in the above five areas has the highest abundance and biomass.

Petroleum and petroleum products are main permanent pollutants of the Black Sea coastal waters, including the Sevastopol water area. Sevastopol Bay is most polluted by the parameter under consideration [10]. It belongs to the water areas of active economic use, the main part of its coastline is occupied by berths and related infrastructure with a total length of 11 km. At the same time, the harbour is home to a significant number of warships and civilian vessels, which are one of the main sources of pollution of the bay with petroleum products. In addition, storm water and sewage runoff are discharged into the water area, and due to impeded water exchange, pollutants accumulate in the bay bottom sediments, worsening its ecological condition.

Mytilasters occur in Sevastopol Bay on all the above described substrates [1, 9, 16] and play an important role in the process of marine environment self-purification from petroleum and petroleum products. This was a prerequisite for studying the dynamics of mytilaster settlements in this polluted area. Laspi Bay was chosen as a conditionally clean water area, the coastal zone of which is characterised as relatively safe in terms of certain physical and chemical and microbiological parameters of seawater [17].

The aim of the work is to analyse the dynamics of settlement of mytilasters on natural and artificial substrates in the coastal waters with different degrees of petroleum pollution (on the example of Sevastopol and Laspi bays) according to the literature data and data of monitoring surveys (2012, 2015, 2018).

Within the framework of the set aim, the following tasks were formulated:

1) to analyse the abundance of mytilasters on various natural and artificial substrates of Sevastopol Bay for 2012–2018 in the conditions of chronic petroleum pollution of the studied water area according to the literature data;

2) to determine the abundance and biomass of *Mytilaster lineatus* mollusks in the Sevastopol Bay muds based on the data of monitoring surveys in 2012, 2015 and 2018, taking into account the pollution of bottom sediments with organic substances, including petroleum hydrocarbons;

3) to determine the contribution of mytilasters to the processes of matter and energy transformation in bottom communities in water areas subjected to chronic petroleum pollution and in conditionally clean water areas;

4) to compare mollusk settlements in conditionally clean and polluted water areas.

Material and methods

To assess the quality of the marine environment at the sites of sampling of mytilaster fouling in Sevastopol and Laspi bays, literature data on the content of petroleum hydrocarbons (PHCs) in water were analysed [10, 18–20] (Figure, *a, c*).

The indicators of abundance and biomass of mytilasters on artificial substrates in Sevastopol Bay were analysed according to literature data [9, 10, 13, 21]. The scheme of location of mollusk sampling stations from the mooring walls is presented in Figure, *b*.

Samples of *Mytilaster lineatus* mollusks and bottom sediments were taken in Sevastopol Bay from 2012 to 2018 at depths ranging from 7 to 17 m (Figure, *a*) during three sanitary and biological surveys conducted systematically by the Laboratory of Chemoecology (formerly the Department of Marine Sanitary Hydrobiology) of Institute of Biology of the Southern Seas.

To determine hydrobionts, bottom sediments were sampled with a Petersen dredge (0.038 m^2 capture area) in two repetitions. The bottom sediment was washed through a sieve (1 mm mesh diameter), fixed with ethanol (96%) and then viewed under binoculars. Next, the abundance and crude weight of the organisms

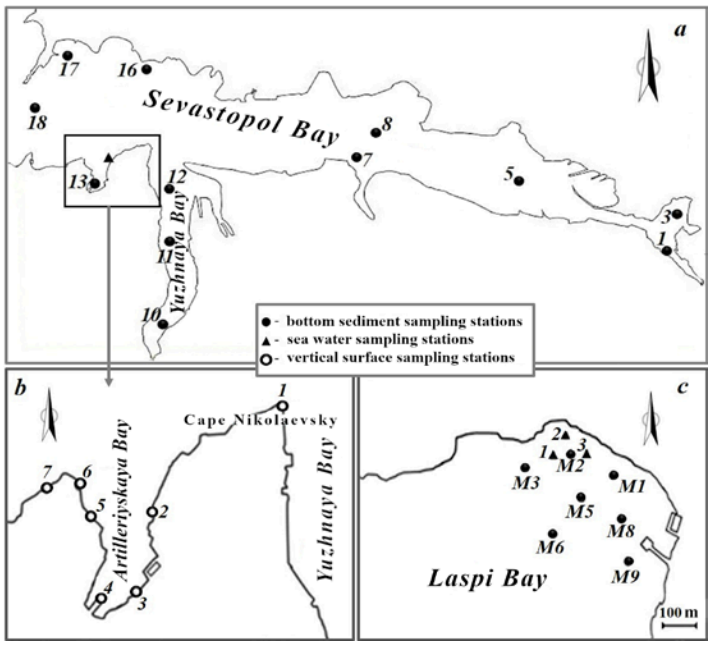

Location of sampling stations for bottom sediment in Sevastopol Bay (*a*), mytilasters from hydraulic structures in Sevastopol Bay (*b*) (literature data [12]) in 2012, 2015, 2018 and seawater and bottom sediment in Laspi Bay in 2017 (*c*) (literature data [22])

were determined. Specimens smaller than 1 mm were not recorded. Bivalves were weighed after they had been opened and the fixing solution had been removed from the mantle cavity.

In recently collected sediment samples, pH and Eh were determined using a pH-150MA meter and natural moisture was determined by weight method.

To determine hydrocarbons, marine sediments were air-dried under laboratory conditions, ground in a mortar and sieved through a sieve with a mesh diameter of 0.25 mm.

In air-dry samples, the amount of chloroform-extractable substances (CES) was determined by weight method, and PHCs were determined by IR spectrometry [3)] using an FSM-1201 spectrophotometer. All results obtained for the CES and PHCs concentrations were converted to 100 g of air-dry bottom sediment (ADBS). Correlation analysis was used for statistical processing of the material. The correlation coefficient was calculated at $P = 0.05$ in Microsoft Excel programme.

To determine the relationship between the analysed environmental parameters (Eh and pH), we used index rH_2 calculated for bottom sediments of the Sevastopol Bay waters using W.I. Clark's formula [22, p. 54]:

$$rH_2 = \mathrm{Eh} / 30 + 2\mathrm{pH}, \quad (1)$$

where Eh is redox potential; pH is hydrogen index.

To assess the role of mytilasters in the transfer of matter and energy on different substrates, we used the index of functional abundance (IFA) calculated by formula [23, p. 88]

$$\mathrm{IFA} = N^{0.25} \cdot B^{0.75}, \quad (2)$$

where B and N are biomass, $g \cdot m^{-2}$, and abundance, $ind. \cdot m^{-2}$, of the taxon.

The IFA for solid natural and artificial substrates of water areas with different anthropogenic load was calculated using data on abundance and biomass of mytilasters from literature sources [10, 15, 18, 20, 24, 25] for 2012–2018. For the bottom sediments of Sevastopol Bay, this index was calculated according to the indicators we obtained in the present work (monitoring surveys in 2012, 2015, 2018). For marine soils of Laspi Bay, the IFA was calculated using literature data.

Results and discussion

Settlement of Mytilaster lineatus on solid artificial and natural substrates under conditions of chronic petroleum pollution and in conditionally clean water areas

In the seawater of Sevastopol Bay, high concentrations of PHCs have been recorded [10, 18], which indicates their constant inflow into the water area. In [19], regular exceeding of sanitary norms for this indicator was noted (see Table 1).

[3)] Oradovskiy, S.G., ed., 1977. [*Guideline for Methods of Sea Water Chemical Analysis*]. Leningrad: Gidrometeoizdat, p. 118–131 (in Russian).

In 2008–2010, the amount of these compounds in water exceeded the MPC on average by 1.5–2 times in 80% of all cases.

Mytilid fouling is ubiquitous on the mooring walls of Sevastopol Bay. Its community undergoes a number of changes under the influence of natural and anthropogenic factors. At the same time, the degree of influence of one or another factor on mytilid communities is variable. Thus, significant changes in fouling were noted after the devastating storm in Sevastopol on 11 November 2007. As shown in [9], mytilid communities on the mooring walls of Sevastopol Bay were almost completely destroyed. Since 2008, they have been gradually recovering in the environment with chronic petroleum pollution, but full recovery of biocenoses took quite a long time.

It was noted [9] that in the spring of 2009, the average abundance of mytilasters on the mooring walls of the bay had increased significantly relative to 2008 and had reached pre-storm values of 2006. In 2006–2009, the abundance of mytilasters increased one and a half to two times in some areas of the bay. The mollusks did not differ in size composition then. It should be noted that the abundance of mussels on the mooring walls decreased by half during the same period.

By 2015, at the same stations, mussel abundance and biomass had declined significantly relative to 2006, with abundance at some stations decreasing four times and biomass six times. These indicators in mytilasters changed to a lesser extent on the surface of the hydraulic structure than in mussels. A twofold increase in the number of abundance and biomass of mytilasters was observed at almost all studied sections of the promenade. In [13], it is noted that in 2015, mytilasters were more numerous than mussels on the concrete promenade of the bay and this phenomenon is frequent for fouling of artificial structures in the Sevastopol waters. Based on the above, it can be noted that under the conditions of regular exceedance of PHCs concentrations in seawater, the community of mytilasters on the mooring walls of Sevastopol Bay recovered after the storm faster than the mussel community. In 2018, a decrease in the abundance and biomass of the studied mollusks was observed at the hydraulic structures of the inner part of the Sevastopol Bay waters compared to 2015 [21]. At the same time, the size composition of the mytilasters has not generally changed over the period under study.

Information on mytilid fouling on artificial substrates of Laspi Bay (mooring walls, concrete slabs and pier of the Laspi children resting camp) is fragmentary or not available. In the waters of Laspi and Sevastopol bays, experiments [26] were conducted to study the potential replenishment of the settlements of mussels and mytilasters during the periods of mass settling of their larvae in different periods. The experiment showed that in the coastal waters of Laspi Bay on artificial substrates (plates with smooth and pile surface), the replenishment of settlements of mytilasters was much higher than in Sevastopol Bay. Potential replenishment of mytilasters in conditionally clean and polluted water areas is higher than that of mussels. Besides the substrate, the reason influencing the difference

in mollusk settlements in conditionally clean and chronically petroleum-polluted water areas can be the quality of their habitat.

Studies [24] of fouling of hydraulic structures in the area of the Southern pier of Sevastopol Bay and a conditionally clean area on the breakwater at the open coast of the town of Alupka (Southern Coast of Crimea (SCC)) showed that the abundance of this species in polluted seawater at the Sevastopol coast was almost twice as high as at the Alupka coast (see Table 1). The biomass of mytilasters in both areas is almost the same. This can be stipulated by the fact that water temperature rises faster in Sevastopol Bay during the spring and summer period than near the SCC. Consequently, the breeding period in the bay can start earlier and more juveniles can settle down by July–August. Such high numbers of mytilasters in the polluted waters indicate that this species is resistant to petroleum pollution and that this anthropogenic factor is not determinant for the functioning of the community. The priority factors affecting the abundance of mollusks are hydrodynamic processes and temperature regime.

Mytilasters are common in waters with different degrees of marine pollution. Thus, we observed mytilasters on rocks in the Laspi Bay waters, where the PHCs concentration in seawater in 2018 was close to the maximum permissible one (MPC = 0.05 mg·L^{-1}) [20] and exceeded the MPC 3–4 times in summer (see Table 1). On average, the PHCs concentration was higher than concentrations typical for Sevastopol bays. At the same time, our studies of hydrocarbon composition of the Batiliman seawater in the period of different recreational load (Laspi Bay) in 2023 [27] showed the absence of petroleum pollution in the water area, and high PH indicators were most likely associated with natural processes (active intake of allochthonous compounds). No petroleum pollution is also indicated by the trace PHCs concentrations in marine soils of Laspi Bay in 2016–2018 [20].

Mytilid fouling of natural hard substrates along the Crimean coast, especially in the SCC waters, has been insufficiently studied in the modern period. The main works in this direction are devoted to the study of the Karadag benthos. In 2014, a study of the taxonomic composition and quantitative indicators of mytilids inhabiting natural substrates of the Cape Martyan Reserve was carried out [28]. The *Mytilaster lineatus* bivalves dominated in terms of quantitative indicators (47% of total abundance and 97% of total macrozoobenthos biomass). This species of mollusks predominates on solid substrates in other areas of the Crimean coast as well. Nevertheless, it is worth noting that the abundance and biomass quantitative indicators of mytilasters (see Table 1) on artificial substrates in the Sevastopol Bay waters are significantly higher than on the SCC natural substrates [2, 13, 26].

The highest IFA values were obtained for the Sevastopol Bay artificial substrates (Table 1). The lowest values were recorded on the SCC natural substrates. This suggests that mytilasters inhabiting the bay hydraulic structures contribute more to the transformation of matter and energy than mytilasters inhabiting

Table 1. Average abundance and biomass of *Mytilaster lineatus* mollusks on artificial and natural substrates with different levels of petroleum pollution (2012, 2015, 2018)

Parameter	Artificial substrates			Natural substrates	
	Sevastopol Bay		Breakwater, Alupka	Karadag	Southern Coast of Crimea
	Southern pier	Promenade			
Abundance, ind.·m^{-2}	11,425	28,388	5654	11,830	9136
Biomass, g·m^{-2}	869	1705	705.1	1700	593.9
Pertroleum hydrocarbons concentration in water, mg·L^{-1}	0.3	0.16	0.1	0.024	0.14
IFA	1655	3444	1186	2761	1176

natural rocks. In general, the values of this index specify that in water areas exposed to chronic petroleum pollution, the contribution of mytilasters to the community is more significant than in conditionally clean water areas.

It can be concluded that the abundance of mytilasters on hard substrates is probably primarily influenced not by marine pollution, but by water temperature and surf-wave phenomena. In addition, it is worth noting that this mollusk is resistant to organic pollution. Its abundance and biomass in the fouling of water areas chronically polluted with petroleum and petroleum products corresponds to and in some areas exceeds these indicators in conditionally clean areas.

Settlement of Mytilaster lineatus on soft soils under conditions of chronic petroleum pollution and in conditionally clean water areas

The studied mollusks do not form mass settlements in muds, but it is known that species diversity of benthic communities can be used to assess the water area ecological conditions, in particular, presence of filter-feeding bivalves, indicating the environmental quality, in the community. Under conditions of chronic petroleum pollution and deterioration of physical and chemical parameters of marine soils, the density of settlement of mytilids decreases [3]. Earlier studies of the Sevastopol

Bay benthic community (2000–2009) showed significant deterioration of the general status of macrozoobenthos: decrease in total biomass in almost all selected water areas [29].

Changes were also noted for mollusks M. lineatus. In 2000, they made a significant contribution to the total biomass and abundance of macrozoobenthos, whereas in 2009, these indicators decreased two times. The key factors influencing the formation and composition of benthic animal biocenoses include the oxygen level in marine soils, salinity, bottom sediment composition, the PHCs and heavy metals level in water and bottom sediments and their accumulation in mollusks [7]. Mytilasters make a great contribution to the total biofilter volume and, consequently, to the processes of self-purification of the water area [3]. They accelerate significantly sediment deposition to the bottom due to their filtration activity.

According to the results of our surveys, mytilasters were found in the Sevastopol Bay bottom sediments represented mainly by black or dark grey muds, sometimes with admixture of sand and broken shell (in 2012 in 58% of samples, in 2015 and 2018 in 50% of samples) (Table 2). In most cases, mytilasters were recorded in muddy bottom sediments, less frequently in sandy sediments with admixture of fine shell. It was noted that mollusks had the lowest biomass in sandy soils.

In 2012, the abundance of mytilasters in the Sevastopol Bay muds varied from 9 to 70 ind.·m^{-2} (Table 2). The highest density of mollusks was recorded in the bay coastal zone in its southwestern part (st. *13*). This station is located at one of the most polluted sites near the mooring walls of Artilleriyskaya Bay (Figure, *a*).

Table 2. The abundance *N* and biomass *B* of *Mytilaster lineatus* mollusks in the bottom sediments of Sevastopol Bay with physico-chemical indicators of their habitat

Year	*N*, ind.·m^{-2}	*B*, g·m^{-2}	pH	Eh, mV	*H*, %	CES, mg·100 g^{-1}	PHCs, mg·100 g^{-1}	IFA
2012	9–70 29.14	0.002–0.184 0.04	7.2–8.2 7.6	–181…–19 –91	36–68 45	100–2200 920	55–799 317	0.22
2015	9–26 16.17	0.002–0.096 0.03	7.3–8.2 7.7	–236…+292 19.3	31–71 58	140–2280 1153	110–887 514	0.13
2018	9–79 36	0.006–0.43 0.09	7.6–7.9 7.8	–188…+24 –65	52–68 60	200–2200 871	134–592 477	0.42

Note: 1. The range of values is in the numerator, the average value is in the denominator.
2. *H* – natural humidity.

The ferry pier and stormwater outfall are located here. The CES concentration at this station was 540 mg·100 g^{-1} ADBS, that of PHCs was 301.7 mg·100 g^{-1} ADBS. These indicators correspond to the 4th level of bottom sediment pollution according to the regional classification [25]. The biomass of mytilasters during this period was within the range of 0.002–0.184 g·m^{-2} (Table 2).

The range of mollusk abundance in 2015 was from 9 to 26 ind.·m^{-2} (Table 2). The density of mytilasters decreased insignificantly compared to 2012. The abundance of mollusks decreased by half in the central part of the bay at st. *8* (Figure, *a*) and by 2.5 times in the southwestern part of the bay (st. *13*). At the same time, relative to 2012, at st. *13*, the CES value increased by four times and the PHCs concentration increased more than twice. The pollution level at this station corresponds to the highest 5th level, whereas earlier the CES content corresponded to the 4th level.

In the bottom sediments of Yuzhnaya Bay, on the shores of which the piers were built (st. *10*) (Figure, *a*), the density of mollusks increased from 18 to 26 ind.·m^{-2}. At the same time, the CES concentration at this station decreased from 2200 to 1800 mg·100 g^{-1} ADBS relative to 2012. Nevertheless, the level of bottom sediment pollution remained the same and corresponded to the 5th level. The biomass values of the studied mollusks in 2015 ranged from 0.002 to 0.096 g·m^{-2} (Table 2). Furthermore, while the abundance of mytilasters in the central part of the bay (st. *8*) decreased, their biomass here increased three times. The CES and PHCs indicators at this station decreased significantly. In other parts of the water area, their values differed slightly.

In 2018, the abundance of mollusks ranged from 9–79 ind.·m^{-2} (Table 2). In comparison with the data of previous years, the density of settlement of mytilasters increased at all stations, except for st. *11* (central part of Yuzhnaya Bay) (Figure, *a*). In 2018, compared to the 2015 data, the level of organic pollution of bottom sediments in the Yuzhnaya Bay water area decreased, the PHCs concentration decreased by 4.5 times. At the same time, as in previous years, the level of bottom sediment pollution corresponded to the highest 5th level.

In the southwestern part of the bay (st. *13*), the abundance of mollusks approached the values of 2012 and was 2.5 times higher than in 2015. The CES and PHCs concentrations were almost unchanged from 2015 to 2018 at this station, but their values were high and corresponded to the 5th level of pollution. The 2018 biomass values ranged from 0.006 to 0.43 g·m^{-2} (Table 2).

In the central part of the bay (st. *7*) (Figure, *a*), the biomass of mytilasters became four times higher compared to 2012. During the same period, the CES indicators remained almost unchanged, while the PHCs concentration increased by six times. These values also correspond to the 5th level of marine soil pollution.

At other stations, a tendency for an increase in the biomass of mytilasters was noted, except for the indicators in the central part of Yuzhnaya Bay (st. *11*) and the southwestern part of Sevastopol Bay (st. *13*). The biomass value in 2018 at st. *11* decreased almost three times compared to 2015, while at st. *13*, the mollusk biomass decreased almost five times, in contrast to the 2012 data. The abundance of mytilasters was almost the same during this period. At the same time, the CES indicators at the studied stations during the same period corresponded to the 5th level of pollution.

The abundance and biomass of mollusks in the years under analysis varied unequally. In general, the analysis of the abundance and biomass average values of the studied mollusks from 2012 to 2018 showed that the abundance of mytilasters in the marine soils of Sevastopol Bay had slightly increased. The average abundance during the study period increased from 29 to 36 ind.·m^{-2}, while the biomass increased from 0.04 to 0.09 g·m^{-2}.

The IFA for marine soils of Sevastopol Bay in the studied years (2012, 2015 and 2018) was 0.22, 0.13 and 0.42, respectively (Table 2). According to this index, in 2018, the contribution of mytilasters to the transformation of matter and energy was higher than in the previous years. In general, the IFA values are very low, indicating an insignificant energetic role of mytilasters inhabiting the Sevastopol Bay soft soils.

In addition to substrate, as mentioned above, community functionality is influenced by physical and chemical indicators that either accelerate or slow down oxidation processes in bottom sediments, thereby changing oxygen levels.

In 2012, pH in bottom sediments ranged from 7.2–8.2, in 2015 it was 7.3–8.2, and in 2018 it was 7.6–7.9 (Table 2). The pH range in these years indicated slightly alkaline environment in most of the analysed samples, except for the Yuzhnaya Bay coastal area (st. *10*) and near Konstantinovsky ravelin (Northern pier) (st. *17*) (see Figure, *a*), where pH increased to 8.21–8.22 (st. *10* in 2012 and 2015, respectively) and 8.2 (st. *17* in 2015), which is likely to be related to the type of precipitation.

The redox potential (Eh) in 2012 had negative values and ranged from −19 to −181 mV (Table 2), indicating reducing environmental conditions. In 2015, Eh fluctuated within a wide range from −116 to +292 mV (Table 2). In the central part of Sevastopol Bay (sts. *5*, *8*) and in the coastal zone of Yuzhnaya Bay (st. *10*) (see Figure, *a*), Eh indicated poorly reducing conditions. In the central part of Yuzhnaya Bay (st. *11*) and in the coastal zone of the southwestern part of Sevastopol Bay (st. *13*) (see Figure, *a*), Eh indicated reducing conditions, whereas at the Northern pier (st. *17*) (see Figure, *a*) it indicated oxidative ones. As in 2015, Eh had a large range from −188 to +24 mV in 2018 (Table 2). At all stations, except for the coastal zone of Sevastopol Bay (st. *13*) (see Figure, *a*), poorly reducing conditions were noted, with st. *13* having the lowest Eh value indicating reducing environmental conditions. These conditions contribute to the accumulation of hydrocarbons, as at low values of the environment redox potential, the processes of bitumoid transformation are slowed down. Reduced Eh values correspond to the water areas where organic matter is concentrated [30].

It is known that Eh value depends on pH. To obtain comparable data in the analysed bottom sediments with different pH values, we calculated the hydrogen potential index (rH_2) using W.I. Clark's formula (1). According to this gradation, oxidative processes predominate at rH_2 above 27, reducing processes at 22–25 and intensive reducing processes below 20. In our case, only one station (st. *17* in 2015)

(see Figure, *a*) showed rH_2 close to 27, hence, oxidative processes prevailed at this station (Northern pier). At other stations, the rH_2 values were significantly lower than 20 during the study period, which indicates intensive reducing processes in the studied marine soils.

Natural moisture content in bottom sediments was 36–68% in 2012, 31–71% in 2015 and 52–68% in 2018 (Table 2). These values correspond to the particle size distribution of bottom sediments. In general, reducing environmental conditions and high concentrations of organic matter accumulated in sediments are observed at most stations in terms of physical and chemical parameters: CES in the range of 100–2280 mg·100 g^{-1} ADBS (Table 2). Widespread occurrence of mytilasters under these conditions confirms the tolerance of mollusks to organic pollution.

In the correlation analysis, only those stations of Sevastopol Bay at which mytilasters had been found were taken into account (n = 15). In 2012, no correlation between mollusk abundance, biomass and physical and chemical parameters of bottom sediments was detected. In subsequent years (2015–2018), a direct relationship between the abundance and CES and PHCs concentration was observed, with correlation coefficients r equal to 0.94 and 0.85, respectively (Table 3). A reverse relationship is observed between abundance and Eh (r = −0.79). The strongest direct correlation was with the CES concentration (r = 0.94). In 2015, a direct correlation between the CES concentration and mollusk biomass was observed (r = 0.72). In 2018, a direct correlation was observed between the biomass of mytilasters and Eh (r = 0.6). An increase in the abundance (2015, 2018) and biomass (2015) of mytilasters at elevated CES concentrations can be observed from the correlation data obtained.

It is known that at high levels of organic pollution (4^{th}, 5^{th}) degradation and reorganisation of biocenoses occurs [25]. Starting from the 3^{rd} level of pollution, the trophic structure of benthos is sharply changed, a change in its qualitative

Table 3. Correlation coefficients between the abundance and biomass of *Mytilaster lineatus* mollusks and the physico-chemical parameters of the environment

Characteristic	Year	pH	Eh, mV	H, %	CES, mg·100 g^{-1}	PHCs, mg·100 g^{-1}
Abundance	2012	−0.32	0.25	0.10	0.03	−0.18
	2015	0.14	−0.79	0.38	0.94	0.85
	2018	−0.47	−0.04	−0.60	0.72	0.89
Biomass	2012	−0.26	0.39	0.20	−0.05	−0.19
	2015	−0.59	−0.34	0.30	0.72	0.40
	2018	0.04	0.60	−0.30	0.23	0.43

composition is observed: some species are eliminated from the community and more resistant to pollution species occupy dominant positions. The increase in the quantitative indicators of mytilasters at the high 5th level of pollution indicates the resistance of this species to organic pollution. Despite the fact that such dependence was observed in the water area with high anthropogenic load, the quantitative indicators in Sevastopol Bay were lower than in conditionally clean water area (Laspi Bay).

For comparison: in the conditionally clean water area of Laspi Bay, the average abundance of mytilasters was 126 ind.·m^{-2} and the biomass – 3.5 g·m^{-2} [31]. The IFA for the Laspi Bay marine soils was 8.57, which makes it possible to speak about a greater energetic contribution of the studied mollusks in the conditionally clean water area than in the water area with chronic petroleum pollution. In Laspi Bay, bottom sediments are represented mainly by sands. The CES content in them on average did not exceed 42 mg·100 g^{-1} air-dry matter, which corresponds to the 1st level of pollution [20]. Despite the exceeding of MPCs of PHCs in seawater in recent years, PHCs in sandy soils were recorded at trace concentrations [20]. Moreover, the CES and PHCs levels in the Laspi Bay bottom sediments remain within the range close to the level of the 1980s, which indicates stable favourable environmental situation in the area. In 2015, the quality of marine waters was assessed using hydrochemical indicators of Sevastopol and Laspi bays. It was established that in some areas of Sevastopol Bay, bottom waters had been in the state of hypoxia, in contrast to the waters of Laspi Bay [4)]. It is also known that sandy soils are more oxygenated than muds. In the latter, in turn, the processes of accumulation of organic substances, including petroleum hydrocarbons, occur faster, which directly affects the quality of bottom sediments and, consequently, the density of settlement and biomass of mollusks.

Conclusion

Mytilasters inhabit various water areas with different degrees of marine pollution by petroleum and petroleum products. These mollusks are widespread, form mass settlements on artificial and natural hard substrates, inhabit muddy and sandy bottom sediments. Due to their abundance, the studied mollusks form a powerful natural biofilter, influencing the marine environment self-purification potential.

The abundance of mytilasters inhabiting hard natural and artificial substrates is primarily influenced not by marine pollution but by water temperature and surf-wave phenomena. This mollusk is resistant to organic pollution, its average abundance (28,388 ind.·m^{-2}) and biomass (1705 g·m^{-2}) at the hydraulic structures of Sevastopol Bay were at the same level under conditions of chronic petroleum pollution of the water area. However, in some areas they were higher than in conditionally clean areas (SCC water area). At the same time, the correlation between

---

[4)] Korshenko, A.N., ed., 2023. *Marine Water Pollution. Annual Report 2021*. Moscow: SOI, 228 p. (in Russian).

the abundance and biomass of mytilasters inhabiting artificial substrates in the bay and the PHCs concentrations in seawater is not observed. The highest IFA values were obtained for the artificial substrates of Sevastopol Bay, which indicates a significant contribution of mytilasters inhabiting these substrates under conditions of chronic petroleum pollution to the transformation of matter and energy.

Analysis of the average values of abundance and biomass of mytilasters in the studied years showed that the number of mollusks in the Sevastopol Bay marine soils had increased at constantly high concentrations of CES (140–2280 mg·100 g^{-1}) and PHCs (110–887 mg·100 g^{-1}). In 2015 and 2018, a direct correlation between the abundance of mytilasters and the level of organic matter contamination of bottom sediments was found (correlation coefficient r was 0.94 for CES and 0.85 for PHCs).

The functionality of the benthic community is influenced by the physical and chemical parameters of bottom sediments, which either accelerate or slow down the oxidation processes, thereby changing the oxygen level. The most important indicator affecting mollusk abundance and biomass is the redox potential of bottom sediments, which was found to be directly dependent on it (r = 0.6). As for other indicators (pH, natural moisture), such a relationship was absent or expressed weakly.

It was revealed that in bottom sediments of conditionally clean water area of Laspi Bay with minimal level of petroleum pollution (PH concentrations in bottom sediments did not exceed 5 mg·100 g^{-1}), the average abundance and biomass of mytilasters had been higher than on the Sevastopol Bay soils with chronic petroleum pollution of marine soils and high CES and PH concentrations in bottom sediments corresponding to the 5th level of pollution.

References

1. Soloviova, O.V., 2007. Role of Mytilids (Mollusca: Mytylidae) in Selfpurification Processes of Seawater from Petroleum Hydrocarbons. *Ekologiya Morya*, 73, pp. 91–100 (in Russian).
2. Solovyova, O.V., 2017. Natural Biofilter of Hydrotechnical Structures of the Crimean Coast in the Recreational Period. *Bulletin of Udmurt University. Series Biology. Earth Sciences*, 27(3), pp. 311–321 (in Russian).
3. Zaika, V.E., Valovaya, N.A., Povchun, A.S. and Revkov, N.A., 1990. [*Mytilidae of the Black Sea*]. Kiev: Naukova Dumka, 208 p. (in Russian).
4. Govorin, I.A., 2006. [The Role of Mussels from the Fouling of Coastal Hydraulic Structures in the Formation of Microbiological Characteristics of the Marine Environment of Beach Water Areas]. *Gidrobiologichesky Zhurnal*, 42(3), pp. 41–50 (in Russian).
5. Jeppesen, E., Søndergaard, M., Lauridsen, T.L., Davidson, T.A., Liu, Z., Mazzeo, N., Trochine, C., Özkan, K., Jensen, H.S. [et al.], 2012. Biomanipulation as a Restoration Tool to Combat Eutrophication: Recent Advances and Future Challenges. *Advances in Ecological Research*, 47, pp. 411–488. https://doi.org/10.1016/B978-0-12-398315-2.00006-5
6. Matishov, G.G., Gargopa, Y.M. and Sarvilina, S.V., 2010. Impact of Atmospheric Circulation Fluctuations on the Zoobenthos Dynamics in the Sea of Azov. *Doklady Earth Sciences*, 430(2), pp. 201–204. https://doi.org/10.1134/S1028334X10020121
7. Korpakova, I.G. and Eletskiy, I.Yu., 2020. Influence of Environmental Factors on the Formation of Biocenosis of Malluscuses in the South-East Area of the Azov Sea.

Environmental Protection in Oil and Gas Complex, (3), pp. 13–18. https://doi.org/10.33285/2411-7013-2020-3(294)-13-18 (in Russian).

8. Soloveva, O.V., 2007. [Flows of Petroleum Hydrocarbons Through the Settlement of Mussels Inhabiting the Southern Breakwater of Sevastopol Bay (Black Sea)]. *Marine Ekological Journal*, 4(4), pp. 61–68 (in Russian).
9. Solovyova, O.V., 2015. Recovery of Mytilidae Fouling of Hydraulic Structures in the Sevastopol Bay (Black Sea). *Bulletin of Udmurt University. Series Biology. Earth Sciences*, 25(3), pp. 70–76 (in Russian).
10. Mironov, O.G. and Alyomov, S.V., eds., 2018. *Sanitary and Biological Studies of the South-Western Crimea Coastal Waters at the Beginning of XXI Century*. Simferopol: ARIAL, 276 p. https://doi.org/10.21072/978-5-907118-89-8 (in Russian).
11. Solovyeva, O.V., 2017. The Dynamics of the Co-Existent Settlements of *Mytilus galloprovincialis* Lam. and *Mytilaster lineatus* Gmel. Along Large Hydraulic Structure in the Conditions of Sevastopol Bay (Black Sea). *Proceedings of the RAS Ufa Scientific Centre*, (3), pp. 83–89.
12. Shurova, N.M., 2013. *Structural and Functional Organization of Population of the Black Sea Mussel (Mytilus galloprovincialis)*. Kiev: Naukova Dumka, 206 p. (in Russian).
13. Soloveva, O.V., 2019. Mytilidae Fouling of Some Hydraulic Structures in the Coastal Water Areas of Sevastopol (Crimea, Black Sea). *Ekologiya i Stroitelstvo*, (2), pp. 27–34. https://doi.org/10.35688/2413-8452-2019-02-004
14. Makarov, M.V., Bondarenko, L.V. and Kopiy, V.G., 2010. [Macrozoobenthos of Natural Solid Substrates of Karantinnaya Bay (Crimea, Black Sea)]. *Scientific Issues Ternopil Volodymyr Hnatiuk National Pedagogical University. Series: Biology,* (3), pp. 149–153 (in Russian).
15. Makarov, M.V. and Kovalyova, M.A., 2017. The Structure of Taxon of Molluscs on Natural Hard Substrates in Aquatorium of Crimean Reserve Areas. *Ekosistemy*, (9), pp. 20–24 (in Russian).
16. Mironov, O.G., Kirjukhina, L.N. and Alyomov, S.V., 2003. *Sanitary-Biological Aspects of the Sevastopol Bays Ecology in XX Century*. Sevastopol: ECOSI-Gidrofizika, 185 p. (in Russian).
17. Atsikhovskaya, Zh.M. and Chekmenyova, N.I., 2002. Water Dynamic Activity Estimation in the Laspi Bay Area (the Black Sea). *Ecology of the Sea*, 59, pp. 5–8 (in Russian).
18. Mironov, O.G. and Mironov, O.A., 2015. Petroleum Hydrocarbons in the Coastal Sea Waters of Sevastopol. *Environmental Protection in Oil and Gas Complex*, (9), pp. 25–29 (in Russian).
19. Mironov, O.G, Alyomov, S.V., Osadchaya, T.S., Guseva, E.V., Mironova, T.O., Muravyova, I.P., Mironov, O.A., Enina, L.V., Aliphanova, D.A. and Volkov, N.G., 2012. Ecological Monitoring of Artilleriyskaya Bay (Sevastopol, Balck Sea). *Marine Ekological Journal*, 12(1), pp. 41–52 (in Russian).
20. Tikhonova, E.A., Soloveva, O.V., Mironov, O.A. and Burdiyan, N.V., 2020. Sanitary and Biological Characteristics of the Laspi Reserve Coastal Waters (the Black Sea). *Ecological Safety of Coastal and Shelf Zones of Sea*, (3), pp. 95–106. https://doi.org/10.22449/2413-5577-2020-3-95-106 (in Russian).
21. Soloveva, O.V., 2021. Dynamics of Mussel and Mytilaster Settlements on the Hydraulic Structures of Recreational Waters. *Aquatic Bioresources and Environment*, 4(3), pp. 38–49. https://doi.org/10.47921/2619-1024_2021_4_3_38 (in Russian).

22. Kiryukhina, L.N. and Mironov, O.G., 2004. Chemical and Bacterial Characteristics of Marine Bottom Sediments in Sevastopol Bays in 2003. *Ecology of the Sea*, 66, pp. 53–58 (in Russian).
23. Maltsev, V.I., 1990. Use of a Functional Abundance Index for Structural Studies of Zoocoenoses. *Hydrobiological Journal*, 26(1), pp. 105–106.
24. Makarov, M.V., Bondarenko, L.V., Kopiy, V.G. and Kovalyova, M.A., 2016. Macrozoobenthos of Biofouling of Hydraulic Engineering Structures in Areas Which are Different in Ecological Conditions near the Crimean Coast (the Black Sea). *Ekologichesky Monitoring i Bioraznoobrazie*, (1), pp. 76–80 (in Russian).
25. Mironov, O.G., Milovidova, N.Yu. and Kiryukhina, L.N., 1986. On Maximum Permissible Concentrations of Petrolium Products in Bottom Sediments of the Black Sea Littoral. *Gidrobiologicheskiy Zhurnal*, 22(6), pp. 76–78 (in Russian).
26. Kazankova, I.I., 2019. Definition of the Potential Recruitment of Mussel, Mitilaster and Anadara Settlements in the Coastal Waters of the Black and Adriatic Seas by Experimental Substrates. *Monitoring Systems of Environment*, (3), pp. 112–119. https://doi.org/10.33075/2220-5861-2019-3-112-119 (in Russian).
27. Tikhonova, E.A., Soloveva, O.V., Tkachenko, Yu.S., Burdiyan, N.V., Doroshenko, Yu.V., Guseva, E.V. and Alyomov, S.V., 2024. The Content of Hydrocarbons and Indicator Groups of Bacteria in the Marine Environment of Laspi Bay (Southern Coast of Crimea). *Ecological Safety of Coastal and Shelf Zones of Sea*, (1), pp. 113–129.
28. Makarov, M.V., Kovaleva, M.A., Kopiy, V.G. and Bondarenko, L.V., 2015. [Macrofauna of Fouling of Natural Hard Substrates (Boulders) in the Water Area of the Cape Martyan Nature Reserve (Black Sea, Crimea)]. In: G. M. Abdurakhmanov and M. Z. Magomedova, eds., 2015. [*Proceedings of the 17th International Scientific Conference "Biodiversity of Caucasus and the South of Russia". Nalchik, 05–06 November 2015*]. Makhachkala: IPE RD, pp. 484–487 (in Russian).
29. Osadchaya, T.S., Alemov, S.V. and Viter, T.V., 2018. The Complex Bottom Sediments–Bentos in Evaluation of the Environmental Status of Sevastopol Bay (Black Sea). In: I. I. Rudneva, ed., 2018. *Pollution of Marine Environment: Ecological Monitoring, Bioassay, Standardization: Collection of the Papers of the Russian Scientific Conference with International Participation Devoted to 125th Anniversary of Prof. V. A. Vodyanitsky, Sevastopol, May 28 – June 1, 2018*. Sevastopol: Colorit, pp. 188–194 (in Russian).
30. Kiryukhina, L.N. and Gubasaryan, L.A., 2000. Biogeochemical Characters of Crimean Shelf's Bottom Sediments from the Black Sea. *Ecology of the Sea*, 50, pp. 18–21 (in Russian).
31. Revkov, N.K. and Nikolaenko, T.V., 2002. Biodiversity of Zoobenthos in the Coastal Zone of the South Coast of Crimea (Laspi Bay Area). *Russian Journal of Marine Biology*, 28(3), pp. 151–162.

Submitted 13.05.2024; accepted after review 14.10.2024;
revised 17.12.2024; published 31.03.2025

About the authors:

Yulia S. Tkachenko, Junior Research Associate, A. O. Kovalevsky Institute of Biology of the Southern Seas of RAS (2 Nakhimova Ave, Sevastopol, 299011, Russian Federation), **ORCID ID: 0009-0001-1752-1043**, **Scopus Author ID: 1220495**, *yulechkatkachenko.90@mail.ru*

Elena A. Tikhonova, Leading Research Associate, A. O. Kovalevsky Institute of Biology of the Southern Seas of RAS (2 Nakhimova Ave, Sevastopol, 299011, Russian Federation), PhD (Biol.), **ORCID ID: 0000-0002-9137-087X**, **Scopus Author ID: 57208495804**, **ResearcherID: X-8524-2019**, *tihonoval@mail.ru*

Tatiana V. Viter, Junior Research Associate, A. O. Kovalevsky Institute of Biology of the Southern Seas of RAS (2 Nakhimova Ave, Sevastopol, 299011, Russian Federation), **ORCID ID: 0000-0002-6792-5548**, **Scopus Author ID: 57208484620**, *tatjana-viter@rambler.ru*

Contribution of the authors:

Yulia S. Tkachenko – preparation of bottom sediment samples, analysis of the results and literature sources on the study topic, writing and execution of the article

Elena A. Tikhonova – study goal and objectives statement, sampling of bottom sediments, determination of physical and chemical parameters of bottom sediments, revision of the article text

Tatiana V. Viter – participation in monitoring surveys of the bay, determination of abundance and biomass of mytilasters in bottom sediments of Sevastopol Bay for 2012–2018, discussion of the results, writing of the article

All the authors have read and approved the final manuscript.